

UNIVERSITÀ DEGLI STUDI DI MILANO

Dipartimento di Chimica

PhD Course in Industrial Chemistry - XXXIV Cycle



(Asymmetric) Photocatalysis Under Homogeneous and Heterogeneous Conditions – Optimization in continuo, Novel Catalytic Reactors and Materials

Coordinator Doctorate Course in Industrial Chemistry: Prof. Dominique Roberto

Tutor: Prof. Maurizio Benaglia

Co-Tutor: Prof Alessandra Puglisi

Co-Referees: Prof. Burkhard König

Prof Timothy Noël

Dr. Miguel Sanz

Fabian Herbrik

R12465

2019-2022



UNIVERSITÀ
DEGLI STUDI
DI MILANO



TECHNOTRAIN

*Enabling TECHNOlogies-driven chemistry: a tailored TRAINing research program for batch
and flow synthesis of chiral amino derivatives*

H2020-MSCA-ITN-2018, Grant Agreement n. 812944

UNIVERSITÀ DEGLI STUDI DI MILANO

(Asymmetric) Photocatalysis Under Homogeneous and Heterogeneous Conditions – Optimization *in continuo* , Novel Catalytic Reactors and Materials

Department of Chemistry

PhD in Industrial Chemistry, XXXIV Cycle



PhD candidate: Fabian Herbrik
Matricola: R12465

Coordinator of the Doctorate Course in Industrial Chemistry:

Prof. Dominique Roberto

Tutor:

Prof. Maurizio Benaglia

Co-Referees:

Prof. Burkhard König
Prof Timothy Noël
Dr. Miguel Sanz

Members of scientific committee:

Prof. Alessandra Puglisi, Dr. Sergio Rossi, Dr. David Bevk, Dr. Sumaira Umbreen

Table of Contents

1.	Introduction	1
1.1.	Interaction of Electromagnetic Radiation and Matter - From a Chemist's Point of View 1	
1.1.1.	Photoredox Catalysis	10
1.1.2.	Showcase of the Lambert-Beer law and consequences for solid supported catalysis....	14
1.2.	Continuous Flow Chemistry and Reactor Technology	19
1.2.1.	Plug-Flow Reactors	29
1.2.2.	Continuous Stirred Tank Reactors.....	30
1.2.3.	Packed Bed Reactors	31
1.3.	(Organo-)Catalyst Immobilization – Strategies and Application	33
2.	Results and Discussion	34
2.1.	Project: Solid Supported Imidazolidinone Catalysts in Photocatalysis	34
2.1.1.	SS-Catalysts in MacMillan's aldehyde alkylation with electrophilic radicals	34
2.1.2.	SS-Catalysts in MacMillan's spin-center-shift benzylation	55
2.1.3.	SS-Catalysts Together With Melchiorre's Nucleophilic Thiocarbamate Catalyst	64
2.2.	Solid Supported Eosin Y and Its Use in (Stereoselective) C-C-Bond Formations	77
2.2.1.	Preliminary Findings using Supported Eosin Y	78
2.2.2.	Supported Eosin Y in Cross-Dehydrogenative Coupling Reactions (CDHC-reactions)..	82
2.3.	Telescoped Synthesis of an API in a Photocatalyzed Stereoselective Way	91
2.3.1.	Preliminary Studies and the Construction of a Novel Photoreactor	91
2.3.2.	Translation into a Continuous Flow Process	95
2.3.3.	Fully Telescoped, Fully Continuous Photoorganocatalyzed API Synthesis	102
2.4.	Photochemistry <i>in Continuo</i> Deep Dive – A Critical Examination of Important Parameters	109
2.4.1.	Introduction to the Field	109
2.4.2.	Explanation of Methodology	111
2.4.3.	Description of Equipment.....	115
2.4.4.	Act I – Dark Ages – Light Ages, Who Knows?	116
2.4.5.	Act II – Renaissance	118
2.4.6.	Act III – Enlightenment.....	122
3.	Conclusion	127
3.1.	SS-MacMillan	127
3.2.	MR-EY	127

3.3.	Telescoped Process.....	128
3.4.	Photochemistry <i>in continuo</i> Deep Dive	128
4.	Experimental Section	129
4.1.	Project: Solid Supported Imidazolidinone Catalysts in Photocatalysis	129
4.1.1.	Description of Equipment.....	131
4.1.2.	Solid Supporting the Catalysts.....	135
4.1.3.	MacMillan Catalyst Precursors for Solid Support	138
4.1.4.	General Procedure for the Stereoselective α -Functionalization of Aldehydes	141
4.1.5.	Continuous Flow Packed Bed Catalytic Reactor enantioselective Cyanoalkylation	157
4.1.6.	Synthesis of Mitiglinide Radical Precursor	159
4.1.7.	Telescoped <i>in continuo</i> Synthesis of a Mitiglinide Precursor	161
4.2.	Solid Supported Eosin Y and Its Use in (Stereoselective) C-C-Bond Formations	166
4.2.1.	Description of Equipment.....	168
4.2.2.	Synthesis and Characterisation of Solid-Supported Eosin Y MR-EY.....	170
4.2.3.	General Procedures for Batch, Continuous Flow and Packed Bed Catalytic Reactions 174	
4.2.4.	Fluidic Synthesis and Characterisation of Products	183
4.3.	Telescoped, <i>In Continuo</i> Synthesis of an API in a Photo-catalyzed Stereoselective Way 192	
4.3.1.	Description of Equipment	194
4.3.2.	General Procedure for Batch Reactions – Benchmarking the Photoreactor	199
4.3.3.	Purification and Characterization of Compounds 3aa, 3ba, 3ca, 3ab, 3ac	202
4.3.4.	General Procedure for Fluidic Reaction (Screening and Synthesis).....	206
4.3.5.	Calculation of Productivity and Space-Time-Yield.....	218
4.3.6.	Procedures for the Telescoped Process	219
4.4.	Photochemistry <i>in Continuo</i> Deep Dive – A Critical Examination of Important Parameters	225
4.4.1.	Description of Equipment.....	226
4.4.2.	General Procedure for the Preparation of Stock-Solutions for Batch and Flow Reactions 231	
4.4.3.	Measurement of Molar Extinction Coefficient to Determine Transmission Through Reaction Medium.....	236
4.4.4.	Irradiation from One Side versus Both Sides. And How to Read the Diffusion Graph..	238
4.4.5.	Actinometry and Photonflux Consideration.	240
4.4.6.	Predicting Reactor Performance Using Photons equivalents.....	242
5.	Bibliography	245

List of Publications

August 2022

Supported Eosin Y as a Photocatalyst for C-H Arylation of Furanes in Batch and Flow - <https://doi.org/10.3390/molecules27165096>

June 2022

Immobilized Eosin Y for the Photocatalytic Oxidation of Tetrahydroisoquinolines in Flow - <https://doi.org/10.1002/cctc.202200461>

March 2022

Enantioselective organophotocatalytic telescoped synthesis of a chiral privileged active pharmaceutical ingredient - <https://doi.org/10.1002/chem.202200164>

October 2021

In-flow enantioselective homogeneous organic synthesis - <https://doi.org/10.1515/gps-2021-0073>

August 2020

Eosin Y: Homogeneous Photocatalytic In-Flow Reactions and Solid-Supported Catalysts for In-Batch Synthetic Transformations
<https://doi.org/10.3390/app10165596>

July 2016

Ruthenium Catalysed Methylation of Amines with Paraformaldehyde in Water under Mild Conditions - <https://doi.org/10.1002/cssc.201600824>

1. Introduction

1.1. Interaction of Electromagnetic Radiation and Matter - From a Chemist's Point of View

Giacomo Ciamician began studying light on the roof of the University of Bologna more than 100 years ago, envisioning a future in which all the energy required by humans would be derived entirely from the sun. In 1912, he imagined an industry based solely on solar energy, avoiding the use of finite resources such as fossil fuels and coal.^[1]

We are still a long way from completely abandoning nonrenewable sources, but significant progress is being made every day, and Ciamician's dream of a sustainable and environmentally friendly industry may become a reality: it is estimated that the sunlight that strikes our planet every day is more than the energy that we consume in a year^[2]. Photochemistry has advanced dramatically over the last century and has been applied to a wide range of topics: the goal of my thesis is to investigate the use of light in aminocatalysis, as well as to investigate novel chemistry involving green processes. Before discussing photocatalysis, it is helpful to understand the fundamental concepts of photochemistry, such as the excitation pathway of a molecule and the laws that govern it. The most basic interaction occurs when one molecule absorbs one photon, resulting in the molecule being promoted to its excited state.

The well-known Bohr equation contains the mandatory condition: ^[3]

$$\Delta E = E_f - E_i = h\nu$$

Equation 1

When the magnetic field of a molecule interacts with light, a photon is absorbed.

The optimal pathway for an excited molecule is determined by the selection rules: for example, the probability of a selected pathway is described by the transition moment (TM), which can be calculated after the Schrodinger equation is solved:

$$TM = \int \phi_i \hat{\mu} \phi_f d\tau_e \int S_i S_f d\tau_s \int \theta_i \theta_f d\tau_N$$

Equation 2

The first term is known as the electronic transition moment: ϕ_i represents the orbitals, and μ is the dipole moment operator. This term is based on the symmetry and overlap

of the two orbitals: to allow the transition between two orbitals, the product of the orbitals' wavefunctions must be antisymmetric; this rule is known as the Laporte rule. The spin-overlap integral, whose value depends on the initial and final spin states of the promoted electron, is equal to one when the initial and final spin states are the same. This rule makes the transition between two different multiplicity states impossible. The third and final term is the overlap integral of the initial and final wave functions for nuclear vibrations, which is based on the Franck-Condon principle and is thus known as the Franck-Condon term. The Franck-Condon principle is especially helpful in determining the shape of an absorption band. To understand what the Franck-Condon principle represents, consider the Potential Energy Surface (PES) in the figure below:

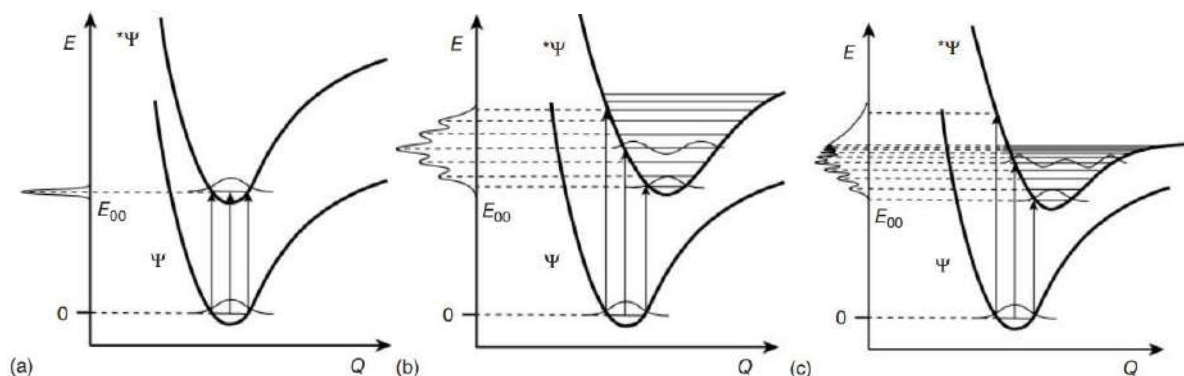


Figure 1. Depiction of the influence of the Franck-Condon principle in the absorption spectra by the PESs. Adapted From "Photochemistry and Photophysics – Concepts, Research, Applications", Balzani V., Ceroni P., Juris A.^[3]

Figure 1 demonstrates an excited state that is identical to the ground state. Because the wavefunctions are the solution to the same problem in this case, there is a strong transition from the ground state to the excited state: the absorption spectrum shows a sharp line corresponding to the 0-0 transition. The inverse case is shown in (b), where there is a strong distortion: in this case, several different 0-n transitions are permitted, forming a distribution; in fact, the shape of this transition is "Gaussian." The final (c) represents the case where the excited state is greater than the molecule's dissociation energy and the vibrational structure is completely lost. Finally, the Franck-Condon principle is demonstrated, which states that during an electronic transition, a change from one vibrational energy level to another is more likely if the two vibrational wave functions overlap significantly.

It is useful to record an emission spectrum and superimpose it with an absorption spectrum to study the distortion of the excited state.

There is no distortion between the ground state and the excited state if there is a significant overlap between the higher wavelength of the absorption spectrum and the lower wavelength of the emission spectrum, the smaller the overlap, the more distorted the excited state. The principle is based on the Condon approximation, which is a restriction of the Born-Oppenheimer approximation: in this restricted approximation, the electronic transition is considered faster than nuclear motion, allowing the nucleus to be assumed fixed in a specific position without changes in nuclear kinetic energy during the transition. Light absorption by a molecule on a vibrational level resulted in a change in kinetic energy, whereas light absorption on v_0 in a distorted molecule resulted in a change in nuclear position. The Jablonski diagram, shown in Figure 2, is a better representation of the PES.; In fact, it is an energy diagram that depicts the molecule's ground and excited states, as well as photophysical processes such as light absorption, emission, and intersystem conversion. Because organic molecules usually exhibit singlet states, the multiplicity state of the molecule is usually omitted; however, for metal complexes, it is useful to mark the energy level with the corresponding multiplicity.

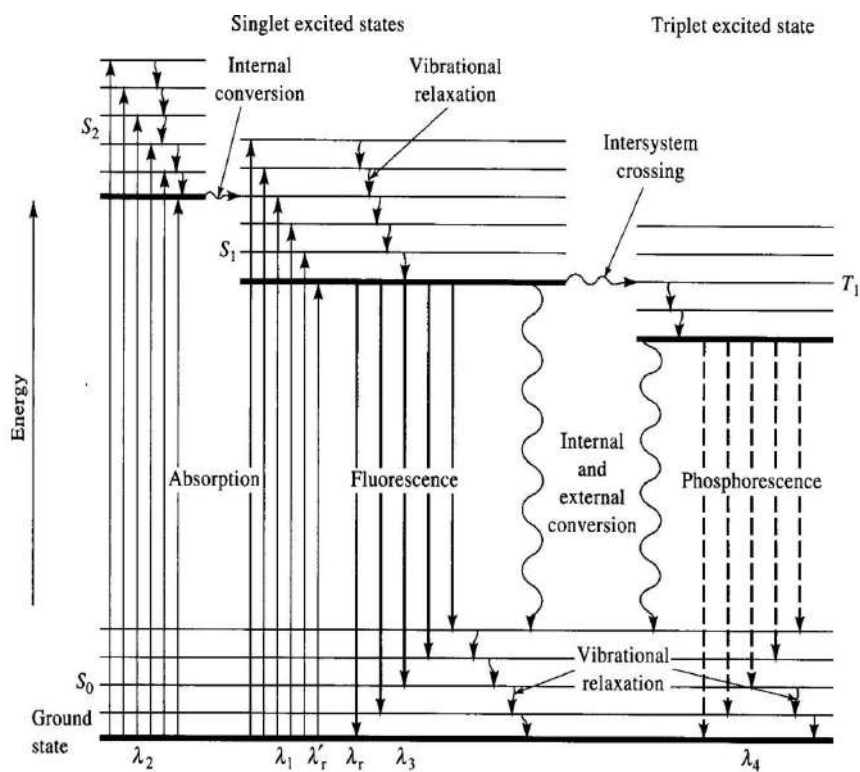


Figure 2. Jablonski Diagram

The diagram's most useful information is as follows:

- The energy difference between S_0 and S_1 is greater than the energy difference between S_1 and S_2 .
- Singlet and triplet states of the same numerical label usually have the same electronical configuration. • Light absorption usually generates the excited state in a high vibrational level due to the Franck-Condon principle if the excited state is distorted.
- Furthermore, if an emission from a highly distorted excited state occurs, the ground state is reached on a high vibrational level.
- The rate of each pathway is critical for understanding the contribution of each pathway.
- Because of the spin-selection rule, the intersystem crossing between the S_1 and T_1 states should be forbidden; however, this transition occurs if there is a significant spin-orbit overlap, such as caused by a heavy atom.
- The solvatochromic shift is an important effect to consider: the solvent can affect the energetic levels and stabilize or destabilize the excited state.
- If the solvent can stabilize the energetic level, a decrease in the E between the ground and excited states is observed; in this case, the absorption and emission spectra are shifted to a higher wavelength.
- If the solvent is unable to stabilize the excited state, the energy gap between the two energetic levels can widen, causing the spectrum to shift to lower wavelengths.
- Absorption and emission spectra remain simple for organic compounds, but they become more complicated for coordination compounds due to the additional transitions caused by the complex's different orbitals. They are typically distinguished by high symmetry and an open-shell d-orbital configuration.

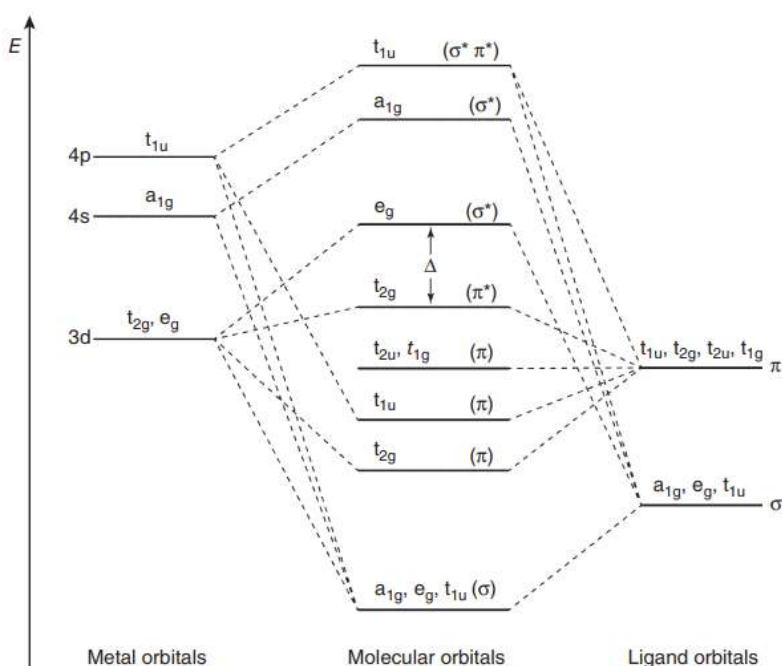


Figure 3. Depiction of MOs diagram for a metal complex. Adapted From “Photochemistry and Photophysics – Concepts, Research, Applications”, Balzani V., Ceroni P., Juris A.

Because of the high symmetry of the molecules, the molecular orbitals of a coordination compound are named differently: they are named with a letter (e, t, or a) based on the number of degenerate levels, and with a specification g (gerade in German, even) or u (ungerade in German, odd). Figure 3 depicts an example of an octahedral symmetry coordination compound, with the ground state being the t_{2g} level and the excited state being the e_g level. These levels are localized on the metal, and the energy difference between t_{2g} and e_g is referred to as crystal field stabilization energy. The orbitals of the ligands can interact with the metal in various ways: e_g and a_{1g} can bond, whereas t_{2g} can only bond; the t_{1u} orbital can give both interactions.

Several transitions can occur in a metal complex: the first is called intra-ligand or ligand centered (LC) and occurs between ligand σ electrons. Another possible transition is the metal-centered (MC) transition, which involves the excitation of an electron centered on the metal to an orbital of the metal. The Metal to Ligand Charge Transfer (MLCT) involves the excitation of a metal electron on the orbital of the ligand: this transition is especially important for the activation of a redox potential; the metal is oxidized and the ligand is reduced. Ligand to Metal Charge Transfer is the inverse of MLCT (LMCT).

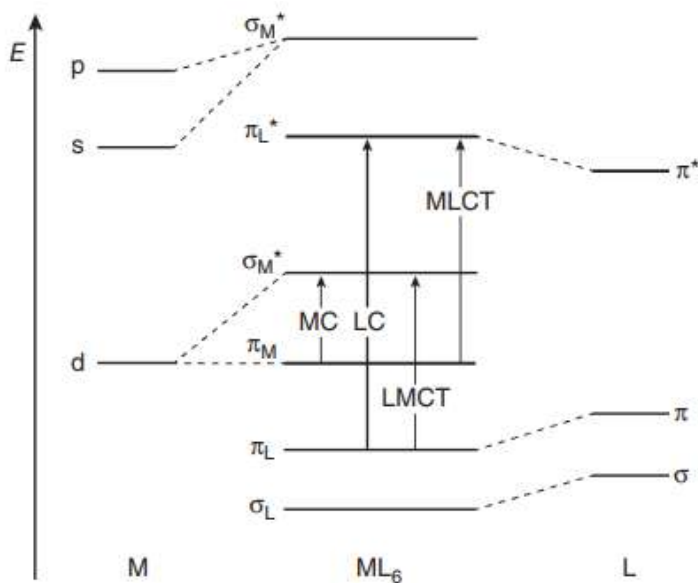
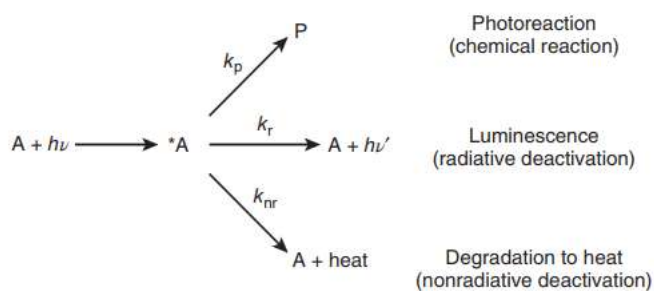


Figure 4. Depiction of transitions that can occur in a metal complex. Adapted From “Photochemistry and Photophysics – Concepts, Research, Applications”, Balzani V., Ceroni P., Juris A.

Deactivation pathways

An excited molecule can take several paths, the most common of which are excited state deactivations, which return the molecule to its ground state. The following scheme describes the most common excited-ground state transitions:



Scheme 1. Depiction of major deactivation pathways.

When a molecule is excited, it can take one of three different paths, as shown in the diagram above. The first pathway is photoreaction, which results in a different product. The other two paths are radiative and nonradiative deactivation, which both lead to the molecule remaining in its ground state via photon or heat emission. Deactivation without using radiation. Internal conversion and intersystem crossing are terms used

to describe radiationless transitions between energy states of the same or different multiplicity. As previously stated, the spin selection rule should prevent intersystem crossing. The multiplicity of the molecule has indeed changed. There are some exceptions to this rule, such as the heavy atom effect caused by increased spin-orbit coupling. If the two states of the molecule have different configurations, the El-Sayed rule allows for intersystem crossing. The El-Sayed rule for organic molecules can be summarized as follows

$^1(n, \pi^*) \rightarrow ^3(\pi, \pi^*)$ $^3(n, \pi^*) \rightarrow ^1(\pi, \pi^*)$ allowed transitions

$^1(n, \pi^*) \rightarrow ^3(n, \pi^*)$ $^1(\pi, \pi^*) \rightarrow ^3(\pi, \pi^*)$ forbidden transitions

The following figure explains when a radiationless deactivation is the most common pathway:

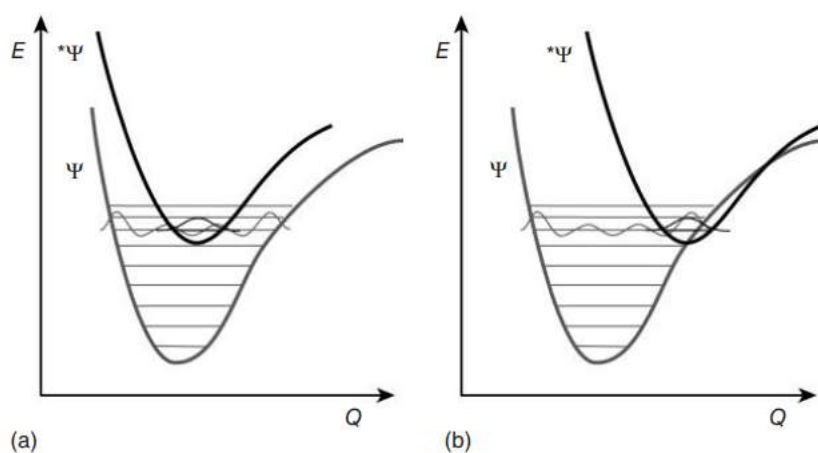


Figure 5. In figure are shown two different cases of deactivation from the excited state. Adapted From “Photochemistry and Photophysics – Concepts, Research, Applications”, Balzani V., Ceroni P., Juris A.

Figure 5 (a) depicts a situation in which there is little vibrational overlap between the vibrational levels: there is a large energy gap between Ψ and Ψ*.

Another example of a radiationless transition is shown in (b), where the energy gap between the two PESs of Ψ and Ψ* is small.

The energy gap law summarizes these two cases: for smaller energy gaps, the rate of conversion between the two energy levels and* is faster.

Deactivation by radiation

The Kasha's rule describes radiation deactivations: emission can occur only from the lowest excited state of any multiplicity.^[3]

Lifetime and Quantum Yield

The molecule can remain in the excited state for a certain amount of time, known as lifetime τ , before deactivating and returning to the ground state via the preferred pathways. The lifetime can be calculated using the process kinetics, as shown in the following equation:

$$\tau(*A) = \frac{1}{k_p + k_r + k_{nr}} = \frac{1}{\sum_j k_j} \quad \text{Equation 3}$$

Then, the efficiency $\eta_i(*A)$, strictly linked to the lifetime, is defined as follow:

$$\eta_i(*A) = \frac{k_i}{\sum_j k_j} = k_i \tau(*A) \quad \text{Equation 4}$$

Another important concept is quantum yield, which is defined for a primary process as the ratio of the number of molecules that go through a specific process to the number of photons absorbed by the reactant in the same time interval.

$$\Phi_i = \frac{\text{number of molecules that follow the process}}{\text{number of photons absorbed by the reactant}} \quad \text{Equation 5}$$

Numerically, it coincides with the efficiency and the equation can be simplified:^[3]

$$\Phi_i = \frac{k_i}{\sum_j k_j} = \eta_i(*A) \quad \text{Equation 6}$$

The quantum yield can be also described by the ratio between the number of photons emitted on the number of photons absorbed:^[4]

$$\Phi_i = \frac{\text{number of photons emitted}}{\text{number of photons absorbed}} = \frac{I_{em}}{I_{abs}} \quad \text{Equation 7}$$

Types of Quenching

A quencher is a molecule that can deactivate another molecule that is excited.

The main quenchers can act in two ways: radiative quenching and non-radiative quenching. The radiative quenching process involves the emission of a photon by the excited molecule and then absorption by another species. Instead, non-radiative quenching can be classified into two types based on the mechanism: coulombic quenching and electron exchange quenching. The Coulombic Mechanism, also known as Forster Resonance Energy Transfer (FRET), is a long-range mechanism that does not require physical contact between the donor and acceptor and is governed by the

dipole-dipole interaction. This mechanism does not follow the Stern-Volmer kinetics in fluid solution. Instead, the electron exchange is referred to as Dexter type and is a short-range mechanism. This is a collisional way in which two species exchange electrons, the excited molecule decays to the ground state while the other species is on the excited specie. The Stern-Volmer straight line is respected in this case, as is the upper diffusion-controlled limit.^[3]

Stern-Volmer Quenching Studies

The presence of a quencher influences the lifetime: it can significantly reduce the concentration of a molecule in its excited state. The deactivation pathway has first order kinetics, but the presence of a quencher causes second order kinetics. The following equation represents the first order kinetic:

$$-\frac{d[*A]_{intra}}{dt} = (k_p + k_r + k_{nr})[*A] = \frac{1}{\tau^0} [*A] \quad \text{Equation 8}$$

In this way it is possible to discover the lifetime of the molecule in its excited state in absence of the molecule B, which is supposed to be the quencher. Instead, the kinetic results in a second order and the new equation is the following one:

$$-\frac{d[*A]_{inter}}{dt} = k_q[*A][B] \quad \text{Equation 9}$$

Where k_q is the rate of the quenching process. The overall kinetic law can be resolved by a simple differential equation:

$$-\frac{d[*A]}{dt} = (k_p + k_r + k_{nr} + k_q[B])[*A] \quad \text{Equation 10}$$

$$[*A] = [*A]_0 e^{-(k_p+k_r+k_{nr}+k_q[B])t} \quad \text{Equation 11}$$

The lifetime in presence of the quencher can be obtained from the equation:

$$\tau(*A) = \frac{1}{\sum_j k_j} = \frac{1}{k_p + k_r + k_{nr} + k_q[B]} \quad \text{Equation 12}$$

From which is directly obtained the Stern-Volmer equation:

$$\frac{\tau^0}{\tau} = 1 + \tau^0 k_q [B] = 1 + k_{SV} [B] \quad \text{Equation 13}$$

This equation is analogous to a straight-line plot in which the intercept must be 1 and the angular coefficient represents the Stern-Volmer constant. The Stern-Volmer

equation is used to calculate the lifetime in the presence of a quencher. The presence of another molecule, which is the specie that is supposed to generate the radical, quenches the molecule in its excited state. To investigate the type of quenching present in the solution, this equation can be rearranged to use quantum yield instead of lifetime.

1.1.1. Photoredox Catalysis

Photoredox catalysts are useful for converting light into energy for a chemical reaction: several different molecules operate on the same mechanism. Metal-based catalysts (such as $[\text{Ru}(\text{bpy})_3]^{2+}$) can be distinguished from organo-based catalysts (like Eosin Y). The reactions based on these catalysts revealed a previously unknown chemistry.^[4] The generic mechanism behind a photoredox catalyst applied in a photochemical reaction is the following one:

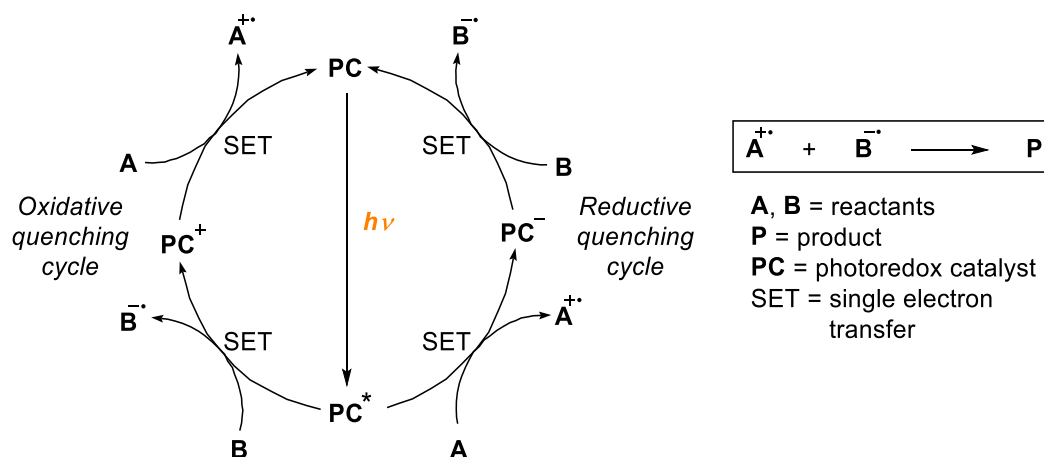
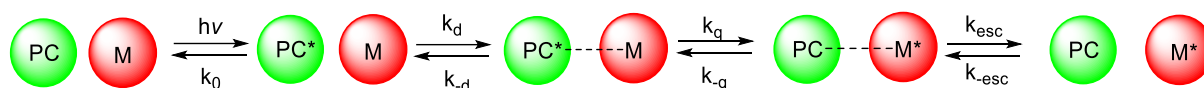


Figure 6. Depiction of a classical mechanism of a photoredox catalyst.

Figure 6 reports two distinct pathways: the preferred one is easily discernible by examining the electric potentials for each electron transfer. The key step in any photocatalytic cycle is the photocatalyst's (PC) absorption of light and the formation of its excited state (PC^*), from which a chemical reaction can occur. Each photocatalyst can take one of two paths, depending on which is thermodynamically preferred.

PC^* can be oxidized (or reduced) to another species and then reduced (or oxidized) to recover PC from the excited state. The polypyridyl complexes of Ru(II) and Ir(III) are the most common metal complexes. To determine which catalyst is best suited for a

reaction, examine the kinetics and thermodynamics of the system: the properties of these complexes are strictly dependent on the structure of the chromophores. Photoredox catalysts are based on an electron transfer process because the excited state increases the species' redox potential. These pathways require the PC to interact with a molecule M to form a "precursor complex," after which the reaction can occur in a variety of ways, one of which is the electron-transfer process. If the product has enough energy to escape from the solvent cage after the reaction, it can diffuse away from the catalyst. If not, the reaction may return to the starting material. The overall path is depicted in the diagram below:



Scheme 2. Depiction of the formation of different species involved in the mechanism.

The photocatalyst must have certain properties, including the ability to adsorb at a specific wavelength with a high quantum yield. Furthermore, the excited state must have a long enough lifetime to form a complex with the molecule M. Analysing the absorption spectra of the compound is useful for understanding the optical and electrochemical properties of the photocatalyst: LC transitions are typically energetic and occur at low wavelengths: these transitions are $\pi L \rightarrow \pi L^*$ transitions. The MLCT is the most common transition at higher wavelengths. The redistribution of electron density within the molecule increases the excited state's reactivity. Charge transfer is typically intense, and it is visible in all absorption spectra. The MC transition causes less intense transitions: this interaction causes photodissociation due to electron promotion in bonding-orbitals on antibonding-orbitals of the metal. The photoredox catalyst's electrochemical properties are critical for recovering it in its ground state after the catalytic cycle. In this case, the energy required to oxidize the metal and reduce the ligand must be calculated using the following equation:

$$E(MLCT) = \left| E_{M^{oxidized}/M} \right| + \left| E_{ligand/reduced\ ligand} \right| \quad \text{Equation 14}$$

Consider that stronger reductant photocatalysts are obtained with ligands that are difficult to reduce and easily oxidized metals, and vice versa. When excited, the PC can also function as an energy donor or electron acceptor/donor. Electron transfer is a useful method of transferring energy because it is followed by bond breaking and/or

formation: the electron transfer mechanism is like the Dexter quenching mechanism described in the previous paragraph, but there are significant differences.

In electron transfer, only one electron is involved, whereas two electrons are involved in the Dexter mechanism. Stern-Volmer quenching studies enable us to investigate the mechanism of a photochemical transformation, as well as the nature of the excited state. Several processes, such as dynamic (or collisional) or static quenching, can have an impact on Stern-Volmer studies. The following differential equation, where Q is the quencher, can be used to study the kinetics of the excited state:

$$-\frac{d[ES]}{dt} = k_0[ES] + k_q[ES][Q] = (k_0 + k_q[Q])[ES] \quad \text{Equation 15}$$

$$= k_{obs}[ES]$$

When the term $k_q[Q]$ is large enough in comparison to k_0 , quenching occurs, and the lifetime of the excited state is reduced: this is only possible if the lifetime is on the nanosecond scale or longer due to mechanical limits. Because of the pseudo first order conditions assuming $[Q]$ constant during the experiment, k_q can be measured when the concentration of quencher is at least ten times that of the photocatalyst. The rate of emission in the presence of several quenchers can be measured using time-resolved emission spectrometry based on Equation 15. The same procedure can be used with steady-state emission spectroscopy instead of rate constants. In the plot (Figure 7), static quenching can be seen (when the chromophore and the quencher are associated in the ground state, there is no influence on the lifetime of the excited state: $k_{obs}=k_0$). With time-resolved emission data, the Stern-Volmer plot is a flat line; with steady-state emission data, it is a slope. If there is dynamic quenching (as previously discussed), the plot is a straight line: the unique feature is that the same data can be obtained using both methods of measurement. If both static and dynamic quenching are present, the plot for the time resolved analysis is a straight line, whereas the plot for steady state emission is a curve due to the presence of both contributions: the overall equation can be resumed as follows:

$$\frac{\Phi_0}{\Phi_q} = (1 + K_D[Q])(1 + K_S[Q]) \quad \text{Equation 16}$$

Where $K_i = \frac{k_q}{k_0}$ and D indicate the case of dynamic quenching, meanwhile S indicate the case of static quenching. Examples are shown in the following figures:

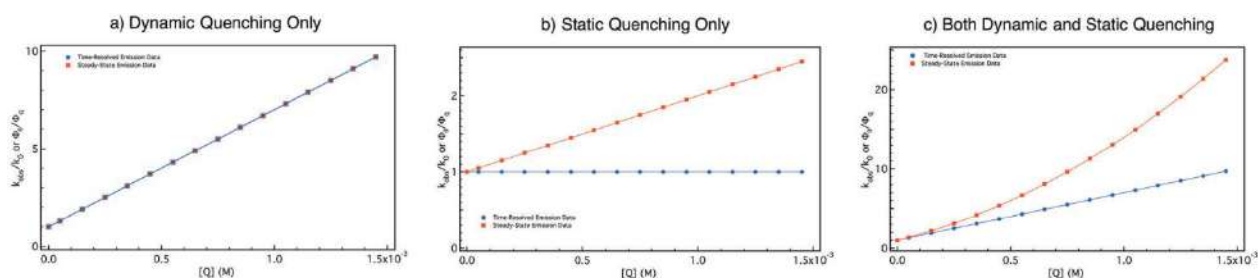
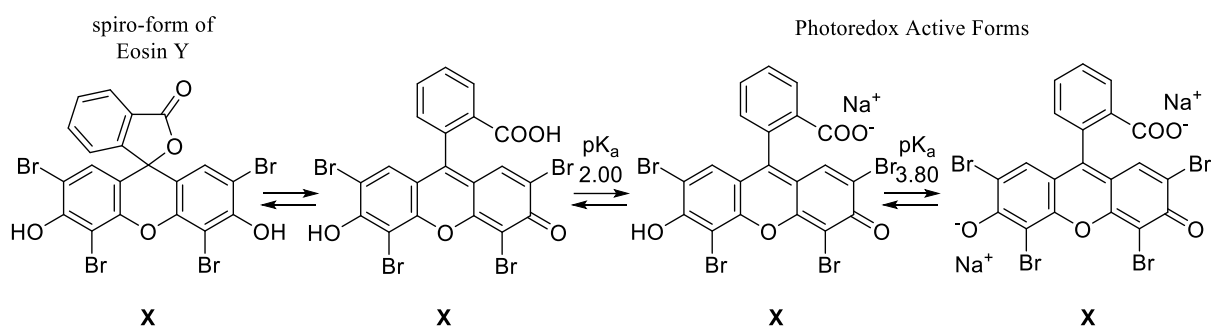


Figure 7. Depiction of Stern-Volmer plots in function of the catalyst. Adapted From “The photophysics of photoredox catalysis: a roadmap for catalyst design” Arias-Rotondo, D. M., and McCusker, J. K.^[4]

As previously stated, the most common metals for photoredox catalysis are iridium and ruthenium: the cost of these metals, as well as their relative scarcity in nature, limit the scalability of the reaction: recently, researchers have developed several new photoredox catalysts based on cheaper and/or more common metals such as Fe, Co, and Cu. The main disadvantage of these new photoredox catalysts is their relatively short lifetime in the excited state when compared to Ir and Ru-based catalysts. Another significant advancement in photoredox catalysis is the ability to use organic photoredox catalysts, the most common of which are Xanthene based ones such as Eosin Y. The photochemical properties of these two organic dyes can be similar to those of metal-based photoredox catalysts, but the reactivity is caused by an intersystem crossing of the excited species from the singlet to the triplet state. The main disadvantage of these organic photocatalysts is their low oxidation potential, which limits their application when compared to metal complexes.^[4,5] One major advantage of using organic catalysts is the ability to expand the characteristics of the catalysts, which leads to a broad functionalization of the photoredox catalysts and the possibility of opening up a previously unexplored chemistry.^[5]

Eosin Y is arguably one of the most studied organophotocatalyst and it exists in four different forms pH-dependent, but only two of these are photoredox active:



Scheme 3. Depiction of the different forms of Eosin Y, the photoredox active species are the anionic and dianionic ones.

A recent application of Eosin Y is the possibility of support it on a solid phase. The first approach is tested by Selvaraj is the usage of Eosin Y as the counter ion of an ion-exchange-resin that resulted useful to perform several transformations such as oxidation of sulfides to sulfoxide. Li and Wang developed the preparation of series of organic nanoparticles by a Sonogashira Cross-coupling with 1,3,5-Triethynylbenzene or 1,4-Diethynylbenzene or directly on inorganic nanoparticles.^[6]

1.1.2. Showcase of the Lambert-Beer law and consequences for solid supported catalysis

This short essay is supposed to serve as a showcase of the physical reality of the Lambert-Beer law in photoredox chemistry. Starting with the authors experience - the effect of the Lambert-Beer law in the daily basis chemistry were severely underestimated.

To begin we look at the Lambert-Beer law. What does it describe?

$$(1) A = \log_{10} \frac{I_0}{I_1} = \epsilon cl, (2) T = \frac{I_1}{I_0} = 10^{-\epsilon cl} \quad \text{Equation 17}$$

A: Absorption, I_0 : initial intensity of photons, I_1 : intensity after absorbing
 ϵ : molar extinction coefficient, c: concentration, l: pathlength of light

T: transmission

To be precise: when we shine light on something, we basically want to know how many photons I_1 will come out at the other side all while knowing the number of photons we emit in the first place I_0 . The physical reality is that there is an exponential decline of

photons that will come out at the other side. While the first equation (Lambert-Beer) (1) has the more practical meaning for chemists, the second equation (2) carries more relevant information for us. In the case of this work, getting significant irradiation (high transmission T) throughout the bulk of the solution is very important. Seeberger *et al* defined in their famous “A hitchhiker’s guide to flow chemistry II” a 1% Transmission cut off at which a photoredox catalytic reaction should still proceed smoothly.^[7] On the basis of this 1% transmission cut off some naïve physical calculations were performed taking into account the dimensions of particle sizes. Surprise unravelled quickly as to how incredibly strong the effect of exponential decline really is.

The author urges the reader to pay careful attention to the displayed graphs and pictures, especially scales and dimensions.

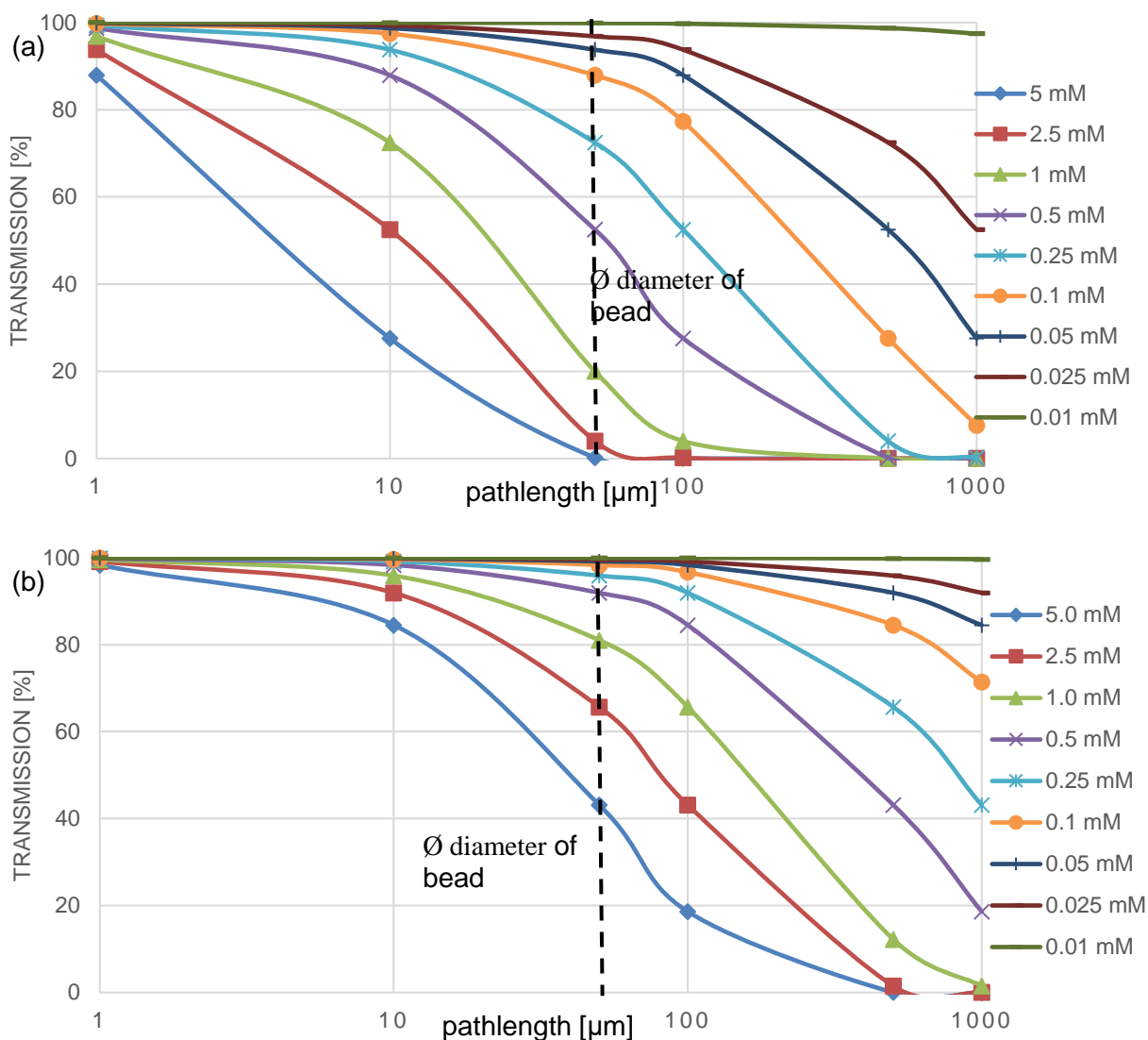


Figure 8: (a) expected transmission [%] through a solution of Eosin Y ($\epsilon = 112000 \text{ M/cm}$) at the indicated concentrations. (b) expected transmission [%] through a solution of Ru[bpy]₃Cl ($\epsilon = 14600 \text{ M/cm}$) at the indicated concentrations. In both the average size of polymer bead used for solid supported catalysts is displayed.

In Figure 8 transmission as function of the pathlength on a logarithmic scale were calculated and displayed. Take home message from these graphs is that you need low concentrations of photoredox catalyst to ensure irradiation of one (!) polymer bead used in solid supported catalysis. Usual concentration for the photoredox catalyst to expect a reasonable reaction rate is about 1-5 mM. To help with the grasping of the effects of these facts some pictures with accurate scales were made.

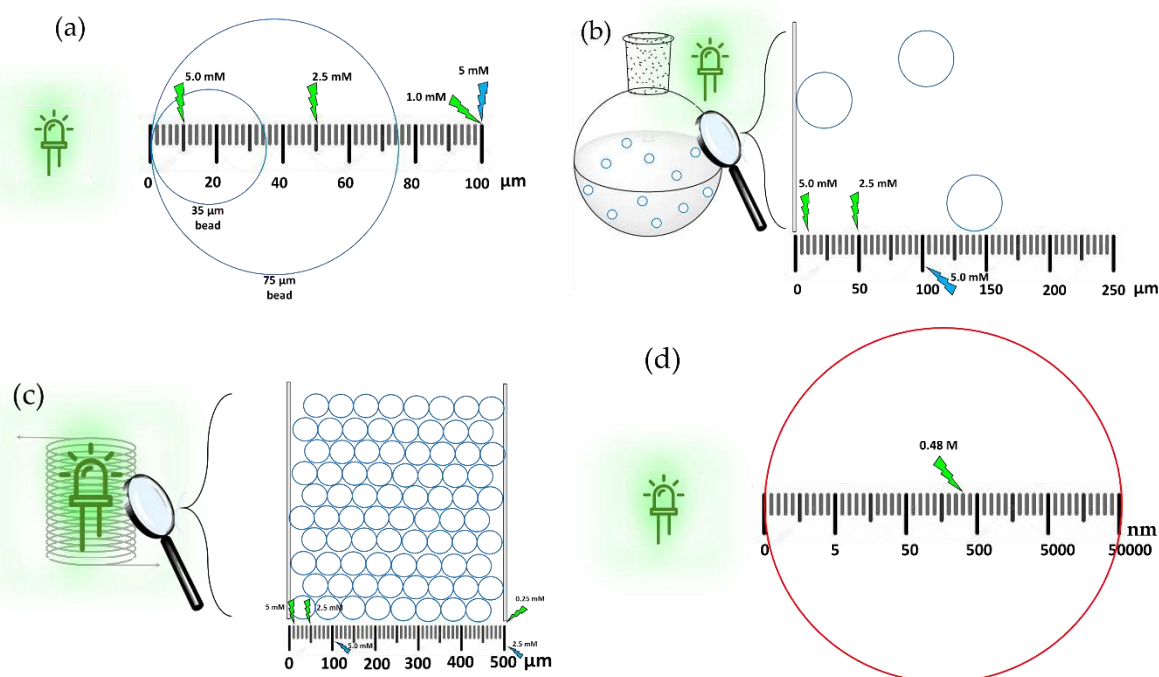


Figure 9: (a) Depiction of beads of Merrifield resin (non-swollen, blue circles) at the minimum and maximum size. The average size of one polymer bead is 50 μm . Green arrows illustrate the depth of penetration of photons at the 1% transmission cut off using Eosin Y (at the indicated concentration) and green light, while blue arrows show the same for Ruthenium complexes (at the indicated concentration) and blue light. (b) (c) Idealized depiction of batch and flow processes, in which the beads are either statistically distributed in the bulk of the reactor volume (batch) or are tightly stacked against each other (flow). (d) Depiction of Eosin Y supported on a bead of Merrifield resin with only a local concentration of Eosin Y of around 0.48 M.

Generally, on the presented scales Eosin Y, due to its high ϵ (112000 M/cm) even at very low concentrations, absorbs most of the light very efficiently. Having the biggest effect in the exponent of equation (2) ϵ is probably the most significant constant. A lower ϵ means higher employable concentration of photoredox catalyst which means higher reaction rates. In the case of the presented batch process (b) the polymer bead needs to be very close to the walls of the reaction vessel. Using a concentration of 5.0 mM at 10 μm deep in the solution a transmission of 1% is expected which might still be enough to lead to a reaction. Though, the reaction rate is, as experienced, abismal. The blue light in the case of metal complexes can penetrate the solution much deeper (100 μm at 5.0 mM).

In the case of flow reactions the dramatic increase of reaction rate is due to the approximately two orders of magnitude increase of interfacial area.^[7] Still it can be

perceived that the bulk of the flow reactor does not receive efficient irradiation. Only at lower concentrations of 0.25 M of Eosin Y all the internal volume of the flow reactor receives efficient irradiation, while in the case of metal complexes all the reactor volume is irradiated at higher concentrations.

Given everything that was learned so far, removing the photoredox catalyst from the liquid phase and immobilizing it onto a solid support (d) has one consequence: the Lambert-Beer law only applies locally to the individual beads, while the bulk of the solution should absorb almost no light.

A few lessons could be learned – out of which a few conclusions could be drawn:

- The exponent in the transmission law (2) coupled with high molar extinction coefficients – low molar concentration needs to be used.
- Bulk of solution is not irradiated efficiently, sometimes not even bulk of one bead receives irradiation. – careful balancing of photoredox catalyst type and concentration. Also remove the photoredox catalyst from the liquid phase by solid support.
- Extremely high local concentration of solid supported photoredox catalyst in one polymer bead means that after light passing through one bead, no more light is left. – decreasing high local concentration of photoredox catalyst.

To summarize this essay in two final thoughts:

the microscopic world absolutely does not scale to the macroscopic world. The quintessence of this essay is the fact that photoredox catalysis is a double-edged sword. On the one hand the photoredox catalyst is supposed to give its excited electrons to reactants and therefor needs to absorb light efficiently; on the other hand, if the catalyst absorbs light too efficiently, it slows down the overall reaction since the irradiation of the bulk volume becomes increasingly inefficient.

Removing the catalyst from the liquid phase is beneficial for irradiation purposes and the chiral imidazolidinone catalyst is supposed to be removed from the liquid phase in the first place. An interesting endeavour would be to synthesize a hybrid material (both catalysts solid supported on the same bead) with a concentration of the photoredox catalyst as low as necessary and the concentration of the chiral organocatalyst as high as possible.

If these two aspects are carefully balanced, one can expect the efficiency of irradiation to increase and by this the overall reaction rate to increase.

1.2. Continuous Flow Chemistry and Reactor Technology

Organic synthesis has traditionally relied on batch reactions. Substrates, solvents, and catalysts are placed in a flask and stirred at a specific temperature for a set amount of time before the crude mixture is analyzed and the product is isolated. Fine chemical production (i.e. drugs, food additives, agrochemicals, or flavors) has always relied on sequential batch processes comprised of multiple unit operations. Flow processes (Figure 10) represent a conceptually different approach to chemical synthesis in which reagents are continuously pumped into a reactor that can be heated, cooled, or irradiated (with microwaves or light) and can contain immobilized reagents, catalysts, or scavengers to eliminate side-products or trace metals.

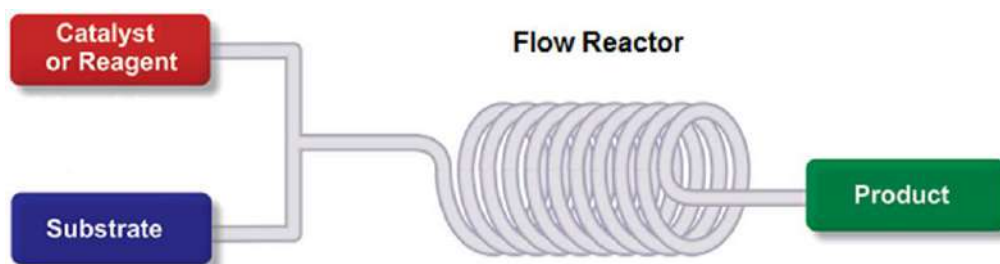


Figure 10. General representation of a continuous flow reaction.

Continuous flow reactors are typically made up of coiled tubing or chip-based devices with a large surface area-to-volume ratio. This has several advantages over traditional batch reactors, most notably improved heat and mass transfers. Because all reaction parameters can be precisely monitored, the process becomes more reliable and reproducible. As a result, reaction time is reduced, efficiency is increased, and substrate mixing is significantly improved. Furthermore, the formation of undesirable byproducts due to hotspots is significantly reduced. The closed environment in which a continuous flow reaction occurs provides additional benefits, primarily in terms of safety: hazardous and highly toxic chemicals or reaction intermediates can be generated in-situ and converted into more elaborated molecules by combining different reagent streams. This reduces the operator's risks because no dangerous species must be handled or isolated. Furthermore, because of the flow reactor's relatively short residence time and sequential operations, reactions involving the formation of unstable

intermediates that cannot be stored or isolated in batch mode become feasible. Flow processes are amenable to automation and allow for the execution of multistep reactions without the isolation of intermediates, as well as real-time analysis for optimal reaction conditions and waste minimization..^[8] The specific reactor chosen is critical, and it is determined by the characteristics of the synthetic process being performed. The physical state of the reagents used (liquids, solids, gases), the reaction thermodynamics (exo- or endo-thermic), reaction kinetics, mixing, heat and mass transfer, and residence time are the most important aspects. There are numerous commercially available systems for performing continuous flow reactions on the market, each offering a solution to a different problem. Laboratory reactor tubes are usually coiled and made of stainless steel hastelloy, copper, polyether ether ketone (PEEK), or perfluorinated polymers. The material chosen is determined by the reaction conditions as well as the chemical stability. Depending on the system's specific requirements, the volumes range from 1 μL to liters, with channel diameters ranging from 100 μm to 16 mm. One of the most difficult challenges in synthetic chemistry is scaling up a given reaction. Several parameters must be considered when transferring production from the laboratory to the production scale in order to avoid unintended complications (e.g. runaway reactions, inefficient mixing or by-product formation). This process usually takes a long time, which raises the overall cost. Scaling up a continuous flow reaction from bench scale to production quantities necessitates little re-optimization and no changes to the synthetic pathway. One possible scaling strategy is to run the reaction in multiple parallel flow reactors (numbering-up approach). Alternatively, the size of the reactor can be increased (scale-up approach). Even though flow reactors have many advantages over batch procedures, some limitations must be overcome. The main issue is the precipitation of solid species, which can cause the reactor to clog. In synthetic chemistry, the precipitation of inorganic salts or insoluble materials during a reaction is a very common occurrence. It is easy to see how this would be a major issue in the case of a flow system. Although new technologies for handling solids in flow have recently been developed, technological advances are still required to avoid undesirable situations. The use of solid catalysts may also represent a flow restriction: due to the generally low turnover number of heterogeneous catalysts, the catalytic species within the reactor must be replaced on a regular basis. When working with multiphase systems, extremely precise

control of reaction parameters is required, as inefficient mixing into the reactor may occur. Recently, some technologies to address this problem have been developed (e.g. tube-in-tube reactor for gas-liquid biphasic systems)^[9] However, some enhancements are still required for large-scale application. The use of continuous flow processes in the pharmaceutical and fine chemical industries is still limited. Until recently, a continuous manufacturing approach was reserved for petrochemical and bulk chemical companies that produced large quantities of relatively simple compounds. The complexity and diversity of the products, as well as the associated complex process conditions, have always posed a challenge for the application of continuous manufacturing in the fine chemical sector. Typically, molecules manufactured by pharmaceutical and agrochemical companies require 6 to 10 synthetic steps (convergent or sequential) and may involve chemo-regio- and stereo-selective transformations requiring quenching, work-up, separation, and purification operations. These items are typically produced in small quantities and have a short shelf life. Batch procedures involving the use of multipurpose plants continue to dominate the production of fine chemicals for these reasons: a small number of temperature- and pressure-controlled vessels can be used for virtually all of the reactions, separations, and purification steps associated with a long and complex synthetic route. However, with the recent development of commercially available modular devices for performing continuous flow synthesis and the growing interest of the scientific community (at both the academic and industrial levels) in flow chemistry, continuous pharmaceutical manufacturing is rapidly expanding and becoming an enabling tool for medicinal chemists.

Key Advantages of Flow Chemistry

Flow chemistry is one of the most advanced technologies in the last twenty years, with the goal of facilitating or improving the ability to complete a reaction.

Microfluidic technology has been discovered to be one of the best ways to perform some chemical reactions; in fact, it is possible to precisely control all the reaction's key parameters. The primary advantages of flow chemistry are:

- better mixing;
- efficient heat and mass transfer;
- faster reaction;
- easy scale-up;
- safety with hazardous chemicals or reactions;
- potential cost savings;
- and a lower environmental impact.
- Less equipment is required to perform chemical reactions, and less space is required.

Furthermore, it is possible to see how Flow Chemistry could be one of the best ways to combine the 12 Green Chemistry principles with the 12 Green Engineering principles. ^[10]

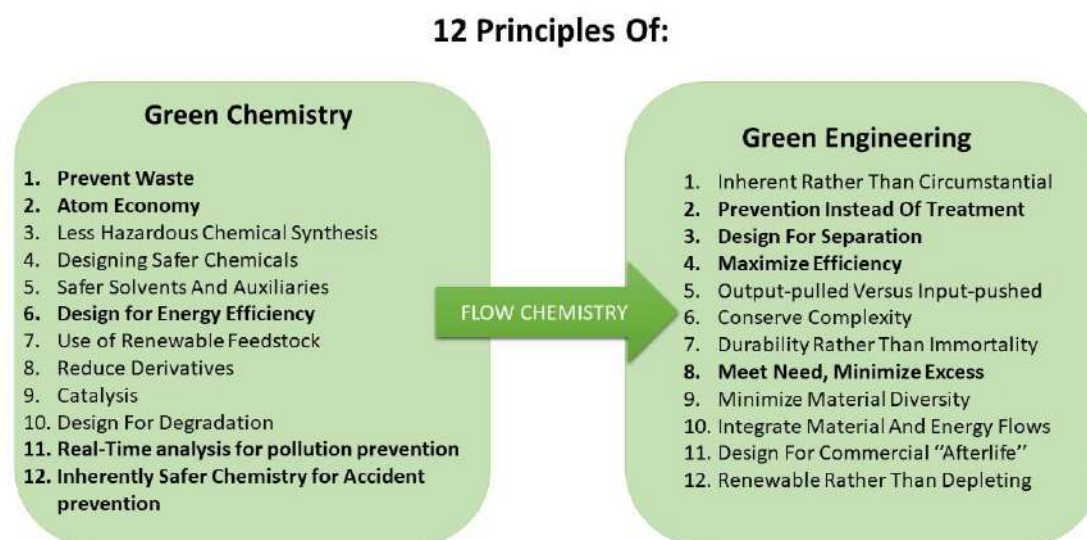


Figure 11. Depiction of the principles of Green chemistry and Engineering, in bold are highlighted the principles met by Flow Chemistry.

One of the principal benefits of flow chemistry is a faster reaction followed by a reduction of waste: batch chemistry is usually formed by 5 different steps (batch reaction, workup, evaporation of solvent, purification, and another solvent evaporation), this is a long sequence that could require several hours or maybe days -all of the steps can be done continuously.^[10] Moreover, it is estimated that for each kilogram of product are produced about 25 Kg of waste.^[11]

Mixing

Several different reactions are performed in batch chemistry in systems composed of different phases, for example, a reaction involving a liquid-liquid interphase or a reaction involving a heterogeneous catalyst. A reaction involving gas phases can also be performed in flow conditions: increasing the gas flow rate can change how the gas is present inside the tube. Using a slow flow rate, it is possible to obtain "bubble flow" (in this case, bubbles can be seen inside the reactors), increasing the rate leads to "slug flow" (a sequence of gas and liquid can be seen inside the tube), and finally "annular flow" (this case is observed when there is a strong flow of gas inside the tube and the liquid on the walls).^[10]

There are two different conditions for a liquid-liquid reactor: laminar flow, which occurs when two different flows parallel inside the tube, and slug flow, which is more common, especially when using a T-mixer, which occurs when you can observe an alternation of phases inside the tube. The main issue with Liquid-Liquid reactions is the mixing of two different phases; flow patterns are related to flow rate: lower flow rates result in equal mass transfer by all flow patterns, whereas high flow rates cause the reactor structure to change the mass transfer characteristics.^[10]

The characteristic of the flow can be analysed by the Reynolds number (Re): low values of Re correspond to laminar flow meanwhile high values lead to turbulent flow, it can be calculated by a simple equation.

$$Re = \frac{Q D_H}{\nu A} \quad \text{Equation 18}$$

Where Q is the flow rate, ν is the viscosity, A is the diameter of the tubing and D_H is the density; laminar flow is obtained for $Re < 2040$.

Both cases are usually present in a batch. In fact, closer to the stirring bar, a turbulent flow is observed, while further away, a laminar flow is observed: the movement of the molecules is generally based on diffusion, which depends on the size of the vessel. The diffusion inside the reactor is faster due to the smaller dimensions of the reactor's tubes. Unfortunately, high diffusion does not imply efficient mixing: to understand this fact, it is useful to examine the Damköhler number (Da), which can be easily calculated using the equation:

$$Da = \frac{\chi d_t^2}{4\tau D} \quad \text{Equation 19}$$

A value of $Da < 1$ indicates that the reaction is slower than mixing, whereas a value of $Da > 1$ indicates that the reaction is faster than mass transport. In this last case, there is the generation of a gradient within the system, which has an adverse effect on the ideality of the reactor and can affect the product's selectivity. Furthermore, flow chemistry has no effect on the kinetics or chemistry: it can be viewed as a useful tool for avoiding gradients that occur in batch conditions. The rate of the reaction and the mixing are critical parameters in determining whether a reaction should be developed in a flow process.

Temperature

Temperature is a critical parameter in a chemical reaction: in batch conditions, the cooling or heating of the reaction is especially important due to the non-homogeneity of temperature in the liquid phase, which leads to different side-products. In fact, the small size of the tubes improves heat transfer performance because it is directly proportional to surface area. However, the heat-conductivity of each material used to prepare the reactor must be assessed: PTFE (Polytetrafluoroethylene) has a low conductivity, whereas stainless steel or silicon have a high conductivity. Because of the system's high control, it is possible to avoid side reactions that are also close in G: in batch conditions, accurate control of the reaction condition is not possible as in flow chemistry. The ability to use lower-boiling solvents due to the pressure generated inside the tube is an intriguing application of heating in flow conditions; this technique is known as "superheating" and can be used in conjunction with microwave irradiation.

It is critical to include a Back-Pressure Regulator (BPR) in the system: this valve allows you to control the pressure inside the system. It is possible to avoid the eventual evaporation of solvents or reagents in batch-heated reactions by maintaining uniform concentration inside the reactor in this manner.

Photochemistry

The Lambert-Beer Law explains the main advantage of photochemistry in flow conditions: at constant chromophore concentration and molar attenuation coefficient of the molecule, a lower optical path allows for lower absorbance (so a higher transmittance). In a reactor tube, the entire reaction mixture is irradiated; however, in a batch reaction, the "back" of the reaction is not. If a UV light was used, it may be useful to consider that glass can absorb light at 360 nm, whereas using HPLC tubing in PFA (perfluoroalkoxy alkane) or HPFA (High purity PFA), light absorption by those materials is low. The scalability of the reaction is a major issue in batch photoredox chemistry: scaling up the reaction requires a longer reaction time due to the smaller surface irradiated by the light. Flow chemistry is found to be the best option for achieving consistent scale-up. In Figure 12, an example has been provided:

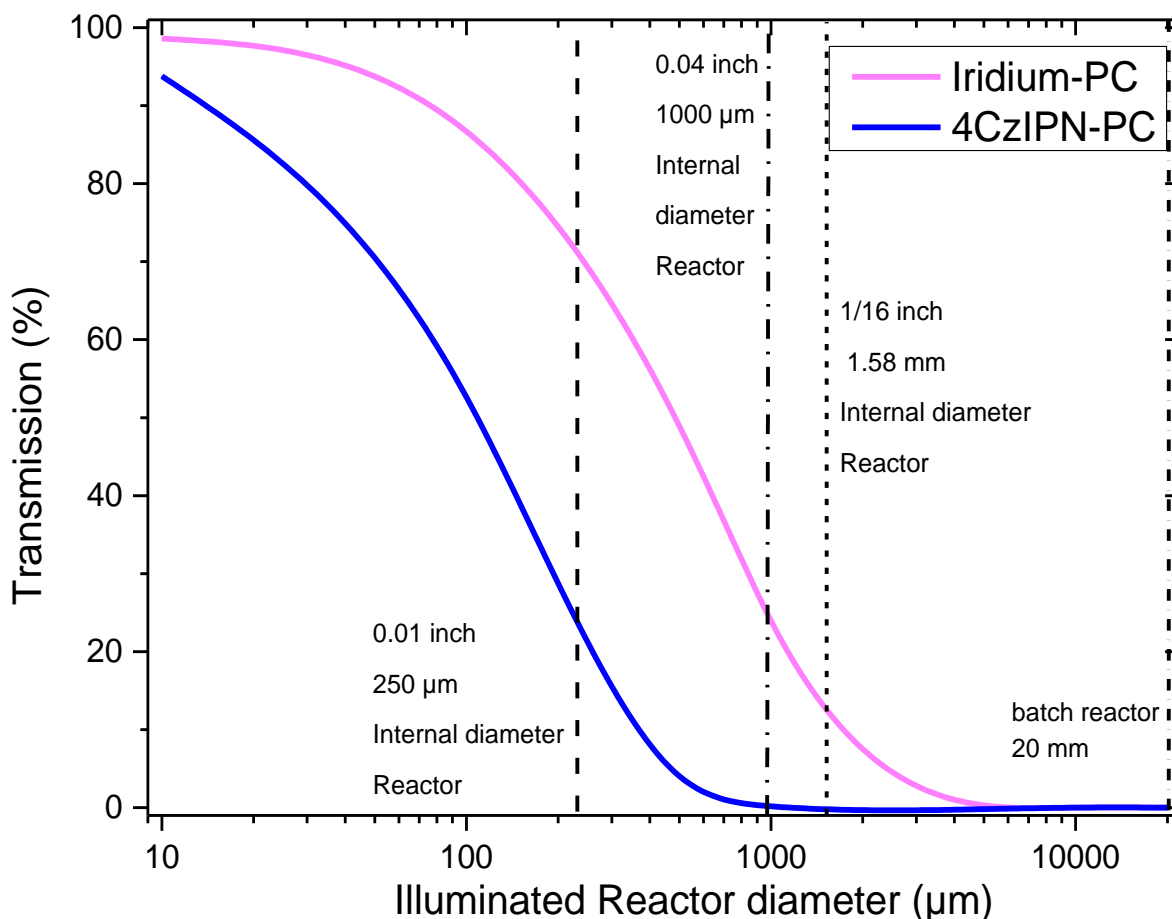


Figure 12. Depiction of the transmittance in function of the optical path/reactor diameter of two different photocatalysts

As shown in Figure 12, the curve has an exponential trend due to the Bouguer-Lambert-Beer law in function of transmittance: in batch condition only a part of the solution is irradiated by light while in flow more of the reactor volume in proportion to batch is irradiated by light. This can be observed by the equation:

$$A = \log_{10} \frac{1}{T} = \log_{10} \frac{I_0}{I} = \epsilon cl \quad \text{Equation 20}$$

Another significant advantage of flow photochemistry is the ability to scale up using two distinct strategies. The first involves extended operation times and increased throughput by increasing the flow rate. This is the most used approach on the laboratory scale due to the ease of optimization required: the key parameter remains the residence time, which must be constant; in fact, by increasing the reactor volume can increase the flow rate and thus productivity. The second strategy for scaling up photochemistry is to run several different reactions in parallel: this is preferred on an

industrial scale. Light is widely regarded as an important traceless and green reagent for photochemical transformations, but this is not entirely correct: laboratory light is artificial and typically derived from non-renewable sources. Due to the presence of the entire spectrum emitted by the sun, the goal is to use sunlight as a reagent for our chemical reaction: nowadays, it is possible to combine the advantage of flow chemistry with the sunlight and perform chemical transformation using only it. Some parabolic concentrators can be used to focus sunlight on a flat-bed reactor containing the solution to increase the intensity of the light. The sunlight selectivity can be obtained by using specific materials to construct the flow reactor: this allows only a subset of the total sunlight emission spectrum to be used.^[12]

Approach to Developing a Flow Chemistry System

Developing a novel or well-known reaction in flow chemistry is more difficult than in batch chemistry: in classical chemistry, it is sufficient to dissolve or suspend the reagents in the solvent and stir it at a defined temperature until the limiting reagent is consumed. A flow system is significantly more complex, which is why batch chemistry was the predominant method used in the previous century. Around the turn of the millennium, interest in flow chemistry skyrocketed due to all of the previously mentioned benefits and the ability to perform otherwise forbidden/impossible transformations. One of the main advantages (and disadvantages) of flow chemistry is that it is a modular technique that allows you to vastly customize your system: the wide range of different modules gives us a lot of options. The system can be divided into six distinct zones, as shown in the diagram below:

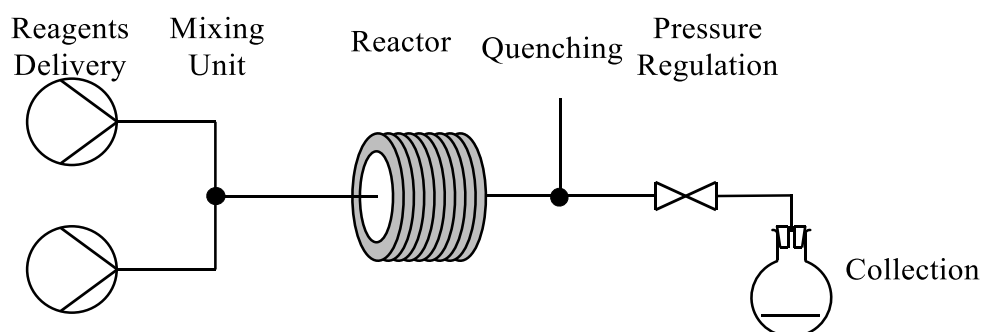


Figure 13. Depiction of a classical setup to perform flow chemistry

In addition, two more units could be added: one for product purification and another for data analysis. The reagents are delivered to a mixing unit, and the reaction mixture can then react in the reactor before being quenched by a quenching unit, which is useful for controlling the residence time. The pressure regulator is the last component of the reactor; it is essential if high pressure is required inside the reactor; the final step is the collection of the reaction mixture. To connect all the system's modules, the same components used for HPLC tubing are used, specifically a series of ferrules and nuts. Polymer-based equipment can usually be used without issue at low and medium pressures (30 bar), but stainless-steel equipment is preferable at higher pressures. The liquids are delivered to the reactor via a pump, which allows you to control the flow rate as well as the residence time and stoichiometry of the reaction. HPLC pumps can also be used when high pressures or flow rates are required. A problem for both could be reagent precipitation inside the system, which can cause clogging or fouling. There are two methods for mixing reagents: passive and active mixing. Active mixing necessitates the use of external energy, such as ultrasonication, whereas passive mixing is dependent on fluid properties (pumping speed, viscosity, etc.). The simplest way to mix a single-phase reaction is to use a T- or Y-shaped connector.^[10]

The core of the system is undoubtedly the location of the chemical reaction, and they are classified into three types: chip, coil, and packed bed reactors. The type of reactor used is determined by the type of reaction under investigation. One advantage of flow chemistry is the ability to analyze the condition inside the reactor in real time: several instruments, such as GC, HPLC, and NMR, are designed to directly analyze the crude. The three main methods of flow purification are liquid/liquid separation, chromatography, and crystallization. The most common purification technique is liquid-liquid separation, which consists of a hydrophobic membrane permeable only to organic solvents. The unmixable solvents flow through the hydrophobic membrane, separating the two phases. It is possible to selectively extract the product by studying its solubility in different conditions, such as changing the pH of the water phase. The chromatography consists of a series of scavengers capable of trapping impurities or a type of column chromatography if a series of impurities is blocked on the silica.^[10]

Continuous crystallization is a novel technique for crystallizing a product. The idea is to create a supersaturated solution inside the flow reactor due to the high pressure and temperature, and then collect the crystallized solution in the flask.^[13]

Final Consideration on Flow Experiments

A flow system capable of performing all chemical reactions does not exist; however, due to the adaptability of the technology, the flow system can be easily adapted to the reaction under investigation. A well-adapted flow system can ensure highly reproducible results, scalable protocols, and the ability to expand synthetic chemistry into new areas. The concentration of the solution is one of the main differences between flow chemistry and batch chemistry: in batch, the concentration of the reagent decreases over time, whereas in continuous, the concentration is constant at the start of the reactor and decreases along the flow reactor. The time spent inside the reactor is known as residence time (t_R), and it is easily calculated using the equation (V is volume and Q is flow rate):

$$t_R = \frac{V}{Q} \quad \text{Equation 21}$$

1.2.1. Plug-Flow Reactors

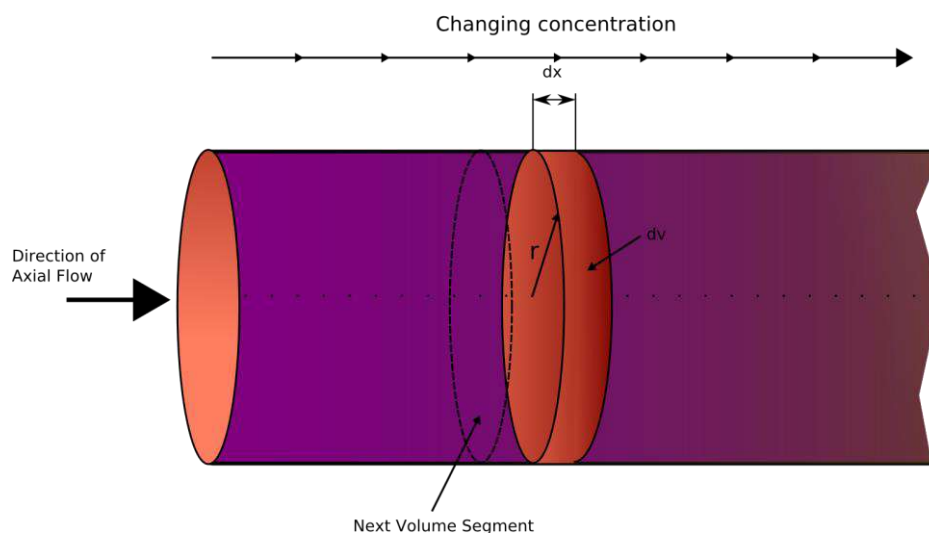


Figure 14. Typical illustration of a reactor following the plug-flow model. Along the reactor length the concentration of the product will increase all while at any given point the concentration of product is static. Adapted from “Difference between batch, mixed flow & plug-flow reactor” Usman Shah.^[14]

The first type of reactor is the Chip-Based Reactor, which is best suited for reactions that require good heat transfer. They are typically made of silicon, glass, ceramics, or stainless steel. [10] Several different reactors have recently been developed using 3D printing. 3D-printable resins that are particularly light-transparent can be used, with specific functional groups capable of immobilizing the catalyst.[10] Unfortunately, because of their light absorbance, some immobilized catalysts are incompatible with photochemistry. [2]

Coil-Based Reactors are less expensive than Chip-Based Reactors and, as a result, are one of the most commonly used reactors. Coils of PTFE, PFA, FEP (fluorinated ethylene propylene), and stainless steel of various diameters can be used. Because the reactor could be damaged, it is critical to consider the reactor materials' compatibility with the chemicals involved in the reaction.

1.2.2. Continuous Stirred Tank Reactors

Another way of mixing reagent is the use of the Continuous Stirred Tank Reactor (CSTR) To be precise, this unit is a tank with a stirring device and entry and exit tubes for continuous material/product delivery into or out of the reactor. As in batch conditions, heterogeneous phases can be mixed in this unit. This unit can be heated or cooled to be used in a variety of conditions. CSTRs work well with non-mixable solvents, for example, in reactions involving Phase Transfer Catalysts (PTC). The following image depicts the various types of mixers:



Figure 15. Photograph of a disassembled CSTR (fReactor) unit.

A CSTR cascade will eventually produce the same result as a plug flow reactor. In practice, 5 units of CSTRs will exhibit the same behavior. The subject of CSTRs is vast in and of itself.[15]

1.2.3. Packed Bed Reactors

The Packed-Bed Reactor is the final type of reactor: these units are distinguished by the presence of a solid inside. Typically, an HPLC column is filled with the heterogeneous reagent and a filter, commonly a frit-septum, is placed on both ends of the tube to prevent material loss. The size of the particles is critical: large particles have a low surface-to-volume ratio, and the conversion may be inefficient, whereas small particles can cause back-pressure problems. The main advantage of this reaction is that it reduces residence time due to the equivalents of catalyst present inside the reactor and does not require any recovery procedure: in batch chemistry, at least, filtration is required to recover the heterogeneous phase. A potential issue could be the possibility of some catalyst leaking, particularly for Transition Metals-based catalysts that may be partially soluble in the reaction conditions. Another issue could be the presence of a "chromatographic effect" inside the column because of the reagent's different affinity for the catalytic material.

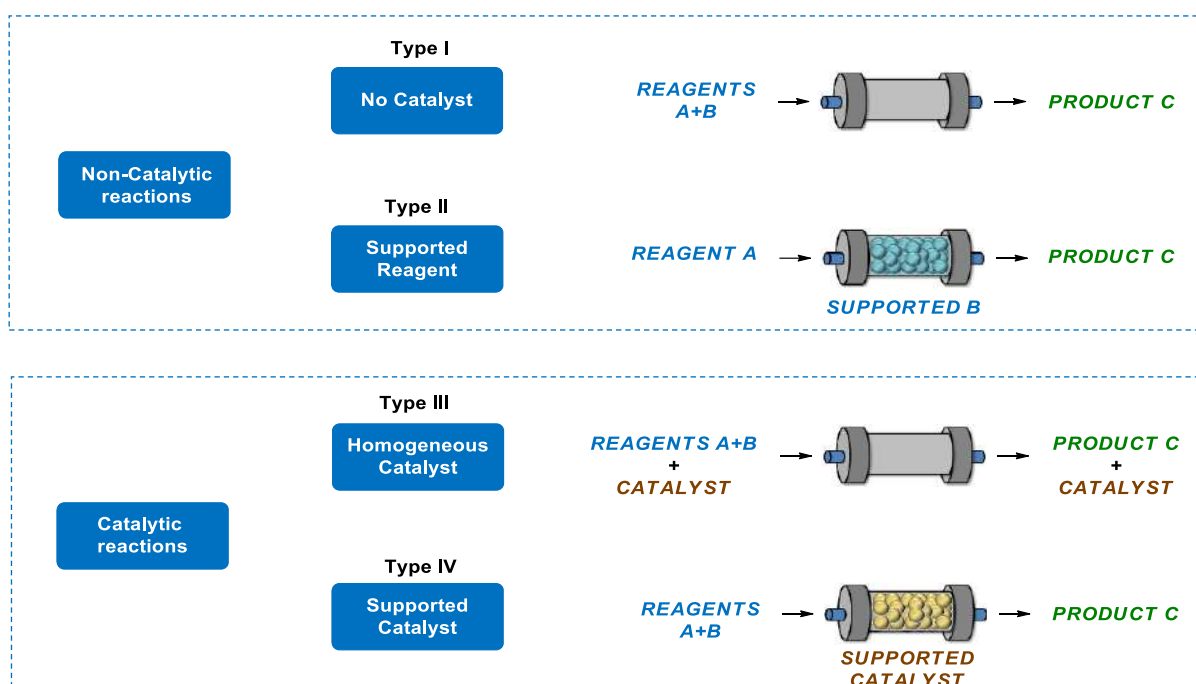


Figure 16. Different types of continuous flow reactions.

As depicted in Figure 16, continuous flow systems are broadly classified into four types. In type I, the reagents (A and B) are directed to the reactor, and the product (C) is

collected at the end of the process. In type II, one of the reagents (B) is supported on a non-soluble material and confined within the reactor; the substrate (A) is then passed through the reactor, and the exiting reaction mixture contains only the desired product (C) (if the reaction goes to completion). Types I and II do not employ any catalytic species during the reaction. A homogeneous catalyst is used in type III: the catalyst flows through the reactor with the reagents and is collected along with the product (C) (a purification step to isolate C is required). Type IV reactors confine the catalyst within the reactor while the reagents pass through; of course, an immobilization step of the catalyst onto a solid support is required, but no separation step to isolate the product from the catalyst is required; type IV reactors enable catalyst recycling. Because catalytic methodologies are now required for the development of sustainable and efficient processes, the latter type (IV) is widely regarded as the most convenient system for performing a reaction in flow.^[16]

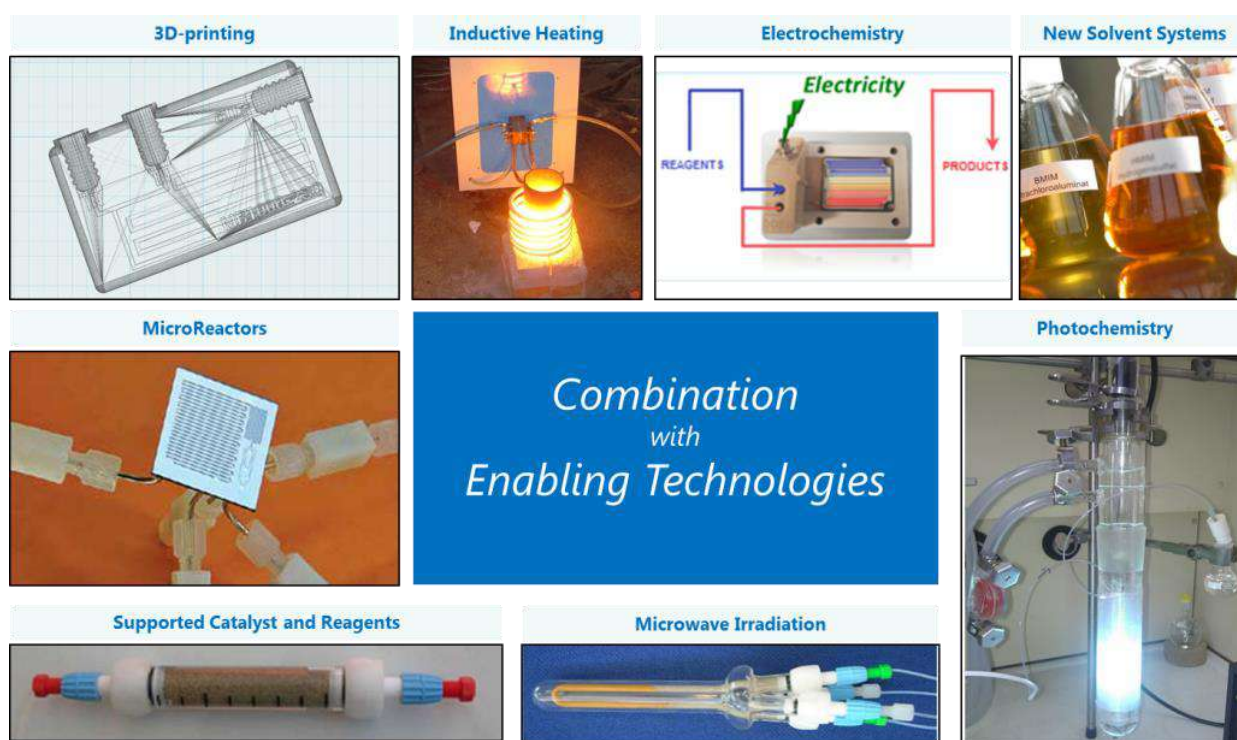


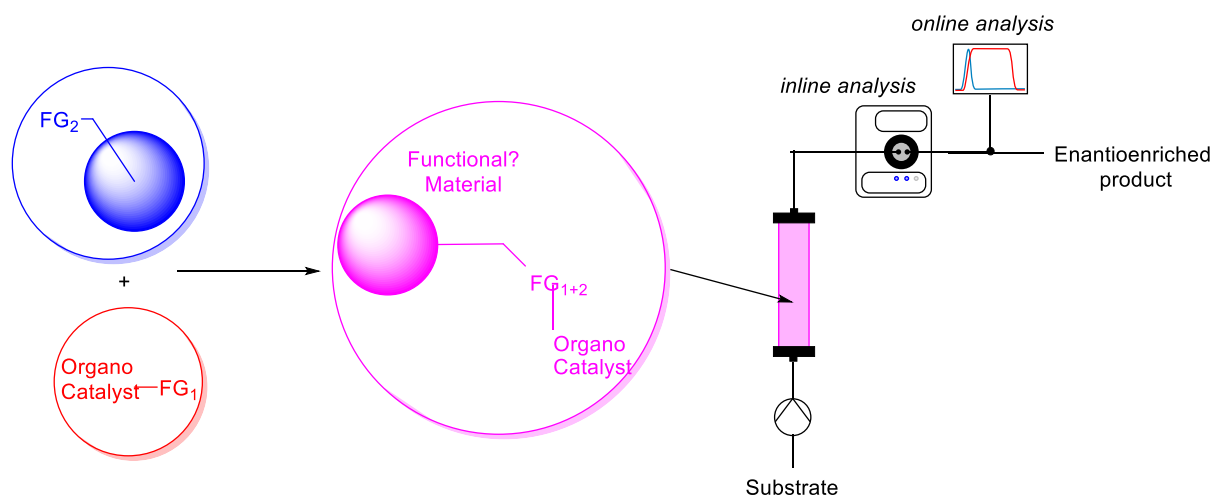
Figure 17. Enabling technologies generally combined to flow processes.

Flow methodologies can be easily combined to many enabling technologies in order to increase process efficiency.^[17,18] Supported reagents or catalysts, microreactor technology, 3D printing, photochemistry, microwave irradiation, inductive heating,

electrochemistry, or new solvent systems are examples of representative enabling technologies combined to continuous processes (Figure 17). This combination enables the creation of fully automated processes with higher throughput.

1.3. (Organo-)Catalyst Immobilization – Strategies and Application

To state that the field of organocatalyst immobilization can be summarized in a short paragraph in a thesis is a huge overstatement. The field is exhaustive. Books have been written, also one by our group.^[19] Generally, when designing a process around an immobilized catalyst a packed-bed reactor design is often preferred. Pericás and coworkers recently summarized the field of continuous flow processes using a packed-bed reactor constructed with solid supported organocatalysts to give some kind of molecule of interest to industry:^[20] Reported examples include e.g. proline-based, diarylprolinol derivatives, primary (di-)amino catalysts such as cinchona derivatives,^[21,22] squaramides, thioureas^[23], phosphoric acids, other phase transfer catalysts, isothiureas, lewis bases,^[24] imidazolidinones.^{[25][26][27]} The citation marks indicate some works published in our group on the topic of solid supported catalysts used in flow applications. As the focus of this work lays heavily on chiral imidazolidinone catalysts (MacMillan type catalysts) a review only detailing these catalysts used in an immobilized way was recently published.^[28]



Scheme 4. Generic scheme to explain how an immobilized catalyst is conceptualized from a material with a suitable functional group an organocatalyst with a complementary functional group and after reaction the new catalytic material is obtained. Construction of a chiral catalytic reactor and process.

The catalyst choice is simply ruled by the type of chemistry that the chemist/engineer wants to do. The immobilization strategy is often undertaken using e.g. copper catalyzed azide alkyne cycloadditions (CuAAC), Williamson-type ether synthesis, amide couplings. They all have in common a robust chemistry that will also lead to a robust bond that is hard to cleave. Bond formations to give esters are also often undertaken but the hydrolytic lability of esters is often detrimental to catalyst life. The material choices vary from soluble polymers to insoluble polymers - nano structured or heavily swelling, inorganic nanostructured materials such as titania/silica/alumina to name only the few most prominent. Recently magnetic nanoparticles also received attention because of their special ease of separation by applying a weak magnetic field.^[19]

2. Results and Discussion

2.1. Project: Solid Supported Imidazolidinone Catalysts in Photocatalysis

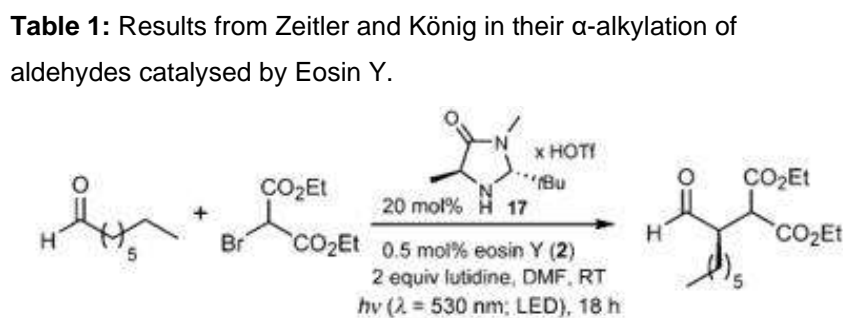
2.1.1. SS-Catalysts in MacMillan's aldehyde alkylation with electrophilic radicals

“One molecule away from magic” is the poetic description of catalysis as uttered by Benjamin List. Together with David MacMillan they were awarded the Nobel Prize for chemistry in 2021 for pioneering asymmetric organocatalysis. The advent of organocatalysis brought with it a sudden boom of generally more environmentally benign methodologies often exploiting the feedstock of chiral molecules from nature as catalysts. Not even 10 years after his initial discoveries MacMillan *et al* combined organocatalysis with photoredox-catalysis furnishing the immense energy of photons to generate electrophilic radicals that readily undergo α -addition to π -nucleophilic species such as enamines – a reactivity that is otherwise not realized in a straightforward manner.^[29] Usually a more complicated malonate-alkylation, decarboxylation protocol is required to give the same molecule but racemic by the nature of the chemistry. After his initial findings MacMillan *et al* published several other photoredox- organocatalytic protocols such as α -cyanoalkylation, α -benzylation, α -trifluoromethylation, *spin-center-shift* α -benzylation and α -amination.^[30–34] Paolo

Melchiorre later showed that a photoredox-catalyst is not strictly required to enable the same reactivity by either the direct photoexcitation of the enamine intermediate,^[35] by the formation of EDA-complexes,^[36] or by pioneering a new class of nucleophilic thiocarbamate catalysts that react first in a S_N2-pathway and then undergo homolytic bond cleavage to give rise to the same electrophilic radicals.^[37] Shortly after the advent of asymmetric organocatalysis, organocatalysts have been immobilized to different materials by employing a large variety of methods. The overall research area of immobilized organocatalysts was recently summarized in a book,^[19] while the more special case of immobilized chiral imidazolidinones in a recent review article.^[28] Our group has published several pieces on asymmetric Diels-Alder reactions catalysed by immobilized chiral imidazolidinone catalysts exploiting different materials such as magnetic nanoparticles or soluble polymers to name only a few examples.^[21,23,25,27,38–40] Also enantioselective metal-free imine reductions by similar catalysts are known to be efficiently catalysed.^[24,41] Lastly enantioselective alkylation of aldehydes with carbocations are reported to be efficiently catalysed in a homemade chiral flow reactor for extended periods of time and low catalyst loadings.^[26] With this last example the advantages of immobilized catalysts are clear: No need for separation from the reaction mixture, manufacturing a catalytic reactor with very high catalyst loadings inside the reactor but due to continuous operation overall miniscule catalyst loadings. The distinction between immobilisation and solid supported is drawn here as the two expressions are often used interchangeably: by solid supported a type of immobilisation is specified in which the material will always remain heterogeneous – as a solid. The term immobilisation includes all types of materials, also soluble polymers and surfactants which do not fall under the first definition. To the best of the authors knowledge examples of using solid supported (or even immobilized) catalysts exploiting the reactivity of photo-generated electrophilic radicals do not exist. This work shall represent a significant addition to the overall portfolio of efficient asymmetric reactions enabled by solid supported catalysts.

The literature on solid supported MacMillan-catalysts in combination with photocatalytic addition of electrophilic radicals was extensively surveyed.^[26,33,39,42–52]

In Figure 18 is depicted a general and simple infographic in which the state of the art is summarized, while the general reaction namely the generation of electrophilic radicals and their addition to enamines to eventually give α -alkylated aldehydes is depicted in Table 1.



Entry	Variation from the standard conditions ^[a]	Yield [%] ^[b]	ee [%] ^[c]
1	none	63	77
2	23 W fluorescent bulb instead of LED	78	80
3	23 W fluorescent bulb instead of LED and [Ru(bpy) ₃]Cl ₂ (8)	75	76
4	T = 0 °C	70	81
5	T = -5 °C	85	88
6	sunlight (T ≈ 30 °C) ^[d]	77	76

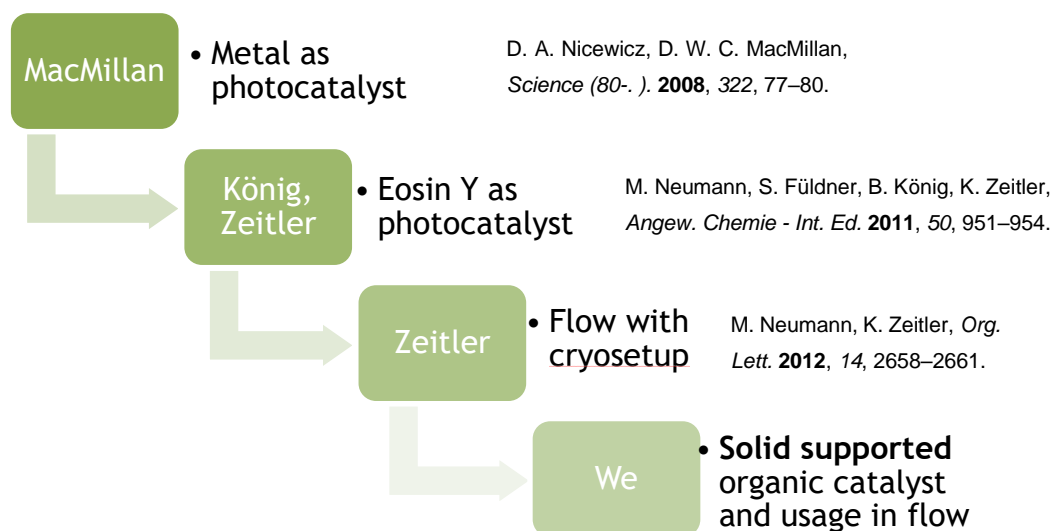
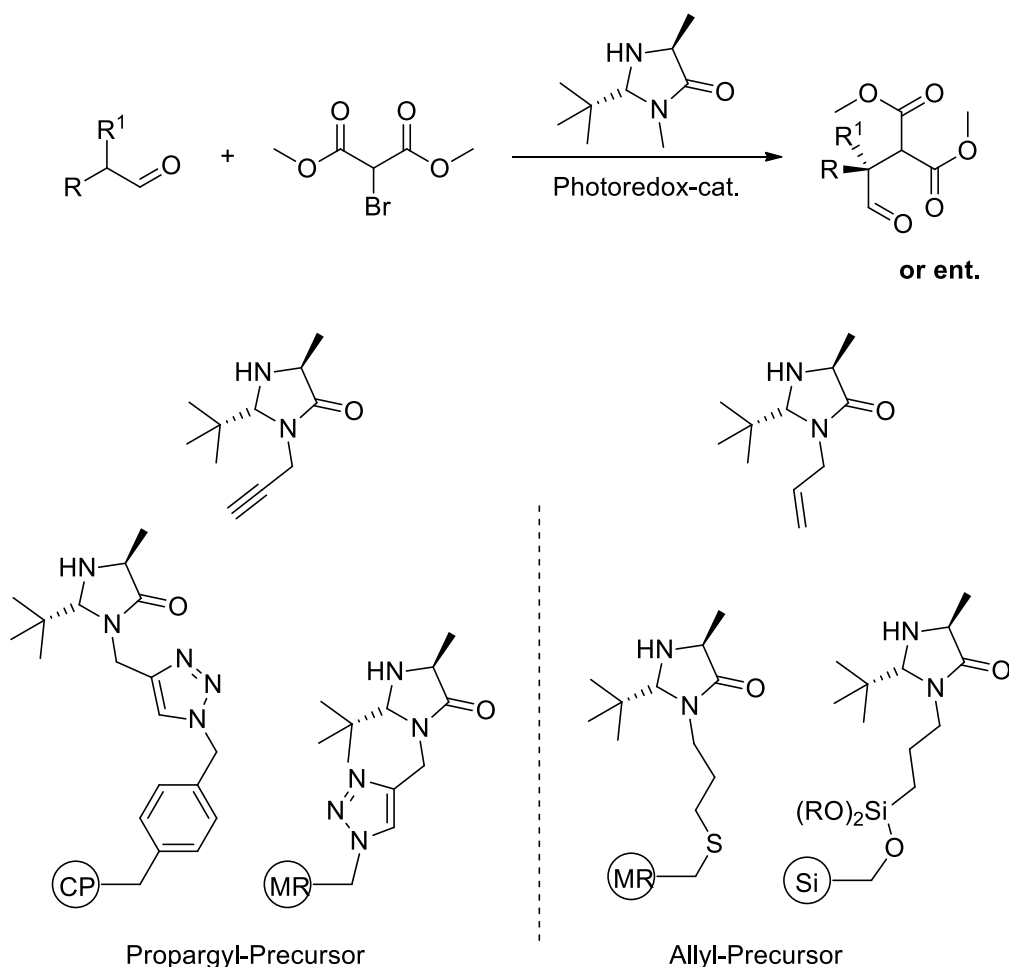


Figure 18: Infographic as summary of the state of the art.

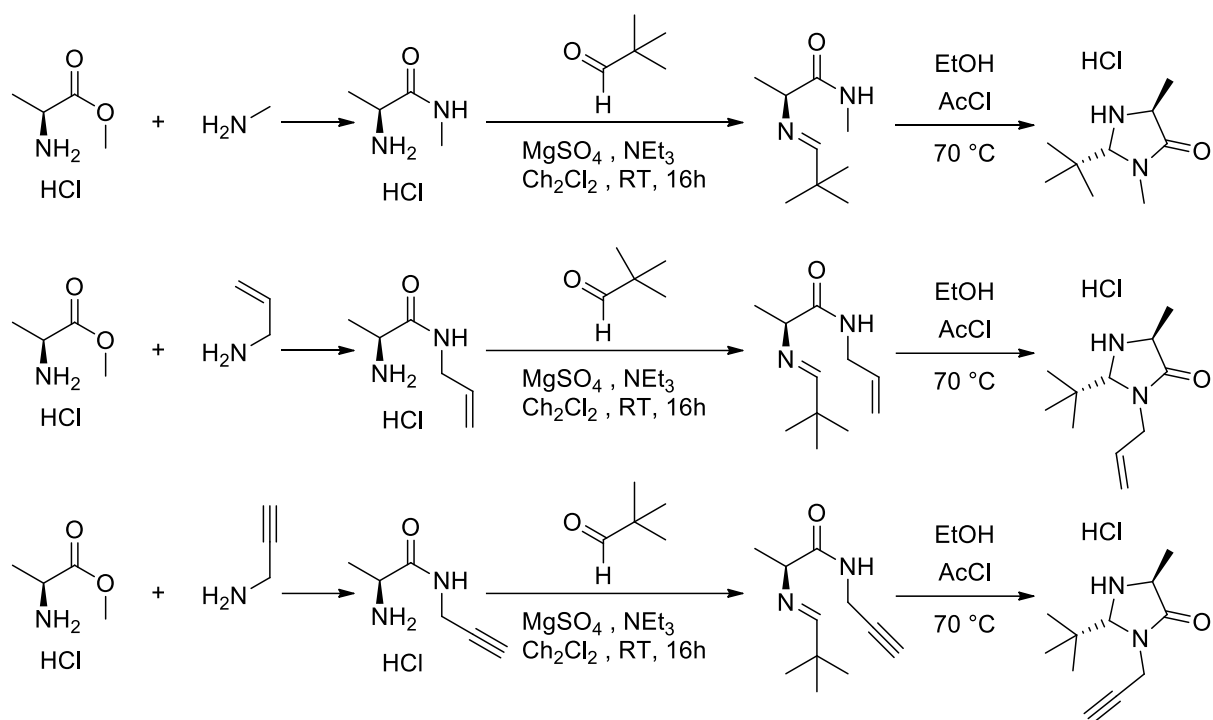


Scheme 5: Depiction of the reaction type, the MacMillan-catalysts in their precursor state for the solid support.

Second is depicted the go-to precursor for the solid-supported strategy. The propargyl-precursor was chosen due to its ability to perform click-reactions with either an azide-functionalized Merrifield-resin (MR) or with a styrene monomer for a copolymerisation-strategy (CP) to form a microporous Polymer.

The allyl-Precursor is used for hydrosilylation to graft it onto silica nanoparticles (Si) and for a radical thiol-allyl coupling to a thiol functionalized Merrifield-resin (MR)

To have a reference to the original MacMillan-Catalyst it was synthesized using the usual amide-imine-cyclisation strategy devised by MacMillan.^[53] The slow crystallization will usually result only in getting the major diastereomer. The same strategy was employed to get the allyl- and propargyl-precursor. All of these reactions were performed on a gram scale.



Scheme 6. Synthesis of the original MacMillan-Catalyst, and the allyl- and propargyl-precursors for the solid support.

Having the two Precursor in hand the two solid supported catalysts with the most convenient access were synthesized first. Therefore the benzylic chloride of the Merrifield-resin was nucleophilically substituted to form the azide functionalized MR and the thiol functionalized MR by employing either sodium azide or thiourea. In the case of the propargyl-precursor the final click reaction for the solid support was successful due to the expected weight difference of the resin beads before and after the reaction. In the case of the thiol-allyl coupling the reaction has most likely not worked, because the weight difference is miniscule.

Scheme 7: Depiction of the Synthesis of the two supported Merrifield-resin supported catalysts.

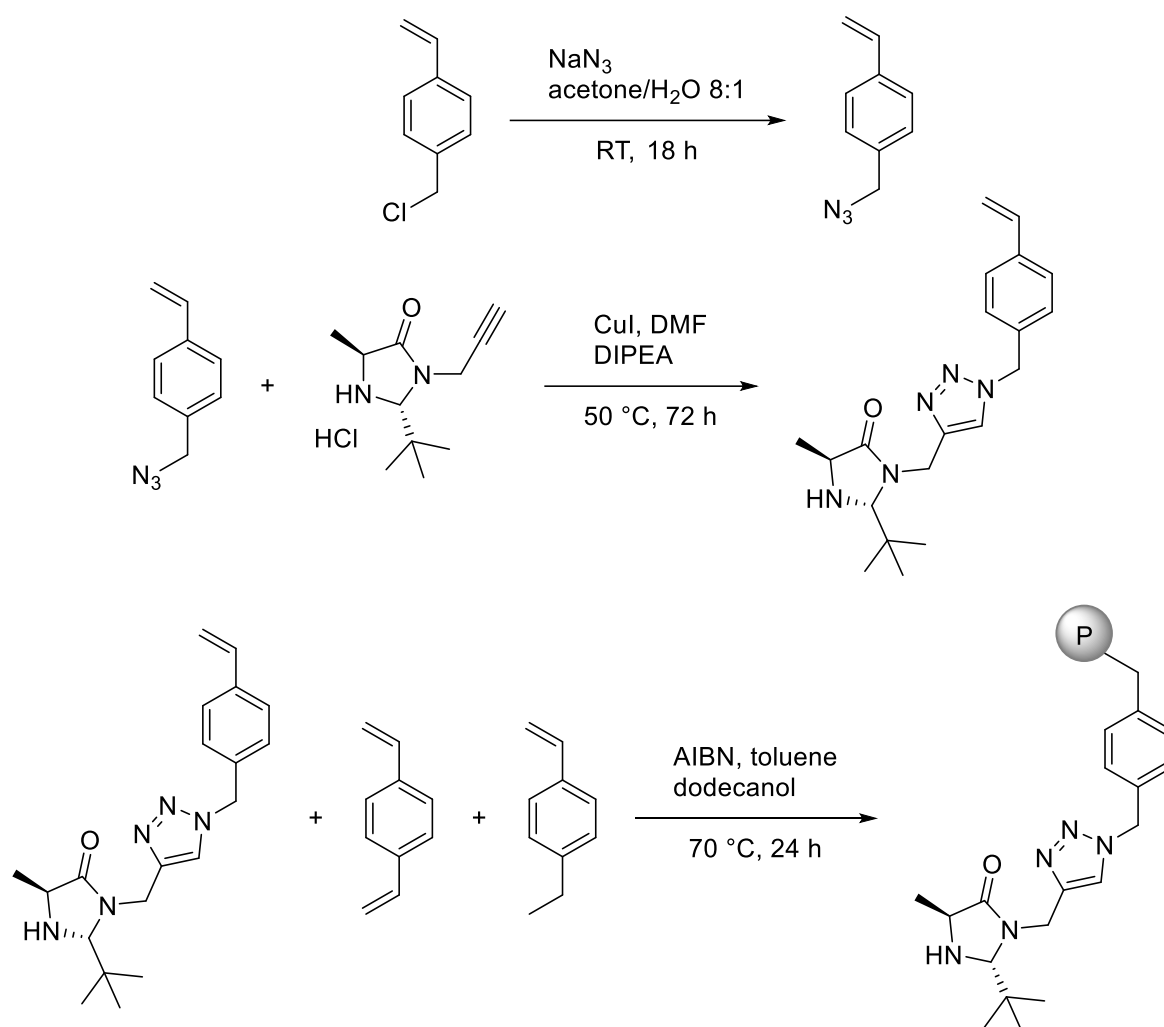
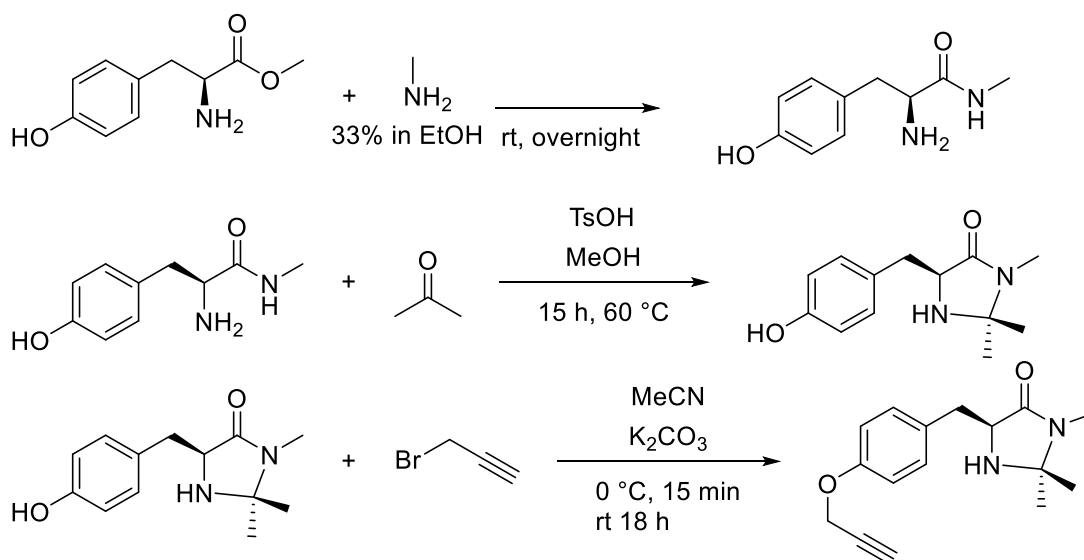


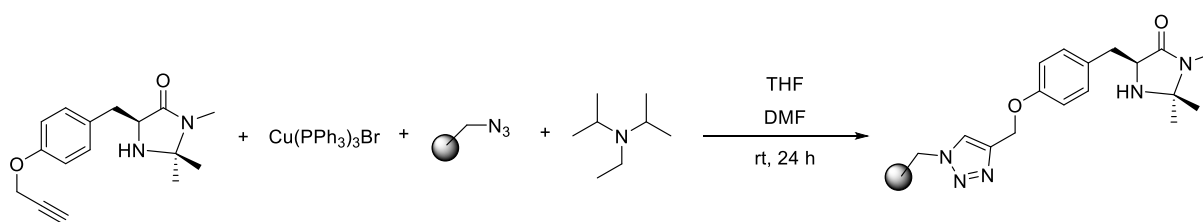


Figure 19. Photographs of the mesoporous copolymer just after the reaction is finished (left). Grinding of the polymer is required to get a fine material (right).

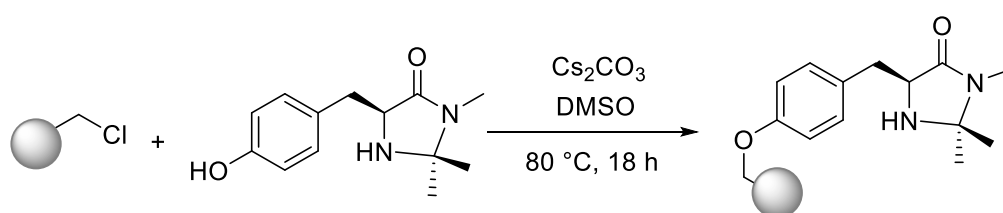
The outstanding results, or better failures of the solid supported second-generation MacMillan catalysts to provide any feasible data in the context of conversion or yield led to the hypothesis that maybe the polymeric backbones were not suitable with the photoredox conditions. To test this hypothesis an experiment was run in which normal store-bought polystyrene was added. The reaction proceeded smoothly in which led to the conclusion that the polymeric backbone does in fact not interfere with the reaction. Unpublished results from Marco Lombardo's (University of Bologna) group showed that a solid support strategy which uses the amide nitrogen is not feasible due to the loss of catalytic activity. To test this a new set of first generation solid supported MacMillan organocatalysts was synthesized due to their overall synthetic accessibility. The syntheses are depicted in Scheme 8-Scheme 11



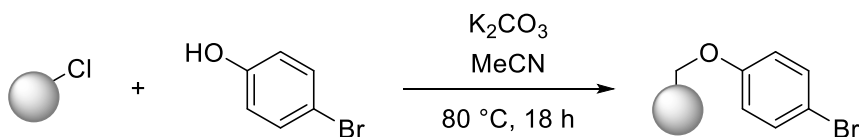
Scheme 8: Illustration of the tyrosine derived MacMillan-catalyst that were synthesized for later supporting on solid material.

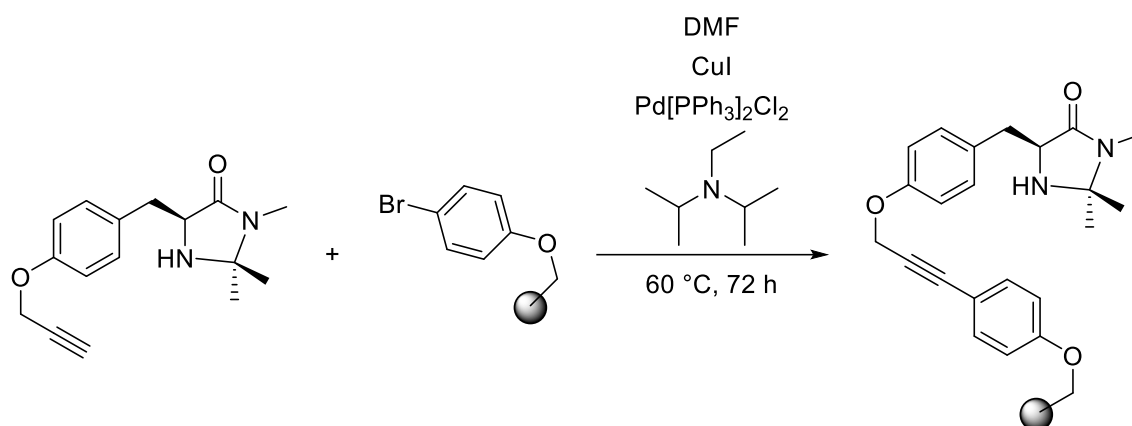


Scheme 9: Illustration of the synthesis of the click chemistry based solid support of the tyrosine MacMillan-catalyst.

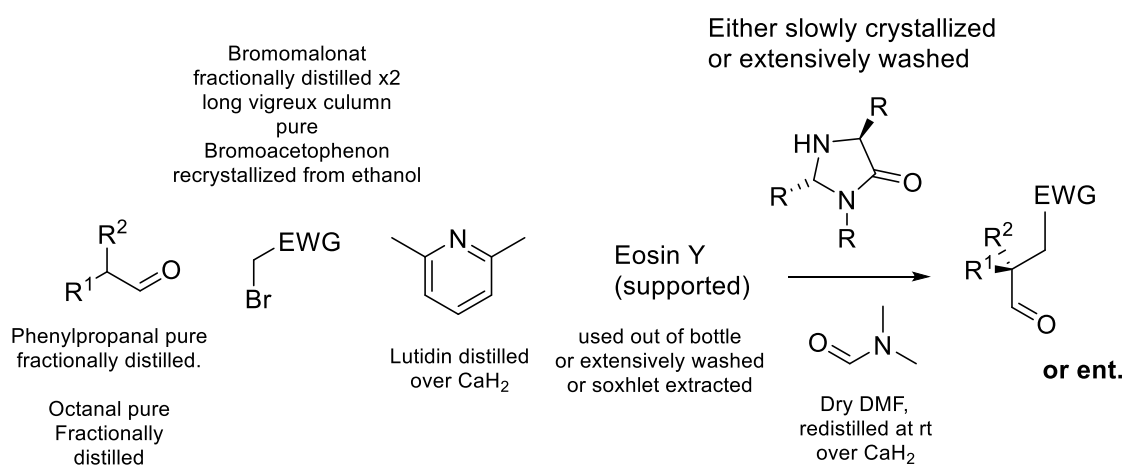


Scheme 10: Illustration of the synthesis of the Williamson phenolether synthesis based solid support of the tyrosine MacMillan-catalyst.





Scheme 11: Illustration of the synthesis of the sonogashira crosscoupling based tyrosin derived MacMillan catalyst.

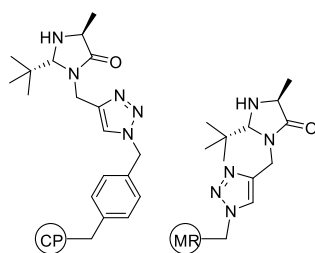


Scheme 12: Depiction of the general scheme for the electrophilic radical addition to enamines. Summary over the reagents used and their purification methods employed to ensure highest levels of purity. In the subsequent table further information for each entry will be given on what reagent exactly was used in the respective catalytic run.

In Scheme 12 is depicted in a general way the performed α -alkylation of aldehydes employing MacMillan's enamine SOMO-activation with his amino acid derived imidazolidinone catalysts. It is also depicted the endeavour that has been undertaken for each reagent to be in its purest form.

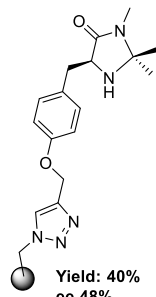
2nd Gen MacMillan Catalysts

Best unsupported results:
Yield: 61%, ee: 76%
(Lit Y: 63%, ee: 77%)

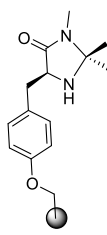


Do Not Work at all

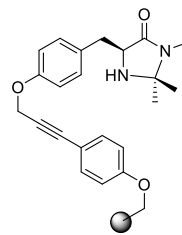
1st Gen MacMillan Catalysts



Yield: 40%
ee 48%

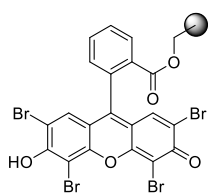


Yield: 33%
ee 59%

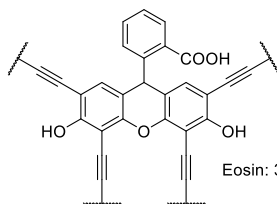


Works but slow
ee nd

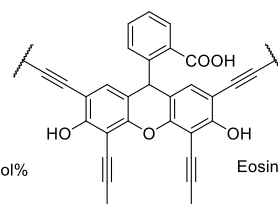
Solid "supported" Eosin Y



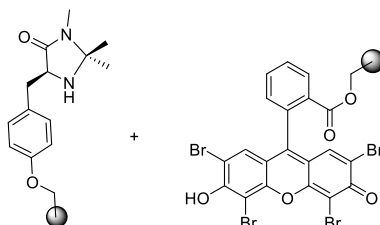
Yield: 50%
ee 69%
used together
with 2nd gen
MacMillan



Works but slow



Works but way too slow



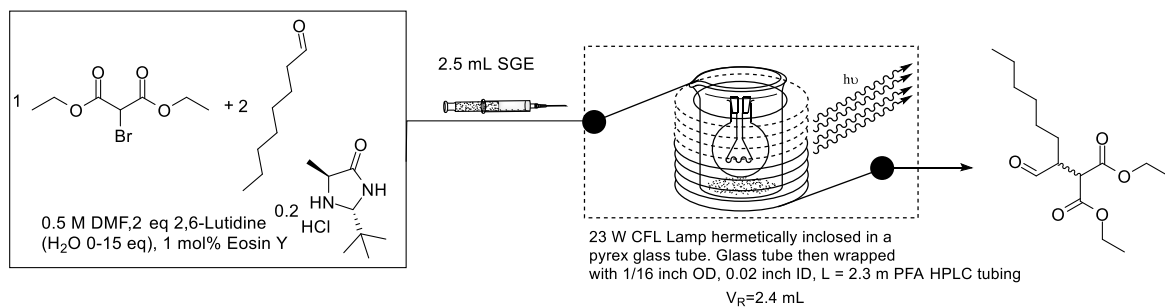
In the same batch, **Did not work**

Figure 20: Preliminary results of all the supported catalysts (organo- and photoredox catalysts).

Those first generation MacMillan catalysts are structurally derived from tyrosine. This time the solid support was performed via the amino acid side chain and not the nitrogen of the amide. The three depicted catalysts are supported via different linkers onto a commercially available Merrifield resin (200 mesh, High loading, Merck AG). As the chemical structure of the linker may play a significant role, three different solid support strategies were employed each leading to a different linker: Those are respectively (from left to right): Click chemistry derived, Williamson ether synthesis derived and Sonogashira coupling derived.

In this work is presented the first merging of solid supported organocatalysis with photoredox catalysis - to the best of our knowledge. In terms of stereoselection and chemical yield the supported catalysts perform subpar but still show a promising start of investigation. The nature of solid supported catalysts allows for the construction of catalytic reactors. In those the catalyst loading at any given time can be super-stoichiometrical but the continuous pumping of reagents in fact leads to a much lower catalyst loading. If the catalyst does not degrade fast it can be used for indefinite amounts of time thus rendering the catalyst extremely efficient. Having at hand solid supported MacMillan catalysts a few first tests, investigations of continuous flow photoredox chemistry were employed, for which the literature is scarce: Those continuous flow experiments showed a drastic increase of productivity, up to 100-fold. This is due to the high molar extinction coefficients of organic dyes and metal complexes which prevent most of the internal reactor volume to receive efficient irradiation under batch conditions, most of the light is absorbed in the first few millimetres of the solution. In continuous flow the increased surface-to-volume-ratio is exploited to achieve much higher levels of irradiation.

In fact when performing MacMillan's α -alkylation of aldehydes under continuous flow conditions with the second depicted first generation solid supported MacMillan catalyst a noticeable acceleration of the reaction was observed- full conversion (GC) after 40 min. The experiment is depicted in Figure 21.



Zoom in on one wrapping of HPLC tubing filled with polymer beads (packed bed reactor type)

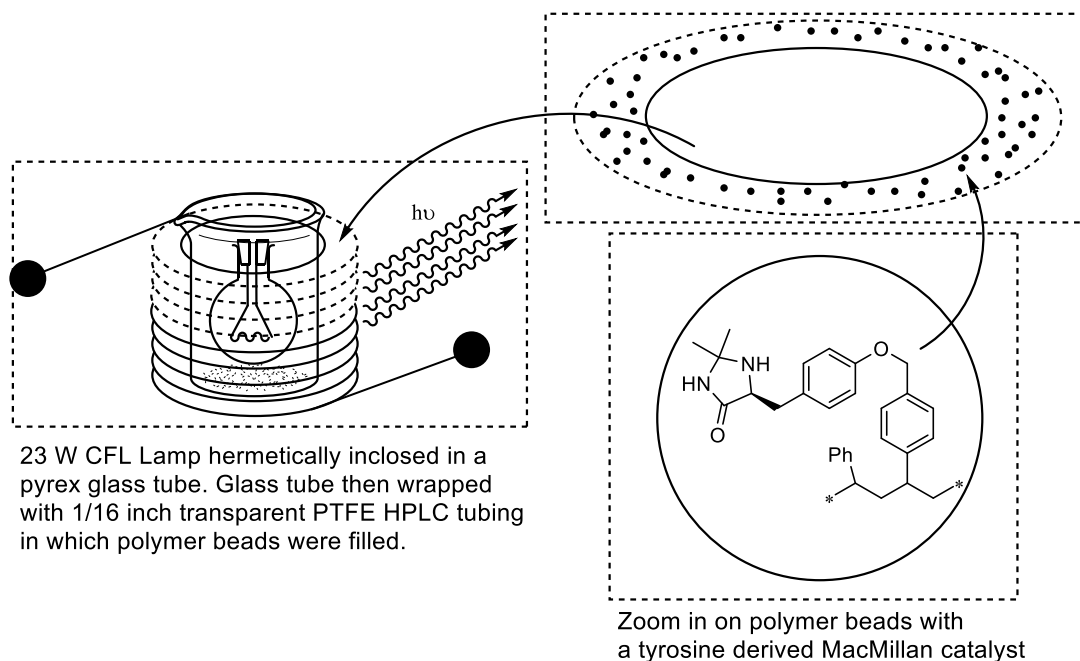
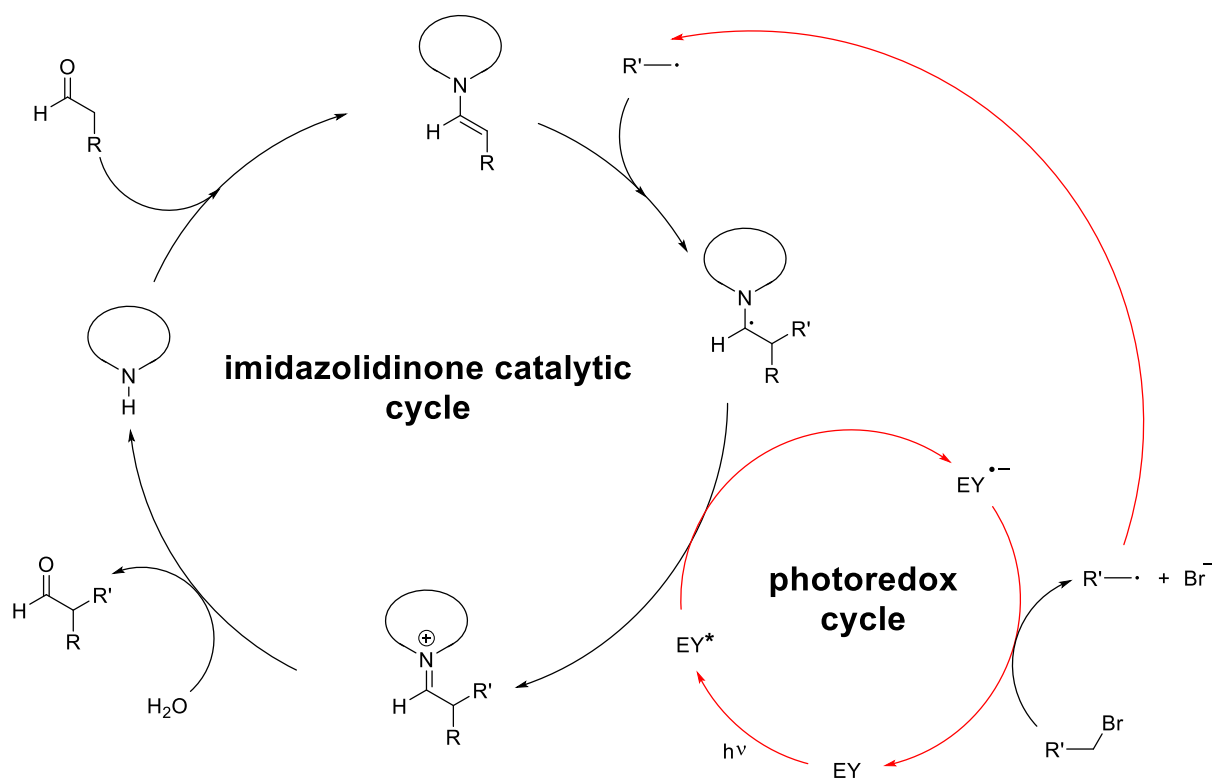


Figure 21: Photographs of the experimental setup for the continuous flow photoredox catalysis. The experiment is explained in further detail in the two times zoomed in scheme. The reaction that was performed is the MacMillan α -alkylation of aldehydes as depicted in Scheme 12. All the reagents were dissolved in DMF and pumped with a syringe pump through the packed bed catalytic reactor. In the first photograph a visible discoloration in the catalytic reactors occurs indicating the reversible photoquenching of Eosin Y. This effect is in general a good indicator for a complete reaction.

Table 2. Reactor dimension: PTFE HPLC Tubing 1/16th inch Internal diameter. 2.3 m long, Reactor volume 2.4 mL. 883 mg of solid supported catalyst

Entry	Flow rate [$\mu\text{L}/\text{min}$]	Residence time [min]	Conversion [Full/Incomplete/None]
1	40	60	Full
2	60	40	Incomplete
3	40	60	none

As illustrated in Table 2 running the reaction inside the reactor for longer times deactivated the catalyst. First we were disheartened about these findings but we soon realized we committed a rookie mistake: Water is absolutely needed for the catalyst turnover and after initial enamine formation water is flushed out of the reactor meaning the iminium ion in the mechanism cannot be hydrolyzed. In Scheme 13 is displayed the mechanism.



Scheme 13. Mechanism for the enantioselective α -functionalization of aldehydes.

In fact when adding equivalents of water into the reaction mixture full consumption of the starting bromomalonate was always observed as displayed in Table 3.

Table 3. Reactor dimension: PTFE HPLC Tubing 1/16th inch Internal diameter. 1.6 m long, Reactor volume 833 μL . 586 mg of solid supported catalyst.

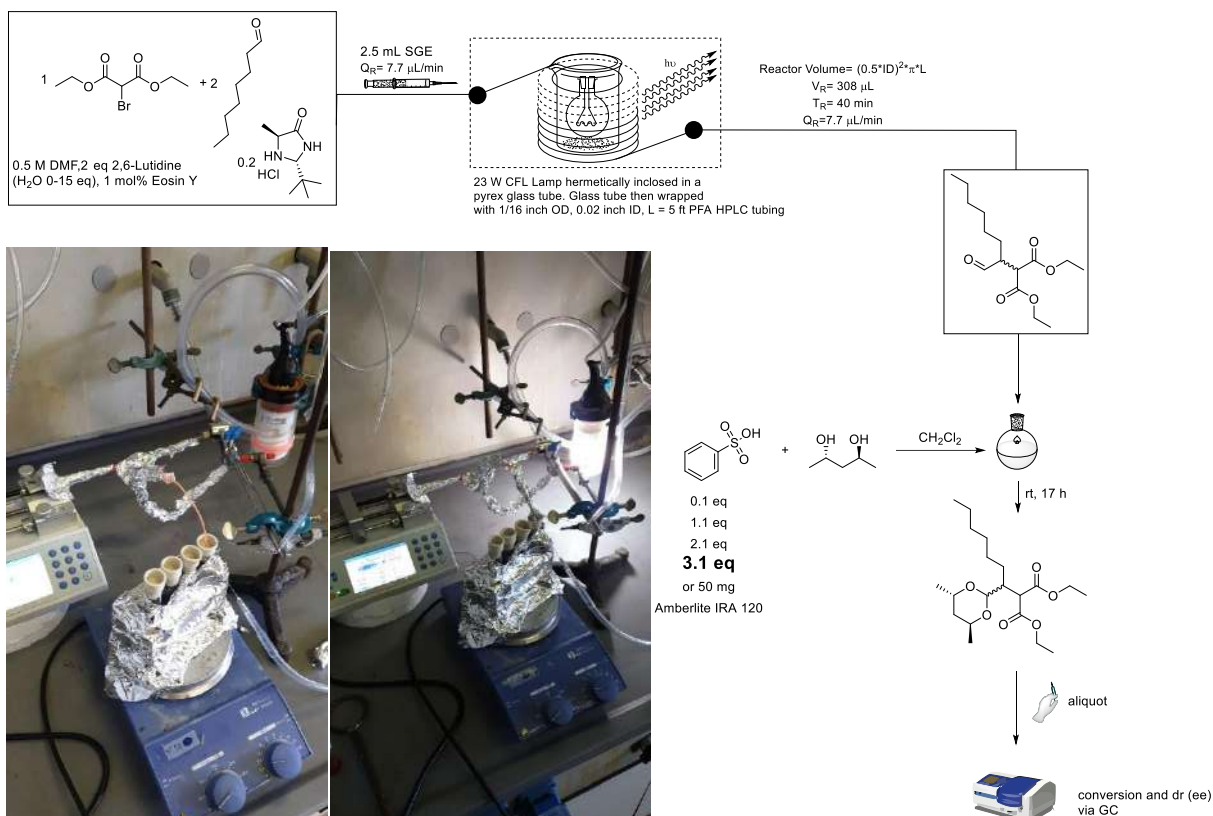
Entry	Flow rate [$\mu\text{L}/\text{min}$]	Residence time [min]	Eq. of Water	Conversion [Full/Incomplete/None]
1	40	40	5	Full
2	60	40	10	Full
3	40	40	15	Full

Leaving the reactor inside a fridge over the weekend unfortunately completely deactivated the catalyst even after flushing the material with solvent as displayed in Table 4

Table 4. Effect of leaving packed bed reactor in fridge over weekend.

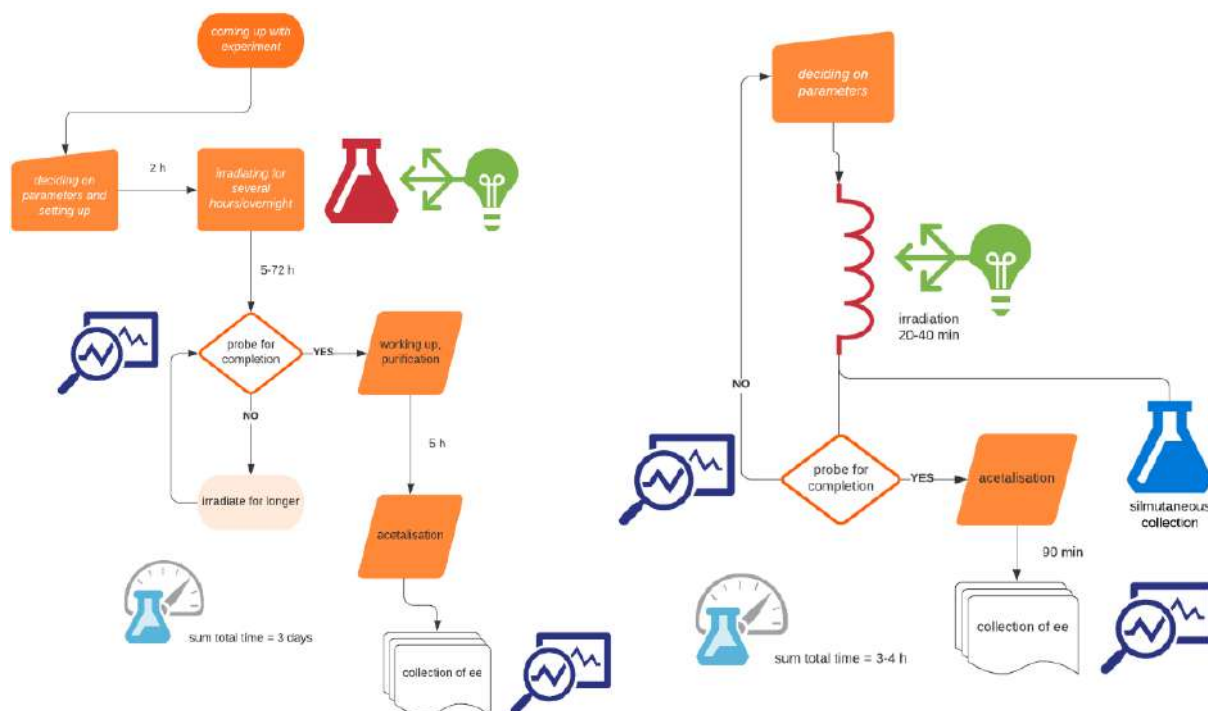
Entry	Flow rate [$\mu\text{L}/\text{min}$]	Residence time [min]	Eq. of Water	Conversion [Full/Incomplete/None]
1	83	10	5	No
2	55	15	5	No
3	42	20	5	No
4	34	25	5	No
5	28	30	5	No
6	24	35	5	No
7	21	40	5	No

Lastly, as we had developed an efficient continuous flow protocol, we wanted to significantly speed up the assay for the determination of the enantiomeric excess. typically, the aldehyde is isolated by chromatographic means, derivatized and then analyzed by NMR. This protocol took at least a full day and as chromatography was the “rate-limiting” step (and also significant epimerisation happens on silica)^[54] we tried to apply an *in situ* derivatisation. For this the outflow of the flow reactor was mixed with the acetalization reaction mixture and different amounts of toluene sulfonic acid were used to neutralize the reaction mixture and lead to slightly acidic conditions for the formation of the diastereomeric acetal.



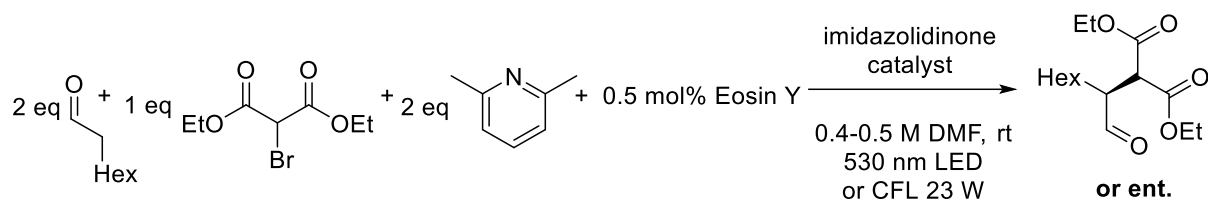
Scheme 14. Setup for the *in situ* derivatization of the aldehyde by mixing the reaction mixture with the acetalization mixture and ever increasing equivalents of toluenesulfonic acid.

Doing as described allowed for a significant speed up of the testing of the reaction conditions. What was before a several days endeavour was shortened to 3-4 h of read out for the results. All of this work was completely in vain though as the newly found “optimized conditions” lead to even more epimerisation than before using column chromatography. The ee dropped to only 11% as displayed in Table 5.



Scheme 15: Depiction of the decision-making process and the general idea of flow vs batch optimisation studies. Realistic time windows are given for each step. Left is depicted the batch process for optimisation of the ee – it is characterized to be time consuming and inefficient as the total time required to get the ee of one sample is expected to be somewhere in the region of 3 days. Right is depicted the continuous flow process – inline probing for ee and generally much shorter reaction times allow for quick access to the ee. Setting up is roughly time equivalent for both processes.

Table 5: Depiction of the best results from optimized batch and flow catalytic runs with its respective imidazolidinone catalyst indicated in the table.



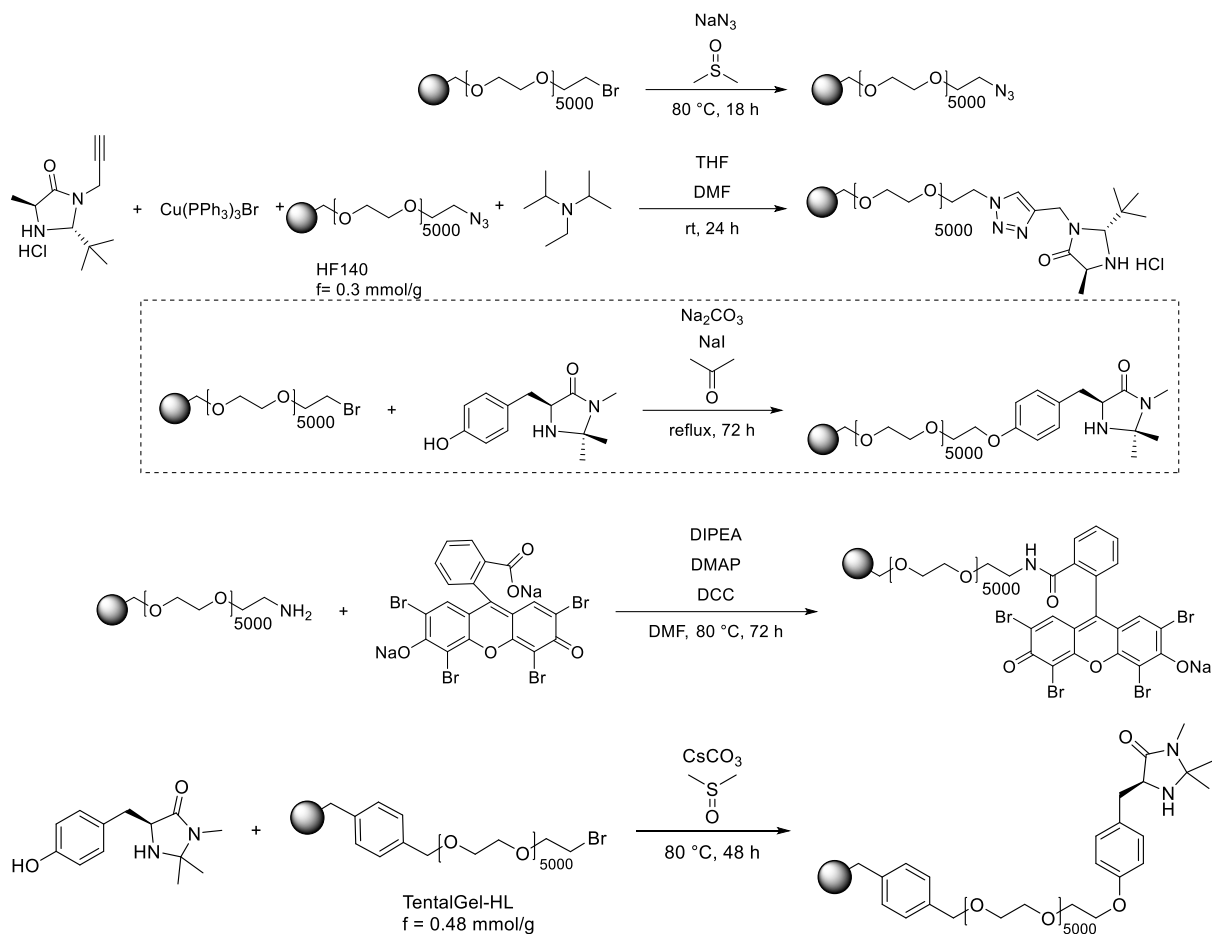
Entry	Type Catalyst	Batch vs Flow	ee
1	 2 nd homogeneous	Batch	76%
2	 2 nd homogeneous	Flow	88%
3	 2 nd supp.	Batch	-
4	 1 st supp.	Batch	59%
5	 1 st supp.	Flow	11%

Disheartened about these findings we tried to tackle a problem that was always present in the new chiral material. Swelling of the material in DMF/water mixtures was low in comparison to swelling in solvents such as dichloromethane. In Table 6 is displayed the different swelling behavior of all sorts of polymer resins used for solid phase peptide synthesis. Noticeable is entry 1 with polystyrene that does not swell whatsoever in water and exhibits poor swelling in protic solvents. Also aprotic polar solvents exhibits subpar swelling. Also noticeable is entry 5 with TentaGel HL that exhibits similar swelling behavior in water, protic solvents, aprotic polar solvents and some not so polar solvents such as dichloromethane and THF. We figured the best chance we have is to use such a material that will “always” swell well.

Table 6. Swelling behaviour of different materials used in solid-phase peptide synthesis.^[55]

resin \ solvent	Water	MeOH	EtOH	CH ₂ Cl ₂	Toluene	DMF	MeCN	THF	Dioxane	Ether	NMP
Polystyrene 1% DVB	--	1.6	1.7	7.5	7.5	4.1	2.0	7.5	7.0	3.5	7.0
TentaGel XV 0.2 - 0.4 mmol/g	3.6	6.2	2.2	18.0	12.6	13.2	8.6	13.4	14.2	2.0	14.4
TentaGel R 0.18 - 0.23 mmol/g	2.9	3.7	1.8	6.8	3.4	5.0	4.5	4.9	5.3	1.9	5.0
TentaGel S 0.25 - 0.3 mmol/g	3.6	3.6	2.9	6.3	4.8	4.7	4.2	5.0	5.4	1.9	4.9
TentaGel HL 0.5 - 0.6 mmol/g	3.1	3.6	3.5	5.7	4.1	4.6	3.9	4.2	4.8	2.4	4.7
HypoGel 200 0.7 - 0.9 mmol/g	1.8	2.8	2.6	7.0	5.1	6.0	3.0	6.5	6.4		
HypoGel 400 0.6 - 0.8 mmol/g	1.8	2.9	2.8	6.9	5.5	5.2	4.6	5.3	5.6	2.6	
TentaPore 0.5 - 1.0 mmol/g	2.8	2.8	3.0	3.8	3.2	3.1					
ScavengePore 0.5- 3.3 mmol/g	2.7	2.3	2.2	4.7	4.2	3.5	2.7	4.1	4.2		

In Scheme 16 are displayed the next round of solid supported catalysts that were synthesized using similar methodologies as before.



Scheme 16. Syntheses of 2nd Gen TG-MacMillan by a click-strategy, 1st gen TG-MacMillan by a S_N-strategy and TG-EY by an amide-bond formation strategy.

The TentaGel-catalysts were isolated as a brown solid (check Figure 22 for the photograph) and already before trying the presumption was had that they will most likely not work very well as they absorb light very efficiently. In fact after showing no activity in practice we were very disheartened and a clear path forward was not obvious.



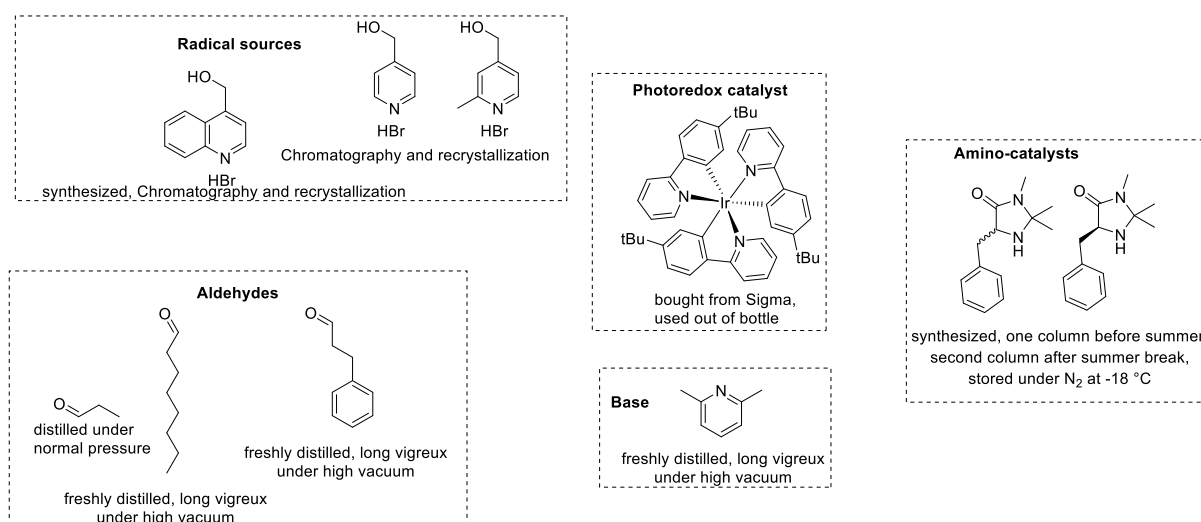
Figure 22. Photograph of the MR-1st-Gen MacMillan (left) and TG-1st-Gen MacMillan (right). Material color indicates absorption of violet-blue light.

2.1.2. SS-Catalysts in MacMillan's spin-center-shift benzylation



Scheme 17. Reaction conditions of MacMillan's spin-center-shift benzylation.

Simultaneously when performing the last set of synthesis of solid supported catalysts, we started to engage in a new type of α -functionalization. We wanted to diversify the chemistry to not be hard stuck and hopefully through some serendipitous findings we could make the solid supported catalysts work under photoredox conditions. In this new reactivity a pyridyl-methanol acts as the radical source.^[32] Very much to our delight the best performing organocatalyst is a first generation MacMillan catalyst that features only one stereogenic center. The first generation solid supported catalysts are much more convenient to work with as they do not lose their activity by epimerization so quickly.^[19] A new photoredox catalyst is employed that can fortunately be purchased.



Scheme 18. Showcase of the different reagents and their purification methods.

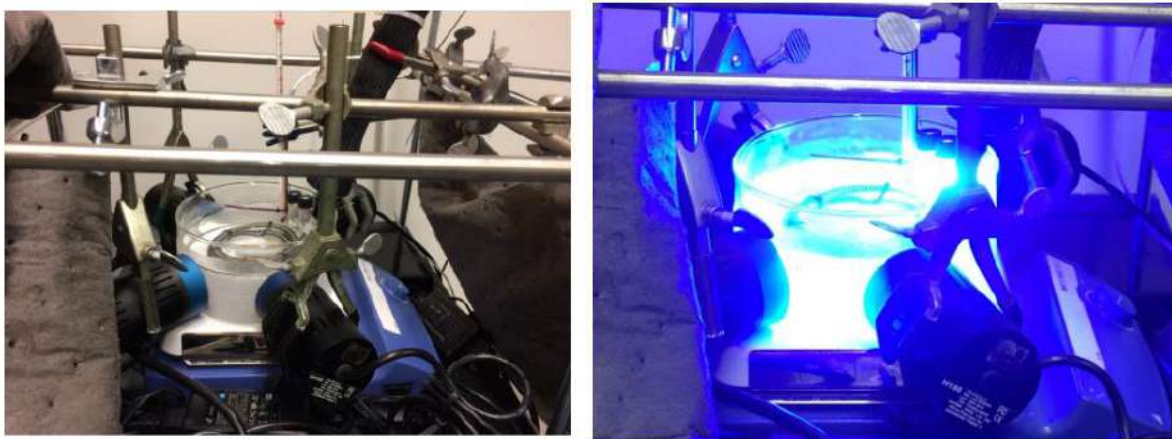


Figure 23. MacMillan's setup. Note the glacier formation on the left picture when the lamps are off.

Interestingly MacMillan employed a quite particular setup, displayed in Figure 23. By using 4 34 W Kessil Lamps with he was able to melt the glacier that formed on the glass. We were intrigued that he needed so much light to make the reaction work. The exact lamps are unfortunately discontinued from the manufacturer. This was already a bad omen to begin with. Our first approaches also with the homogeneous MacMillan in batch using a normal compact fluorescence lamp showed no conversion. Even when translating into microfluidic conditions with a 50 W halogen lamp showed miniscule conversion, the setup is detailed in Figure 24



Figure 24. Photograph of the microfluidic translation.

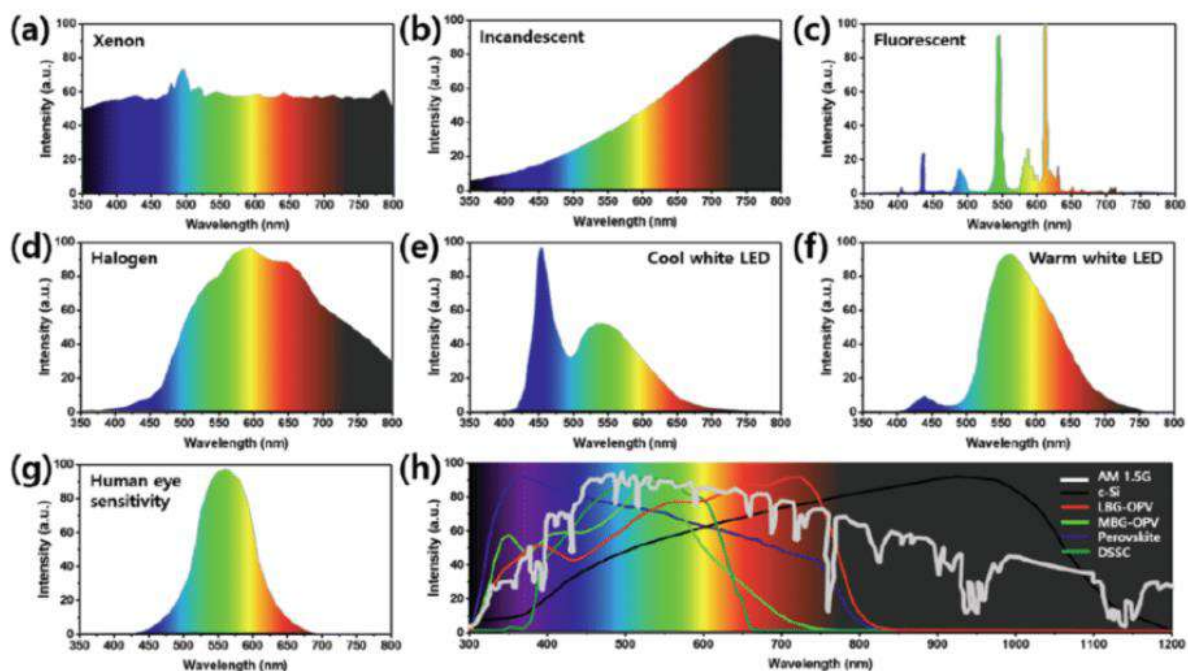


Figure 25. UV-Vis-spectra of several different light sources.^[56]

In Figure 25 are displayed the UV-Vis spectra of different light sources. Basically none of the lamps (apart from Xenon lamps) showed a large peak at the maximum of the photocatalyst ($\lambda_{\text{max}}=380$ nm). We figured we were forced to use a highly intense monochromatic LED at possibly close to 380 nm.

As cryogenic reaction conditions were required, and we did not want to “melt the ice” with lamps through a dish. We would rather build a photoreactor that can be used under cryogenic conditions.

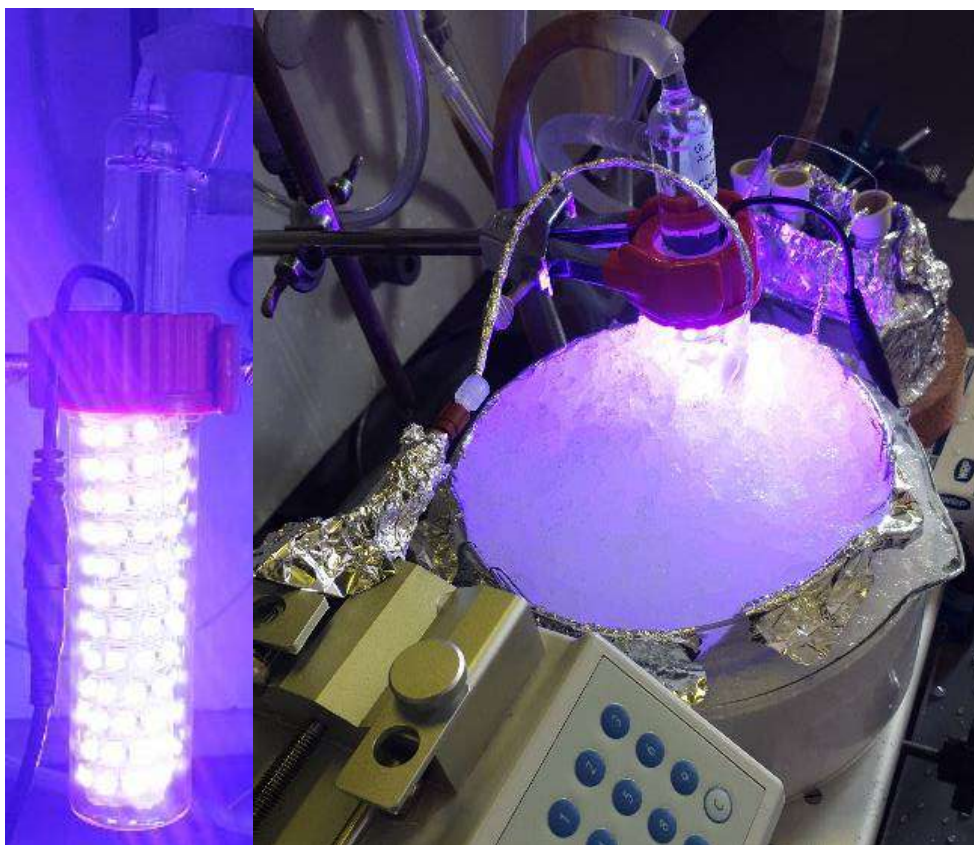


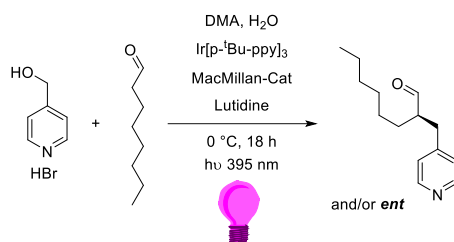
Figure 26. Immersion photoreactor where LEDs are water-cooled and hermetically encased in a glass-tube to allow operation at any temperature in a cryo-/heat-bath.

In Figure 26 is detailed a novel type of photoreactor that is perfectly suited for cryogenic (or generally temperatures that deviate from room temperature) conditions by immersion in a temperature regulated bath. The goal was to build a photoreactor for such conditions using only readily available and low-cost equipment that can be found in any organic chemistry laboratory. The herein presented Photoreactor can be immersed in any cryobath for temperature regulation as the LEDs are *hermetically sealed* inside a Pyrex glass tube to avoid glacier formation, which can obstruct efficient irradiation due to the high albedo of water ice that would form from atmospheric moisture. The heat generation which tends to burn high power LEDs under sealed conditions is counteracted by wrapping the LED-Strips around a central sublimator glass-piece which is water cooled. With this innovative reactor design, it is possible to run a continuous flow photoreaction at any temperature by simply immersing the photoreactor and coil reactor couple in a temperature-controlled liquid (Ice-mixtures,

dry-ice mixtures, cryostat-baths, oil-baths). The here presented Reactor performed for over 300 h and is still fully operational.

After trying out the new photoreactor we were delighted to see that at least the homogeneous catalyst (Table 7, entries 1-3) showed high levels of conversion and enantioselectivity running the reaction over night in small vials. In contrast, the solid supported MacMillan catalysts **MR 1** and **TG 1** showed now conversion.

Table 7. Summary of the obtained results using the novel photoreactor and



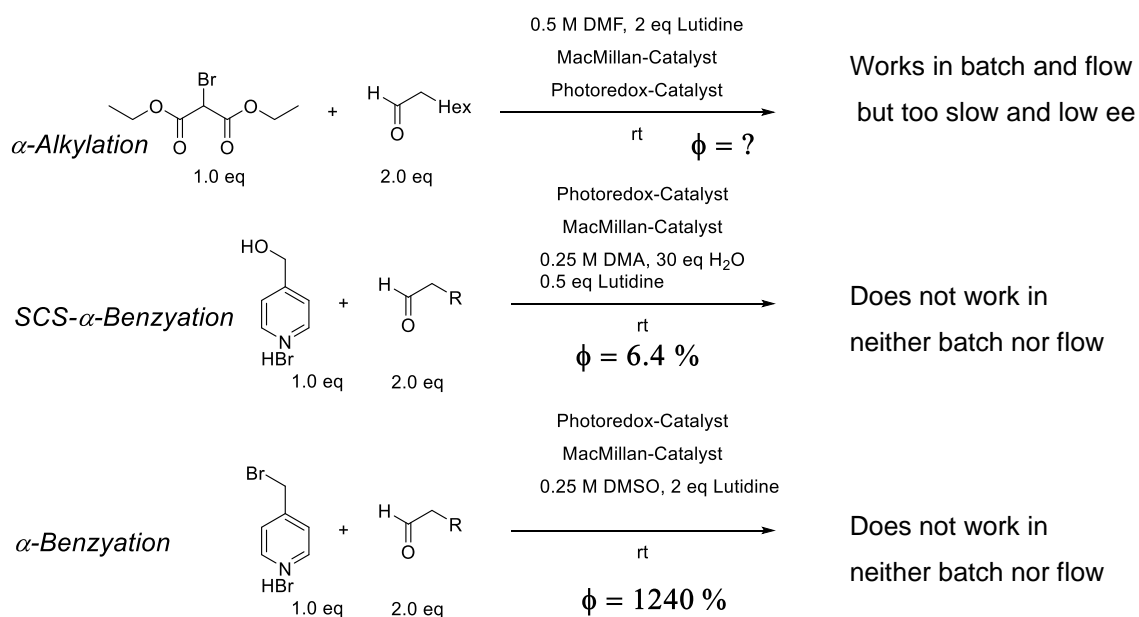
Entry	Batch vs Flow (Reaction time)	Cat.	Conversion ^a	ee ^b
1	Flow (90 min)	 <i>rac</i>	Full	rac
2	Batch (18 h)		81%	91% (Lit: 96%)
3	Batch (18 h)		70%	93%
4	Batch (18 h)		0%	---
5	Batch (18 h)		0%	---

Again, we make the intense coloration of the material responsible for this behavior. The intense light requirements indicated a poor quantum yield of the reaction.

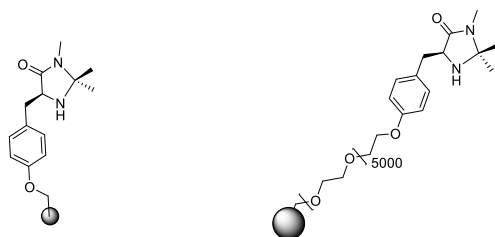


Figure 27. Photograph of the MR-1st-Gen MacMillan (left) and TG-1st-Gen MacMillan (right). Material color indicates absorption of violet-blue light.

In fact when looking up the quantum yield $\Phi=0.06$ of the reaction we figured out that the combination of low quantum yield and highly absorbing solid supported catalyst was not the best combination. Using the catalyst under the reported standard α -benzylation protocol (that has a high quantum yield as indicated in Scheme 19). We also saw miniscule conversion to the product. The starting material was consumed probably due to autocondensation of the pyridine benzylic bromide.

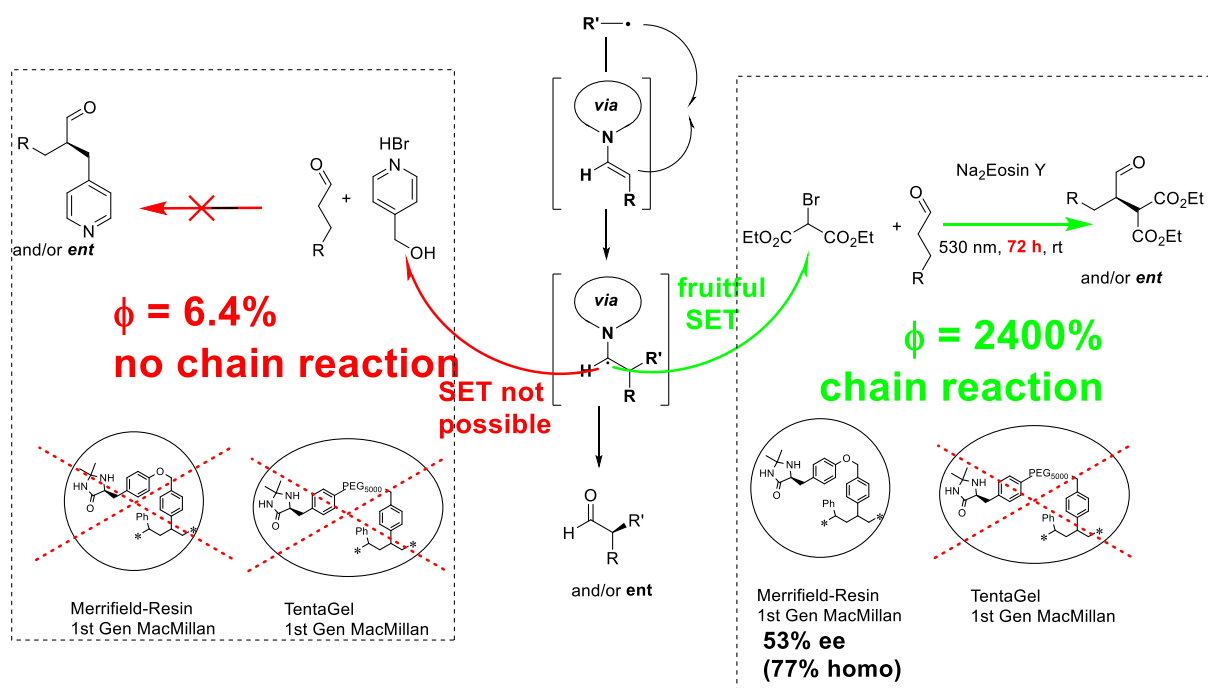


Scheme: Published standard conditions for the α -functionalisation of aliphatic aldehydes



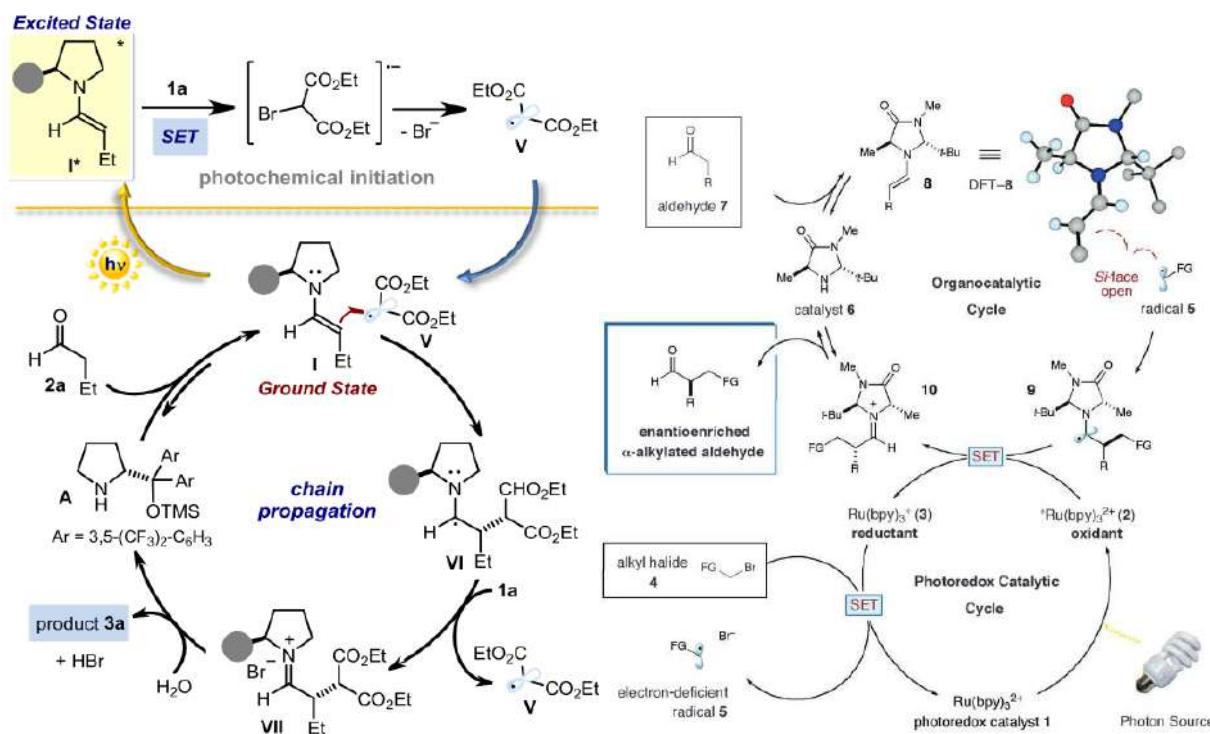
Scheme: Solid supported MacMillan-catalysts used in the above mentioned reactions

Scheme 19. Summary of the results so far using first generation MacMillan catalysts solid supported on to Merrifield resin and TentaGel resin.



Scheme 20. Infographic to make the concepts clearer that were outlined so far.

In Scheme 20 is displayed in an illustrative way the reason why probably the solid supported catalysts in this work were not performant so far. While the benzylation reaction with a low quantum yield does not any product formation, the alkylation protocol that is able to sustain the chain reaction show product formation but with slow conversion and overall low enantioselectivity. The chain reaction mechanism vs the “normal” photoredox cycle is displayed in Scheme 21.



Scheme 21. Comparison of the two different mechanisms for the alkylation of aldehydes, made possible by either an EDA-Complex from a electron-rich enamine in a radical chain initiation. mechanism or the standard MacMillan photoredox-cycle where a photocatalyst is doing the initial reduction for the radical chain initiation mechanism. Adapted from Nicewicz, D. A.; MacMillan, D. W. C. *Science* (80-.). 2008, 322 (5898), 77–80 and (1) Arceo, E.; Jurberg, I. D.; Álvarez-Fernández, A.; Melchiorre, P. *Nat. Chem.* 2013, 5 (9), 750–756.. [29,57]

2.1.3. SS-Catalysts Together With Melchiorre's Nucleophilic Thiocarbamate Catalyst

The combination of 1st generation chiral imidazolidinone catalyst, readily available photocatalyst and starting material led us to try out this reaction under solid supported conditions. After having synthesized the 1st generation chiral imidazolidinone catalyst on a Merrifield-resin (high loading) we were quickly disillusioned. After ruling out possible polymer-matrix effects (by running the reaction with homogeneous catalyst and plain unfunctionalized Merrifield-Resin) potential swelling issues were next evaluated. The commercial supplier of Merrifield-Resin provides a table indicating less than optimal swelling behaviour in polar solvents and no swelling in water.^[55] As this methodology employs both we sought out to synthesize another solid supported 1st generation chiral imidazolidinone catalyst – this time on TentaGel, a polystyrene resin with lower amounts of crosslinking and with additional PEG₅₀₀₀ units grafted to the benzylic position. Unfunctionalized TentaGel has a wide range of swelling behaviour and generates a gel/solvent-like behaviour in which even small proteins can diffuse easily.^[55] With this new catalyst at hand at least traces of the product in LC-MS assays were visible. When comparing a critical parameter for photoreactions – quantum yield – between several of MacMillan's work it was obvious that the SCS-benylation methodology is an inefficient photoreaction, the quantum yield is low because the oxidation-potential of the intermediate α -amino-radical is too low to efficiently make the SET to a new molecule of starting material. Thus, a chain-propagation mechanism is not possible. MacMillan's alkylation protocol on the other hand has an almost three orders of magnitude higher quantum yield. One absorbed photon will make more than 24 molecules of product by a chain reaction. Employing both the aforementioned catalysts under modified MacMillan conditions,^[58] we were delighted to see after extended periods of irradiation (72 h) full consumption of bromo-malonate but the levels of enantioinduction remained subpar (59% ee) employing **MR-1**. Interestingly **TG-1** shows no sign of conversion probably due to the intense red color of the material which absorbs the necessary green photons for the excitation of the photocatalyst Eosin Y. Under homogeneous conditions, the reaction proceeds with higher levels of enantioinduction (75% vs 59% ee) and lower reaction times (typically <10 h). Under the employed methodologies there seemed to clearly be a problem regarding the

overall efficiency of the photo-process only that it was unclear at which level the problem manifests itself. One possible scenario is that the solution absorbs all incident photons before sufficient photons even hit a small bead of the resin. To test this hypothesis measurements of the absorption behaviour at 1 mm pathlength were undertaken and from this was calculated by applying the *Lambert-Beer-Law* the transmission curves of the two different methodologies so far tried out. As depicted in Figure 28 it is evident that the reaction mixture for the α -alkylation (Eosin Y) absorbs all incident photons before even reaching the macroscopic size of one resin bead (70 μm average). On the other hand, the reaction mixture containing Iridium photoredox catalyst for the SCS-benylation has plenty of photons left but the low quantum yield makes this already slow reaction even slower, presumably.

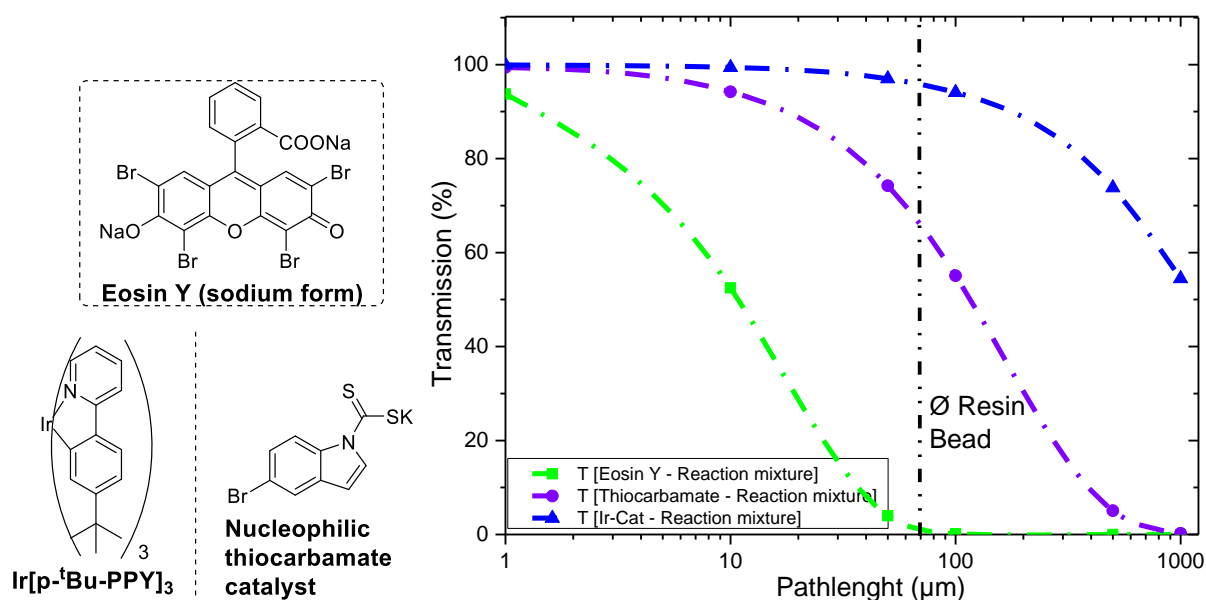
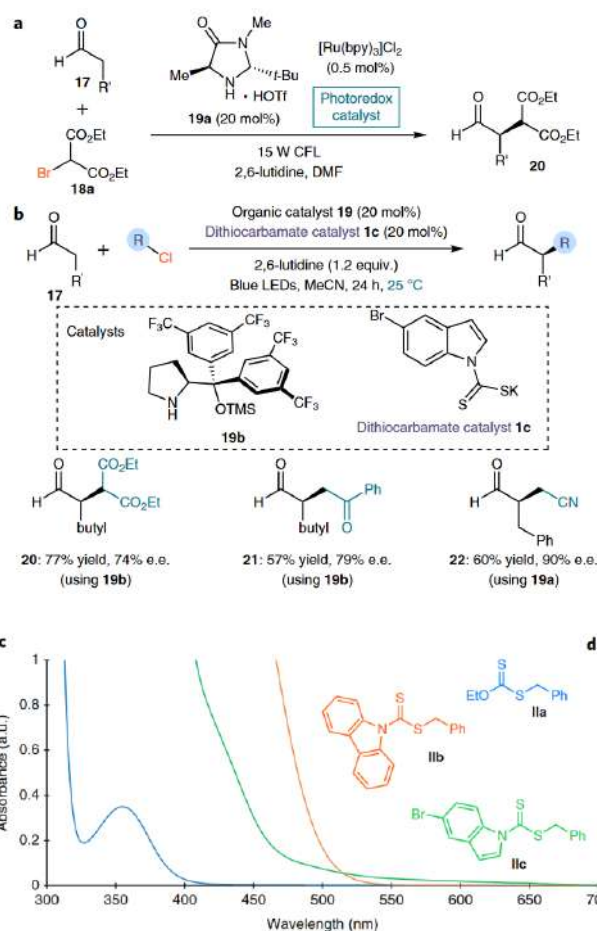


Figure 28. Depiction of the transmission curves of the three different methodologies for the enantioselective α -functionalisation of aldehydes. Dashed line represents the macroscopic average size of the polymer/resin bead onto which the chiral imidazolidinone catalysts were grafted.

The nucleophilic thiocarbamate catalyst by Melchiorre *et al* on the other hand when inside the reaction mixture shows promising transmission behaviour: at the bead-size there are still plenty of photons left, it reaches high levels of absorption at the size of 1 mm which would even allow the construction of continuous flow reactors. Of course, it must be highlighted that the transmission was measured without the solid-supported catalysts inside the cuvette. Diffraction by the material leads to isotropic behaviour

which ultimately defeats the idea of UV-Vis spectrometry. These measurements were still useful to give an idea about the order of magnitude.



Scheme 22. Depiction of Melchiorre's new strategy for the alkylation of aldehydes by the invention of a new nucleophilic thiocarbamate catalyst. Adapted from Schweitzer-Chaput, B.; Horwitz, M. A.; de Pedro Beato, E.; Melchiorre, P. *Nat. Chem.* 2019, 11 (2), 129–135. [54]

Indeed when combining Melchiorre's thiocarbamate catalyst together with the solid supported chiral imidazolidinone catalyst we were delighted to find out, that after 24 h of reaction time product could be isolated (Table 8, entry 1). The overall procedure for product isolation and purification was also changed. Direct *in situ* derivatization stops time critical epimerisation of the stereogenic center while also providing an excellent chromophore for detection.

After a quick dilution with methanol the samples were purified, evaporated, transferred and gravimetrically evaluated in a semi-automatized, mostly parallelized workflow that

was initially designed to purify and evaluate hundreds of molecules per day in library synthesis.^[59] This workflow is illustrated in Figure 29.

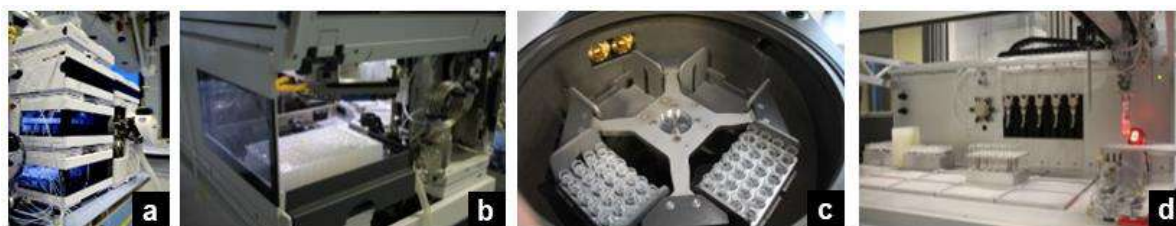
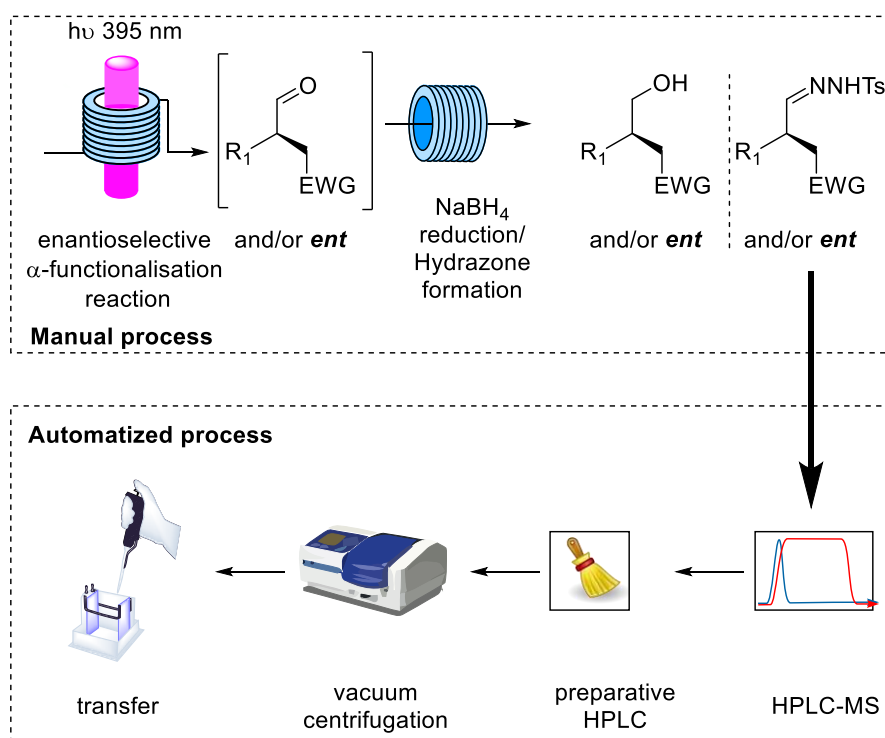
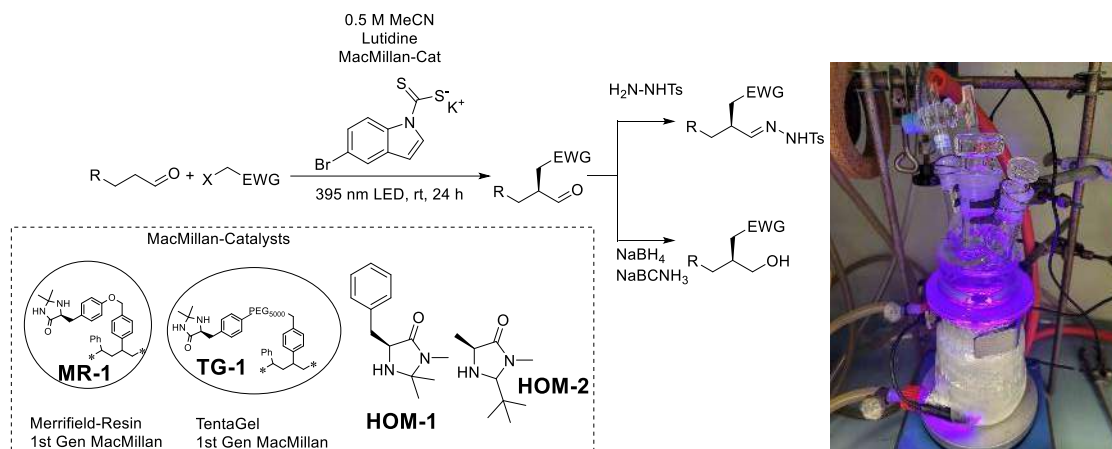
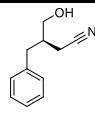
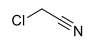
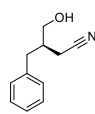
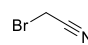
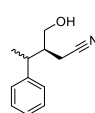

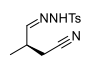
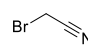
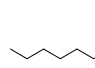
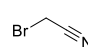
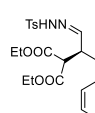
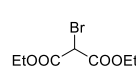


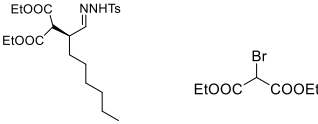
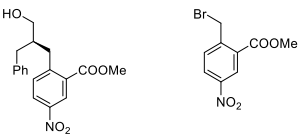
Figure 29. Semi automatized evaporation, purification, evaporation, transferring, weighing, after manual phase separation. (photos left-to-right: a) HPLC-MS , b) Pipetting and weighing robot, c) Vacuum centrifuge, d) analytical preparation sample)

The levels of enantioinduction were promising, chemical yield was low due to chloroacetonitrile as starting material not sustaining the chain reaction mechanism. Also, poorly swelling Merrifield-resin supported catalyst **MR-1** was showing low levels of conversion. **TG-1** on the other hand performed similarly as the homogeneous catalyst **HOM-1**. Indeed when employing bromoacetonitrile as radical precursor decent yields were achieved while simultaneously achieving excellent levels of enantioinduction with **TG-1** (96% ee, entry 2). Using branched aldehydes or aliphatic aldehydes provides the product in satisfactory yields and ee (entries 3-5). Changing the radical precursor to bromomalonate provides the product in decent yield and when using phenylpropionaldehyde and octanal in 90%+ ee (entry 6+7). The aliphatic product with this radical precursor gives lower level of enantioinduction, but still comparable to literature reports.^[54] When switching to a α -benzylation protocol we were surprised to achieve also high levels of enantioinduction of 90% ee (entry 7). **TG-1** performed better in most cases in comparison to **HOM-1** probably due to the positive stabilisation of the phenolic part of the chiral imidazolidinone which can undergo cation- π -interaction to stabilize the iminium-species. It is also conceivable that the polymeric backbone of TentaGel-resin provides additional levels of directionality explaining the observed high levels of enantioinduction when using aldehydes bearing aromatic residues or aromatic radical precursors.

Table 8. Summary of the employed conditions for the asymmetric α -functionalization of aldehydes using solid supported chiral imidazolidinone catalysts. Comparison with the obtained results with homogeneous catalysts. Variation from the conditions outlayed in the scheme is also indicated.



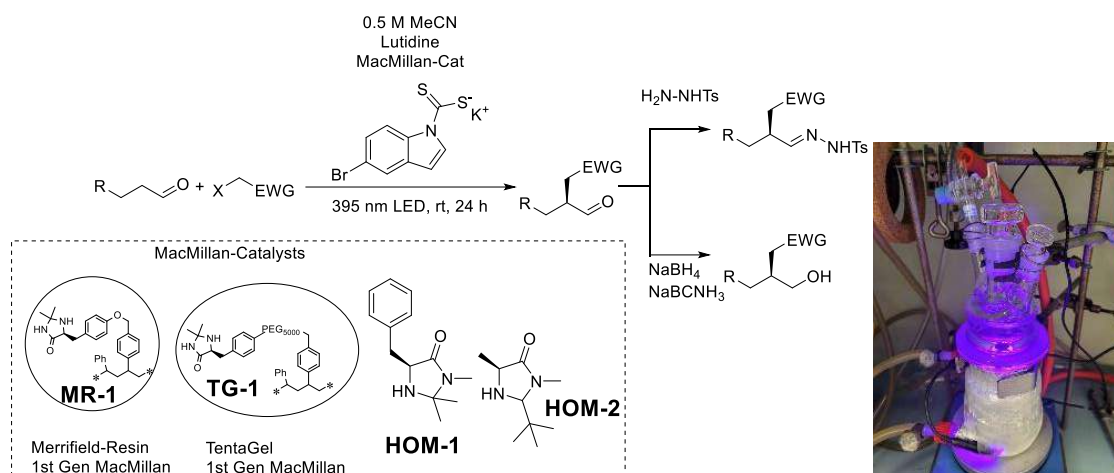
Entry	Product	Electrophile	Catalyst	Variation	ee [%]	Yield ^[a]
1			HOM-1	None	84	53%
			TG-1	None	78	33%
			MR-1	None	77	6%
			HOM-1	20% H ₂ O	74	25%
2			HOM-1	None	92	80%
			TG-1	None	96	81%
			HOM-1	20% H ₂ O	96	78%
			TG-1	20% H ₂ O	95	79%
3[b]			HOM-1	None	2.2:1 d.r.	61%
					86 (maj)	
					80 (min)	
			TG-1	None	2.1:1 d.r.	57%
		88 (maj)				
		89 (min)				
4			HOM-1	None	62	74%
			TG-1	None	77	84%
5			HOM-1	None	77	76%
			TG-1	None	91	72%
6			HOM-1	None	70	69%
			TG-1	None	90	61%

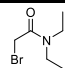
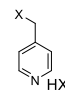
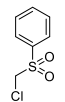
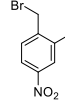
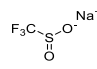
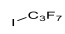
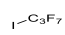
7		HOM-1	None	56	73%
		TG-1	None	73	76%
		Hom-2	Eosin Y, DMF ^[c]	75	60%
		MR-1	Eosin Y, DMF ^[c]	59	58
8		HOM-1	None	71	52%
		TG-1	None	90	48%

[a] Isolated yield after chromatographic purification. [b] racemic starting aldehyde: combined yield of diastereoisomers. [c] typical MacMillan conditions employed. Eosin Y instead of nucleophilic carbamate catalyst, DMF as solvent as instead of acetonitrile, 23 W compact fluorescence lamp, with **MR-1** as catalyst – 3 d of reaction time.

Indicated in Table 9 are electrophilic radical sources that did not lead to significant conversion. Trying out the α -bromoamide (entry 1) shows one of the limitations when the chain reaction mechanism cannot even be sustained with bromide as leaving group. The electron-withdrawing group needs to be activating enough to enable the reactivity. The benzylic pyridine chlorides and bromides (entry 2) probably undergo auto-substitution as consumption of starting material was indicated but no appearance of product could be seen in a significant amount. Chloromethyl sulfone did not show any conversion to the product (entry 3). Electron-poor nitro-fluoro benzylic bromide (entry 4) showed only miniscule conversion. Langlois' reagent for radical trifluoromethylation (entry 5, trifluoromethylsulfinate) under a variation of standard conditions indicated traces of product. Perfluoroalkylation using perfluoroiodopropane (entry 6) showed traces of conversion. A strategy to *in situ* reduce I_2 , a powerful radical quencher, showed no traces of conversion indicating something wrong with our hypothesis I_2 being detrimental to catalytic turnover.

Table 9. Summary of the employed electrophilic radical sources that did not show any kind of significant conversion. Also the appearance of traces of product in uHPLC-MS assays is indicated.



Entry	Electrophile	Conditions	Catalyst	Traces? [Yes/No]
1		As outlayed	Hom-1 TG-1	No No
2	 X: -Cl, -Br	As outlayed	Hom-1 TG-1	Yes Yes
3		As outlayed	Hom-1 TG-1	No No
4		As outlayed	Hom-1 TG-1	Yes Yes
5		No Nucleophilic catalyst but photosensitized with anthraquinone	Hom-1 TG-1	Yes Yes
6		As outlayed	Hom-1 TG-1	Yes Yes
7		Biphasic (10%) NaS ₂ O ₃ to quench I ₂	Hom-1 TG-1	No No

For the described reaction conditions a watercooled photoreactor was devised from a jacketed glass-reactor through which water cooling was applied. Around the outer layer of glass were wrapped the high intensity LEDs (1.07 W/cm²). For the translation *in continuo*, into the middle of the reactor was placed a coiled reactor made from perfluoroalkoxyalkane (PFA) which was filled with the polymer beads onto which the chiral imidazolidinone catalysts are solid supported to build a packed bed reactor with a high surface area. Flow-in, flow-out and a nitrogen atmosphere were applied through the lid of the reactor, having 3 openings with septa. In a T-junction was made the *in situ* reduction with aqueous (basic) sodium borohydride solution. After a uHPLC-MS assay conversion was plotted into a graph (left). Transmission with the respective sizes of polymer beads and tubing were made and compared to the Eosin Y methodology (middle). And lastly a schematic representation (to size) of the packed bed reactor was drawn (right).

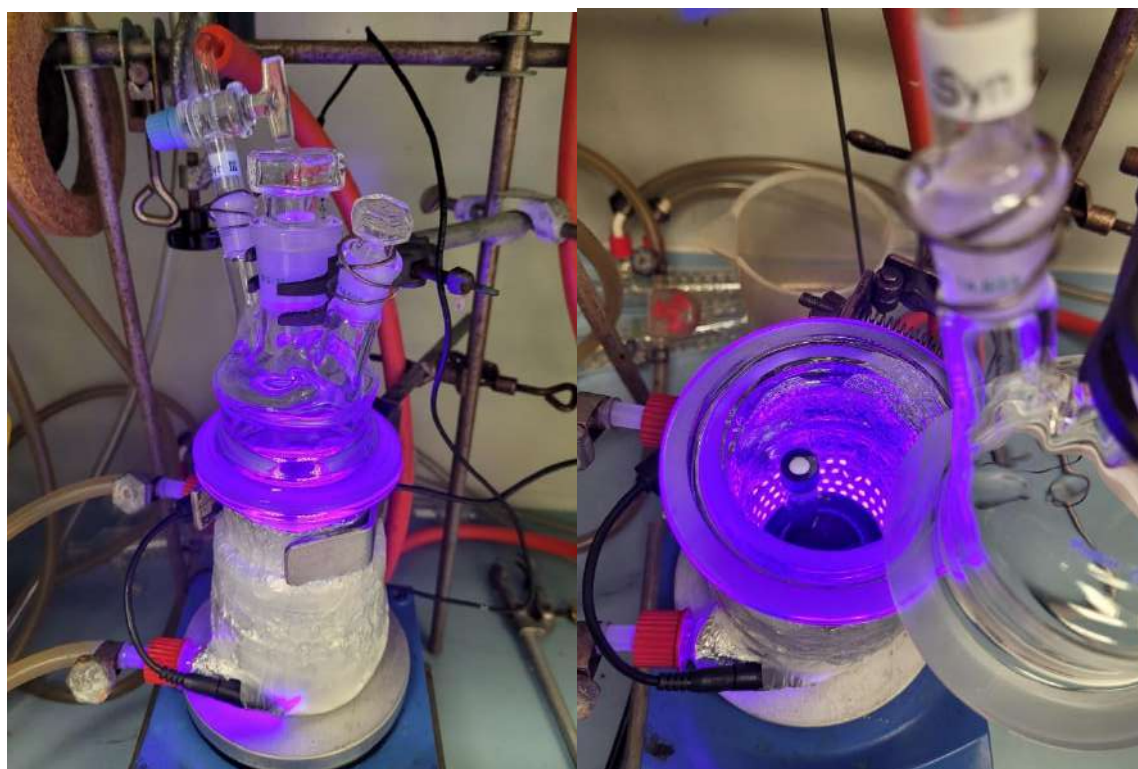
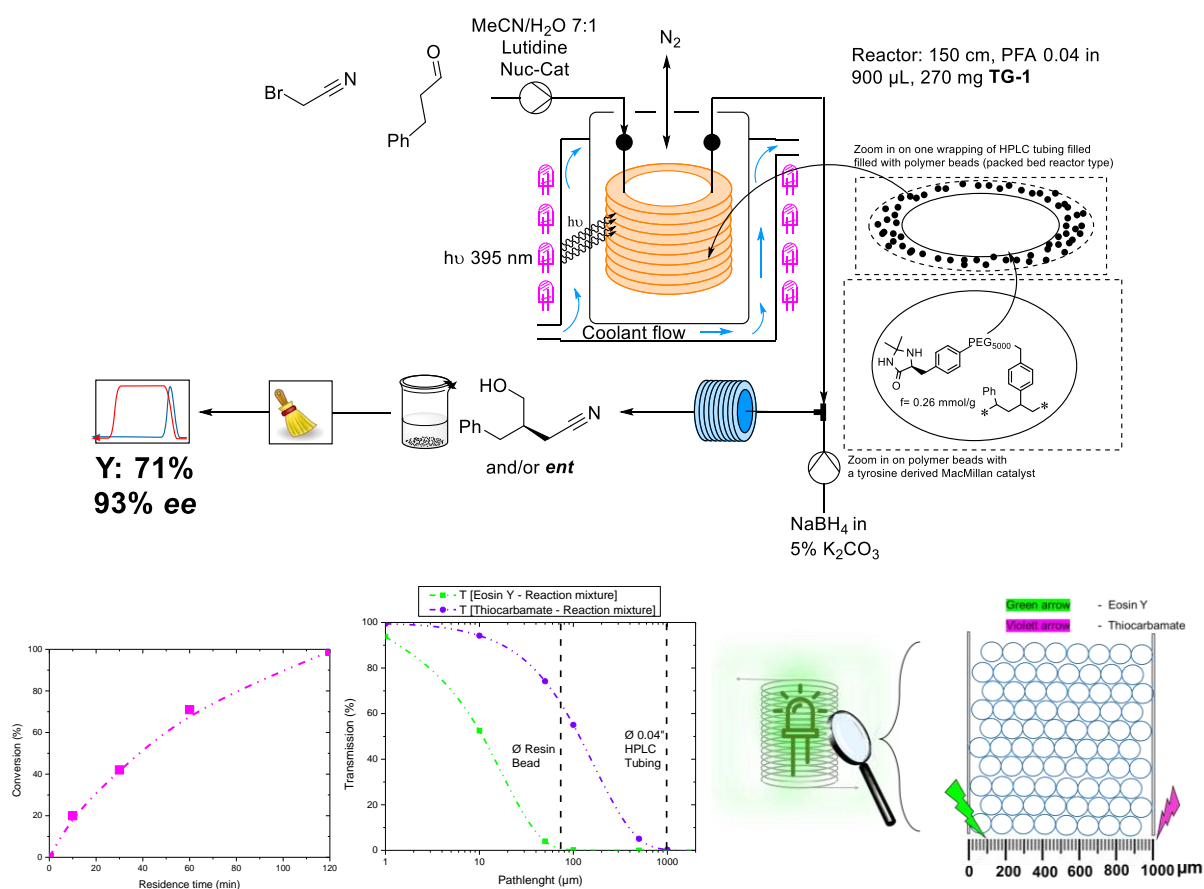


Figure 30. Photographs of the novel photoreactor.

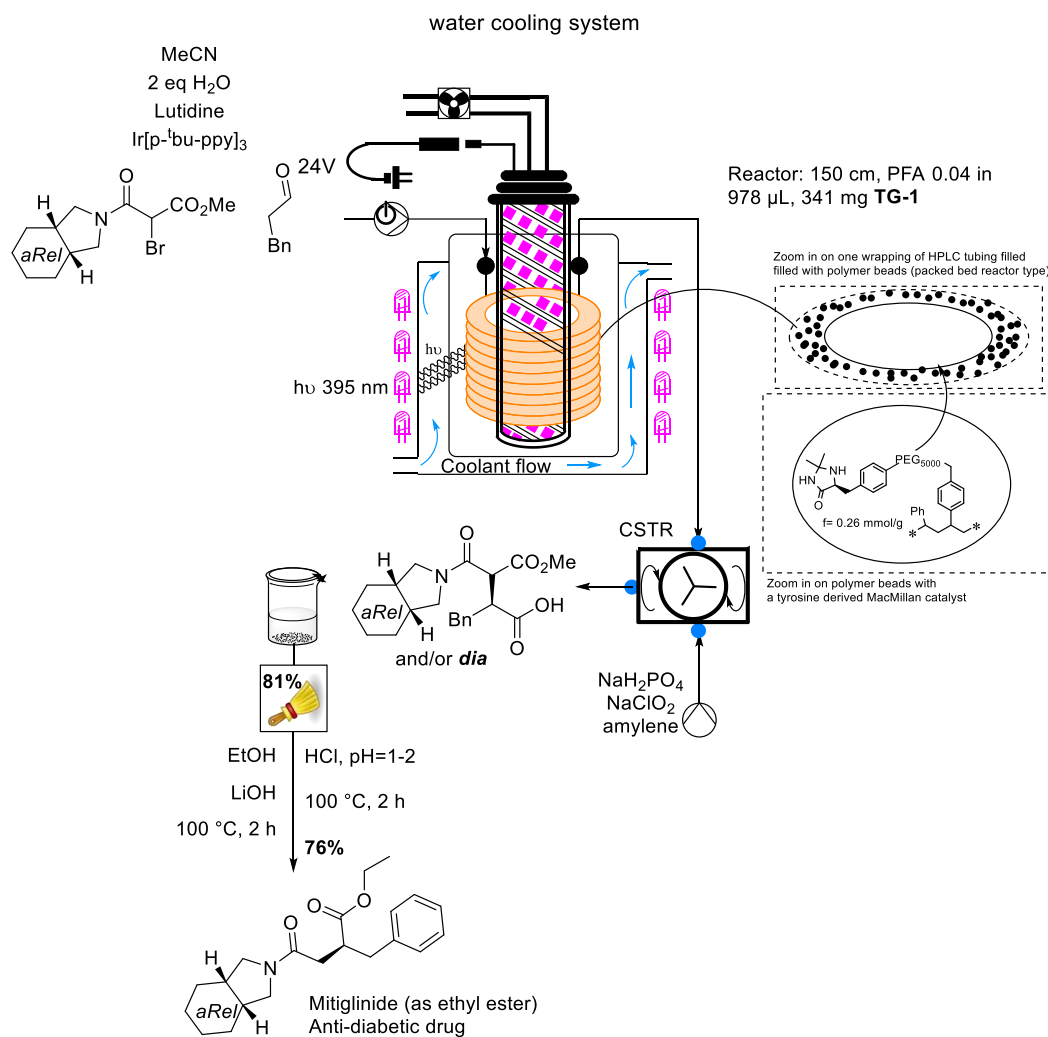
Having an efficient solid supported catalyst, a continuous flow process with a chiral reactor was devised.^[60] In general, this allows for an overall process with low loading due the continuous operation and the spatial separation of reaction mixture and solid supported catalyst. For this around 150 cm of PFA-HPLC-tubing with an internal diameter of 0.04 inches (1.00 mm) was taken and filled with the polymer beads while they were suspended in a mixture of acetonitrile/water. Up until the dimensions of this reactor no significant back-pressure was observed. At any given time inside the reactor, the loading is roughly twice as high as under batch conditions, while for the overall process, loading was less than a tenth compared to batch. After having found conditions that reproducibly give full conversion (120 min residence time) continuous operation to collect equally as much product under flow as under batch conditions was undertaken (work-up and purification was exactly alike). Yield and ee are in good agreement with both processes. Compared to the batch process productivity (as here defined as mmol/h of product) is increased by 1200% (2 h vs 24 h).



Scheme 23. Schematic representation of the translation of the solid supported methodology into continuous flow.



Figure 31. Photograph of the packed bed reactor (HPLC-tubing) filled with the solid supported 1st generation MacMillan catalyst.



Scheme 24. Continuous operation of packed-bed TG-1 reactor for the enantioselective synthesis of a precursor of mitiglinide, an approved drug. After purification a saponification, decarboxylation and esterification reaction cascade gave mitiglinide (as ethyl ester).

Ultimately to show the applicability of **TG-1** we engaged in the enantioselective synthesis of mitiglinide, an antidiabetic drug. There exist numerous enantioselective synthesis, often starting *ex chiral pool* or engaging in some kinetic resolution techniques.^[61] Clearly the asymmetric α -alkylation protocol can elegantly furnish the required stereogenic center. The axially chiral amide building block was synthesized from cheap and readily available starting materials in excellent yield. The racemic resolution of the axially chiral amine was not the scope of this work and thus was not engaged in but was rather used as a racemate. Batch protocols indicated successful conversion to the aldehyde product which was directly in-situ derivatized to the carboxylic acid. The final product was obtained after a high-yielding decarboxylation-

esterification cascade in 66% overall yield. After these invigorating findings the next step was clear to us: Development of a – at least partial – telescoped process *in continuo*. For this we again build a packed-bed reactor from HPLC-tubing and **TG-1**. To our delight the continuous operation showed high conversion initially. After 10 hours of operation conversion dropped to 60% and after 22 hours conversion was as low as 5%. Several mechanisms for catalyst inactivation are discussed in literature, catalyst oxidation and hydrolysis to only name a few. Overall for the operation *in continuo* the catalyst-stoichiometry inside the reactor was roughly 70% higher than under batch conditions. When considering the prolonged operation, the catalyst-stoichiometry was as low as 3 mol%. After successful alkylation, the output of the reactor was infused into a homebuilt continuous stirred tank reactor (CSTR) in which a Pinnick-oxidation protocol was undertaken. After purification, the acid-product was further reacted to eventually form mitiglinide which was isolated in 76% yield and with 70% ee.

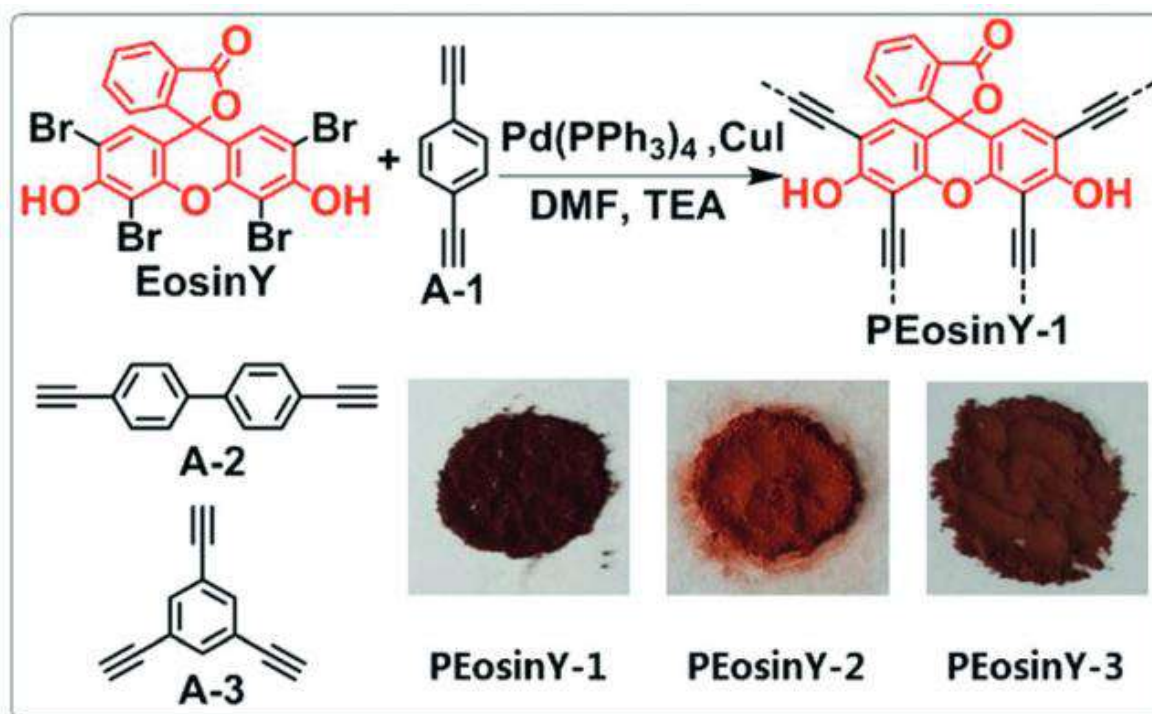
2.2. Solid Supported Eosin Y and Its Use in (Stereoselective) C-C-Bond Formations

David MacMillan, Nobel Laureate, refocused attention on photochemistry, specifically photoredox catalysis, in his 2008 Science study.^[62] Combining photochemical processes to generate reactive radical species that are then trapped by chiral enamine produced by an organocatalytic cycle. Significant progress has been made since his initial studies, particularly in replacing the expensive and toxic metal-based photocatalysts with more environmentally friendly organic dyes. Organic molecules can be tailored to have a wide range of either highly oxidizing or highly reducing potentials, as Zeitler et al. recently demonstrated.^[63] Eosin Y is a versatile dye with intermediate oxidation and reduction potential, making it an ideal all-purpose photoredox-catalyst similar to Ru[bpy]₃Cl₂. Eosin Y found numerous applications at a fraction of the cost of metal photocatalysts (1%). As the Lambert-Beer-Law dictates a negative exponential attenuation of photons through the reaction mixture, photochemistry suffers from poor scalability in general. Most of the volume of a batch reactor will not be irradiated efficiently. Continuous flow reactors are frequently used to overcome this limitation due to their inherent higher surface-to-volume-ratio.

The pre-pilot water treatment reactor by Noël et al. and the luminescent solar concentrator reactor by Noël et al. are notable examples of the combination of continuous technologies and Eosin Y.^[2,64] Another method for overcoming photon attenuation is to use solid-supported photocatalysts, which work best in small particulate forms with a large surface area.

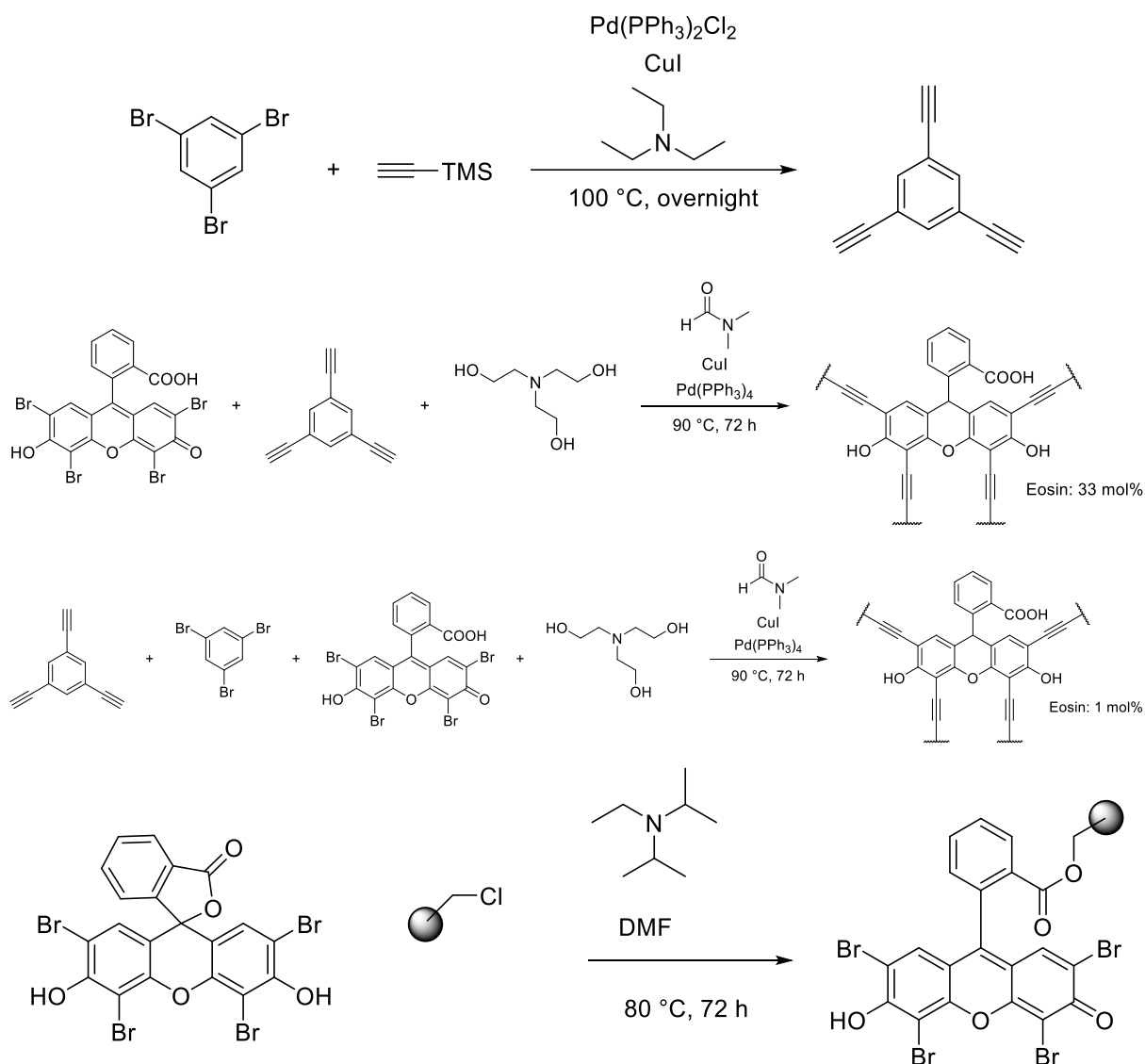
In this regard, Eosin Y has been studied by using it as the counter-ion to ion-exchange resin,^[65] on magnetic nanoparticles by ionic tethering,^[66] graphene oxide,^[67,68] backbone of metal organic frameworks,^[69,70] backbone of porous conducting organic polymers.^[71,72] Work-up and purification are greatly facilitated in all cases. Recently, our group published a review article on the topic of combining Eosin Y with various technological platforms.^[6] We hope to contribute a new easy-to-synthesize solid supported Eosin Y and its application in the development of a catalytic continuous flow reactor with this research.

2.2.1. Preliminary Findings using Supported Eosin Y



Scheme 25. Synthesis of a porous organic conducting polymer of Eosin Y. Adapted from Wang, C.-A.; Li, Y.-W.; Cheng, X.-L.; Zhang, J.-P.; Han, Y.-F. *RSC Adv.* 2017, 7 (1), 408–414.^[73]

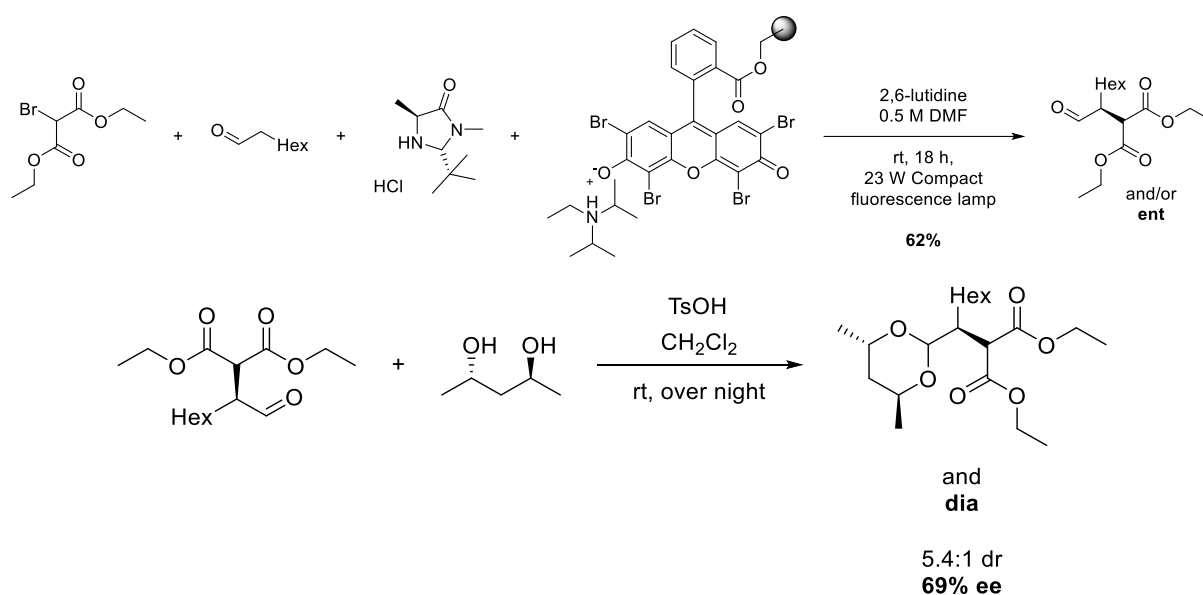
In Scheme 25 is displayed a novel porous organic conducting polymer of Eosin Y. We found this publication serendipitously. So far, the idea was mostly to solid support the organocatalyst. Solid supporting the photocatalyst may be beneficial as well. The condensed phase will obviously absorb light much more efficaciously, but the bulk of the solution will receive irradiation. Also, when the solid material has a sufficiently high surface area it might still perform better than a solution of a photocatalyst. At least that was what we thought. This promptly also gave rise to us considering other strategies to solid support Eosin Y.



Scheme 26. Depiction of several forms of solid supported Eosin Y.

In Scheme 26 are summarized the reaction conditions for several types of solid supported Eosin Y. First the normal porous organic conducting polymer is displayed, then a “diluted” form of the porous polymer is displayed. Also a supported version of Eosin Y on Merrifield resin was undertaken.

All three were also tested in the enantioselective α -alkylation protocol. Most effective proved to be MR-EY which catalyzed the reaction seamlessly and provided the product in satisfactory yield and levels enantioinduction that are comparable to using homogeneous Eosin Y, as displayed in Scheme 27. The porous polymers both got discolored during the reaction and did not lead to full conversion.



Scheme 27. Depiction of the α -alkylation protocol with MR-EY.

With the new effective material at hand it was tried to build a catalytic reactor by filling inside coils and chip reactors. In both cases the poorly swelling material got stuck and the reactors were destroyed as detailed in Table 10. Only when filling it inside an Omnifit column that was previously filled with glass balls that were stacked in an alternating fashion to ensure a tight ball packaging. The glass balls were introduced to increase the internal irradiation, as depicted in Figure 32

Table 10. Results of trying to build different types of catalytic packed bed reactors.

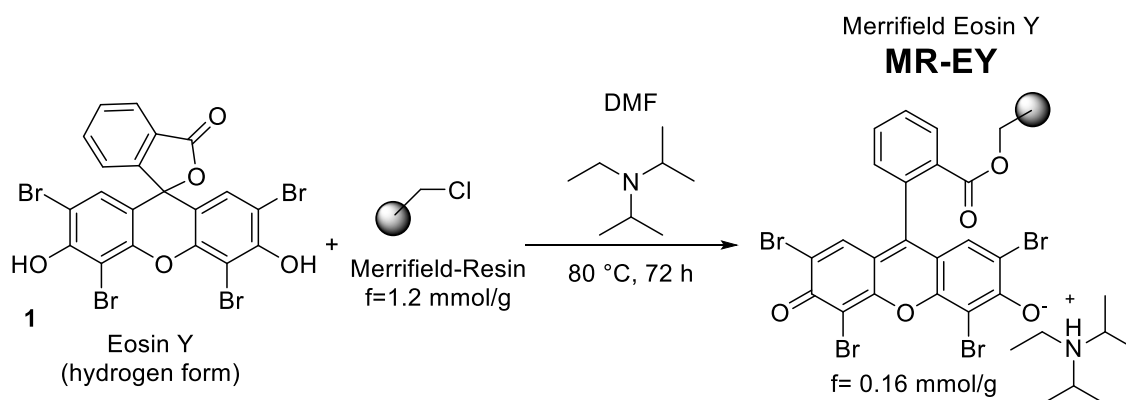
Entry	Type of Reactor	Material	Success
1	Coil 1/16 in ID	MR-Eosin HL	No
2	Coil 0.02 in ID	MR-Eosin HL	No
3	Coil 1/16 in ID	MR-Eosin LL	No
4	Coil 0.02 in ID	MR-Eosin LL	No
5	3D-Printed 1 mm channels fractal	MR-Eosin LL	No (ruined)
6	3D-Printed 1 mm channels straight	MR-Eosin LL	No (ruined)
7	Omnifit 100 mm L 10 mm ID 32x 4 mm Glassballs as filler	MR-Eosin HL	Yes



Figure 32. Photograph of the packed bed reactors that was build from an omnifit column, glass balls and MR-EY.

2.2.2. Supported Eosin Y in Cross-Dehydrogenative Coupling Reactions (CDHC-reactions)

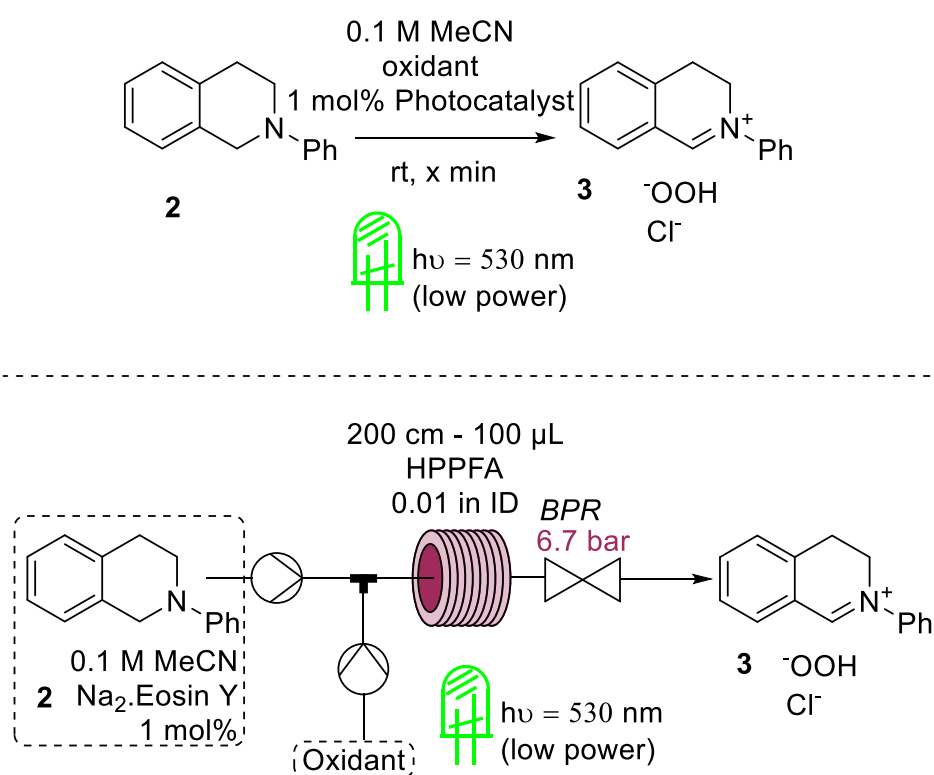
We want to report on a new easy-to-synthesize solid supported Eosin Y and its application in the development of a catalytic continuous flow reactor used to perform tertiary amine oxidations followed by a nucleophile addition to achieve a diastereoselective Mannich type reaction. As previously stated, condensation of the strongly absorbing photocatalyst into small particulate forms is a viable option for overcoming the problem of inefficient irradiation of the reaction mixture. As a result, we decided to investigate the use of an Eosin Y immobilized on Merrifield-resin, the most used precursor polymer for solid phase peptide synthesis. It is a terpolymer composed of styrene, 4-vinylbenzylchlorid, and 1-2 percent divinylbenzene as a crosslinker. The resulting polymer beads from emulsion polymerization are macroscopic in size ($\varnothing=75$ μ m) and become a free-flowing powder when swollen, but sufficiently soft that they do not grind down each other when agitated. The previously described strategies for solid supported Eosin Y investigated either complicated bottom-up approaches for new material synthesis or weak undirected interactions for immobilization, such as ionic interactions (limiting scope and usability). In Scheme 28 a straightforward synthetic strategy for the immobilization of Eosin Y onto Merrifield-resin (High-loading 1.2 mmol/g) is displayed.



Scheme 28. Synthesis of solid supported Merrifield-resin Eosin Y (MR-EY).

The inactive hydrogen form of eosin Y is deprotonated and reacts as a nucleophile with the Merrifield-resin (20 g scale). After three days, the mixture is poured into a glass

sintered funnel and thoroughly washed until there is no longer any pink color in the running liquids. In theory, this covalent approach to the preparation of solid supported catalyst should result in a more durable material. SEM analysis on MR-EY and the presence of Br in the new material both confirmed the support's morphological integrity. (For more information, see the Supporting Information). The newly synthesized material's efficacy was then investigated by using it in a well-established transformation: the oxidation of a tertiary amine to the respective iminium-ion (catalyzed by the material), followed by Mannich-type nucleophile addition (not by the material). Because of the extensive conjugation, the iminium-ions can usually be isolated and even stored for long periods of time when using 1,2,3,4-tetrahydroisoquinolines as amines, making them ideal substrates for this transformation. Under homogeneous conditions, the CDHC was studied with the sodium salt of Eosin Y as a starting point (Scheme 29).



Scheme 29. Reaction conditions for batch and flow oxidation under homogeneous conditions.

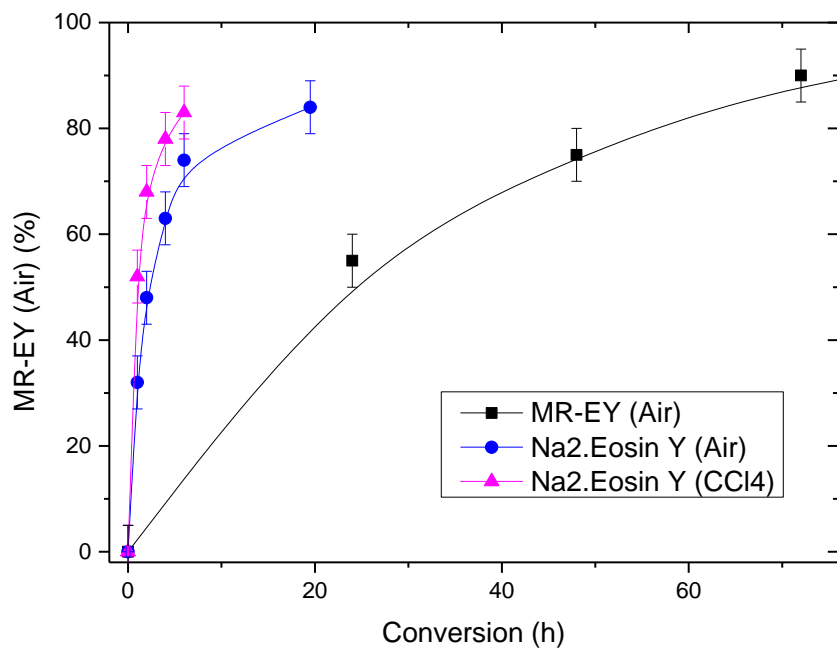


Figure 33. Conversion vs Reaction time graph of MR-EY and standard Eosin Y under batch conditions.

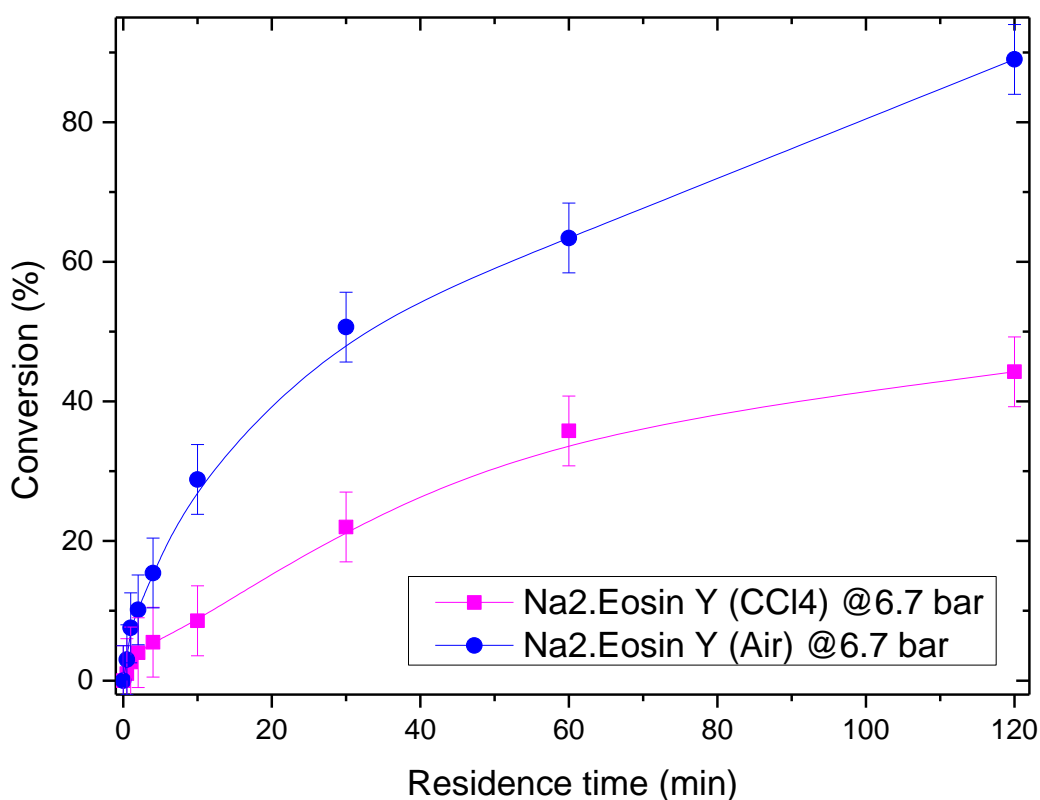
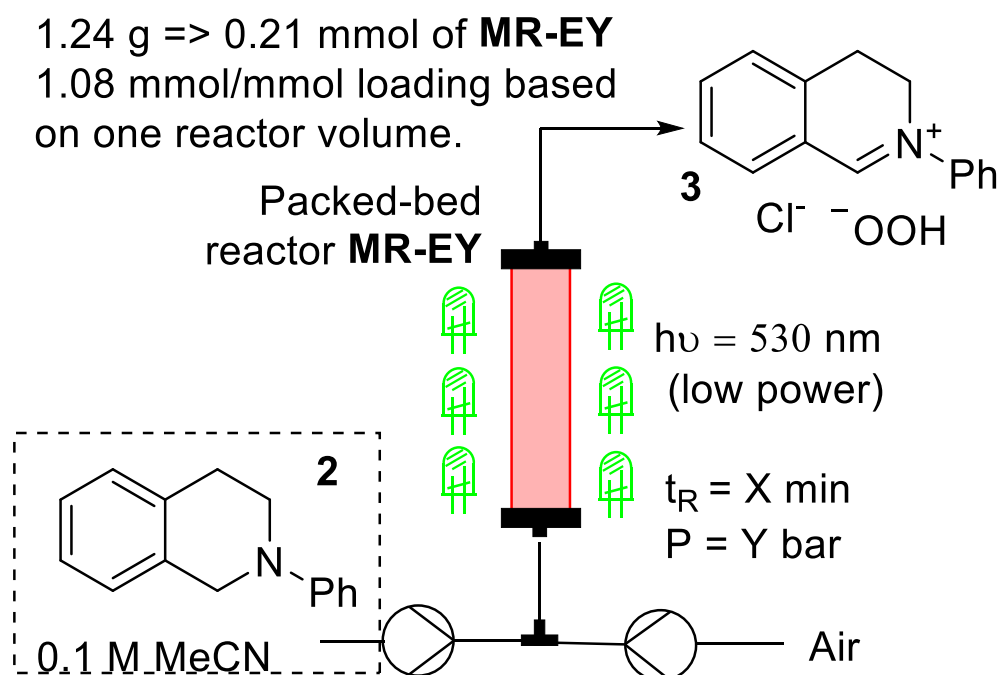


Figure 34. Reaction Conditions for batch and flow oxidation under homogeneous conditions.

Using either air or carbontetrachloride as the terminal oxidant, the reaction typically proceeds to high levels of conversion only after a long time (10-20 h). When MR-EY is

used, the reaction is slowed by a factor of four. The observed lower reactivity is due to the combination of a triphasic reaction mixture (solid-liquid-gas) with an additional critical reaction parameter - light - that imposes another interfacial challenge as mixing becomes more and more turnover limiting. When Eosin Y is used in a coiled microfluidic reactor setup, a significant speed increase (x8) is observed using air as the oxidant and a sevenfold increase in pressure, resulting in a 90 percent conversion after 120 minutes. When designing a packed-bed catalytic continuous flow reactor, the aforementioned additional interfacial challenges can be taken advantage of. A 100x10 mm omnifit column was first maximally filled with 5 mm glass balls stacked alternately, and then MR-EY was filled inside as an acetonitrile suspension. This novel reactor design aims to increase internal irradiation of the reactor bulk while decreasing catalytic reactor loading. This reactor is then wrapped in a 2.6 W/m low-power LED-strip emitting at 530 nm. (Scheme 30). We were ecstatic to discover that the catalytic reactor outperforms the microfluidic reactor with homogeneous Eosin Y. After 120 minutes, 86 percent conversion was achieved, outperforming batch methodology by a factor of ten.



Scheme 30. Solid supported Eosin-promoted in-flow oxidation in a packed-bed reactor.

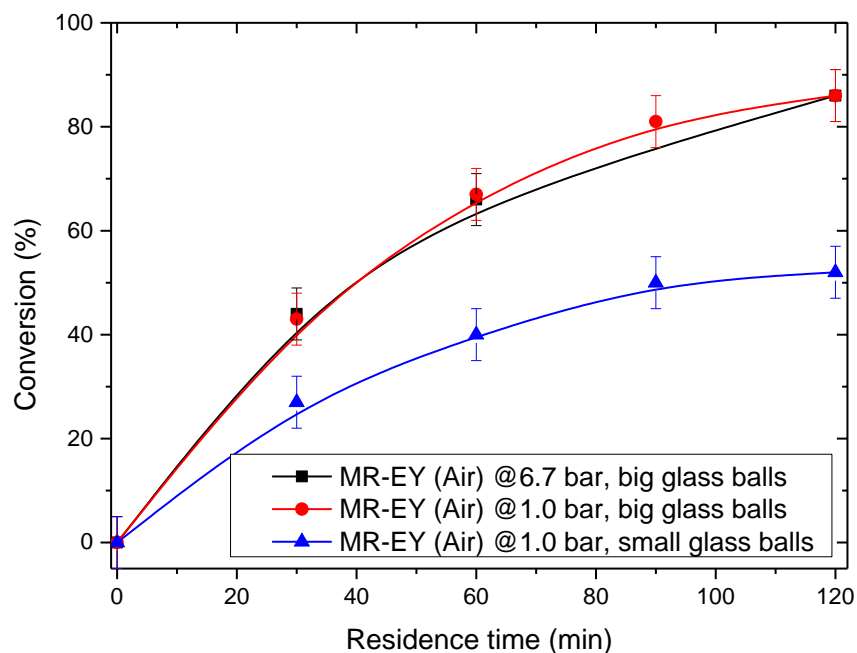
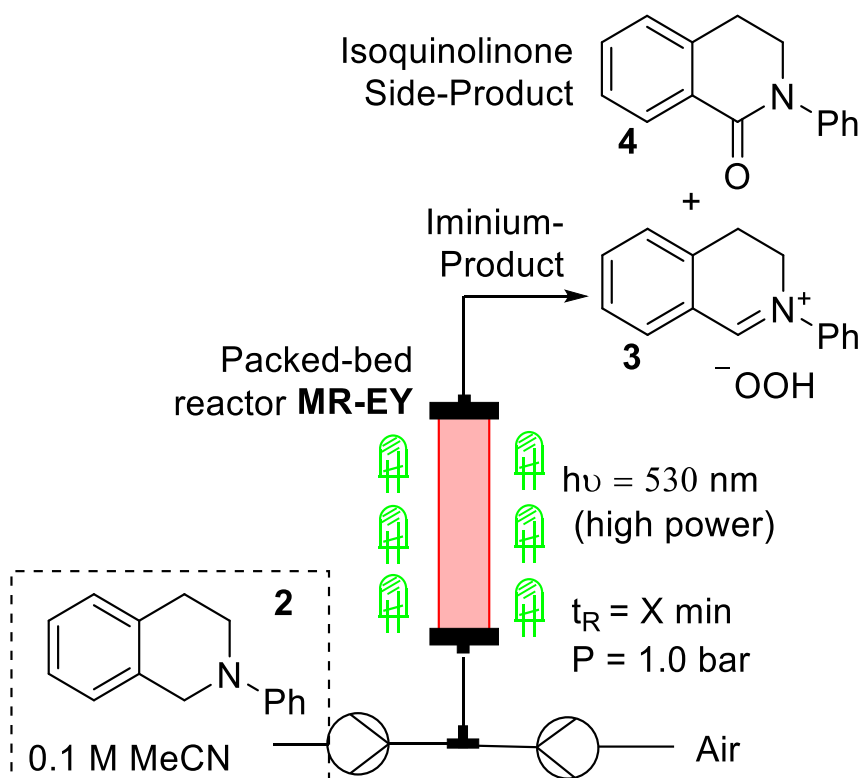


Figure 35. Conversion vs Residence time graph of solid supported Eosin Y in a packed bed reactor under continuous flow conditions.

There was no significant difference when 6.7 bar of air pressure was applied. Only when the size (and thus the number) of glass balls inside the reactor was reduced did a significant difference in behavior occur, cutting productivity in half and causing a plateau effect. The difference in the amount of MR-EY inside the two catalytic reactors is not large enough to explain this difference in behavior. As a result, it is hypothesized that the phenomenon is caused by an irradiation effect. Next, a high-power LED-strip (24 W/m) was used to investigate the effect of photon density further. Wrapping it around the catalytic reactor proved hazardous because the LEDs heated the setup above the boiling point of acetonitrile. Even with a 5 cm distance between the LEDs and the reactor, air cooling did not cool the catalytic reactor sufficiently to reach room temperature. By wrapping the LEDs around a double-walled glass piece that could be water-cooled, a new device was created. In Scheme 31 are summarized the findings with high power LEDs.



Scheme 31: In-flow oxidation with high-intensity LED together with MR-EY packed-bed reactor.

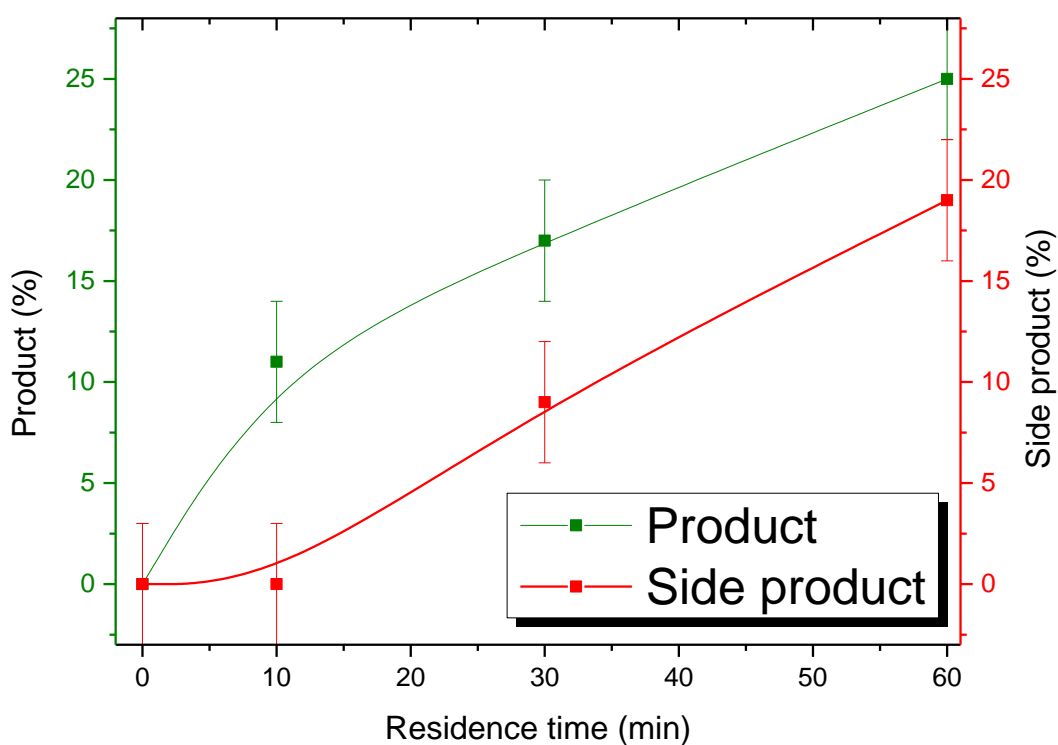
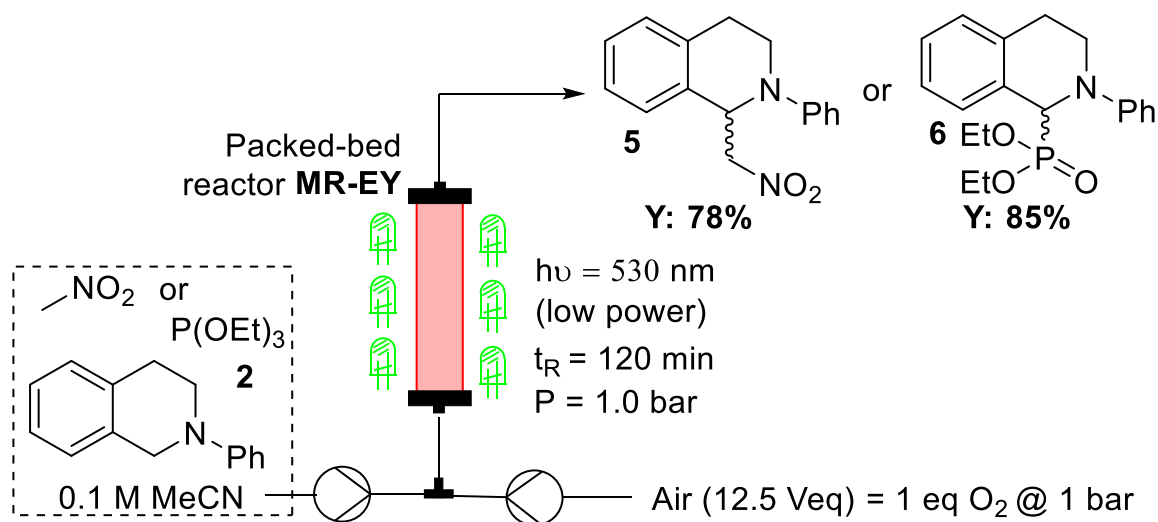


Figure 36: Conversion (to the product and isoquinolinone side product respectively) vs residence time graph for the In-flow oxidation with high-intensity LED together with MR-EY packed-bed reactor.

Unfortunately, the reaction did not speed up as expected, but a significant amount of the isoquinolinone side-product began to form, which was previously only hinted at in the HPLC-MS assay that had been used to quantify it.

Assuming that an additional equivalent of oxygen is required for over-oxidation to the side-product, the conversion of product vs side-product (roughly 20% + 20% respectively) indicates that roughly 60% of the 1.0 equivalents of oxygen infused into the reactor were consumed (at 1 h residence time), which is comparable to consumption using low-power LED-strips. (Scheme 30). After identifying conditions for high productivity of iminium-ion generation, in situ nucleophile addition was attempted. As nucleophiles, nitromethane and triethylphosphite were chosen in preliminary studies. Before infusing the tetrahydroquinoline solution into the catalytic reactor, ten equivalents of nitromethane or one equivalent of triethyl phosphite were mixed with it in acetonitrile, as displayed in Scheme 32. After 120 min of residence time and collection, the Aza-Henry-product **5** was isolated in 78% yield after chromatographic purification. Similarly, the phosphonate-product **6** was obtained in 85% isolated yield.

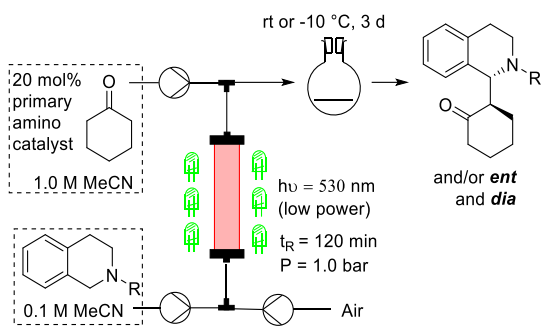


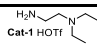
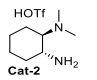
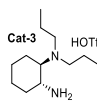
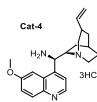
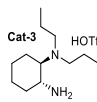
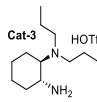
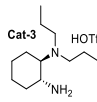
Scheme 32. All-in-flow in situ addition of nucleophiles to generated iminium-ions.

Following that, a diastereoselective Mannich-protocol was converted into continuous flow.

Two different metal-based catalysts were required in a recently published visible-light-promoted asymmetric cross-dehydrogenative coupling of tertiary amines to ketones, one for photooxidation and the other to reduce nitrobenzoic acid to close the net

oxidative process.^[17] We decided to improve on this protocol using our catalytic reactor by removing the metal catalysts and replacing them with air as the terminal oxidant. Several chiral diamines were studied as organocatalysts in the reaction of tetrahydroquinolines with cyclic ketones as Mannich donors and acceptors (see Table 11). We envisioned a two-step process to avoid any potential side-reactions with the amino-catalyst inside the catalytic reactor. Yang et al discovered in their study that running the reaction under air conditions would result in subpar performance, which could be attributed to catalyst decomposition.^[17] Thus, after photooxidation with the cyclic ketone and diamino catalyst, the iminium-ion mixture was combined and left to react semi-batch in a temperature controlled environment. The findings from the collection and chromatographic purification of Mannich products derived from the combination of cyclohexanone with variously substituted tetrahydroquinolines are summarized in Table 11. In general, low levels of diastereo- and enantioinduction were obtained when the Mannich-reaction was performed at room temperature (entries 1-4). As a result, this protocol was modified and optimized at room temperature using the most efficient catalyst (cat 3) (entry 3). After three days at -10 °C, the product was obtained in 69 percent yield with greatly improved diastereoselectivity (83:17) and very good enantioselectivities (88 percent ee, entry 5). Similar results were obtained in the reaction with the N-p-bromo and p-chlorophenyl tetrahydroquinoline derivatives, with high diastereoselectivities and enantioselectivities of up to 90% e.e (entries 6-7).

Table 11. Diastereoselective Mannich-reaction.


Entry	R	Catalyst	T [°C]	d.r.	e.e.	Yield
1	Ph		rt	60:40	---	64%
2	Ph		rt	60:40	Rac (min) 2% (maj)	71%
3	Ph		rt	55:45	67% (min) 70% (maj)	64%
4	Ph		rt	15:85	33% (min) 45% (maj)	67%
5	Ph		-10	83:17	88% (maj) 28% (min)	69%
6	<i>p</i> -Cl-Ph		-10	80:20	90% (maj) 20% (min)	68%
7	<i>p</i> -Br-Ph		-10	3.8:1	87% (maj) 5% (min)	61%

Finally, the supported photocatalyst's recyclability was investigated. No significant deterioration of MR-EY was observed under the used reaction conditions; for example, the same catalytic reactor was used to perform the initial screening experiments at 1.0 bar pressure (Scheme 30), when ten reactions at five different residence times were performed. The experiments were then repeated, but no discernible change in catalyst activity was observed. A single reactor was also used to run various stereoselective Mannich reactions, as shown in Table 11. After each reaction, the reactor was thoroughly washed (>20 reactor volumes) to ensure that the out-flow running liquids were free of contaminants. Following washing, different reaction conditions were used, with the reactor remaining constant. The diastereoselective nucleophile additions (Scheme 32) were carried out in the same reactor that had been reused for weeks in our study and did not require any modifications.

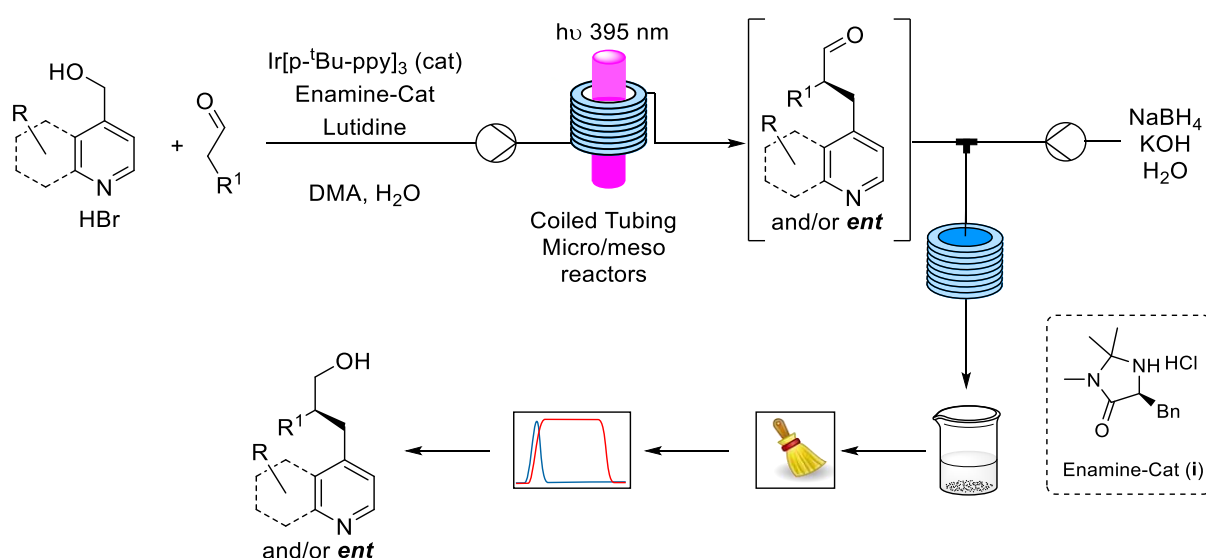
2.3. Telescoped Synthesis of an API in a Photocatalyzed Stereoselective Way

2.3.1. Preliminary Studies and the Construction of a Novel Photoreactor

Continuous flow technologies have emerged as an effective means of preparing highly functionalized molecules.^[1] Highly efficient telescoped processes,^[1] aimed at the synthesis and even production of active pharmaceutical ingredients,^[3] have been reported, as have some remarkable examples of automated organic synthesis.^[4] However, in the case of chiral molecules, the majority of the works relate to the in-flow synthesis of the racemic product, whereas reports of in continuo enantioselective catalytic synthesis are extremely rare, highlighting the need for new contributions in the field.^[5] If enantioselective organophotoredox catalysis is used in the synthesis of the target molecule, efficient in flow asymmetric catalytic processes must be developed.^[6] Under batch conditions, the majority of the volume of a photochemical reaction does not receive efficient irradiation; continuous flow reactors frequently have a surface-to-volume ratio that is two orders of magnitude higher.^[12] Seeberger defines a 0.1 percent transmission cut-off in his famous review "A hitchhikers guide to flow chemistry " as a guiding rule at which a photochemical reaction mixture with a certain transmittance can still operate efficiently.^[7] The combination of photochemistry and organocatalysis allows for easy access to molecules that would otherwise be difficult to obtain. Shortly after MacMillan et al pioneering contribution,^[74] Zeitler et al. translated the new methodology to be run in continuous mode using custom built coiled polymer tubing wrapped around a compact fluorescence lamp, increasing productivity by roughly x100.^[9] However, examples of asymmetric organocatalyzed photochemical reactions translated into continuous flow are scarce, with only two other studies to date - the E/Z-isomerisation, cyclisation, and asymmetric reduction cascade with a chiral Brnsted-acid by Rueping et al and the asymmetric photo—oxidation of carbonyl compounds in the presence of a chiral phase transfer catalyst by Meng et al.^[58,75,76]

We would like to share our findings on in-flow catalytic asymmetric alkylation of aldehydes in order to provide some insight into the process of 100x scaling-up an

asymmetric catalytic photochemical reaction: Going from microfluidic conditions to a 10 mL mesofluidic reactor resulted in a nearly 18000 percent increase in productivity. Finally, for the first time, a stereoselective photoredox organocatalytic continuous flow reaction for an API was achieved with 95 percent enantioselectivity in a fully telescoped process. MacMillan's spin-center-shift benzylation was chosen as the best reaction for scaling up and translating into continuous flow conditions (Scheme 33).^[32] After reacting the aldehydes with 4-pyridyl methyl alcohols, the products were reduced to the corresponding alcohols for HPLC enantioselectivity analysis to avoid issues related to stereogenic center lability in the α -position to a carbonyl group.



Scheme 33. Continuous two-step enantioselective α -benzylation of aldehydes and NaBH₄ reduction, offline collection, chromatographic purification and HPLC-assessment of the enantiomeric excesses.

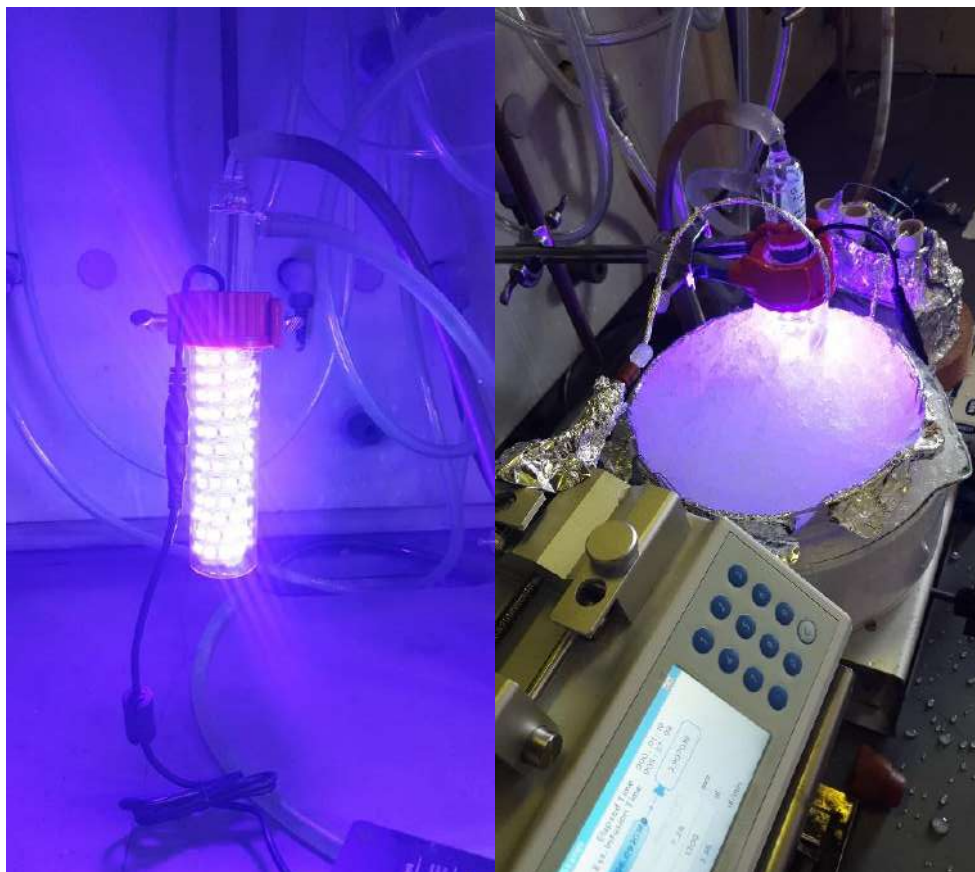
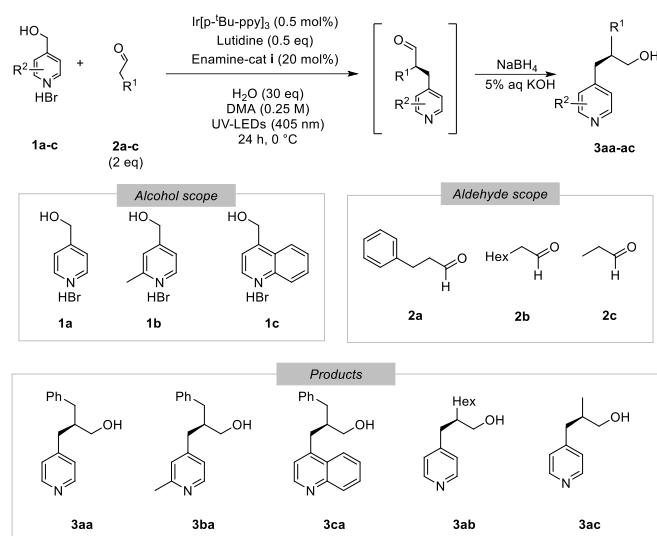


Figure 37. Immersion photoreactor where LEDs are water-cooled and hermetically encased in a glass-tube to allow operation at any temperature in a cryo-/heat-bath.

After determining the best performing LEDs,^[13] a homemade, custom-designed photoreactor was tested under batch conditions before being compared to continuous flow processes (for the description and picture of the photoreactor see the SI).

After 24 hours, the reaction of alcohols 1a-c and aldehydes 2a-c produced products 3aa, 3ba, 3ca, 3ab, 3ac with moderate yields but excellent enantioselectivities, as shown in Table 12.

Table 12. In batch experiments to generate values for benchmarking the reactor in terms of productivity



Entry	Product ^[a]	Yield ^b	ee [%] ^[c]
1	3aa	43%	96
2	3ba	32%	97
3	3ca	32%	96
4	3ab	31%	94
5	3ac	44%	96

^[a] Conditions: 0 °C, 24 h, c=0.25 M - 250 μmol - 1.0 eq 1a-c, 2.0 eq 2a-c, 0.5 eq lutidine, 20 mol% enamine cat., 0.5 mol% Ir[p-Bu-ppy]₃. 5% KOH, 10 eq NaBH₄. ^[b] Isolated yield after chromatography. ^[c] Determined by HPLC on chiral stationary phase.

Following a quick aqueous preparation with phase separation, the samples were purified, evaporated, transferred, and gravimetrically evaluated in a semi-automated, mostly parallelized workflow that was originally designed to purify and evaluate hundreds of molecules per day in library synthesis.^[59] Figure 38 shows an example of this workflow.

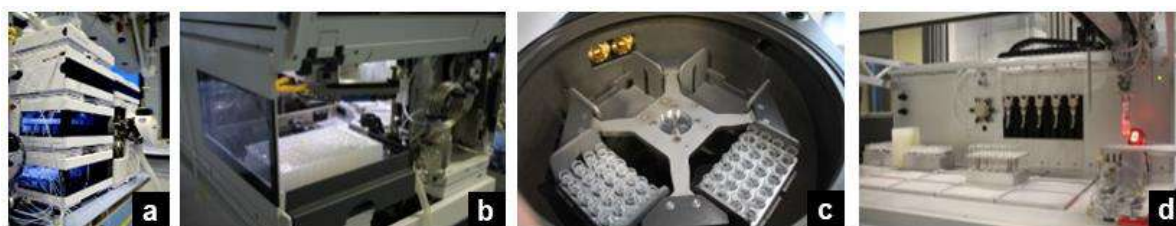
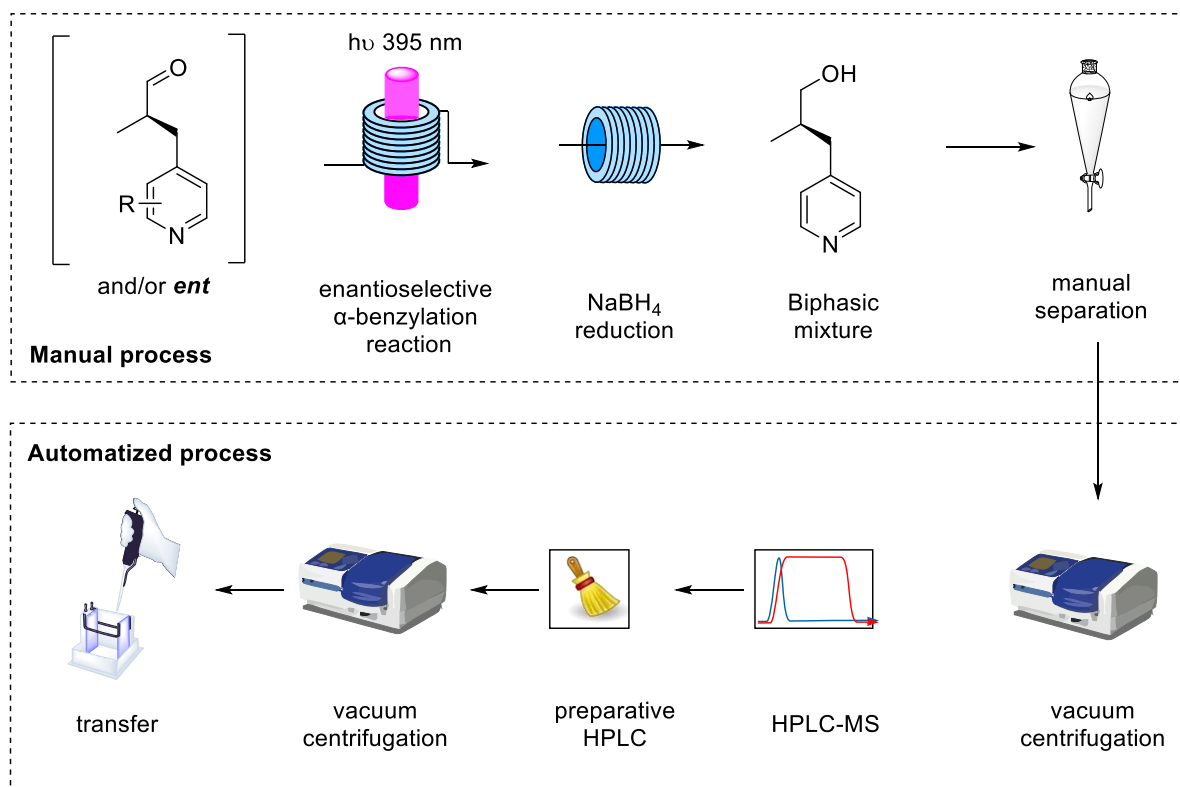


Figure 38. Semi automatized evaporation, purification, evaporation, transferring, weighing, after manual phase separation. (photos left-to-right: a) HPLC-MS , b) Pipetting and weighing robot, c) Vacuum centrifuge, d) analytical preparation sample)

2.3.2. Translation into a Continuous Flow Process

Preliminary considerations suggested that when translating the reaction into continuous flow, using HPLC tubing with different diameters (0,25 - 1 mm), the irradiation efficiency should not be compromised by complete photon absorption.

Based on a few examples of pilot-plant kilogram-scale continuous flow (tubular) photoreactors in industry,^[77,78] perfluoroalkoxyalkane (PFA) HPLC-tubing was chosen for the cryogenic water-cooled photoreactor. Screening under microfluidic and mesofluidic conditions resulted in a 100x fold upscaling of the enantioselective reaction. When compared to batch conditions, microfluidic reactions occur

approximately 20 times faster (60 min for high conversion) (24 h). Only the electron-rich quinoline alcohol, as previously described, has a significantly slower reaction kinetic.^[32]

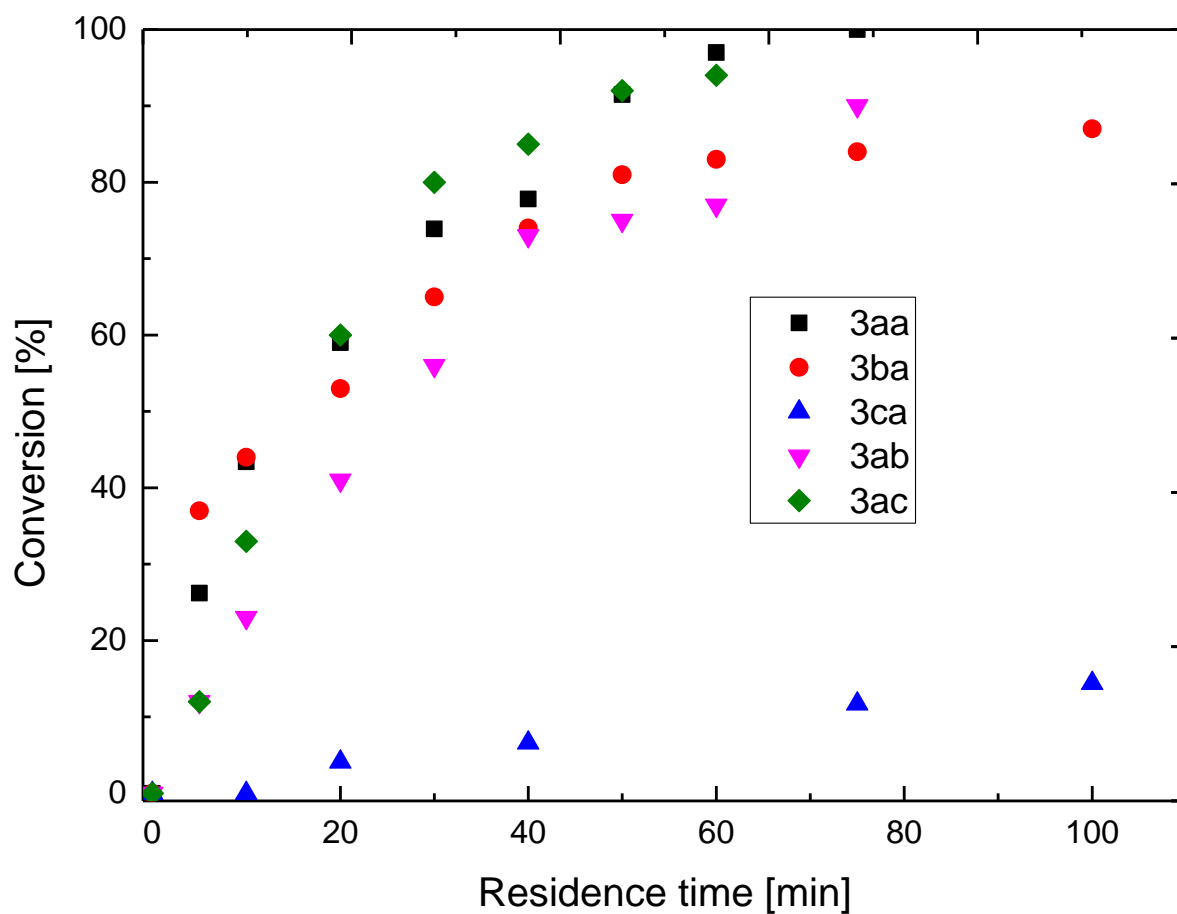


Figure 39. Conversion vs. residence time under microfluidic conditions.

Increasing reaction time at the flatter end of the curve results in only minor increases in (theoretical) isolated yield. The goal of this work is to achieve high productivity while maintaining acceptable levels of conversion. This compromise is best estimated at the point on the conversion curve where the slope changes from steep to flat. Figure 39 depicts the productivity curve of one selected example (3aa).

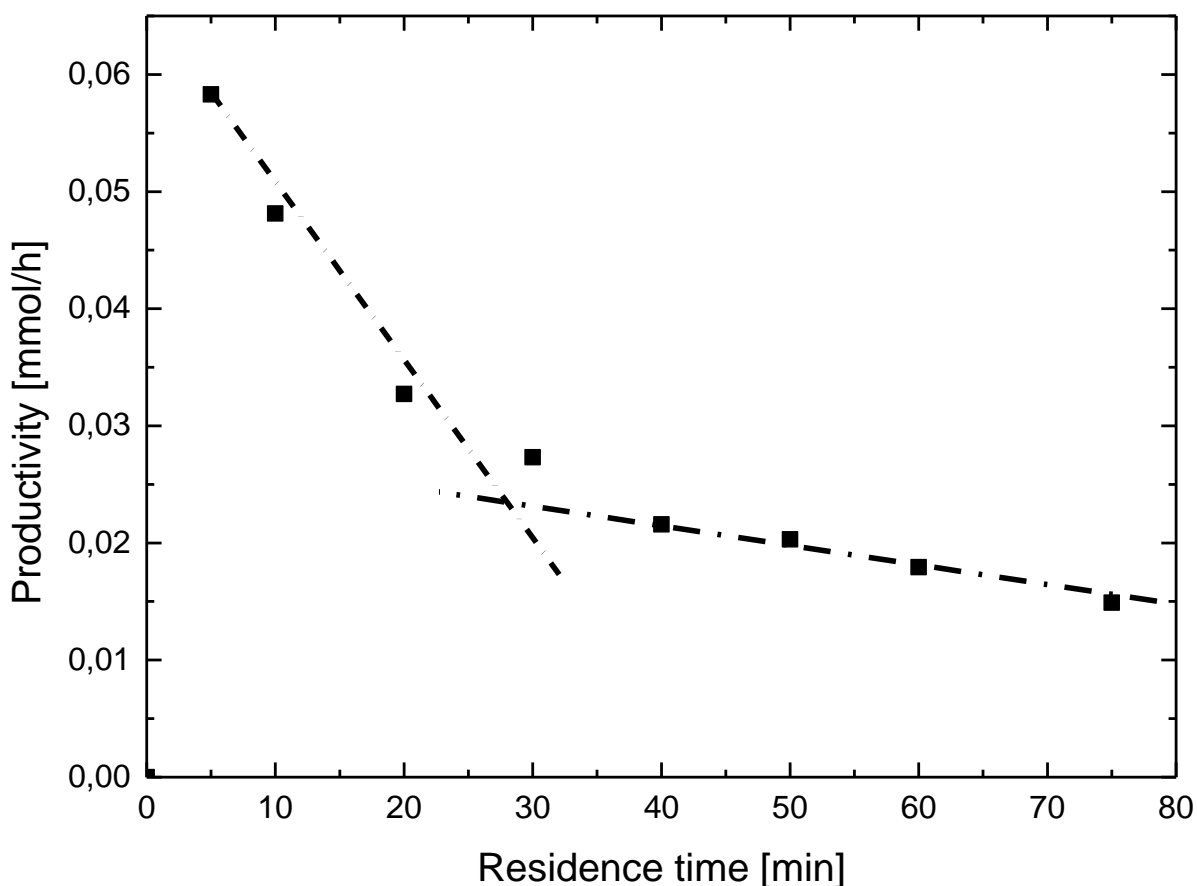
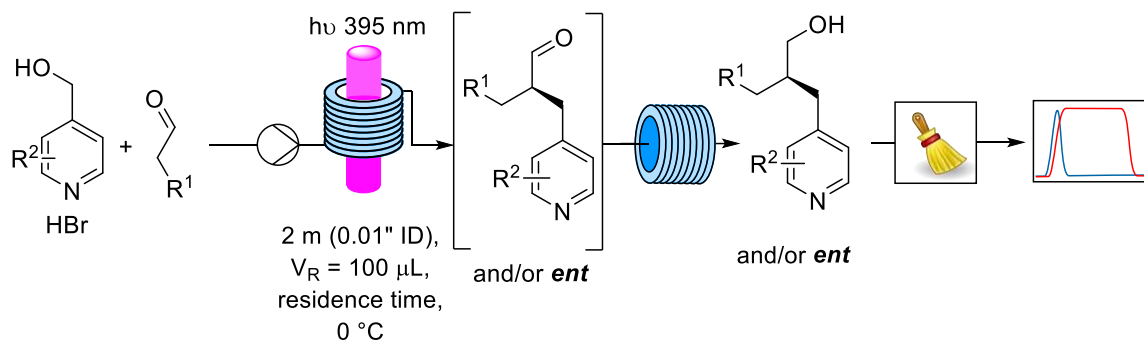


Figure 40. Illustration of the double regression strategy to determine the sweet spot for conversion of molecule 3aa.

The steep slope is followed by a steady decline until the point of flattening is reached in this curve. A double regression strategy was used, with the intersection representing the point at which a steep slope becomes a flatter slope. For this specific example, the best compromise was 30 minutes. With the best compromise conditions available, each molecule was synthesized by collecting the reactor output for the time required to produce the same mole of product (assuming quantitative yield) as under batch conditions for maximum comparability. Table 13 summarizes the results of those experiments. In batch conditions, yields and enantioselectivities are comparable. For the quinoline scaffold 1c, a stop-flow experiment was performed by filling a 1 mL reactor with the reaction mixture and irradiating it for 24 hours, as in batch conditions; the isolated yield nearly doubles due to the increased surface (Table 12, entry 3, table 2 entry 3).

Table 13. Results from the microfluidic experiments to generate values for benchmarking the reactor in terms of productivity.



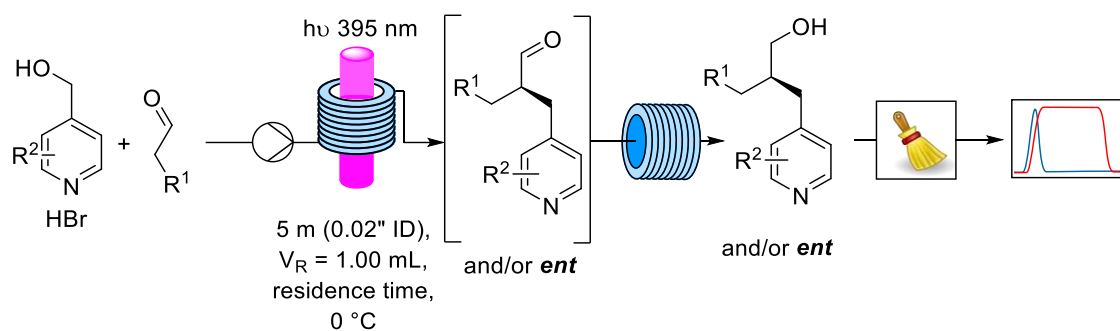
Entry	Molecule	Residence Time [min]	ee [%]	Yield ^[b]
1	3aa	30	98	43%
2	3ba	35	99	55%
3 ^a	3ca	1440	91	62%
4	3ab	40	94	57%
5	3ac	25	96	83%

^[a]Stop flow experiment, reaction time 24 h in a 1 mL Reactor. ^[b]isolated yield after chromatography corrected by conversion. Reaction mixture was collected to get 250 μmol of product, assuming quantitative yield

Following that, a tenfold increase in size was attempted. A reactor with an internal volume of 1 mL was built and tested under microfluidic screening conditions by doubling the internal diameter and roughly doubling the reactor length (Table 14).

When compared to microfluidic conditions, the overall efficiency drops slightly; conducting the reaction at room temperature rather than 0 °C (entries 3 and 7) increased the yield of 3aa while decreasing the yield of compound 3ac. Longer residence times resulted in higher isolated yields and improved productivity for compound 3ac (entries 4 and 5). An additional 50% increase in residence time did not result in significant improvements.

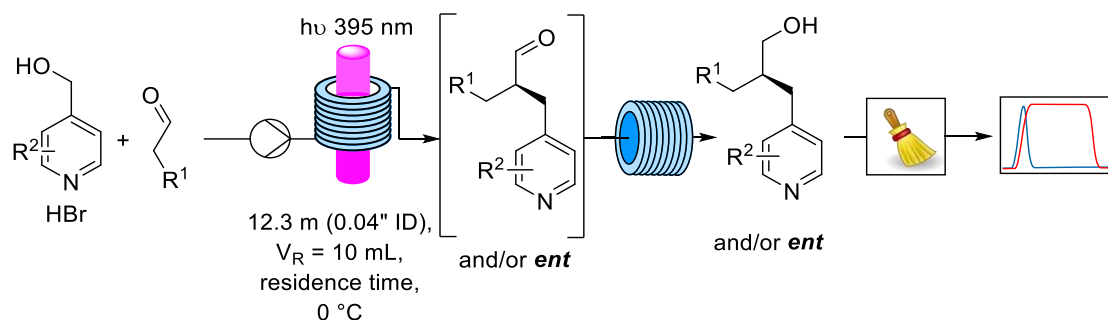
Table 14. Results from mesofluidic (1 mL) experiments to generate values for benchmarking the reactor in terms of productivity.



Entry ^[a]	Molecule	Residence Time [min]	ee [%]	Yield ^[b]
1	3aa	30	98	28%
2	3aa	60	98	47%
3 ^a	3aa	60	96	62%
4	3ac	25	96	31%
5	3ac^b	50	95	64%
6	3ac	75	95	77%
7 ^a	3ac	50	93	31%

^[a]Experiment conducted at room temperature. ^[b] isolated yield after chromatography (not corrected) Reaction mixture was collected to get 250 μ mol of product, assuming quantitative yield

Internal diameter and tubing length were roughly doubled for the next factor 10 upscaling step, yielding a reactor with a volume of 10 mL. Due to the high cost of the photoredox catalyst (\$120/50 mg), the 10 mL reactor was first tested under segmented flow conditions, in which an immiscible solvent (n-heptane) is pumped after the reaction solution. This procedure significantly reduces overall costs and the amount of "waste" generated while collecting the same moles as batch conditions. As shown in Table 15, a slight reduction in efficiency was observed with the 10 mL reactor (35 percent yield vs 47 percent with the 1 mL reactor). Although the isolated yield increased when the residence time was doubled, it was still subpar (entry 3). Using propionaldehyde, the segmented flow transitioned into a Taylor-flow regime, with reaction mixture droplets followed by larger droplets of heptane. Fluorescence of the heptane droplets began to occur as well, indicating the presence of a photoredox catalyst. This observation may help to explain why compound 3ac's overall process is less efficient (entries 4-6).

Table 15. Results from segmented flow (10 mL) experiments.

Entry	Molecule	Residence Time [min]	ee [%]	Yield ^[b] [%]
1 ^[a]	3aa	30	96	21%
2 ^[a]	3aa	60	97	35%
3 ^[a]	3aa	120	97	48%
4 ^[a]	3ac	25	96	8%
5 ^[a]	3ac^a	50	97	25%
6 ^[a]	3ac	75	95	38%

^[a] segmented flow conditions used. ^[b] isolated yield after chromatography. Reaction mixture was collected to get 250 μmol of product, assuming quantitative yield

The results of the segmented flow experiments were directly translated into a standard continuous flow experiment, yielding comparable results (38 percent vs 35 percent in segmented flow), with excellent enantioselectivity (92 percent e.e.). When no flow splitting occurs, the segmented flow method can be used to save reagents while still gaining insight into reactor efficiency and productivity. When compared to the yields achieved by MacMillan et al in the original publication that inspired this work, the isolated yields of most of the continuous flow experiments are rather low. Several contributing factors lowered the yield considerably: When photon flux is considered, the organocatalytic cycle becomes rate limiting. The formation of enamine was found to be slow, and iminium-ion hydrolysis was found to be even slower. There are probably too many benzylic radicals produced. This effect is mitigated under batch conditions by a predominantly "dark" reactor. Side reactions previously described by MacMillan et al became more prevalent (benzylic radical reduction or recombination), resulting in poor overall selectivity. One approach to overcoming this limitation is to build a "darker," more optimized reactor with a better balance of radical generation and the organo-catalytic cycle. As previously stated, a tubular continuous flow reactor has

an increased surface-to-volume ratio of up to two orders of magnitude, making it ideal for photoredox chemistry. Table 16 summarizes the final comparison and judgment of productivities of the various types of reactors, using a similar method to determine productivity as Zeitler et al.^[58] Productivity nearly triples under microfluidic conditions (low reactor volumes). Every factor 10 increase in productivity that followed was seamlessly translated. The 10 mL mesofluidic reactor can increase productivity by nearly 18000 percent while maintaining stereochemical efficiency, giving the product > 95 percent e.e. This seamless upscaling was further demonstrated when the realized space-time-yield (STY) was considered, which is an excellent metric for comparing reactors of different volumes. As shown in Table 16, there was a significant increase in STY when switching from batch to microfluidic (x33). Every factor 10 upscaling only resulted in a 20% decrease in STY, indicating that upscaling by increasing the length and diameter of the tubing worked flawlessly. Again, when considering photon-flux and transmission behavior, even at the 10 mL meso-fluidic reactor with a diameter of 1 mm, there are plenty of photons available, resulting in a "bright" reactor. Increasing the diameter of the tubing is obviously no longer a viable option due to the negative exponential attenuation of photons at some point. As a result, industrially sized continuous-flow (tubular) reactors frequently deal with tubing that is hundreds of meters long.^[77,78]

Table 16. Numerical comparison of productivities of different reactor types and of normalized relative factors.

Entry	Method	Productivity ^[a] [mmol/h]	Rel. Factor	STY ^[b] [mmol/mL*h]
1	Batch	4.0E-3	1	3.7E-3
2	Microfluidic	1.2E-2	2.8	1.2E-1
3	1 mL Meso	9.4E-2	22	9.6E-2
4	10 mL Meso	7.6E-1	177	7.8E-2

^[a] Productivity as in moles of product (calculated from isolated yield) divided by the collection time it took to collect 250 μ mol of product, assuming quantitative yield.^[b] Space-time-yield as in moles of product in reactor, divided by residence time and reactor volume.

2.3.3. Fully Telescoped, Fully Continuous Photoorganocatalyzed API Synthesis

We decided to use a fully telescoped continuous process after developing an efficient, highly enantioselective in-flow protocol for alkylation of aldehydes. Figure 40 depicts a chiral patented API with the 4-methylpyridine scaffold,^[79] a favored motif in several APIs.^[31,32] At nanomolar concentrations, the compound inhibits cyclin dependent kinase 9, making it an effective API for a potential cancer drug.^[80] The published synthesis consists of six linear steps (6 percent overall yield), the final of which is a low yielding Buchwald-Hartwig type aromatic amidation (Scheme 34). To the best of our knowledge, no previous article on a stereoselective photoredox organocatalytic continuous flow reaction in a telescoped process for an API has been published.

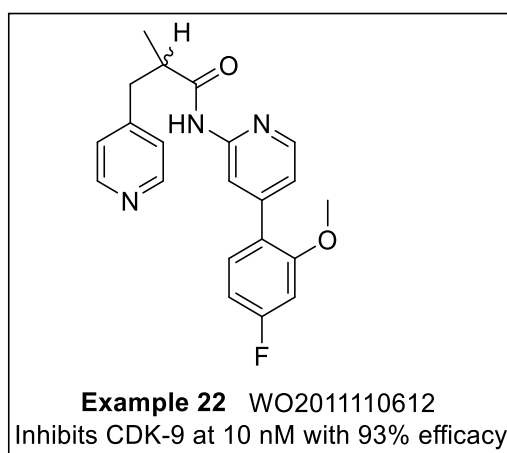
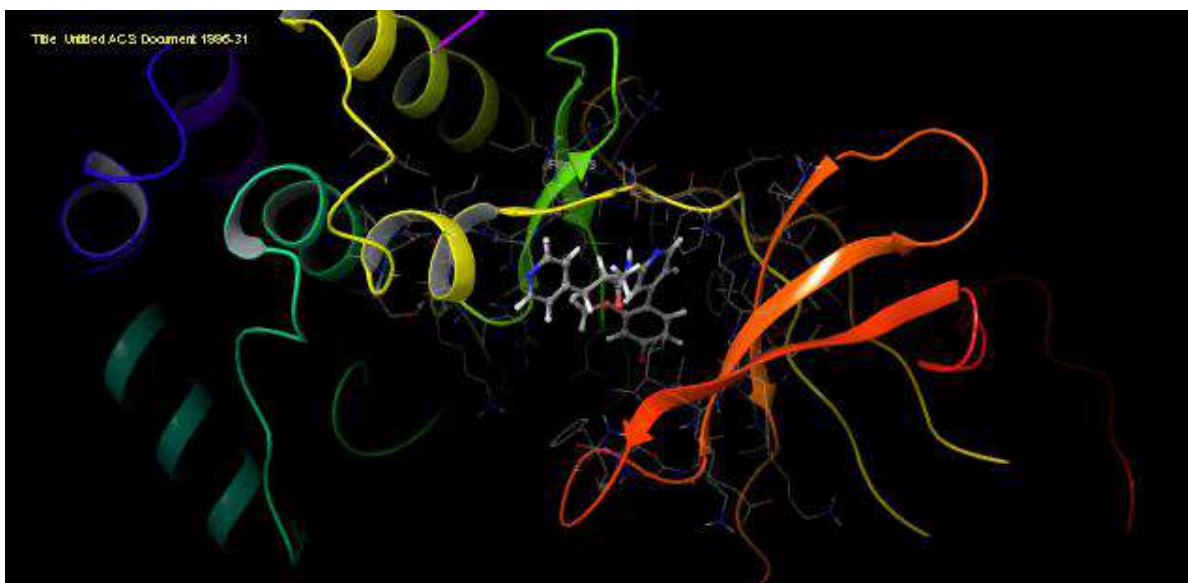


Figure 41. Chemical structure of the API for which the telescoped process was to be developed.

- Leland H. Hartwell, J. Hoonhorst, R. Timothy Hunt, and Paul M. Nurse received the 2001 **Nobel Prize in Physiology or Medicine** for their complete description of **cyclin and cyclin-dependent kinase mechanisms**, which are central to the regulation of the cell cycle.
- Inhibiting CDKs can be an effective anti-cancer therapy
- Pfizer (2015), Novartis (2017 and Lilly (2018) have CDK-Inhibitors in the market.

Nobel Prize, Recent market releases, Photoredox chemistry, Continuous Flow

- No record in Literature for the photoredox- and organocatalyzed, continuous asymmetric synthesis of small molecule antagonist.



(R)-Example22 DockingScore=-10.557 Kcal/mol



(S)-Example22 DockingScore=-10.311 Kcal/mol

Figure 42. Molecular docking studies(High Precision mode) using the Schrödinger Software suite to possibly determine which stereoisomer bind preferably to CDK-9.

A Molecular docking study, as detailed in Figure 42, was undertaken to possibly determine which of the stereoisomers of the API will bind preferentially to CDK9. The difference in docking score of only 0.34 Kcal/mol is not a significant difference. In the binding pose the residue where the pyridine motif is located is pointing into two different directions for each stereoisomer.

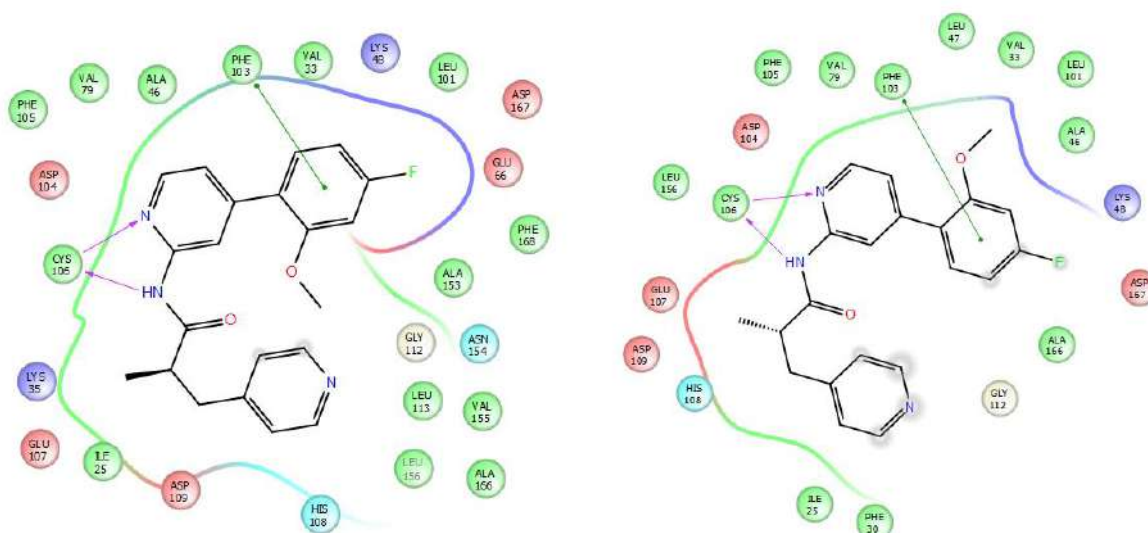
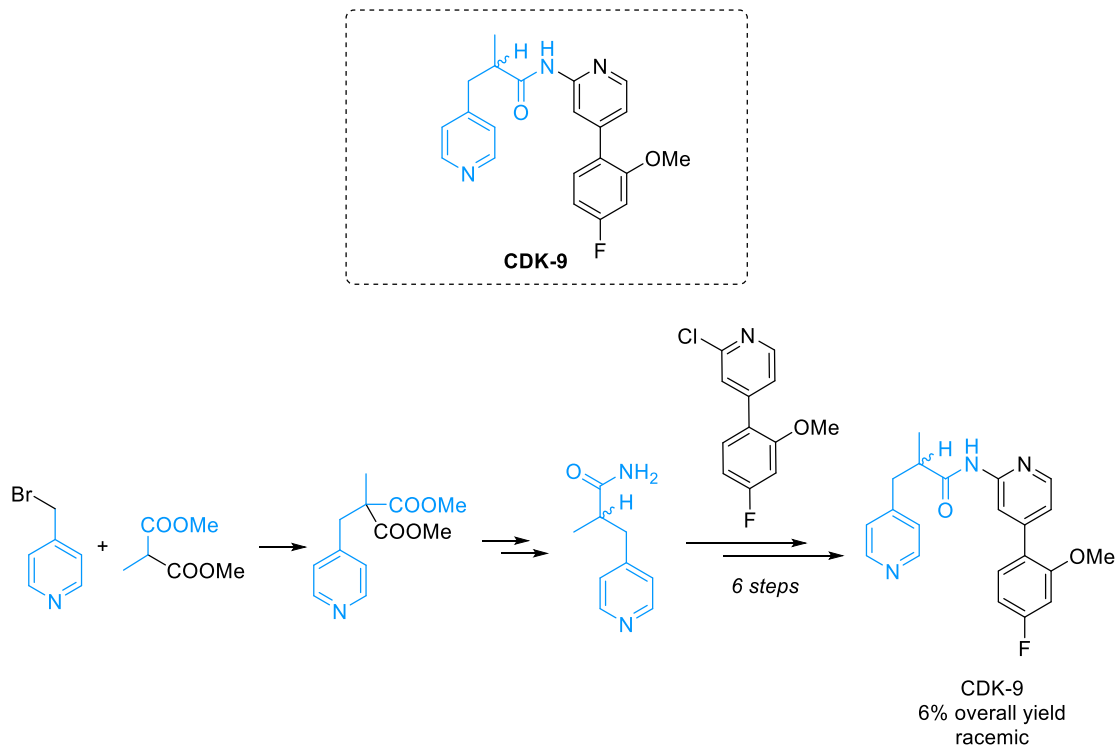


Figure 43. Interaction diagrams of (*R*)-enantiomer (left) and (*S*)-enantiomer (right). Noteworthy are the two different orientations in which the fluorinated aryl moiety is bound inside the hydrophobic binding pocket.

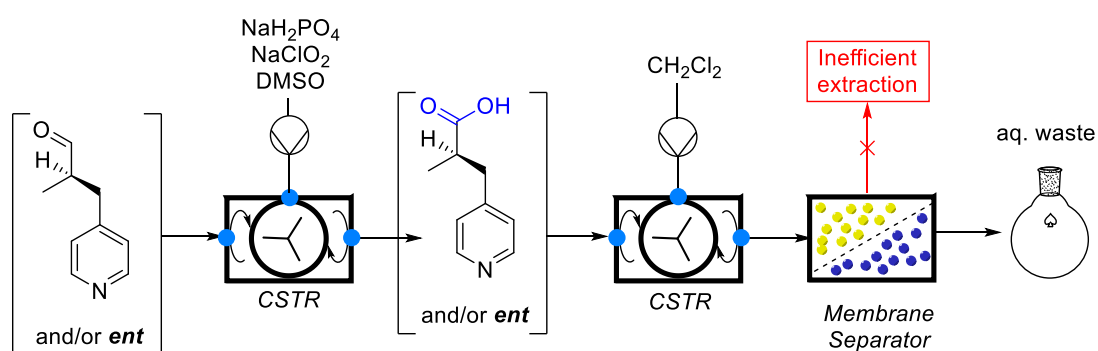
The same conclusion can be drawn when considering the interaction diagram displayed in Figure 43. The aminopyridine building block is bound almost the same, while the pyridine moiety does not show any strong directionality.



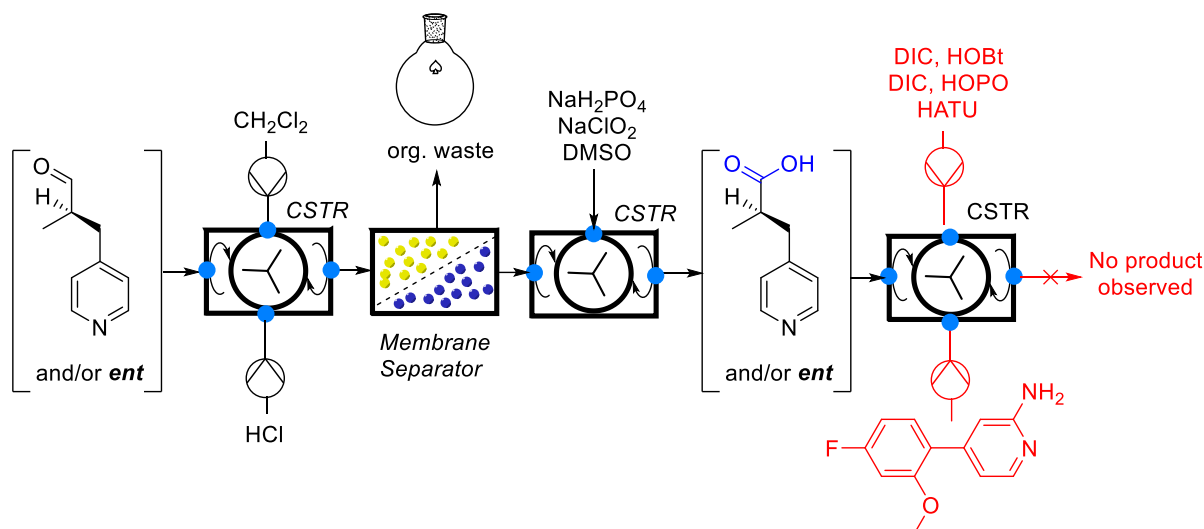
Scheme 34. Synthesis of a patented API for a potential cancer drug.

To prevent the critical epimerization of the aldehyde, a first approach involved oxidizing it to carboxylic acid. The carboxylic acid was to be reacted with the aminopyridine building block in an amide coupling. As shown in Scheme 33, two distinct strategies were tried and failed. In the first attempt, the entire reaction mixture was pumped into a continuous stirred tank reactor (CSTR) and reacted with a sodium chlorite solution for the mild and selective Pinnick oxidation, which is known for preserving stereogenic center integrity. While the oxidation was highly efficient, the subsequent continuous phase separation with a membrane separator did not go well, most likely due to the carboxylic acid's zwitterionic nature.

Strategy 1: Pinnick-Oxidation then inline extraction into organic phase then amide coupling



Strategy 2: Inline extraction into aqueous phase then Pinnick oxidation then amide coupling



Scheme 35. Attempted oxidation – amide coupling strategies.

The aldehyde was first extracted with high efficiency into the aqueous phase using the same continuous membrane separator by pumping in an acidic buffer sodium phosphate solution in the second approach. Because most of the reagents remained in the organic waste, this extraction step significantly cleaned the reaction mixture. The aqueous phase was then used in continuous operation to carry out the Pinnick oxidation; however, all attempts to achieve an aqueous amide coupling failed.^[81,82] Figure 44 depicts a failed attempt to obtain at least the hydroxy pyridine N-oxide (HOPO) active ester.

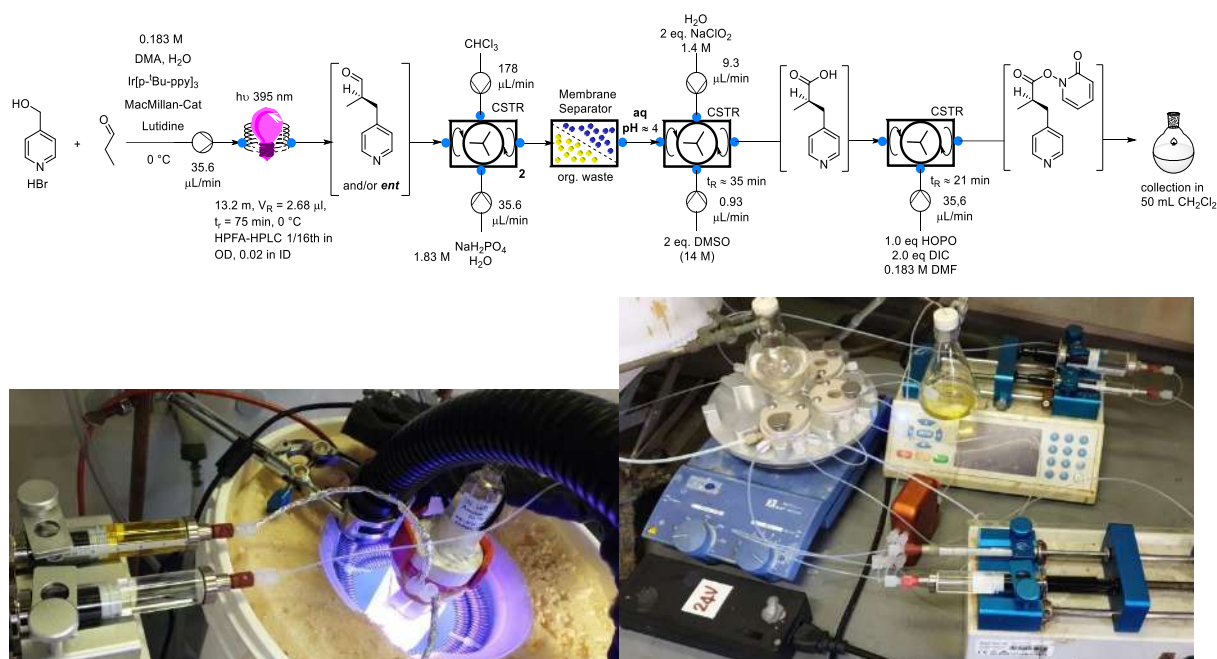
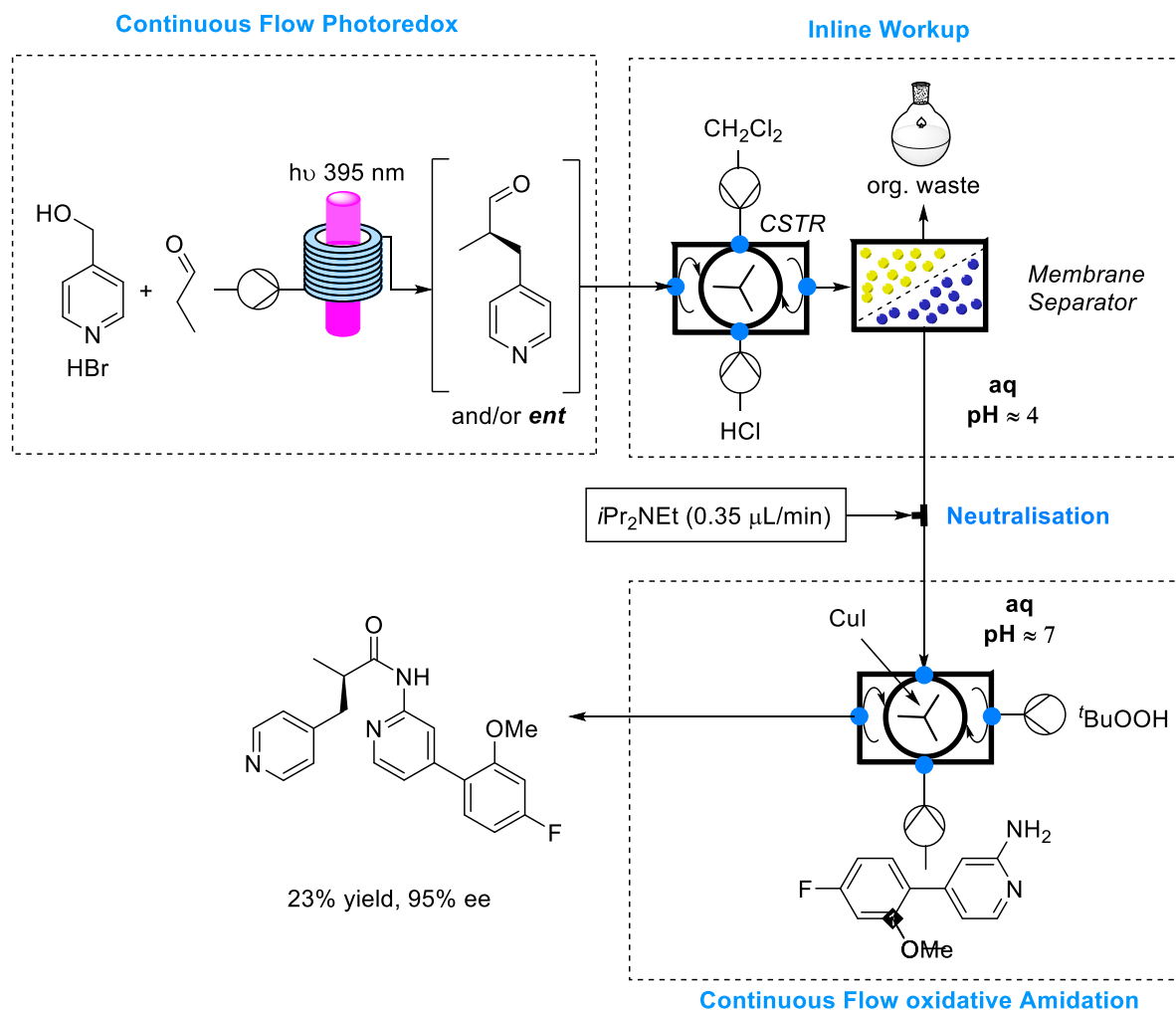


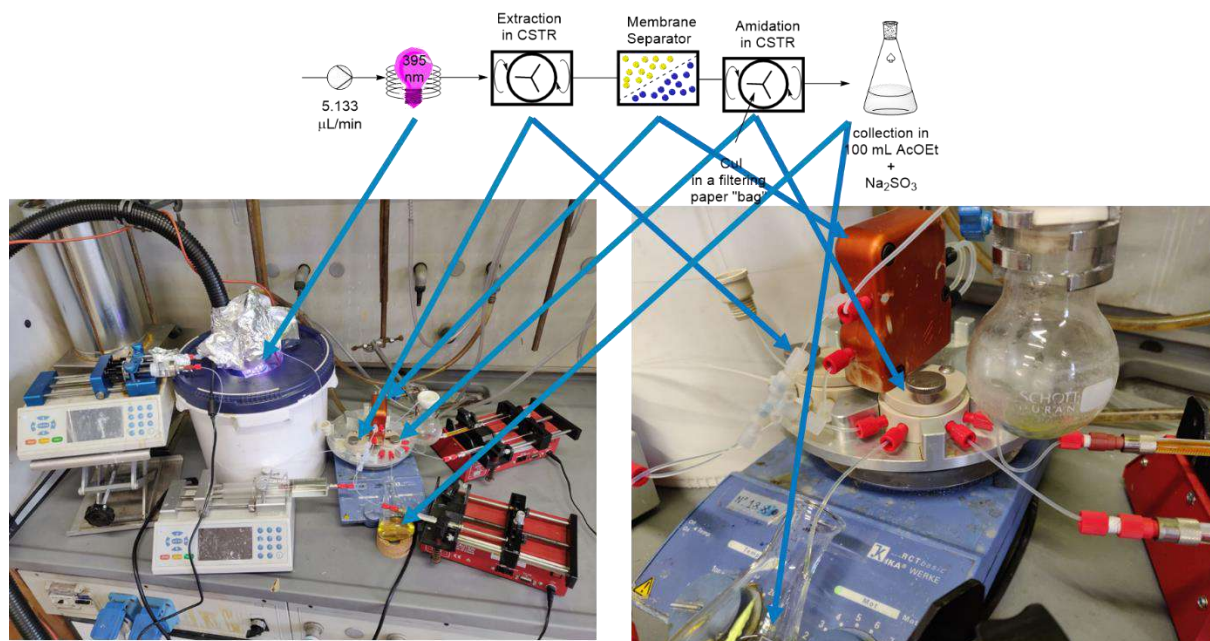
Figure 44. Schematic representation and photographs of the unsuccessful telescoped synthesis of the HOPO-active ester precursor molecule for the final API.

As alternative strategy, we investigated the direct oxidative amidation of aldehydes with aminopyridines catalyzed by Cu(I) in combination with *tert*-butyl hydroperoxide (Scheme 36).^[83]



Scheme 36. Fully telescoped, fully continuous synthesis of a privileged API.

After some successful batch reactions, this methodology was incorporated into the continuous flow process, and the fully continuous, fully telescoped process to synthesize a complex API was realized. The final process consists of four operational units: asymmetric benzylation in continuous flow, inline continuous work-up, neutralization, and the final oxidative amidation (Scheme 36). The final product had a 23 percent overall yield and a 95 percent ee. By removing four linear steps, the overall yield was increased by a factor of four, demonstrating the potent methodology of stereoselective benzylation *in continuo*.



Scheme 37. Photograph with indicators for the individual parts of the telescoped process.

2.4. Photochemistry *in Continuo* Deep Dive – A Critical Examination of Important Parameters

2.4.1. Introduction to the Field

Photochemistry experienced a sudden renaissance more than one decade ago by the outstanding publication in *Science* by David MacMillan, showcasing a particularly useful chemical transformation that is otherwise difficult to achieve.^[74] The only problem with photochemistry is the extraordinarily challenging upscaling – which can be done efficiently only when exploiting the higher surface area of continuous flow reactors as detailed by Seeberger and Noël in their famous reviews respectively.^[7,12] Traditional upscaling under batch conditions is not viable due to the excessively prohibitive negative exponential light attenuation through matter as described by the Lambert-Beer law. König recently asked the provocative question “Visible-Light Photocatalysis: Does It Make a Difference in Organic Synthesis?” and compared classical approaches versus their photochemical analogues and found generally milder reaction conditions,^[84] all while Rehm recently also reviewed the possibility of the strategic usage of photochemistry in flow in organic synthesis and also summarized the reactor technologies to do so efficiently.^[85,86] More than a century ago the legendary Giacomo Ciamician dreamed of a solar photochemistry of the future where most of humanity’s need for chemicals comes directly from the sun itself.^[1] Even though we are far from reaching this dream, considerable steps forward have been achieved as recently summarized by Noël.^[87] Sometimes the combination of photochemistry with more traditional fields in chemistry such as heavy metal catalysis gives rise to astonishing reactivity such as N-Aryl coupling chemistry or decarboxylative sp^2 - sp^3 -cross coupling reactions both first introduced in *Science* by David MacMillan.^[88,89] Of the latter was recently developed an enantioselective version by MacMillan.^[90] These new reactivities are so powerful that recently it came to a sudden boom in publications regarding the upscaling to beyond kilogram-scale in industry, always employing flow conditions, with even some cross industry and cross border collaborations. To our delight the niche existence of photochemistry has come to an end – by great engineering and chemistry endeavors. To name some of the most

outstanding examples: Merck's two different kilogram photo-flow-reactors,^[77,91] Merck's, Eli Lilly's and Macmillan's cooperation regarding an automatized batch protocol that accurately mimics flow conditions,^[92] GlaxoSmithKline's and Astra Zeneca's small footprint UV-reactor for kilogram-scale reactions,^[93] Abbvie's Laser driven process inside a continuous stirred tank,^[94] and lastly Corning Reactor Technologies' and Kappe's multi-kilogram per hour reactor.^[95] The popularization of photochemistry in flow has also moved way beyond the level of chemistry/chemical engineering journals, academia and industry, for example by the two Ted^x talks (a platform that has billions of views) given by Noël and Gupton to a wider audience explaining their dreams of a medicine-on-demand flow chemistry platform for the synthesis of pharmaceuticals or the same dream as Ciamician regarding a brighter and greener future with the usage of solar (flow)chemistry.^[96,97] Science Communicator and YouTube legend Sir Martin Poliakoff, a distinguished Professor in green chemistry, recently published a study in Nature Chemistry about a continuous photocatalytic green synthesis of Artemisinin with the respective YouTube video (elegantly titled "Fighting Malaria with Green Chemistry") gaining hundreds of thousands of views.^[98,99] Also Poliakoff and Green together recently published a photochemical route to new lactones at the multi-kilogram scale in flow reactors.^[100] In the authors' opinion photochemistry in flow has made the breakthrough in industry. Therefore, the presented work in this study shall serve as a practical guide on how to scale-up photochemical reaction *in continuo* by showing the critical parameters, how to measure them, how they should influence decision making and explain the pitfalls if those are being ignored by the chemist/engineer.

2.4.2. Explanation of Methodology

Before detailing the exact methodology employed in this study it is first of utmost importance to understand exactly why scaling a photochemical reaction is so extraordinarily challenging. In Figure 45 is plotted the transmission of light through a reactor as a function of the reactor width/pathlength and as a function of the product of concentration and the molar extinction coefficient ϵ (note the double logarithmic scales). The white line intersection between the green part and the red part marks the 1% transmission threshold where a photoreaction could be seen still viable. As in general reactor productivity scales linearly with the reactor volume and concentration, high reactor diameters and concentrations are preferable. The graph visually explains why we can only have one of the two. Only at low concentrations (and/or low molar extinction coefficient ϵ) we can have a “thick” reactor. Likewise, only at narrow reactors we can have concentrated solutions (and/or high molar extinction coefficient), otherwise, the reactor will be inside the red zone and not receive any kind of efficient irradiation. It must be noted that if the dimension of the reactor is sufficiently low and the reaction kinetics dictate a rather slow reaction, mixing by diffusion completely counteracts the phenomena. An addition to this statement would be that at industrially sized reactors diffusion mixing (due to the thick reactors) can often be considered negligible.

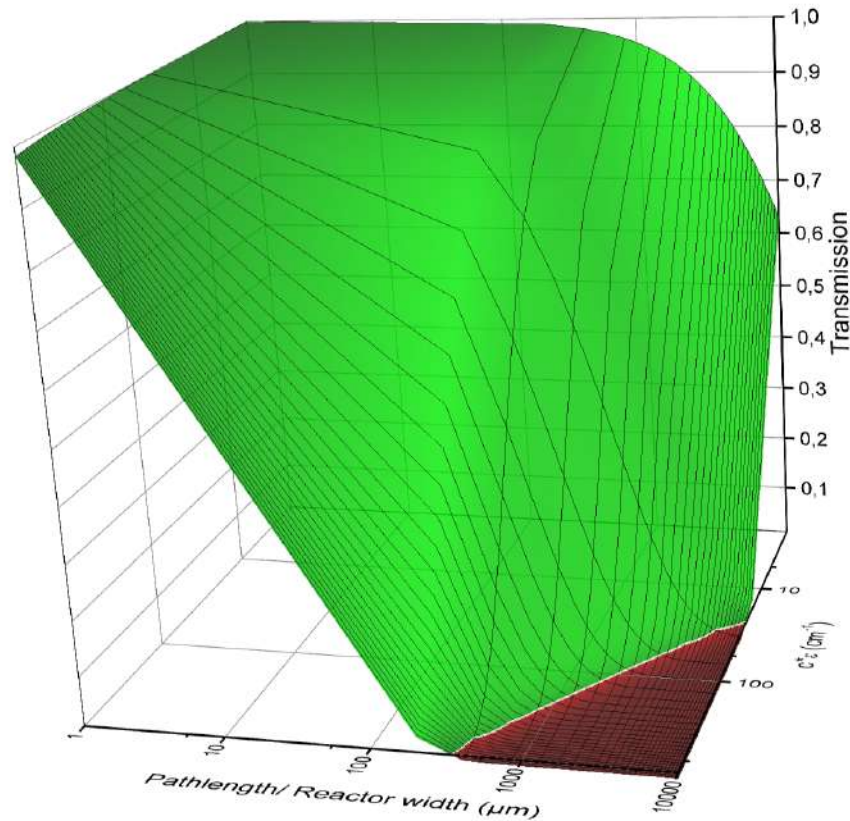


Figure 45. 3D-Graph of transmission as a function of pathlength and concentration times the molar extinction coefficient.

Which physical quantities constitute an efficient reactor? In general reactor productivity P can be described by:

$$P = \frac{n_{prod}}{t_R}, \quad \frac{P}{V_R} = STY = \frac{n_{prod}}{t_R V_R} \quad \text{Equation 22}$$

with n_{prod} : moles of product, t_R : residence time and V_R : reactor volume. Likewise, a productivity dependent on reactor volume can be defined as space-time-yield (STY), which is a metric comparing directly different reactors with each other and giving a good indication of which reactor should be used for upscaling purposes. By algebraic substitution STY can be further changed into:

$$STY = \frac{q c_{prod}}{V_R} \quad \text{Equation 23}$$

With q : volumetric flow rate and c_{prod} : concentration of product. An elegant (yet simplistic) way to look at a photochemical reaction is to set into relation the molar flowrate of substrate that enters the reactor (left side) and the “molar flowrate” of

photons (also known as photonflux or photon-density) that enter the reactor (I_R), that get absorbed ($1-T$) and that will lead to a product molecule (\emptyset). In the most efficient photoreactor imaginable the two are the same, like indicated below. In this case you can estimate the molar flowrate of your desired product that flows out of your reactor after the reaction.

$$q c_0 = \emptyset I_R (1 - T) = 1 \rightarrow c_0 \cong c_{Prod} \quad \text{Equation 24}$$

It is not surprising that at a certain point in your upscaling endeavors your reaction rate will be limited by the power of your photoreactor which directly translates to the amount of photons (“molar flowrate of photons”) that enter your reactor. After algebraic substitution you will get the following relationship:

$$STY = \frac{\emptyset I_R (1 - T)}{V_R} \quad \text{Equation 25}$$

The term $\emptyset I_R (1 - T)$ is central to this piece of work. Understanding it is the first step to then exploit it later. \emptyset is called the quantum yield and we have little control over it as it depends mostly on the chemical reaction. It is a numerical representation of the fraction of absorbed photons that will lead to a product molecule. I_R is called the photonflux in your reactor. It depends on the Light source you use, the number of it, the reactor geometry, reflectance of the reactor material. It is a quantity that is difficult to simulate but at a later point it will be explained how this quantity can be obtained. The last term ($1-T$) dictates how many photons will be absorbed by your reaction mixture. As it is the most straightforward tool in photochemistry in continuous flow, the presented work will focus on the exploration of the effects it may have on a photochemical process.

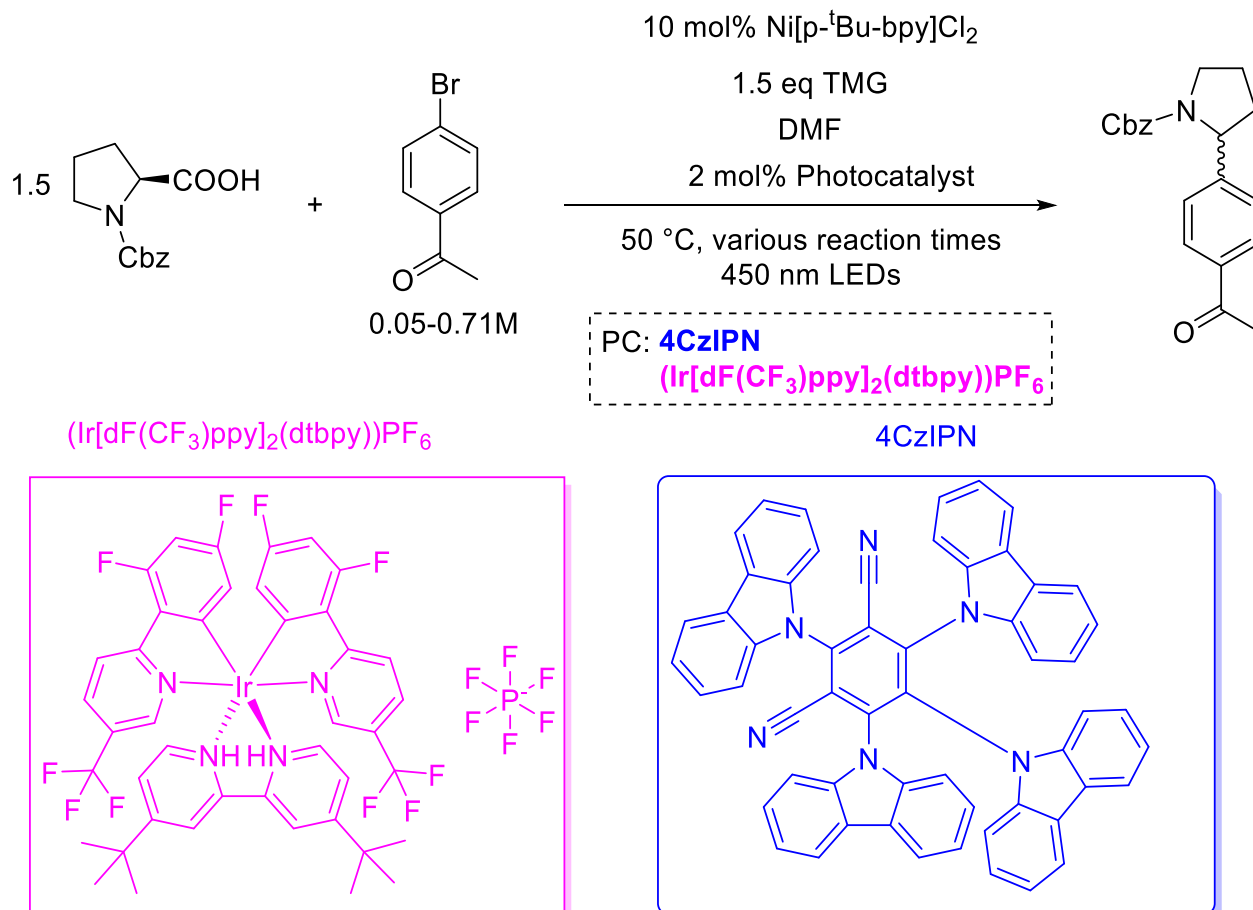
$$T = 10^{-\epsilon c l} \quad \text{Equation 26}$$

If considered that Transmission T scales negative exponentially with the molar extinction coefficient ϵ , concentration c and optical pathlength l the most drastic differences in reactor performance can be achieved just optimizing this term.

MacMillan’s decarboxylative cross-coupling reaction shall serve as the perfect chemistry to choose for this study.^[89] It is as previously detailed of great industrial interest, the reaction was extensively optimized in batch and *in continuo*,^[92,101] it was described to work with different photoredox catalysts that possess significantly different

molar extinction coefficients and it is robust against water and oxygen (the latter even being required for catalysts turnover).^[102] The exact conditions are detailed in Scheme 38. It must be highlighted that this study is not about the chemistry!

MacMillan's decarboxylative sp^3 - sp^2 -cross-coupling by merging Ni- and photoredox-catalysis



Scheme 38. Showcasing the reactions conditions. Note the general color coding in this scheme will apply to the rest of this study with the Ir-PC being violet due its absorption maximum at 390 nm and 4CzIPN being blue due its absorption maximum being at 440 nm.

To showcase the drastic difference in performance the chemist/engineer may obtain in a photochemical process we wanted to engage in a play/simulation in three acts. More and more thought will be invested with each act:

Act I – Translating into Continuous Flow **ignorant of all critical parameters** (ϵ , photonflux I_0 , Reactor diameter)

Act II – Measuring ϵ of reaction mixture more wisely choosing concentration of Reaction mixture and Reactor diameter **making sure reactor is not too dark/bright**. Using different Photocatalysts with different ϵ to show how it affects the performance.

Act III – Measuring the photonflux inside your Reactor and thus **knowing the limits** of your reactor capabilities. Using photons as an effective scaling method.

Finally a comparison of the different approaches - Knowing the Lambert-Beer-Law drastic differences are expected. **How bad of a Reactor can you build** is basically what this study is supposed to showcase!

2.4.3. Description of Equipment

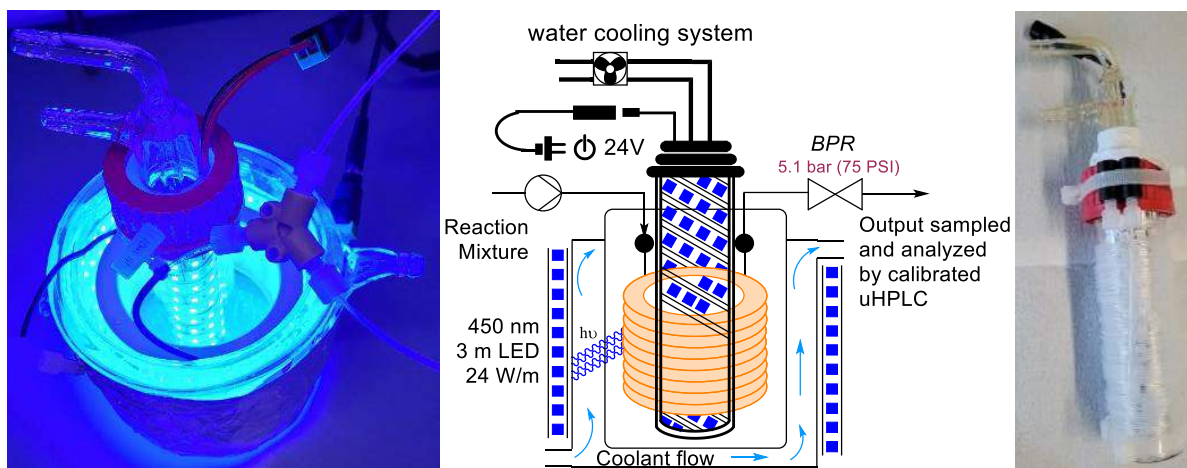


Figure 46. Depiction and photographs of the continuous flow reactor (plug-flow) and the photoreactor setup.

We chose to irradiate with blue light at a maximum of 460 nm where both the photocatalysts (4CzIPN+Ir) are absorbing. To render the process more efficient it was irradiated from both sides of the plug flow reactor. For this two distinct photoreactor were used as demonstrated in Figure 46, one irradiating from inside out (right), the other one from outside to the inside (left). As temperature control was important, the LEDs were attached to jacketed, double-walled glassware so that a cooled/heated liquid could be passed through them. These photoreactor were originally designed for cryo-operation in our laboratories.^[103] Essentially the temperature of the liquid circulating inside can be self-regulated. In the case of running the reactions *in continuo* conveniently when no circulation of water was occurring the temperature inside the

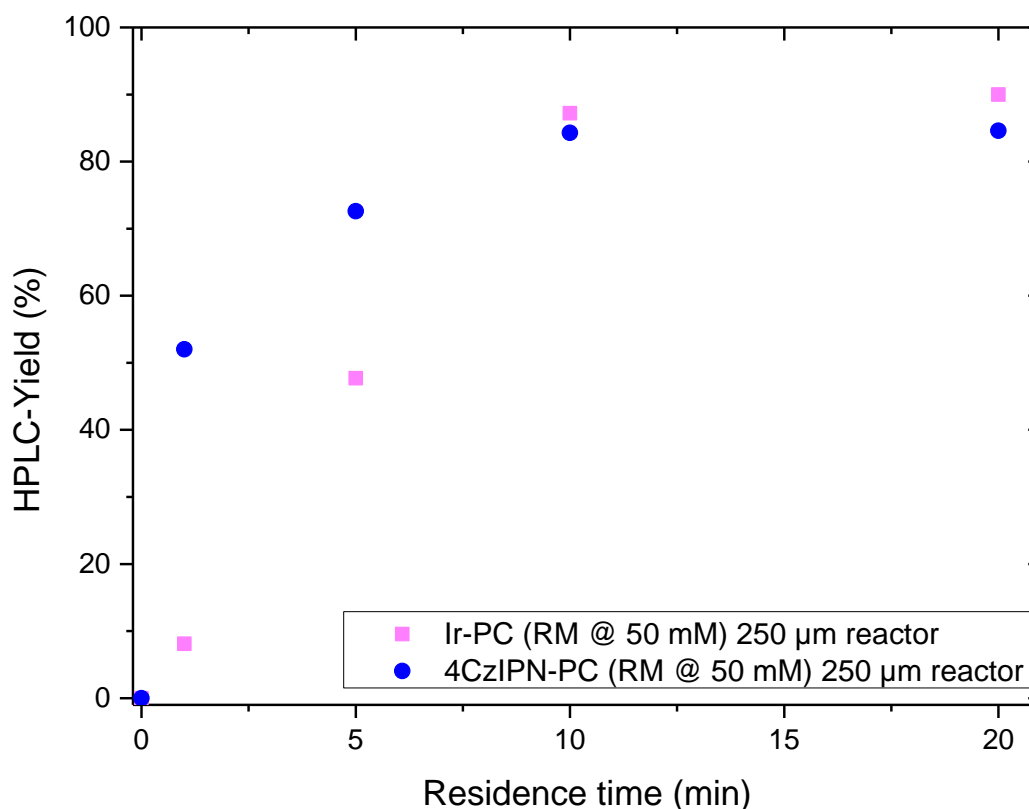
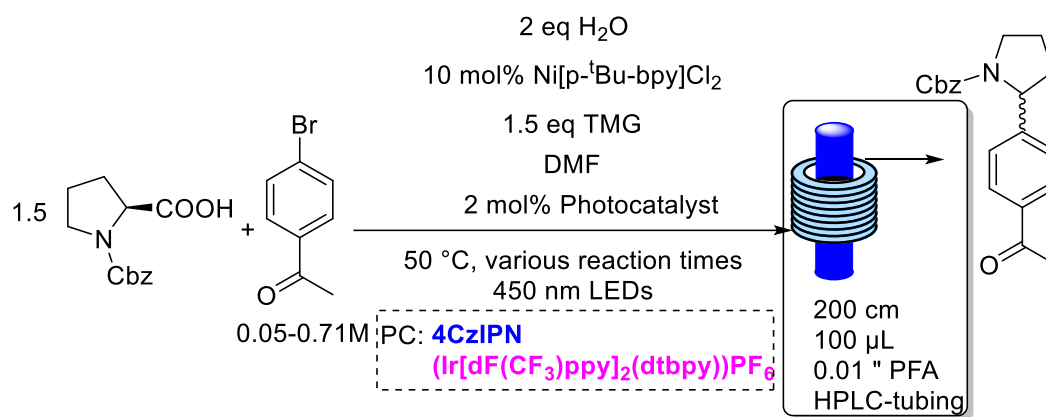
reactors equilibrated to around 50 °C due to the LEDs' 72 W of electrical power consumption. To the different plug flow reactors was connected either a syringe pump (microfluidic) or a VapourTec EasyScholar peristaltic pump delivering the reaction mixture. As significant amounts of carbon dioxide are formed when running the reaction, a back-pressure regulator giving 5.1 bar of counter-pressure to keep the mixture homogeneous. After the output was collected it was directly injected into a uHPLC employing a similar protocol as was previously described (internal standard).^[77] A more detailed description of the experimental Setup can be found in the supporting information.

2.4.4. Act I – Dark Ages – Light Ages, Who Knows?

As previously outlined in the first act, the scientist does not know whether the reaction mixture absorbs too many/too little photons. The original batch set-up from MacMillan was recreated – 20 mL of reaction mixture inside a 50 mL round-bottom flask, moderate stirring speeds (not specified) and irradiating from all sides. Not surprisingly under these conditions the reaction proceeds sluggishly. As detailed in Table 17 after 23

Table 17. Batch experiments for benchmarking purposes.

Entry	Catalyst	Reaction time [h]	HPLC-Yield
1	Ir-PC	23	77
2	4CzIPN	23	75



Scheme 39. Depiction of the reaction conditions with reactor specifications under microfluidic conditions. Depiction of reaction progress as a function of residence time.

In contrast, when performing the reaction under microfluidic conditions the reaction accelerates by a remarkable amount. Instead of taking 23 h until high levels of yield, it now takes only 10 min to reach even higher levels, as displayed in Scheme 39. This corresponds to a whopping factor x150 increase in space-time-yield. One could argue we are off to a good start – what else is there to come?

2.4.5. Act II – Renaissance

In general, when the reader is interested in a physicochemical and engineering approach to the herein described principles, Noël's recent summary is a good read.^[104] In the present study the underlying principles will be explained in a more illustrative and graphic way to help scientists who are new to the field to understand and give a point of reference to be able to return to always.

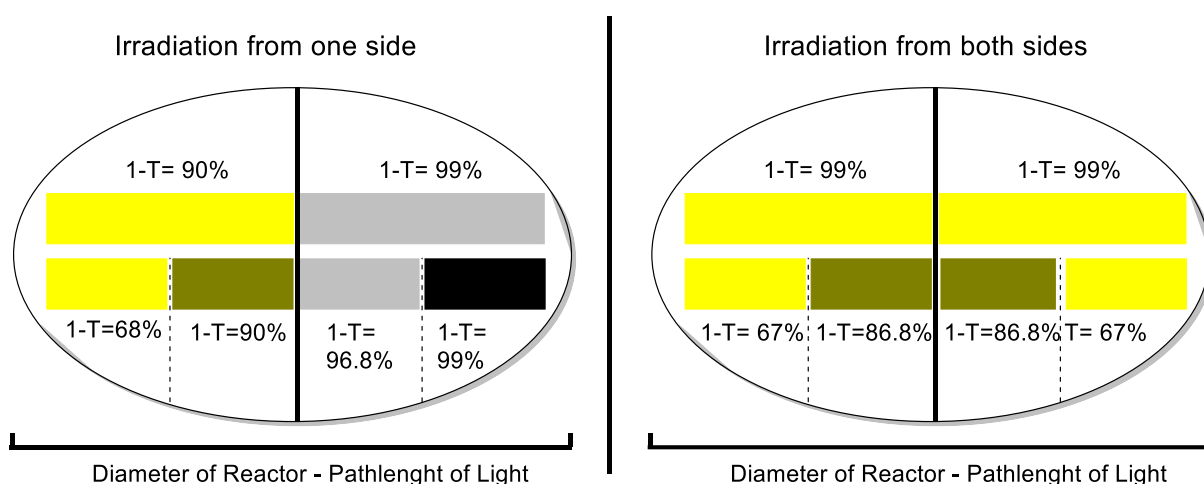


Figure 47. Transmission (T) profile of a reactor cross-section. Left is displayed the case where irradiation is taking place only from one side of the reactor. Right is displayed the case where irradiation is taking place from both sides of the reactor. Dark zones, as characterized by low transmission zones, are much less prevalent on the right side.

A key issue that is often overlooked is the topic irradiation from one side against both sides. As depicted in Figure 47, the transmission profile of a photoreactor changes completely when irradiating from both sides. In this example the basic assumption is that at the given reactor diameter the measured transmission is $T=1\%$ ($1-T=99\%$). In the left example half of the reactor experiences insufficient irradiation while in the right example both reactor-halves experience sufficient irradiation. When the dimensions of the reactor are sufficiently small the effects of insufficient irradiation are counteracted completely by diffusion.

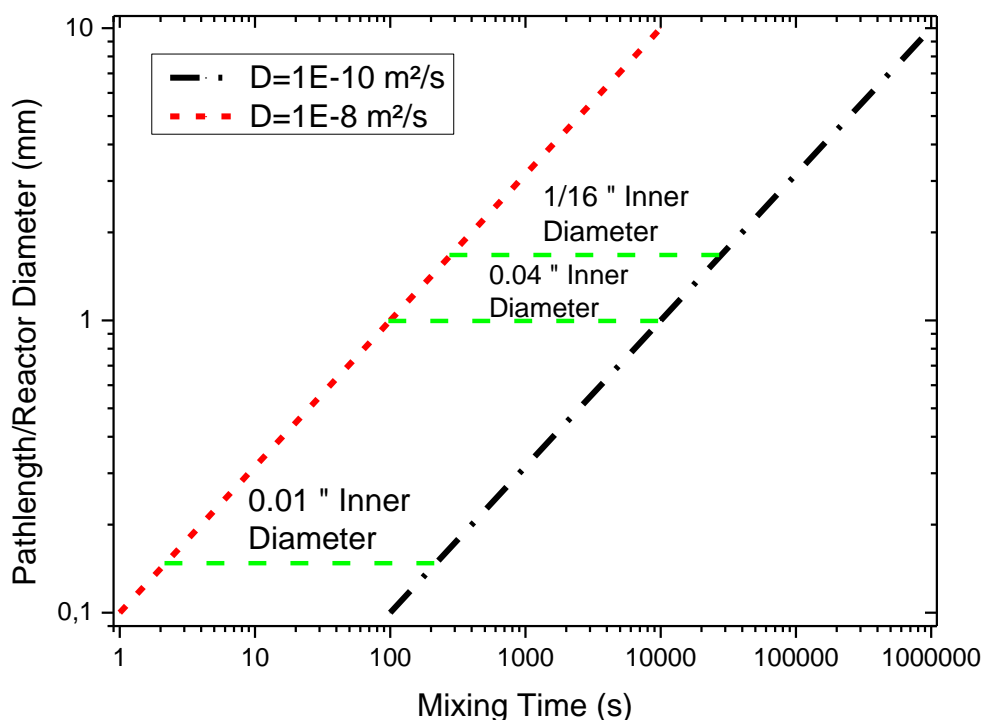


Figure 48. Reactor size (Diameter) versus mixing time. In small reactors laminar flow regimes are predominant, leading to mixing being limited by diffusion.

When dealing with capillaries/tubes in the micrometer to few millimeter dimensions basically flow regimes will always be characterized by laminar flow. In this case the mixing time is characterized by the Einstein-Smoluchovski equation:

$$t_{mixing} = \frac{L^2}{D} \quad \text{Equation 27}$$

L: diffusion length, D: Molecular diffusivity. In Figure 48 is displayed a graph of the Einstein-Smoluchovski equation with the range of molecular diffusivity constants D typically predominant in liquids.^[104] In this graph are also displayed with the green lines the three different reactor inner diameter used in this study. Inside the smallest diameter reactor diffusion is in the order of magnitude of seconds to minutes. In the 1 mm reactor diffusion is in the order of magnitude of minutes to hours. In the 1.6 mm reactor the diffusion is roughly three times slower. When reinvestigating the previous examples of irradiation from either one or two sides the drastic difference of the two is now even more apparent when considering diffusion times. As half of the reactor is not getting irradiated a practical way to look at it is to look up in the graph (or calculate) the value of diffusion time for half of the inner diameter of the reactor. Conversely one

might make the same considerations when dealing with a reactor that gets irradiated from both sides only in this case half of one of the reactor halves that gets insufficient irradiation – so one quarter. Generally, diffusion-controlled reactions follow the Arrhenius-law – every 10 °C the rate increases by a factor of 2. This is also an important consideration when looking up the values for diffusion.

For all these previously discussed considerations, it is of utmost importance to know the transmission behavior of the reaction mixture. For this the molar extinction coefficient of the reaction mixture must be measured, which you do by simply measuring the absorption of a dilution protocol of the reaction mixture. After making a linear regression of it against the concentration one obtains the value from the slope of the line. From the molar extinction coefficient, the optimum concentration of the reaction mixture, for a given reactor diameter, can be calculated (again using the Lambert-Beer law). When using either of the photocatalysts the optimum concentration could unfortunately not be obtained in this study due to solubility issues. The highest concentration of the limiting reagent that could be obtained without changing the stoichiometry of everything else was $c=0.71$ M (@1 mm reactor diameter) which corresponds to a factor x14 intensification of the prior $c=0.05$ M. Having concentration and the molar extinction coefficient, one might then plot the transmission curve using the Lambert-Beer law. Both discussion points are displayed in Figure 49.

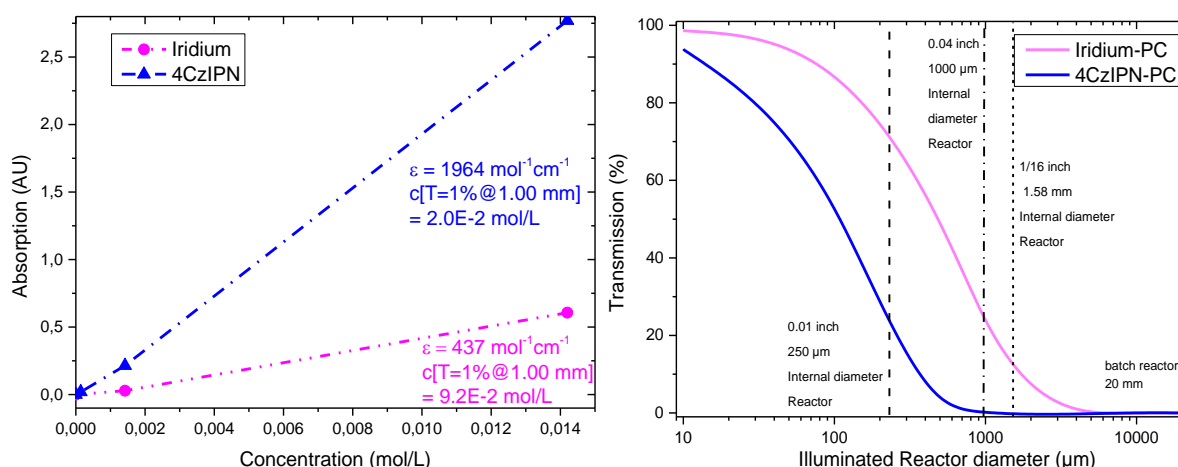
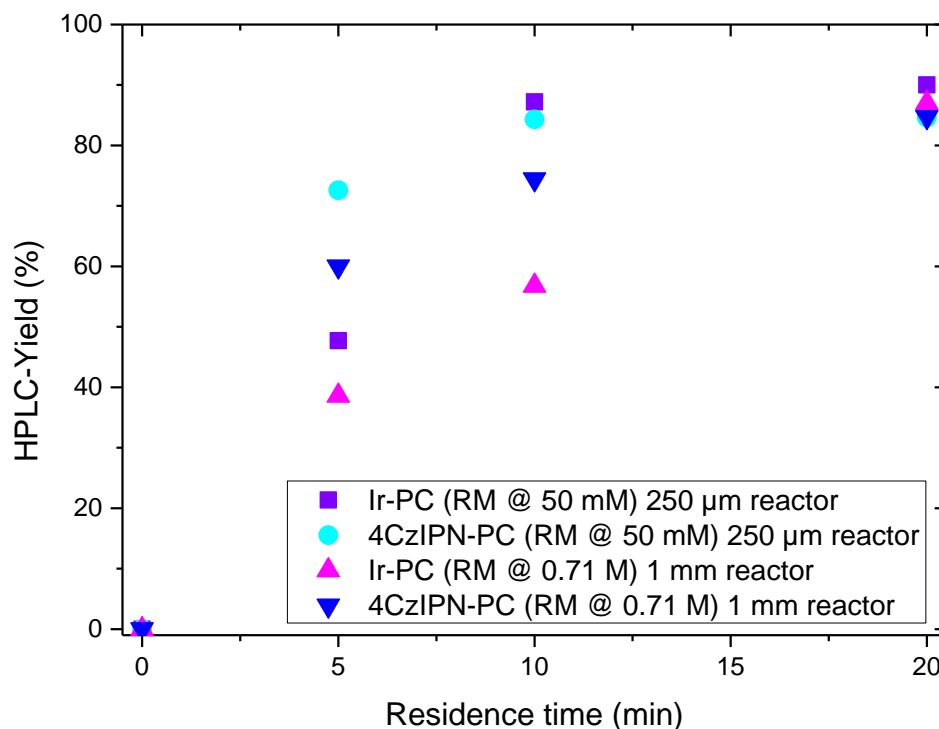
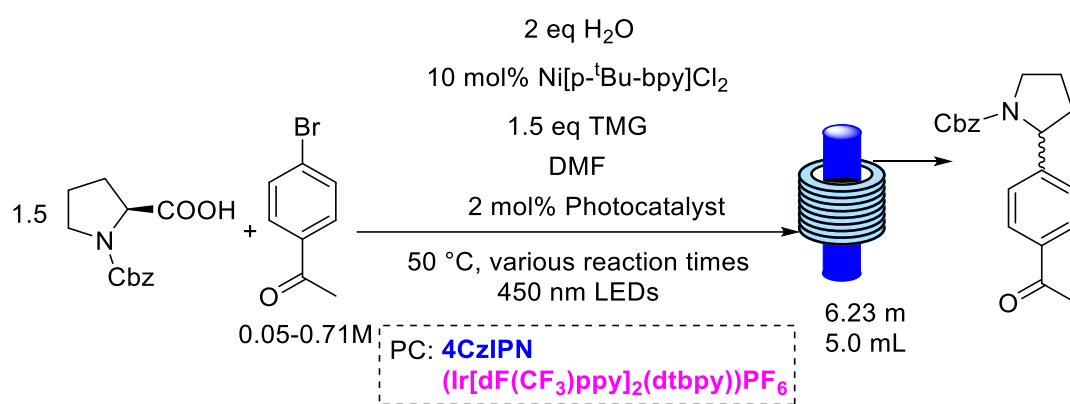


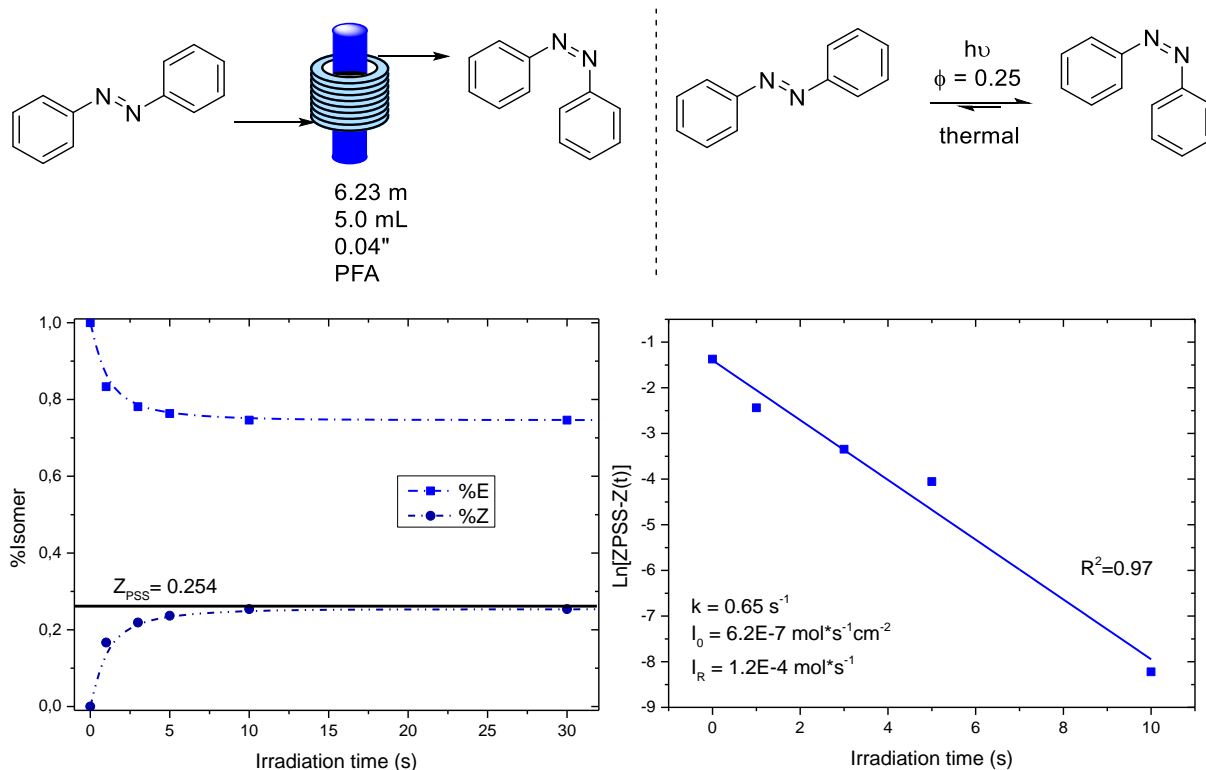
Figure 49. Graphical display of the determination of the molar extinction coefficient and the optimum concentration of the reaction mixture. Calculated transmission curve with inlayed lines with the corresponding reactor diameters.

As upscaling is a scope of this study, we decided to scale up by a factor x50. Coupled with the factor x14 concentration intensified process the productivity was expected to increase significantly. Given the fact that we are irradiating from both sides and that we have deal with a roughly 30 °C increased temperature, the diffusion was estimated to be in the order of magnitude of seconds – the reactor productivity should not be compromised by inefficient irradiation. This is also elegantly displayed in Scheme 40 where the unoptimized microfluidic conditions are displayed against their upscaled, intensified – optimized conditions. At the end of the curve when all starting material is consumed the curves all end at the same level.



Scheme 40. Conversion curve of unintensified microfluidic conditions against their intensified and upscaled conditions.

2.4.6. Act III – Enlightenment



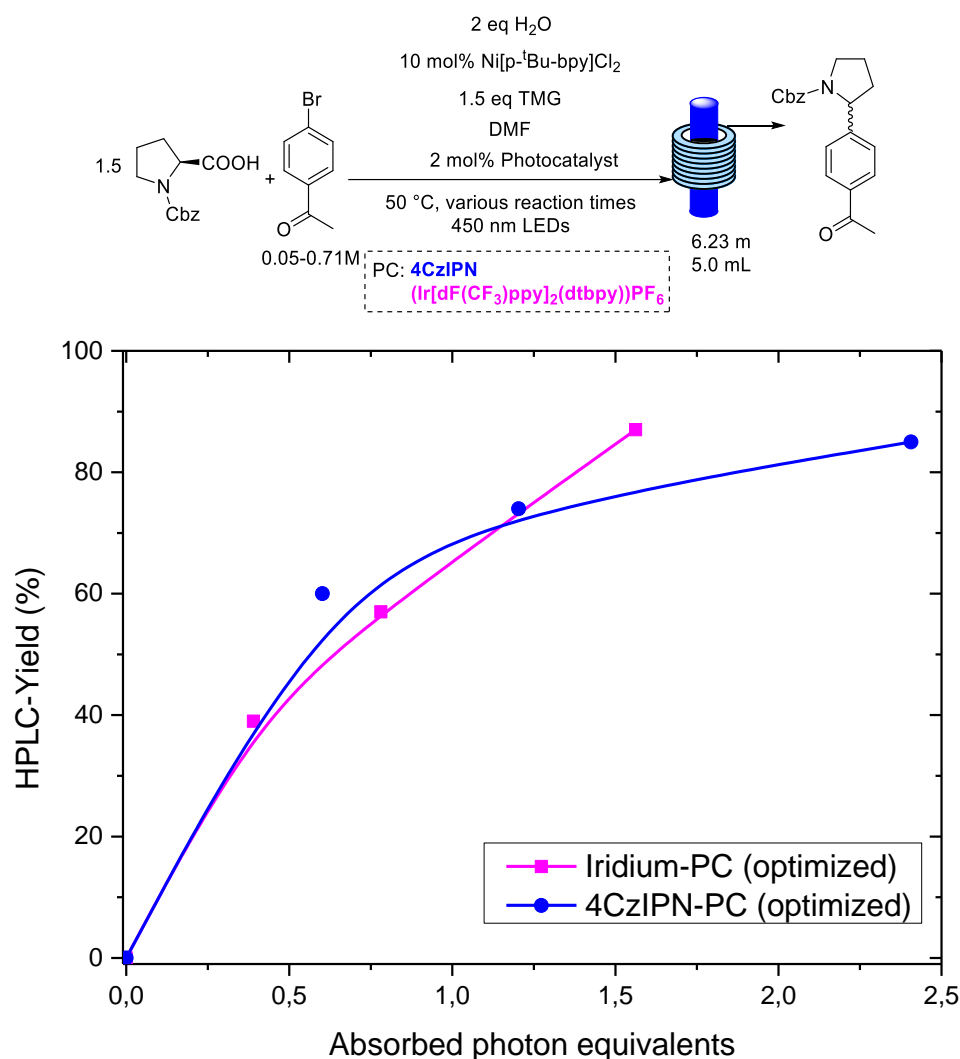
Scheme 41. Illustration of the actinometry experiments: Graph of *E*- vs *Z*-Isomer against irradiation time (residence time). Graph of first order rate kinetics, based on the first graph, to determine the kinetic constant from which the incident photonflux I_R inside the reactor (also photonflux per unit area I_0) can be calculated.

$$STY = \frac{\phi I_R (1 - T)}{V_R} \quad \text{Equation 25}$$

As we have previously discussed, a given space-time-yield of an efficient reactor should scale linearly with the incident photonflux I_R and the quantum yield ϕ . If you have done the optimizations from Act II you have made sure your reactor is efficiently irradiated. To know the maximum productivity or STY of your reactor you need to engage in chemical actinometry, the physical measuring process of the photonflux. If you are interested in the field of chemical actinometry you might find the recent review article by Bolton and co-workers helpful.^[105] In this review the authors summarize the most established actinometers and explain their (dis-)advantages. What is an actinometer you might ask? Generally, an actinometer can be defined as a photochemical reaction for which the quantum yield is beyond a shadow of a doubt well-known, and for which an easy to measure assay exists to know the

conversion/yield of the product of said reaction. From knowing how many photons will lead to a product and how many moles of product are present it can be easily inferred the number of photons that had to reach the reactor. In Scheme 41 is detailed the azobenzene actinometer, a recently published extremely practical and convenient actinometer due to its ease of measurements.^[106] The azobenzene actinometer relies on the *E/Z*-isomerisation, easily measurable by ¹H-NMR in non-deuterated solvents. This isomerisation goes to a temperature and wavelength dependent equilibrium. Time-dependent irradiation and measurements of the *E/Z*-ratios will give you the first graph. Making first order rate kinetics will give you the second graph from which the kinetic rate constant can be extracted from the slope of the linear correlation. Having the constant *k* at hand and looking up the other constants (ϵ and ϕ) in the aforementioned publication you may calculate I_0 . Multiplication of I_0 with the illuminated surface of your reactor finally gives you the photonflux inside your reactor I_R in mol/s. The illuminated surface area is based on geometric considerations about your reactor: plug flow or chip reactor, irradiation from one side versus two sides. All the discussion above is summarized in Equation 28.

$$I_R = A_{irrad} I_0 = A_{irrad} \frac{Z_{PSS} k}{\phi_{azobenzene} \epsilon_{azobenzene} \ln 10} \quad \text{Equation 28}$$



Scheme 42. Graph of the HPLC-yield as a function of the absorbed photon equivalents.

Finally, the knowledge about I_R inside the reactor allowed us to assess the maximum productivity (or STY) of our reactor. In Equation 29 is depicted the mathematical relationship and the concept of photon equivalents. The terms in numerator and denominator are already known to us. If we substitute the residence time that we used so far in our graphs we get Scheme 42. We can see that with one photon equivalent we get around 70% HPLC-yield of the product, indicating an excellent predictor of the overall process. We have thus created an efficient reactor in terms of absorption and in terms of absorbed number of photons that lead to a product in a given amount of time.

$$\frac{\phi I_R (1 - T)}{q c_0} = E q_{\text{photon}} \quad \text{Equation 29}$$

Lastly, we increased the reactor diameter by a factor x1.6. The steady increase in STY that we got by intensification was only further observed in case of the Iridium-photocatalyst. In case of the Isophthalonitrile-photocatalyst the next upscaling step performed worse in comparison to the upscaling step before. This is because we have created an inefficiently irradiated reactor as detailed in Figure 49. In simple terms, the reactor is probably too dark. In case of the Iridium-photocatalyst the reactor is still bright. Mostly, the roughly 5x higher molar extinction coefficient is to blame in this case. As was already teased in the part where the methodology is explained, drastic differences in reactor performance are to be expected when little to no thought is invested instead of doing a bit of optimization work. This relationship is beautifully illustrated when looking at Figure 50. The main takeaways from the graph are: Making a “large” scale photoreaction in batch is nonsensical indicated by the extremely low STY. Going from batch to flow without investing too many thoughts will probably still reward a huge boost in STY. *In continuo* upscaling alone will logically not reward you with a higher STY but greatly increase your productivity. Measuring the molar extinction coefficients and thus creating an efficient reactor by process intensification will greatly increase your STY. At some point Up-scaling will decrease STY as you get an increasingly inefficiently irradiated reactor.

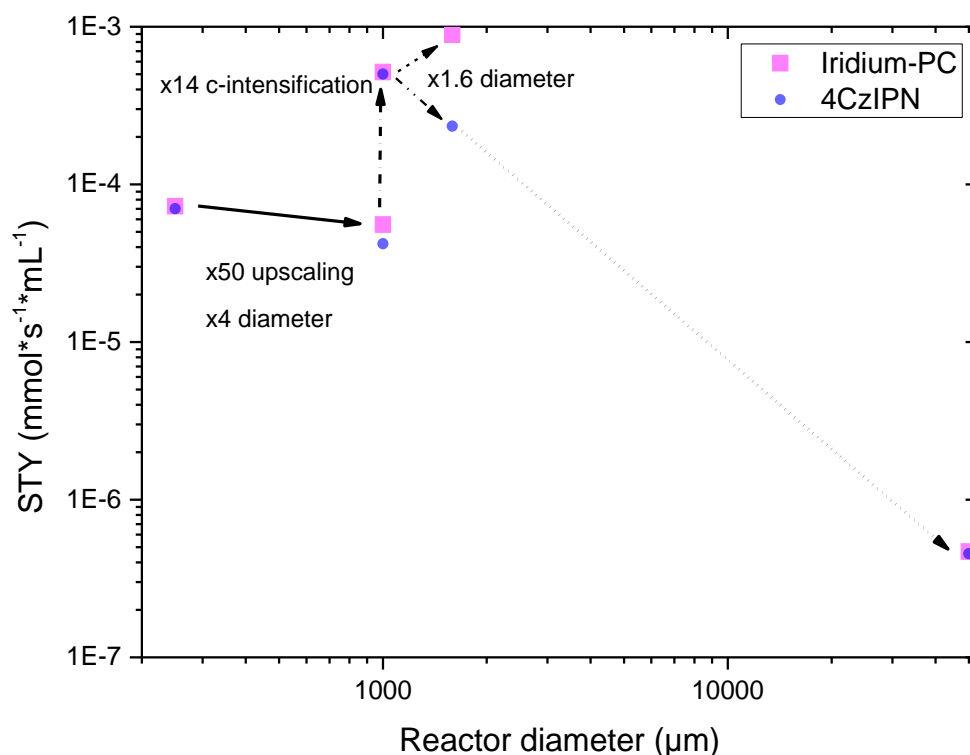
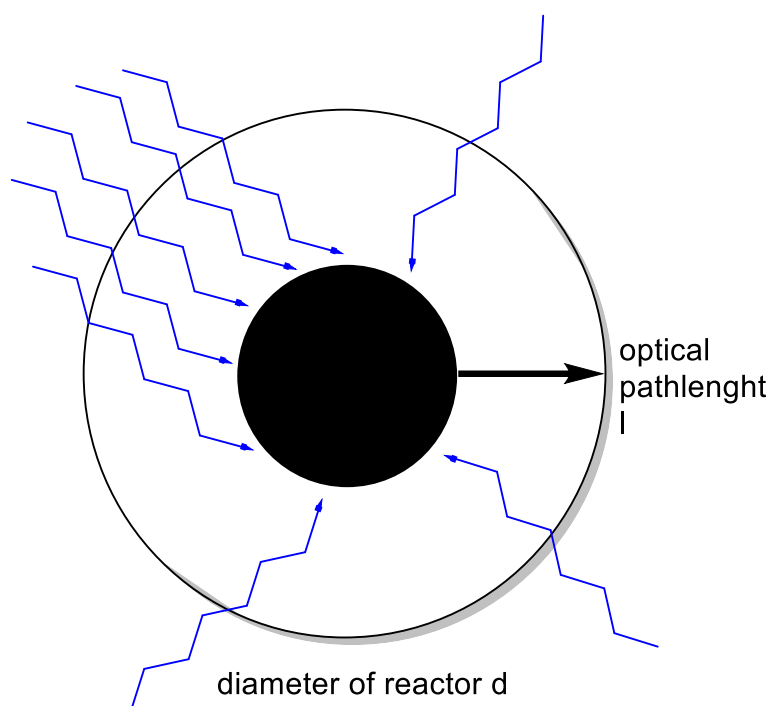


Figure 50. Space-time-yield as a function of the reactor diameter.

Assuming a reactor diameter which is so large that diffusion is significantly slower than the reaction kinetics, a few basic considerations about the efficiency loss can be made. A new effective reactor volume can be defined as the white part in Figure 51. With the reactor diameter d and the optical pathlength until which light will reasonably provide a reaction rate that is sufficient. Here we have some ambiguity about what is a “reasonable reaction rate”. It is up to the scientist to decide that himself but nevertheless Equation 30 holds. As the light penetration scales negative decadic exponentially small increments in reactor diameter will result in huge dark zones inside the reactor.



$$Efficiency\ loss = 100\% - \frac{V_{eff}}{V_R} = 100\% - \frac{2dl - l^2}{d^2} * 100\%$$

Equation
30

Figure 51. Depiction of a tubular reactor with a central dark spot.

3. Conclusion

3.1. SS-MacMillan

Solid supported catalysts exhibit several advantages over the homogenous ones – to name only a few: ease of catalyst separation and low catalyst loadings under continuous operation. This work shows how careful fine-tuning of solid supported material, transmission-based considerations (photocatalyst choice, concentration, and other methodologies) allowed to overcome the difficulties with the inefficient irradiation of reaction mixtures. Generally, the herein described solid supported catalyst shows higher degrees of enantioinduction than its homogeneous counterpart often even higher degrees than previously reported in literature by MacMillan *et al* and Melchiorre *et al*. By building a homemade chiral reactor for continuous flow operations productivity was greatly increased when comparing to the batch process, with significantly decreased catalysts loading. Ultimately the applicability of the material was proven by employing it in the telescoped synthesis of an approved antidiabetic drug – Mitiglinide in high yield and satisfactory enantioselectivity.

3.2. MR-EY

Finally, efficient photooxidation of tertiary amines was achieved using the simple new material MR-EY, particularly when operating with continuous flow catalytic reactors. The increased mass transfer efficiency of fluidic devices increased overall productivity by an order of magnitude. Using iminium-ions in situ or through a telescope, the resulting Mannich-products could be isolated with high diastereoselectivity and enantioselectivity (up to 90% *ee*). Notably, previous studies required a metal-based photocatalyst for the initial photooxidation, as well as another metal-based catalytic cycle with nitrobenzoic acid, to enable the same chemistry that we achieved simply by using air as the terminal oxidant. In this study, the same reactor was reused numerous times without loss of efficiency or material degradation, suggesting good stability and recyclability of solid-supported MR-EY.

3.3. Telescoped Process

This work is another example of how photoredox chemistry can be performed efficiently under continuous flow conditions. Tubular reactors have a higher overall efficiency than in-batch processes by more than two orders of magnitude. Understanding how to develop an upscaling strategy requires insight from photophysical measurements. Having an efficient continuous flow photoredox reactor on hand allowed for the incorporation of a fully telescoped, fully continuous highly enantioselective synthesis of a chiral privileged API as a single unit of operation.

3.4. Photochemistry *in continuo* Deep Dive

“How bad of a photochemical process can you design?” was effectively the scope of this work. In an exemplary fashion the challenges, strategies to overcome them and pitfalls of designing an efficient photochemical process were explored. With the recent boom of industrial interest in photoredox chemistry a general practical guide to translating a chemical process *in continuo* was made by highlighting all the critical parameters (transmission, quantum yield, photonflux, reactor productivity) were explored, by willfully ignoring them and comparing the results with optimized results. The negative decadic exponential scaling of light transmission and the inversely quadratic scaling of diffusion time with the reactor diameter are the major challenges that are easy to be underestimated and special care has to be applied in order to not render upscaling endeavors futile. The chemistry and reactor technologies explored in this chapter are of a lesser importance. The key principles always apply. Be wary fellow scientists.

4. Experimental Section

4.1. Project: Solid Supported Imidazolidinone Catalysts in Photocatalysis

General Description of Reagents and Methods

All reactions were carried out under a positive pressure of nitrogen (5 cm of mercury, or with a spring loaded silicon oil bubbler set to 50 mbar). Oxygen being an effective quencher of the photoredox-catalyst it was taken special measures to avoid oxygen such as bubbling nitrogen through the stock solution for at least 30 min. As most reactions involved water as (co)-solvent no special care was taken to avoid water residues. If not otherwise stated reagents, solvents, and such were used without further purifications. HPLC-grade water was degassed and stored under nitrogen. Octanal and propanal were flushed through a plug of basic aluminium oxide and then distilled under nitrogen and stored under nitrogen. Propanal when used in the reaction was not added before degassing the stock-solutions but was rather degassed separately each time and then was added to the stock-solutions due to its volatility. 3-phenyl-1-propanal (hydrocinnamaldehyde) was distilled under reduced pressure and then stored under nitrogen. (*rac*)-3-phenyl-butanal was purchased from Sigma and used without further purification. 2,6-lutidine was first refluxed and then distilled over calcium hydride and stored under nitrogen. Chloroacetonitrile and Bromoacetonitrile were purchased from Acros and were used without further purification. Diethylbromomalonate was purchased in technical grade from Acros and was insufficiently pure (dibromo- and unreacted malonate as impurities), fractional distillation under vacuum failed, only when using a long Vigreux column of about 50 cm essentially pure diethyl-bromomalonate (GC-MS) was obtained. 3-Nitro-2-bromomethyl methylbenzoate was purchased from Sigma and used without further purification. TentaGel HL Bromo functionalized (0.48 mmol/g) and Merrifield-Resin Chloro-functionalized HL (1.2 mmol/g) were bought from Merck and used without further purification. Methyl malonoyl chloride was bought from TCI chemicals and used without further purification. *trans*-Octahydro-1*h*-isoindole hydrochloride was purchased from combiblocks and used without further purification. Paratoluene sulfonylhydrazide

was purchased from Sigma and used without further purification. The chiral imidazolidinone catalysts of 1st generation **HOM-1** (*R*- and *S*-enantiomer) were purchased from Sigma-Aldrich as the hydrochloride salt and used as received. The chiral imidazolidinone catalysts of 2nd generation **HOM-2** (*S*-enantiomer) were synthesized according to the optimized gram scale chromatography-free procedure of MacMillan and coworkers,^[107] using allylamine (purchased from Sigma) and propargylamine (purchased from sigma). In all three cases single diastereoisomers were obtained. The nucleophilic thiocarbamate catalysts first introduced by Melchiorre and coworkers was synthesized following their reported procedure in 15 g scale and 95% yield.^[54] Eosin Y (hydrogen form) was purchased from TCI chemicals and used without further purification.

Reactions were monitored by thin layer chromatography (TLC) on Macherey-Nagel pre-coated silica gel plates (0.25 mm) and visualized by UV light. Flash chromatography was performed on Merck silica gel (60, particle size: 0.040–0.063 mm). ¹H NMR ¹³C NMR and ¹⁹F NMR spectra were recorded on Bruker Avance III HD 600, Bruker Avance-400, Bruker Avance-300 or Bruker Avance-250 spectrometer in CDCl₃ as solvents at room temperature. Chemical shifts for protons are reported using residual solvent protons (¹H NMR: δ = 7.26 ppm for CDCl₃) as internal standard. Carbon spectra were referenced to the shift of the ¹³C signal of CDCl₃ (δ = 77.0 ppm). The following abbreviations are used to indicate the multiplicity in NMR spectra: s - singlet; d - doublet; t - triplet; q - quartet; dd - double doublet; ddd – doublet of doublet of doublets; dt - doublet of triplets; m - multiplet; quint – quintuplet; sext -sextuplet sept - septet; br - broad signal; dq – doublet of quartets.

High resolution mass spectra (HRMS) were acquired using a Bruker solariX XR Fourier transform ion cyclotron resonance mass spectrometer (Bruker Daltonik GmbH, Bremen, Germany) equipped with a 7 T refrigerated actively shielded superconducting magnet. The samples were ionized in positive ion mode using a MALDI or ESI ionization sources.

Automatic weighing and transferring of liquids were made with a Zinssler Analytics custom robot “Calli”.

Samples were evaporated in a parallel fashion by employing a Genevac HT-4X vacuum centrifuge Series II System.

Preparative HPLC-MS was conducted on an Agilent 1260 Infinity Series (Autosampler, Fraction Collector, DAD, Pumps, Check valves, all while coupled to a Agilent 6120 LC-MS Quadrupole mass-spectrometer. MS-traces were generated in positive/negative switching mode and ESI/APCI as ionization method was used in tandem.

uHPLC-MS (ultrahigh performance) was conducted on a Agilent 1260 Infinity Series (Autosampler, Pump was 1290 Infinity Series) all while coupled to an Agilent 6120 LC-MS Quadrupole mass-spectrometer. MS-traces were generated in positive/negative switching mode and ESI/APCI as ionization method was used in tandem.

Chiral HPLC was measured on a Agilent 1100 Series (DAD, Autosampler, Pumps). The respective chiral stationary phase is indicated in the characterization part.

Experimental Procedures

4.1.1. Description of Equipment



Figure 52: Photograph of the ignited watercooled high intensity LED photoreactor for cryogenic continuous flow operations. Photograph of the coil-reactor Perfluoroalkoxyalkane (PFA) HPLC-Tubing that is wrapped around the aforementioned photoreactor.

A versatile LED-based photoreactor for continuous flow reactions under *cryogenic conditions* is unprecedented in Literature. The goal is to build a photoreactor for such conditions using only readily available and low-cost equipment that can be found in any organic chemistry laboratory. The herein presented Photoreactor can be immersed in any cryobath for temperature regulation as the LEDs are *hermetically sealed* inside

a Pyrex glass tube to avoid glacier formation, which can obstruct efficient irradiation due to the high albedo of water ice that would form from atmospheric moisture. The heat generation which tends to burn high power LEDs under sealed conditions is counteracted by wrapping the LED-Strips around a central sublimator glass-piece which is water cooled. With this innovative reactor design, it is possible to run a continuous flow photoreaction at any temperature by simply immersing the photoreactor and coil reactor couple in a temperature-controlled liquid (Ice-mixtures, dry-ice mixtures, cryostat-baths, oil-baths). The here presented Reactor performed for over 300 h and is still fully operational.



Figure 53. Photographs of the assembled and disassembled water-cooled photoreactor for cryogenic continuous flow operations

Construction of the continuous flow Photoreactor: The central sublimator glass-piece is first wrapped to the desired length with heavy duty aluminium foil to generate a socket for the LED-strip that possesses high heat conductive properties. Around this first layer is then coiled and glued (doublesided adhesive tape) the LED-strip which is further secured in place at the top and bottom with electric isolating tape. The cable is guided through the silicon rubber seal by puncturing it. The final reactor is then assembled as presented in Figure 2. Video of the assembly can be found separately uploaded under supporting files.

Construction of the batch photoreactor. As oxygen is a powerful quencher of photoreactions a plausible cause for the subpar performance of MacMillan's protocol when repeated in our labs, could be unsuccessful attempts to exclude oxygen from our reaction especially under prolonged reaction times. To overcome this issue a photoreactor was build based on a jacketed-water cooled reactor purchasable from <https://www.neubert-glas.de> (catalogue number: 5020-06-0250) with the respective lid (catalogue number: 5103-06-291414). A silicone ring and a metal clamp (excluded for clarity) ensured Schlenk-type conditions. Positive nitrogen pressure during the reactions ensured no oxygen quenching. Around the glass body were wrapped the later described UV-LED-strips and fixed in position with adhesive tape. Contacts were sealed with electrical isolating tape and everything was once again wrapped with several layers of aluminium foil. The aluminium foil cover was then wrapped with parafilm to protect it from eventual chemical exposure. The whole reactor ensemble is displayed in Figure 54. It is conceivable to connect a temperature regulated circulating liquid and thus perform reactions under elevated temperatures.

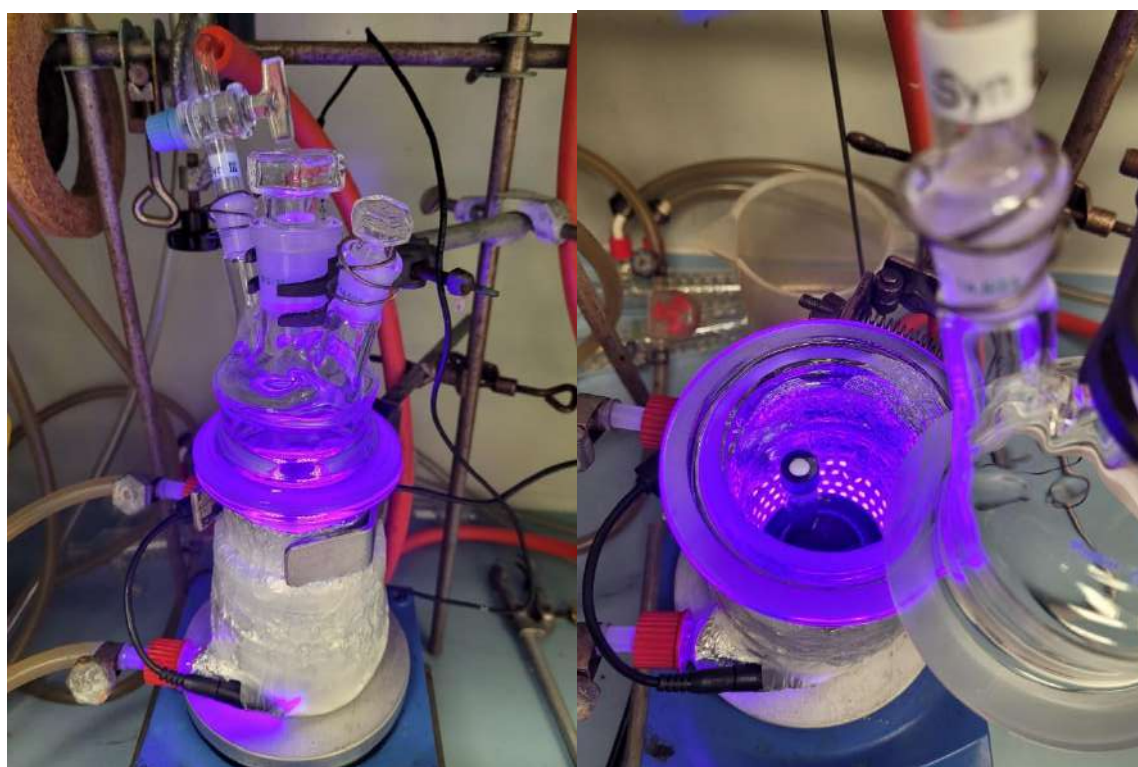


Figure 54. Photograph of the assembled batch photoreactor in a jacketed double-walled glass-piece to be able to put the whole setup under inert-gas.

Led-Specifications: Aftertech® 24v 24w UV 1m Strip 120 LEDs SMD5050 ultraviolet (395 nm), with a self-adhesive tape that holds the strip light safely and securely to the photoreactor support. The LEDs wavelength emission profile together with their specific light intensity (expressed as mW cm^{-2}) have been determined before their use. In particular, the spectrum has been obtained by using a compact CCD spectrometer (model CCS200/M) connected to a multimode optical fiber, purchased from Thorlabs. Ultraviolet LEDs are characterized by an almost monochromatic emission profile (with a full width at half-maximum intensity of ca. 10-20 nm) showing a maximum of intensity located at ca. 395 nm. The light power intensity was thus checked using a Thorlabs PM200 power meter equipped with a S130VC power head with a Si detector. The measured light intensities, though slightly decreasing by moving the maximum of LEDs emission towards longer wavelengths, was $I = 70.94 \text{ mW cm}^{-2}$ (std 0.0034).

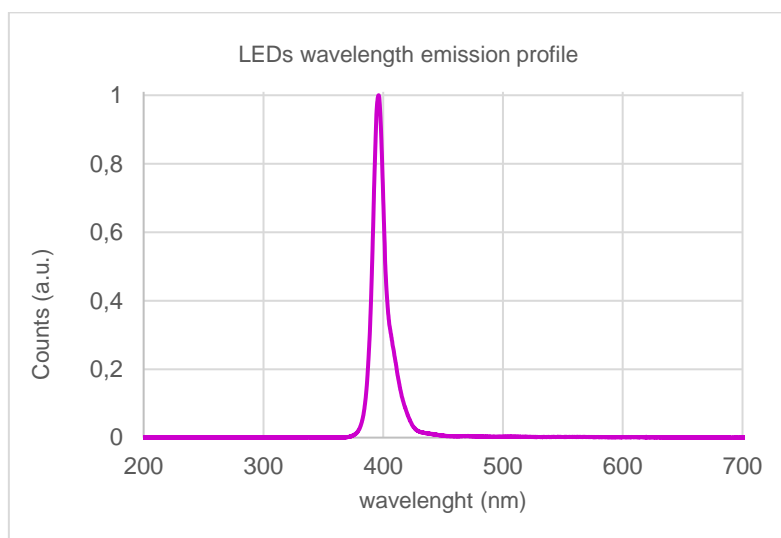
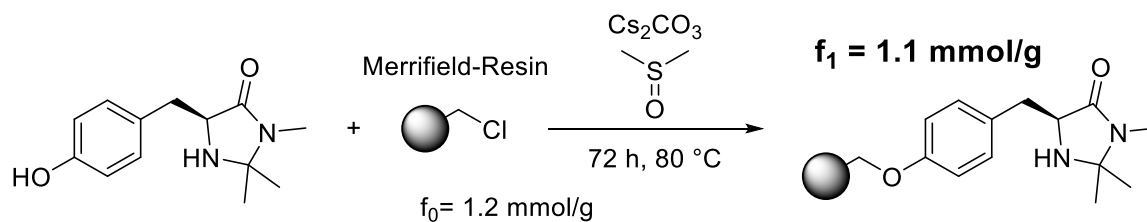


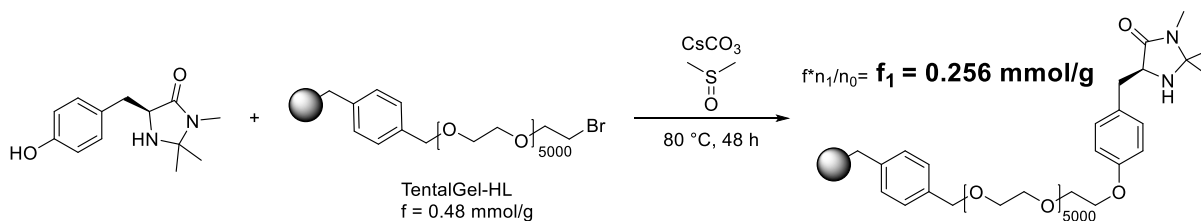
Figure 55. Graph of UV- LEDs wavelength emission profile

4.1.2. Solid Supporting the Catalysts



Reactants			Products		
Formula	C₁₃H₁₈N₂O₂	C₂H₆OS	CCs₂O₃	Formula	C₁₄H₁₉N₂O₂
MW	234,30	78,13	325,82	MW	247,32
Limiting?	Yes	No	No	Equivalents	
Equivalents	1,00		3,00	%Completion	
Sample Mass	1,02g	341,13mg	4,27g	Expected Mass	1,08g
%Weight				Expected Moles	4,37mmol
Molarity		125,00mM		Measured Mass	
Density				Purity	
Volume		34,93mL		Product Mass	
Reactant Moles	4,37mmol	4,37mmol	13,10mmol	Product Moles	
Reactant Mass	1,02g	341,13mg	4,27g	%Yield	

Funnel empty: 127.292 g funnel full: 131.726 g m = 4.434 g $\Delta m = 0.794 \text{ g}$
 $\Delta M = 234.3 - 36.46 = 197.84 \text{ g/mol}$ $\Delta n = 4.01 \text{ mmol}$ $\Delta n/n^*f_0 = f_1 = 1.1 \text{ mmol/g}$



Reactants				Products		
Formula	C₁₃H₁₈N₂O₂	C₁₂H₁₆BrO₂	C₂H₆OS	CCsO₃	Formula	C₂₅H₃₃N₂O₄
MW	234,30	272,16	78,13	192,91	MW	425,55
Limiting?	Yes	No	No	No	Equivalents	
Equivalents	2,00	7,65		3,00	%Completion	
Sample Mass		10,00g		2,78g	Expected Mass	2,04g
%Weight					Expected Moles	4,80mmol
Molarity					Measured Mass	
Density					Purity	
Volume			100,00mL		Product Mass	
Reactant Moles	9,60mmol	36,74mmol	4,80mmol	14,40mmol	Product Moles	
Reactant Mass	2,25g	10,00g	375,14mg	2,78g	%Yield	

The indicated reagents were dissolved or dispersed in the indicated solvent. To this mixture the material was added and heated at the indicated temperature for the indicated time keeping the stirring speed low as possible so that the dispersion did not settle at the bottom of the flask. For large quantities (above 2 grams of Material for

solid support) mechanical stirring was employed and the blades of the agitator were placed and tightly secured in the rotor such that the walls of the flask were not in direct contact. Low stirring speeds and distance of the blades from walls was employed to avoid grinding the material and rendering it less active.

After the reaction was completed the reaction mixture was poured into an oven-dried glass sintered funnel (pore size 4, pre-weighed) and special care was taken to remove almost all the material out of the flask with generous amounts of methanol. The residue was infused with a mixture of water/THF/methanol and stirred with a glass rod. After infusing for 5 minutes vacuum was attached and the washing liquid was filtered off. Vacuum was detached and the whole process was repeated 15 times. After this generous washing process the process was repeated for three times using dichloromethane. The washing flasks was changed and the remains in the funnel were dried by running a constant air stream through them for 5 hours by attaching a vacuum. After this time the filter was weighed again and by the difference in weight a preliminary catalyst loading calculated.

Characterisation of Solid Supported Catalysts

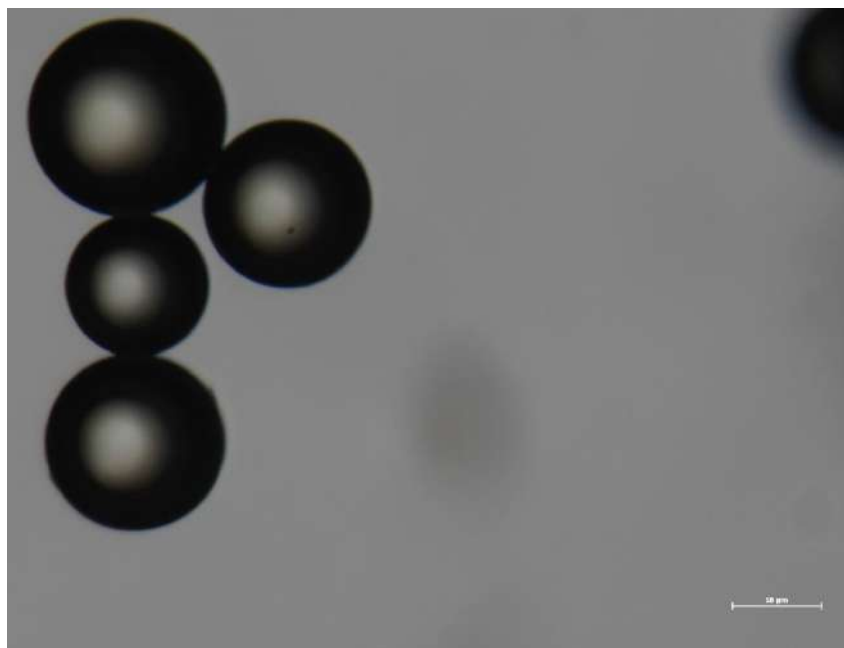


Figure 56. Optical microcroscope image of Merrifield resin supported MacMillan-Catalyst. The spherical structure is uncompromised. X216 Magnification.

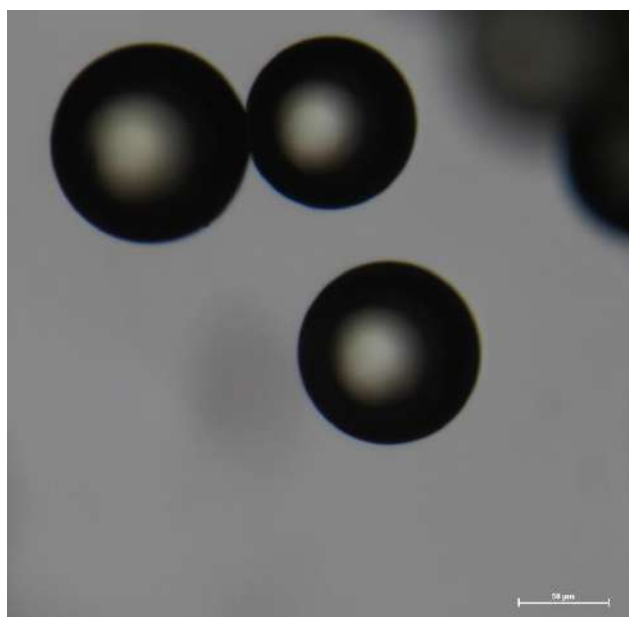
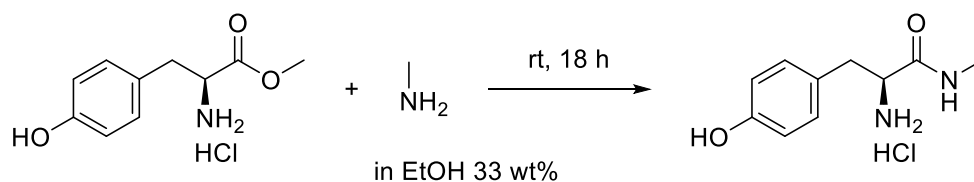


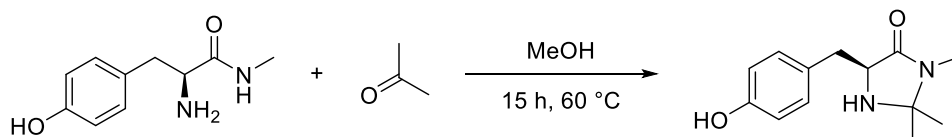
Figure 57. Optical microcroscope image of TentaGel resin supported MacMillan-Catalyst. The spherical structure is uncompromised. X216 Magnification.

4.1.3. MacMillan Catalyst Precursors for Solid Support



<i>Reactants</i>			<i>Products</i>	
Formula	C₁₀H₁₄ClNO₃	CH₅N	Formula	C₁₀H₁₅ClN₂O₂
MW	231,68	31,06	MW	230,69
Limiting?	Yes	No	Equivalents	
Equivalents	1,00	10,00	%Completion	
Sample Mass	4,63g	18,82g	Expected Mass	4,61g
%Weight		33,00%	Expected Moles	20,00mmol
Density		756,00mg/mL	Measured Mass	4,60g
Volume		24,90mL	Purity	
Reactant Moles	20,00mmol	200,00mmol	Product Mass	4,60g
Reactant Mass	4,63g	6,21g	Product Moles	19,94mmol
			%Yield	99,70%

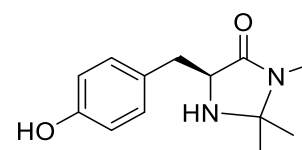
Into a round bottom flask was weighed the respective amino acid, a stirring bar was added, and the indicated amount of methylamine-methanol solution was added. After stirring it at ambient temperature for the indicated time (tlc monitoring) the volatiles were removed *in vacuo* and backfilled with dichloromethane which was removed *in vacuo* again. This was repeated until the residues were solid to ensure complete evaporation of the free methylamine as remains can hamper the aminal formation in the next step. At this point dissolution in dichloromethane may fail and methanol was added to dissolve it. The volatiles were removed *in vacuo* to yield the respective *N*-methylamide of the amino acid.



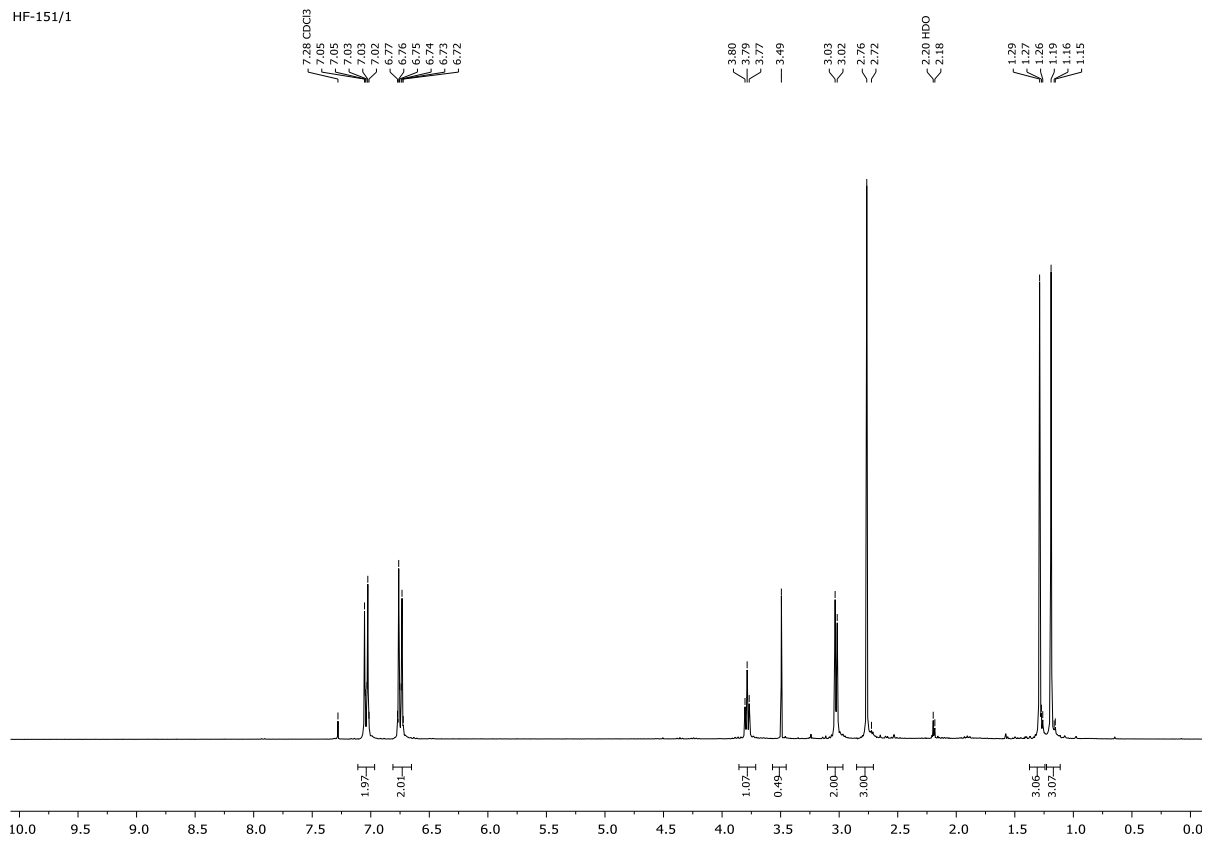
Reactants			Products		
Formula	C₁₀H₁₄N₂O₂	C₃H₆O	CH₄O	Formula	C₁₃H₁₈N₂O₂
MW	194,23	58,08	32,04	MW	234,30
Limiting?	Yes	No	No	Equivalents	
Equivalents	1,00	5,00		%Completion	
Sample Mass	3,88g	5,81g	640,84mg	Expected Mass	4,69g
Molarity			500,00mM	Expected Moles	20,00mmol
Density		748,00mg/mL		Measured Mass	4,04g
Volume		7,76mL	40,00mL	Purity	
Reactant Moles	20,00mmol	100,00mmol	20,00mmol	Product Mass	4,04g
Reactant Mass	3,88g	5,81g	640,84mg	Product Moles	17,24mmol
				%Yield	86,19%

The amide from the first step was dissolved in the indicated amount of methanol and acetone. To this mixture the indicated amount of *p*-toluenesulfonic acid was added and the mixture refluxed for the indicated time. After completion of the reaction the volatiles were removed *in vacuo* and the resulting mixture was dissolved in methanol followed by addition of 10 times the weight of the residue of Florisil and evaporation of the solvent *in vacuo*. The mixture was purified by liquid chromatography using silica as the stationary phase with an eluent of methanol/dichloromethane 1-2% with 0.1% of triethylamine. After evaporation of the volatiles 4.04 g (86%) were obtained of a yellow viscous oil that slowly started to crystallize at room temperature.

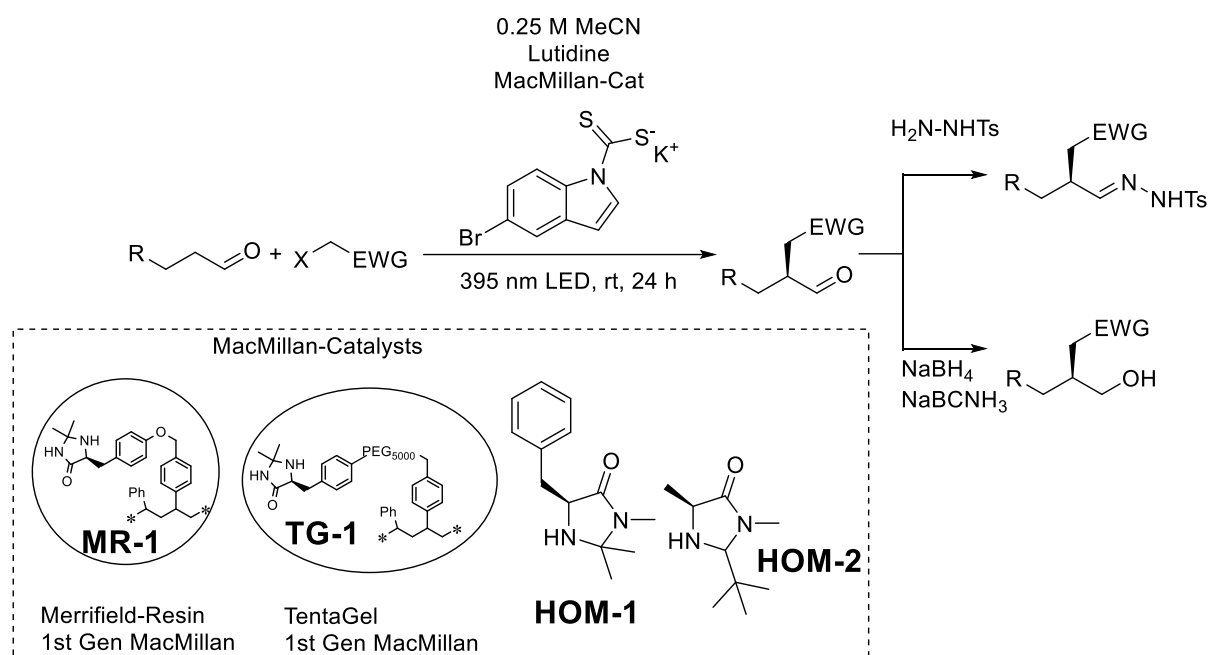
¹H NMR (300 MHz, Chloroform-*d*) δ 7.13 – 6.94 (m, 2H), 6.85 – 6.67 (m, 2H), 3.79 (t, *J* = 5.4 Hz, 1H), 3.49 (s, 0H), 3.03 (d, *J* = 5.4 Hz, 2H), 2.76 (s, 3H), 1.29 (s, 3H), 1.19 (s, 2H).



HF-151/1



4.1.4. General Procedure for the Stereoselective α -Functionalization of Aldehydes



In a 4 mL screw-neck vial with Teflon septum, equipped with a teflon coated stir-bar, were placed 193 mg (50 μ mol, 0.20 eq) of **TG-1** imidazolidinone catalyst followed by 16.0 mg (50.0 μ mol, 0.20 eq) of the nucleophilic thiocarbamate catalyst and in case the radical source was a solid, 250 μ mol (1.00 eq) of it. The solids were dissolved (suspended) in 1 mL of acetonitrile and to the mixture were sequentially added 38 μ L (318 μ mol, 1.20 eq) 2,6-lutidine, followed by 750 μ mol (3.00 eq) of the respective aldehyde and in case the radical source was a liquid 250 μ mol (1.00 eq) of it. The mixture was degassed by bubbling nitrogen through the solution for 15 minutes all while stirring vigorously. After degassing the vial was quickly placed inside the previously inertized batch photoreactor. Because the lid of the photoreactor was opened briefly, after closing it again the atmosphere inside the reactor was exchanged with nitrogen by leaving one of the stoppers floating in the nitrogen stream for 10-15 minutes. After this time the stopper was reattached and the reactor irradiated for 24 h.

In-situ derivatization of aldehydes: In order to fix the labile stereogenic center of the aldehyde product it was directly derivatized in the same vial it was initially prepared.

For this after the irradiation was over, to the vigorously stirred reaction mixture was added in case of

reduction, 100 μL of a saturated solution of sodium borohydride in 5% potassium carbonate solution (~15 M, freshly prepared). The resulting mixture was left to react for 15 minutes after which 1 mL of methanol was added and the mixture stirred until the bubbling stopped and the samples were directly infused into the preparative HPLC-System.

Hydrazone-formation, 1.00 mL of a 0.75 M solution of toluene sulfonyl hydrazide in methanol and it was left to stir at room-temperature for 15 minutes. The mixture was then directly infused in to the preparative HPLC-System.

Automatized Purification Sampling and weighing protocol

The resulting remains were purified using preparative RP18-Silica and a gradient of water/acetonitrile with 0.5mM NH_4HCO_3 using an in-house generated protocol for the semi-automated purification, evaporation. After the automatic chromatographic purification of the compounds the solvent was evaporated in a parallelized fashion inside a vacuum centrifuge. The tube positions with product containing fractions were submitted automatically to the transfer robot. The robot then backfills the tubes with acetonitrile to redissolve and transfers this to barcode-vials which were weighed by robot before filling. The bar-code vials containing the solutions of the product were then evaporated again in a parallel fashion and the robot after weighing the vials again communicates the final yield. This workflow is illustrated in Figure 58.

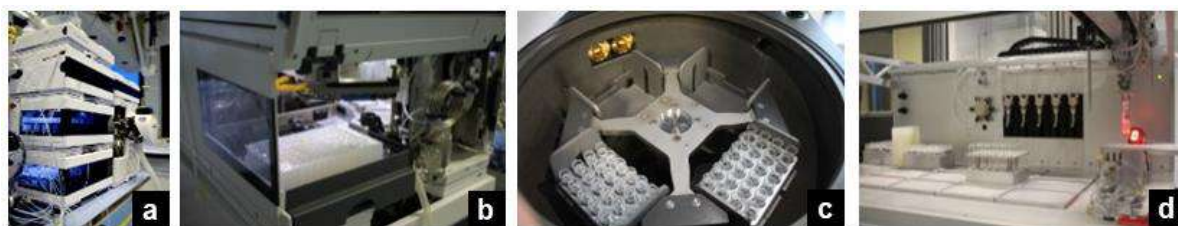
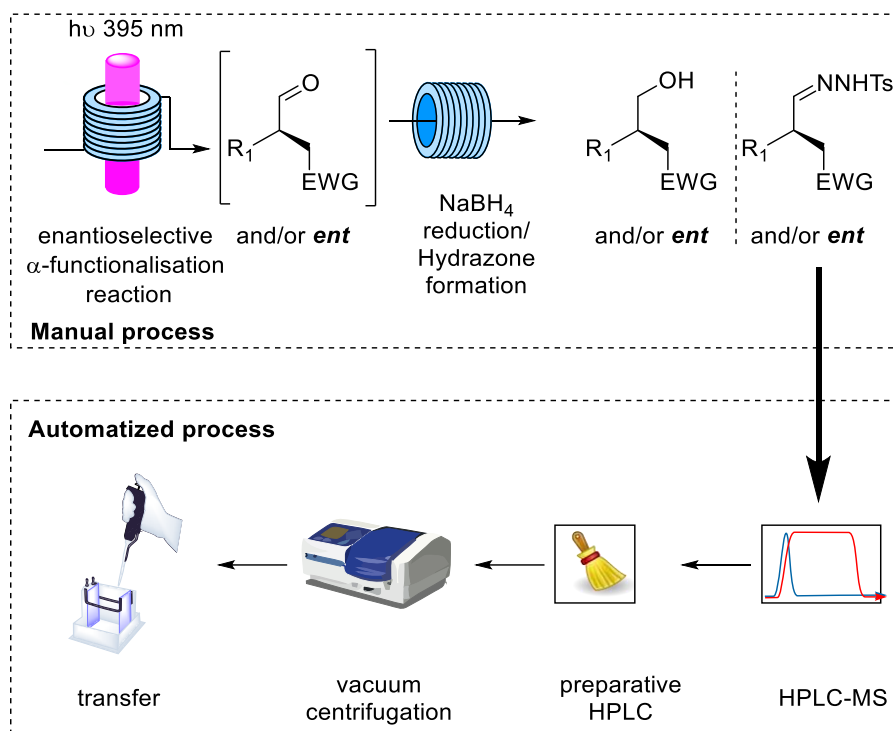
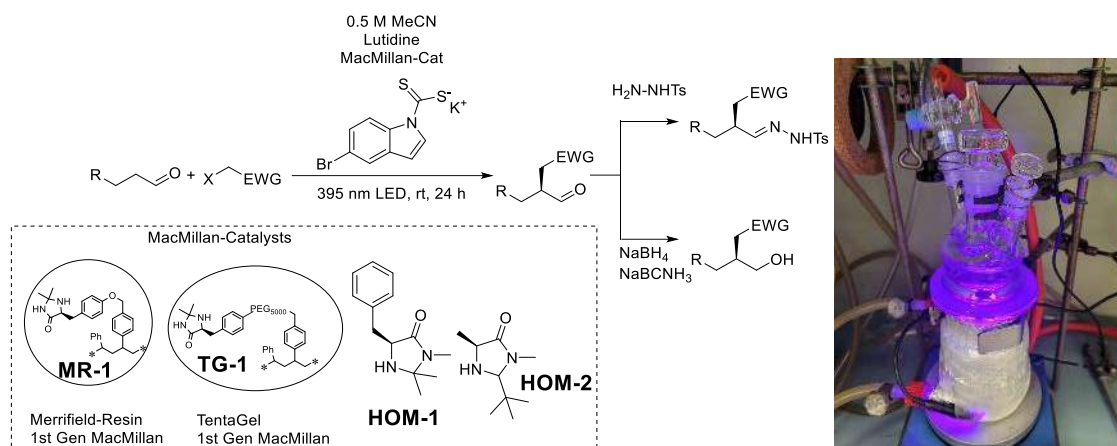
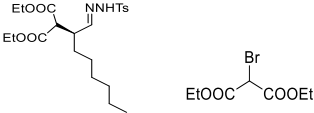
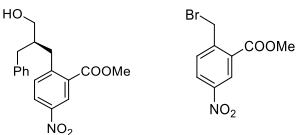


Figure 58. Semi automatized evaporation, purification, evaporation, transferring, weighing, after manual phase separation. (photos left-to-right: a) HPLC-MS , b) Pipetting and weighing robot, c) Vacuum centrifuge, d) analytical preparation sample)

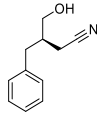
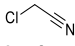
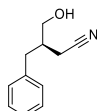
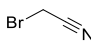
Table 18. Summary of the employed conditions for the asymmetric α -functionalization of aldehydes using solid supported chiral imidazolidinone catalysts. Comparison with the obtained results with homogeneous catalysts. Variation from the conditions outlayed in the scheme is also indicated.



Entry	Product	Electrophile	Catalyst	Variation	ee [%]	Yield ^[a]
1			HOM-1	None	84	53%
			TG-1	None	78	33%
			MR-1	None	77	6%
			HOM-1	20% H ₂ O	74	25%
2			HOM-1	None	92	80%
			TG-1	None	96	81%
			HOM-1	20% H ₂ O	96	78%
			TG-1	20% H ₂ O	95	79%
3 ^[b]			HOM-1	None	2.2:1 d.r.	61%
					86 (maj)	
					80 (min)	
			TG-1	None	2.1:1 d.r.	57%
				88 (maj)		
				89 (min)		
4			HOM-1	None	62	74%
			TG-1	None	77	84%
5			HOM-1	None	77	76%
			TG-1	None	91	72%
6			HOM-1	None	70	69%
			TG-1	None	90	61%

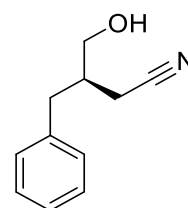
7		HOM-1	None	56	73%
		TG-1	None	73	76%
		Hom-2	Eosin Y, DMF ^[c]	76	60%
		MR-1	Eosin Y, DMF ^[c]	59	58%
8		HOM-1	None	71	52%
		TG-1	None	90	48%

[a] Isolated yield after chromatographic purification. [b] racemic starting aldehyde: combined yield of diastereoisomers. [c] typical MacMillan conditions employed. Eosin Y instead of nucleophilic carbamate catalyst, DMF as solvent as instead of acetonitrile, 23 W compact fluorescence lamp, with **MR-1** as catalyst – 3 d of reaction time.

Entry	Product	Electrophile + amount	Aldehyde + amount	Catalyst + amount	Variation	ee [%]	Yield ^[a] [xx mg]
1		 17 μ L	Phenylpropanal 104 μ L	HOM-1, 12 mg	None	84	53% [24.5]
				TG-1, 193 mg	None	78	33% [15.4]
				MR-1, 54 mg	None	77	6% [2.9]
				HOM-1, 12 mg	20% H ₂ O	74	25% [23.0]
2		 24 μ L	Phenylpropanal 104 μ L	HOM-1, 12 mg	None	92	80% [35]
				TG-1, 193 mg	None	96	81% [35.6]
				MR-1, 54 mg	20% H ₂ O	96	78% [34]
				HOM-1, 12 mg	20% H ₂ O	95	79% [34.5]

Habitus: orange oil.

Purification Analytic HPLC: product at 4,95 min.; m/z=175;
 Column: XBridge BEH Prep C18 5 μ m, 19 mm X 150 mm
 Mobile phase: Acetonitrile / Water+5mM NH₄HCO₃
 Flow rate: 32 ml/min
 Gradient:
 0-0.5 min 19:81
 0.51-10,5 min 79:21
 10,5-12,5 min 98:2



¹H NMR (300 MHz, Chloroform-*d*) δ 7.37 – 7.02 (m, 5H), 3.78 – 3.37 (m, 2H), 2.84 – 2.51 (m, 2H), 2.36 (dd, *J* = 12.8, 5.9 Hz, 0H), 1.98 – 1.74 (m, 1H)

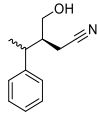
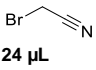
MS m/z = 175 [M+H⁺]

(ESI+APCI)

Chiral Column: Chiralpak AS-3

HPLC Eluent: Hexane/IPA 90:10 @1.0 mL/min

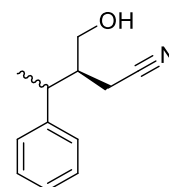
*t*_R (minor) 14.7 min, *t*_R (major) 13.4 min

Entry	Product	Electrophile + amount	Aldehyde + amount	Catalyst + amount	Variation	ee [%]	Yield ^[a] [xx mg]
3 ^[b]			3-phenylbutanal 110 μ L	HOM-1 13 mg	None	2.2:1 d.r. 86 (maj) 80 (min)	61% [29]
				TG-1 193 mg	None	2.1:1 d.r. 88 (maj) 89 (min)	57% [27]

Habitus: orange oil.

Purification Analytic HPLC: product at 4,59 min.; m/z=189;
 Column: XBridge BEH Prep C18 5 μ m, 19 mm X 150 mm
 Mobile phase: Acetonitrile / Water+5mM NH₄HCO₃
 Flow rate: 32 ml/min
 Gradient:
 0-0.5 min 12:88
 0.51-12,5 min 72:28
 12,5-14,5 min 98:2

¹H NMR (300 MHz, Chloroform-*d*) δ 7.36 – 6.99 (m, 5H), 3.92 (dd, *J* = 8.5, 4.8 Hz, 1H), 3.77 (d, *J* = 7.6 Hz, 1H), 3.60 – 3.41 (m, 0H), 3.34 (s, 0H), 2.79 (dt, *J* = 9.9, 7.1 Hz, 1H), 2.57 (dd, *J* = 10.4, 5.7 Hz, 0H), 2.31 (dd, *J* = 16.6, 4.3 Hz, 1H), 2.16 – 2.05 (m, 0H), 2.04 – 1.91 (m, 1H), 1.53 (s, 1H), 1.26 (dd, *J* = 7.0, 4.1 Hz, 3H).



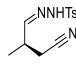
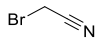
¹³C-NMR (75 MHz, Chloroform-*d*) δ 144.28, 144.02, 128.88, 128.76, 127.27, 127.22, 126.90, 126.81, 118.85, 77.42, 77.20, 77.00, 76.58, 62.45, 61.66, 43.94, 43.87, 39.93, 39.79, 19.44, 19.23, 17.90, 17.17.

HR-MS m/z =calculated 212.1046 [M+Na⁺], found 212.1052 (ESI+APCI) [M+Na⁺]

Chiral Column: Chiralpak AS-3

HPLC Eluent: Hexane/IPA 90:10 @0.4 mL/min

*t*_R (minor) 32.8+51.4 min, *t*_R (major) 24.1+31.9 min

Entry	Product	Electrophile + amount	Aldehyde + amount	Catalyst + amount	Variation	ee [%]	Yield ^[a] [xx mg]
4		 24 μ L	Propanal 100 μ L	HOM-1, 13 mg TG-1, 193 mg	None None	62 77	74% [49] 84% [56]

Habitus: off-white solid.

Purification Analytic HPLC: product at 4,76 min.; m/z=265
 Column: XBridge BEH Prep C18 5 μ m, 19 mm X 150 mm
 Mobile phase: Acetonitrile / Water+5mM NH₄HCO₃
 Flow rate: 32 ml/min
 Gradient:
 0-0.5 min 14:86
 0.51-10,5 min 74:26
 10,5-12,5 min 98:2

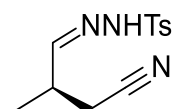
¹H NMR (300 MHz, Chloroform-*d*) δ 8.31 (s, 1H), 7.81 – 7.67 (m, 2H), 7.25 (d, *J* = 7.9 Hz, 3H), 7.10 (d, *J* = 3.9 Hz, 1H), 2.74 – 2.58 (m, 1H), 2.48 (dd, *J* = 16.8, 5.8 Hz, 1H), 2.42 – 2.28 (m, 5H), 1.12 (d, *J* = 7.0 Hz, 3H).

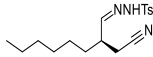
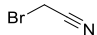
¹³C-NMR (75 MHz, Chloroform-*d*) δ 150.97, 144.44, 134.85, 129.74, 127.88, 118.07, 33.40, 21.64, 21.12, 17.20.

HR-MS m/z =calculated 288.0777 [M+Na⁺] found 288.0779 (ESI+APCI) [M+Na⁺]

Chiral Column: Lux Cellulose 3

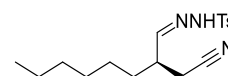
HPLC Eluent: Hexane/IPA 92:8 @1.0 mL/min
 t_R (minor) 40.4 min, t_R (major) 47.2 min



Entry	Product	Electrophile + amount	Aldehyde + amount	Catalyst + amount	Variation	ee [%]	Yield ^[a] [xx mg]
5		 24 μ L	Octanal 110 μ L	HOM-1, 13 mg TG-1, 193 mg	None None	77 91	76% [64] 72% [60]

Habitus: off-white solid.

Purification Analytic HPLC: product at 5,96 min.; $m/z=335$;
 Column: XBridge BEH Prep C18 5 μ m,
 19 mm X 150 mm
 Mobile phase: Acetonitrile / Water+0.1% formic acid
 Flow rate: 32 ml/min
 Gradient:
 0-0.5 min 23:77
 0.51-8,5 min 98:2
 8,5-10,5 min 98:2



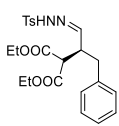
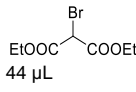
¹H NMR (300 MHz, Chloroform-*d*) δ 8.40 (s, 1H), 7.83 – 7.62 (m, 2H), 7.24 (d, J = 8.0 Hz, 2H), 7.09 (d, J = 4.6 Hz, 1H), 2.42 (dd, J = 8.8, 6.2 Hz, 1H), 2.35 (s, 3H), 1.43 (dd, J = 9.7, 5.2 Hz, 2H), 1.30 – 0.93 (m, 7H), 0.79 (t, J = 6.9 Hz, 3H).

¹³C-NMR (75 MHz, Chloroform-*d*) δ 150.73, 144.34, 134.89, 129.72, 127.88, 118.09, 38.30, 31.66, 31.53, 29.00, 26.14, 22.53, 21.62, 19.54, 14.04.

HR-MS m/z =calculated 358.1560 [$M+H^+$] found 358.1560
 (ESI+APCI) [$M+Na^+$]

Chiral Column: Lux Amylose 1

HPLC Eluent: Hexane/IPA 90:10 @0.8 mL/min
 t_R (minor) 56.3 min, t_R (major) 59.7 min

Entry	Product	Electrophile + amount	Aldehyde + amount	Catalyst + amount	Variation	ee [%]	Yield ^[a] [xx mg]
6		 44 μ L	Phenylpropanal 104 μ L	HOM-1, 13 mg TG-1, 193 mg	None None	70 90	69% [80] 61% [71]

Habitus: off-white solid.

Purification Analytic HPLC: product at 5,7 min.; $m/z=460$;
 Column: XBridge BEH Prep C18 5 μ m, 19 mm X 150 mm
 Mobile phase: Acetonitrile / Water+5mM NH₄HCO₃
 Flow rate: 32 ml/min
 Gradient:
 0-0.5 min 18:82
 0.51-10,5 min 98:2
 10,5-12,5 min 98:2

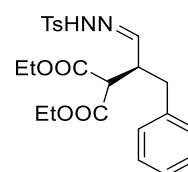
¹H NMR (300 MHz, Chloroform-*d*) δ 7.88 (s, 1H), 7.67 (d, J = 8.3 Hz, 2H), 7.20 (dd, J = 9.5, 6.6 Hz, 3H), 7.12 (d, J = 7.1 Hz, 2H), 7.03 – 6.82 (m, 2H), 4.15 – 3.81 (m, 3H), 3.48 (d, J = 7.1 Hz, 1H), 3.29 – 3.13 (m, 1H), 2.74 (dd, J = 11.5, 7.5 Hz, 2H), 2.35 (s, 3H), 1.14 (td, J = 7.1, 3.7 Hz, 6H).

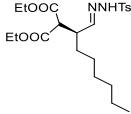
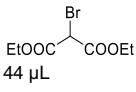
¹³C-NMR (75 MHz, Chloroform-*d*) δ 168.20, 167.83, 150.70, 137.86, 135.41, 129.56, 129.16, 128.53, 127.91, 126.60, 61.75, 61.69, 53.48, 42.88, 36.17, 21.60, 14.01.

HR-MS m/z =calculated 483.1560 [M+Na⁺] found 483.1564 (ESI+APCI) [M+Na⁺]

Chiral Column: Chiralpak AS-3

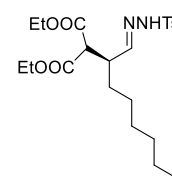
HPLC Eluent: Hexane/IPA 45:55 @0.8 mL/min
 t_R (minor) 14.5 min, t_R (major) 24.0 min



Entry	Product	Electrophile + amount	Aldehyde + amount	Catalyst + amount	Variation	ee [%]	Yield ^[a] [xx mg]
7		 44 μ L	Octanal 110 μ L	HOM-1, 17 mg	None	56	73% [83]
				TG-1, 193 mg	None	73	76% [87]
				Hom-2, 11 mg	Eosin Y, DMF ^[c]	76	60%
				MR-1, 54 mg	Eosin Y, DMF ^[c]	53	xx

Habitus: off-white solid.

Purification Analytic HPLC: product at 6,17 min.; m/z=454
 Column: XBridge BEH Prep C18 5 μ m, 19 mm X 150 mm
 Mobile phase: Acetonitrile / Water+5mM NH₄HCO₃
 Flow rate: 32 ml/min
 Gradient:
 0-0.5 min 23:77
 0.51-10,5 min 98:2
 10,5-12,5 min 98:2



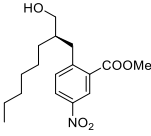
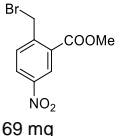
¹H NMR (300 MHz, Chloroform-*d*) δ 7.95 (s, 1H), 7.81 – 7.62 (m, 2H), 7.35 – 7.12 (m, 3H), 4.17 – 3.91 (m, 3H), 3.47 (d, *J* = 7.9 Hz, 1H), 2.89 (s, 0H), 2.34 (s, 3H), 1.51 – 1.28 (m, 1H), 1.28 – 0.92 (m, 8H), 0.79 (t, *J* = 7.0 Hz, 3H).

¹³C-NMR (75 MHz, Chloroform-*d*) δ 168.09, 167.91, 151.57, 143.90, 135.36, 129.52, 127.94, 77.47, 77.04, 76.62, 61.61, 61.58, 54.34, 41.46, 31.57, 30.19, 29.07, 26.48, 22.55, 21.57, 14.06, 14.03, 13.99.

HR-MS m/z =calculated 477.2030 [M+Na⁺] found 477.2036 (ESI+APCI) [M+Na⁺]

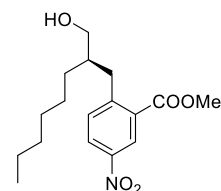
Chiral Column: Chiralpak IA

HPLC Eluent: Hexane/IPA 80:20 @1 mL/min
 t_R (minor) 7.95 min, t_R (major) 9.79 min

Entry	Product	Electrophile + amount	Aldehyde + amount	Catalyst + amount	Variation	ee [%]	Yield ^[a] [xx mg]
8		 69 mg	Phenylpropanal 104 μ L	HOM-1, 13 mg TG-1, 193 mg	None None	71 90	52% [43] 48% [39]

Product was reduced with a methanolic solution of 2.5 M sodium cyanoborohydride to not reduce the nitro-group and not as indicated in the general procedure with sodium borohydride. Habitus: orange oil.

Purification Analytic HPLC: product at 6,18 min.; $m/z=323$
 Column: XBridge BEH Prep C18 5 μ m, 19 mm X 150 mm
 Mobile phase: Acetonitrile / Water+5mM NH₄HCO₃
 Flow rate: 32 ml/min
 Gradient:
 0-0.5 min 23:77
 0.51-10,5 min 98:2
 10,5-12,5 min 98:2



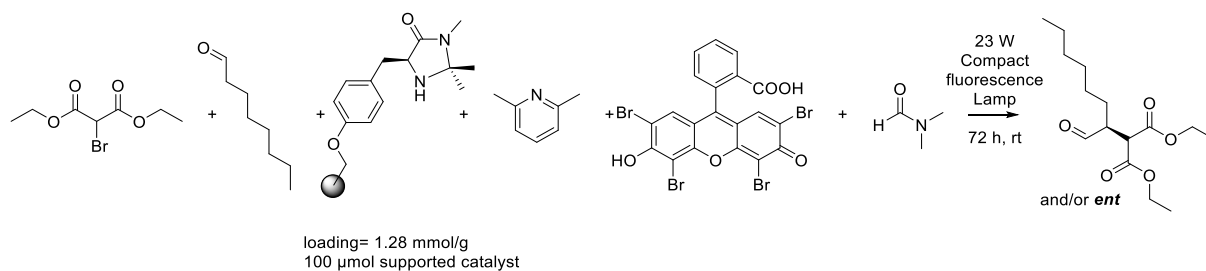
¹H NMR (300 MHz, Chloroform-*d*) δ 8.68 (d, J = 2.6 Hz, 1H), 8.20 (dd, J = 8.4, 2.5 Hz, 1H), 7.41 (d, J = 8.6 Hz, 1H), 7.19 (s, 1H), 3.89 (d, J = 2.7 Hz, 4H), 3.47 – 3.33 (m, 2H), 3.24 (dd, J = 13.0, 8.4 Hz, 1H), 2.83 (dd, J = 13.0, 6.1 Hz, 1H), 1.19 (d, J = 4.5 Hz, 10H), 0.95 – 0.69 (m, 5H).

¹³C-NMR (75 MHz, Chloroform-*d*) δ 166.59, 150.98, 145.97, 133.16, 130.78, 126.02, 125.97, 63.56, 52.89, 43.19, 35.59, 31.79, 31.30, 29.55, 27.04, 22.64, 14.09.

HR-MS m/z =calculated 346.1625 [M+Na⁺] found 346.1626 (ESI+APCI) [M+Na⁺]

Chiral Column: Lux Cellulose 5

HPLC Eluent: Hexane/IPA 90:10 @0.5 mL/min
 t_R (minor) 31.8 min, t_R (major) 30.0 min



20.7 mg (100 μ mol, 20mol%) of 2nd generation MacMillan catalysts **OR** 78 mg (100 μ mol, 1.28 mmol/g, 20 mol%) of solid supported Merrifield 1st-generation MacMillan catalyst **MR-1** were weighed into a 2.5 mL catalytic vial with a screw cap and an inert septum. Before addition of the liquid components the vial was equipped with a stirring bar and was flushed for 5 minutes with nitrogen by puncturing the septum with a needle that also serves as the entry for the nitrogen. To this 1 mL of dry *N,N*-dimethylformamide, 83.0 μ L (500 μ mol, 1.00 eq) diethyl bromomalonate, 173 μ L (1.00 mmol, 2.00 eq) octanal and 116 μ L (1.00 mmol, 1.00 eq) of 2,6-lutidine were added under inert atmosphere. After the addition the mixture was degassed by bubbling nitrogen through the solution for 30 min while stirring.

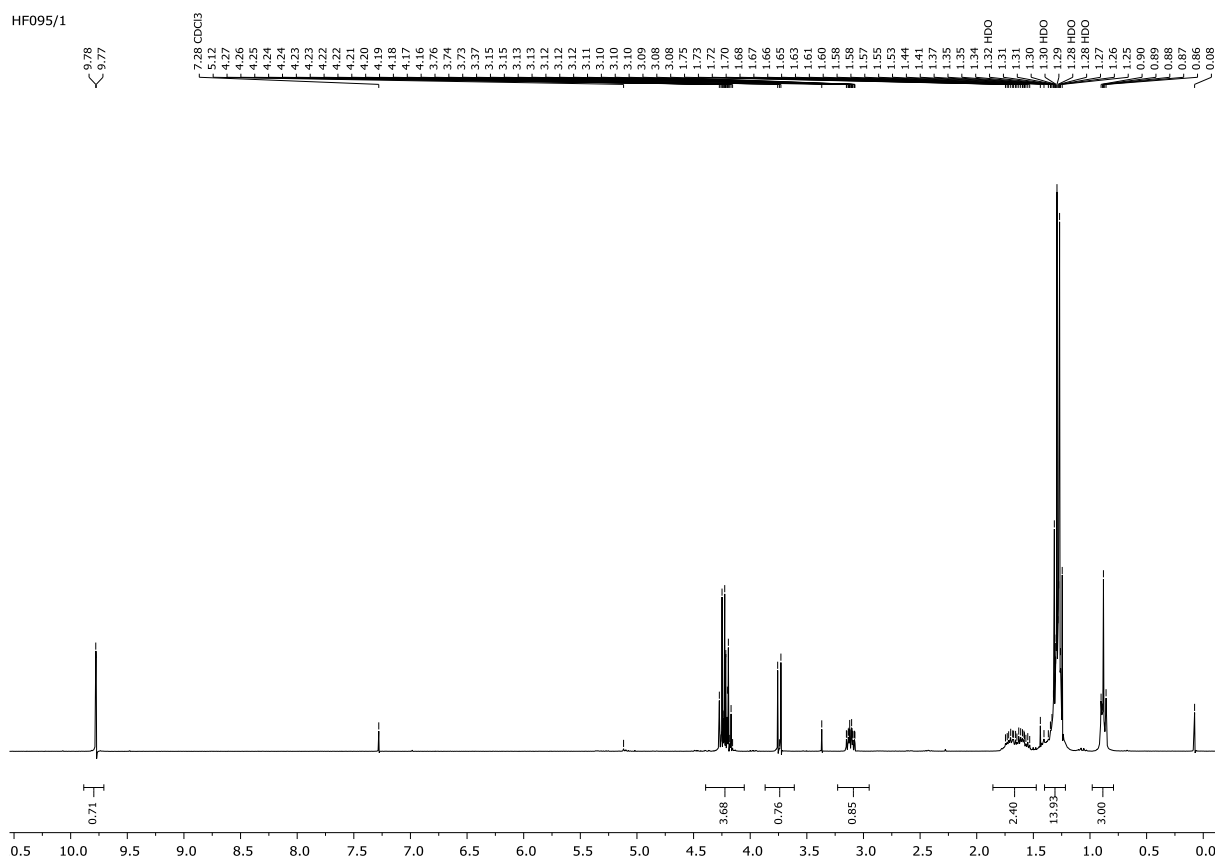
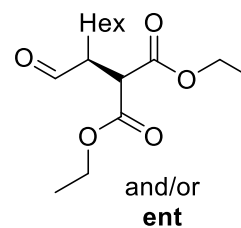
In a constant stream of nitrogen, the screw cap of the catalytic vial was rapidly replaced with a screw cap which possesses an intact septum. The degassed vial was placed directly adjacent (1 cm) to a 23 W compact fluorescence light bulb (CFL) and irradiated for the 17 h (72 h in the case of **MR-1**) all while employing constant pressurized air cooling at ambient temperature. The reaction was monitored taking an aliquot of ~25 μ L (two drops) and injection into a GC-FID after dilution in 1 mL ethyl acetate. Completion of reaction was indicated by assessing the consumption of starting material. The reaction mixture was diluted with saturated aqueous NaHCO₃ and extracted three

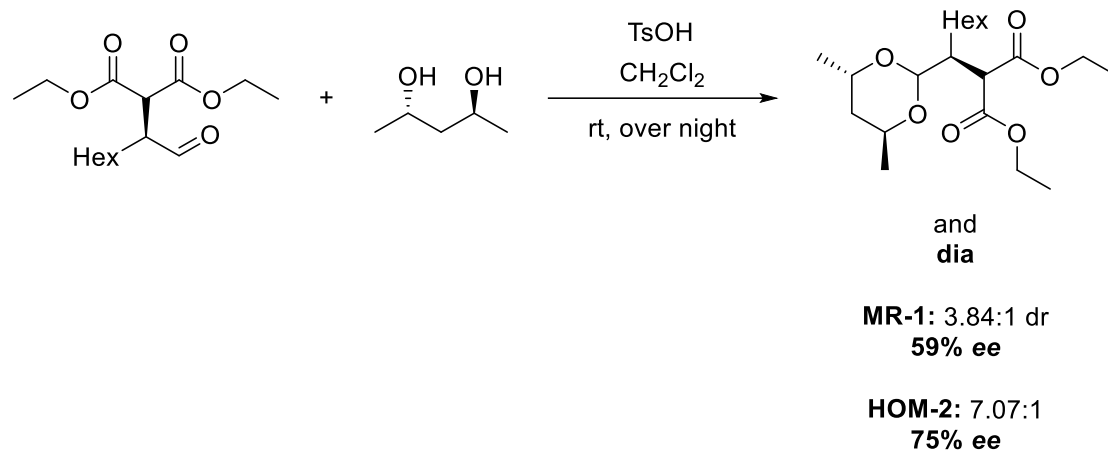
times with diethyl ether. After drying over magnesium sulfate the volatiles were removed *in vacuo* avoiding higher than ambient temperatures. The residues were absorbed onto Florisil and the dry powder was purified using flash column chromatography employing 100 mass equivalents of silica eluting isocratically with diethylether/hexane 1:6. 88.8 mg (293 μ mol, 62%) of a colorless oil were obtained.

R_f (p-anisaldehyde) 0.25

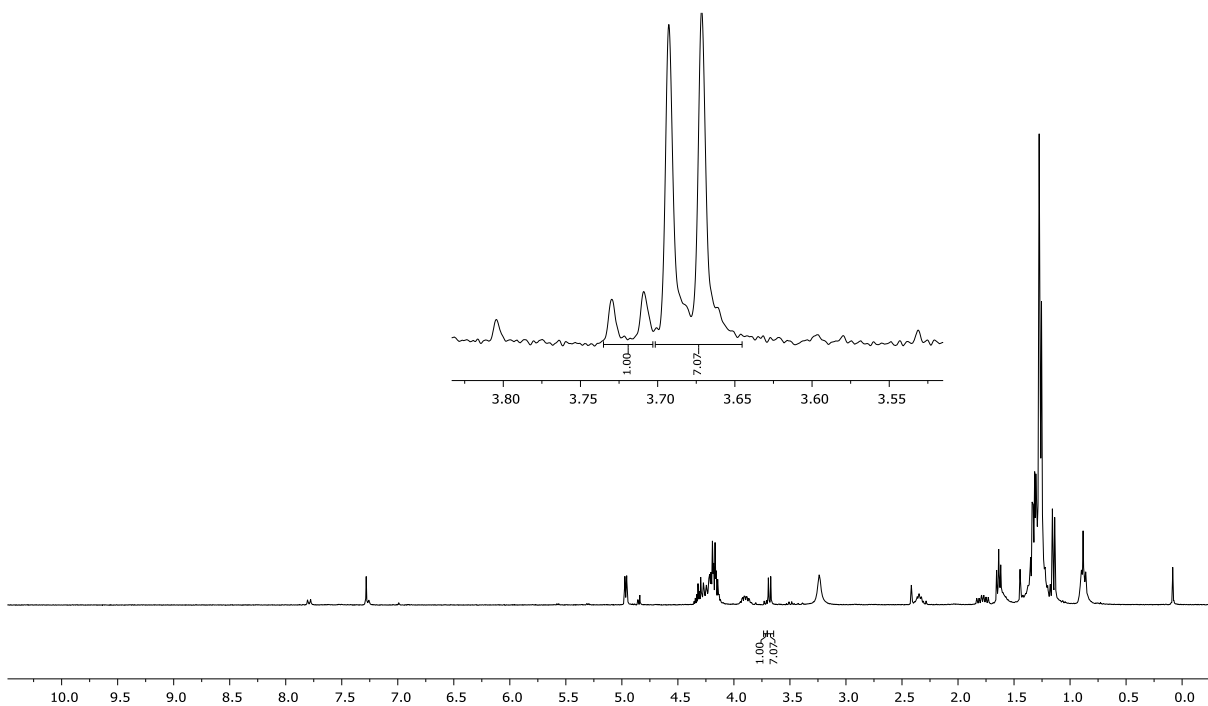
Et₂O/Hex 1:6

¹H-NMR δ [ppm] 9.78 (d, *J* = 1.2 Hz, 1H), 4.28 – 4.16 (m, 4H), 3.74 (d, *J* = 8.6 Hz, 1H), 3.11 (dddd, *J* = 8.8, 7.8, 5.1, 1.2 Hz, 1H), 1.83 – 1.51 (m, 2H), 1.39 – 1.21 (m, 17H), 0.93 – 0.83 (m, 3H).



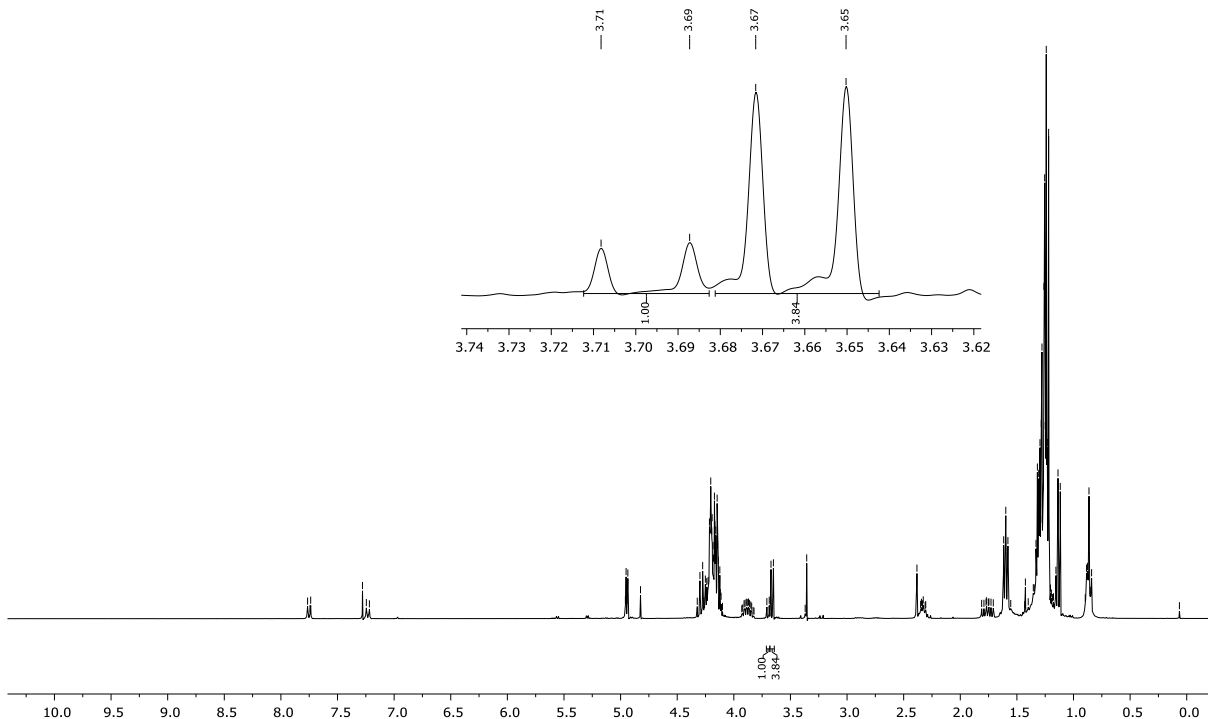


44 mg (148 μmol , 1.00 eq) of the previously synthesized aldehyde was dissolved in 1.1 mL of dichloromethane. To this mixture was added 2.50 mg (15.0 μmol , 10mol%) of *p*-toluenesulfonic acid and 19.3 mg (1.86 μmol , 1.20 eq) (2*S*,4*S*)-pentane-2,4-diol and it was stirred overnight at ambient temperatures. The following day the volatiles were evaporated and backfilled with deuterated chloroform and the mixture analysed in H-NMR and the *ee* was assessed by integration of the diastereomeric acetal protons.

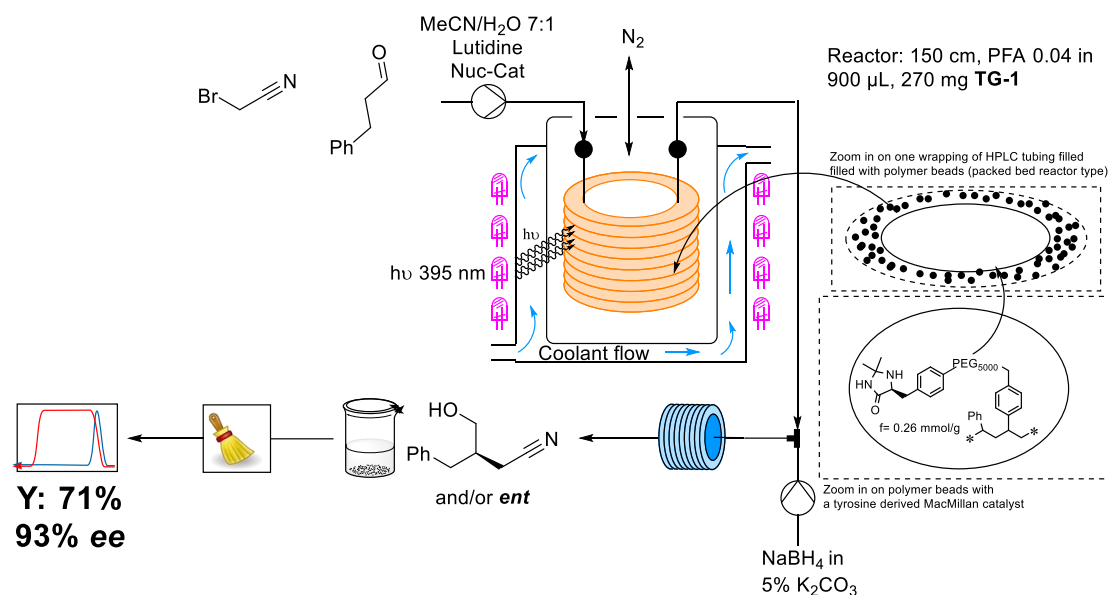


HF098/1

7.76 7.74 7.28 7.25 4.95 4.94 4.94 4.82 4.32 4.30 4.26 4.25 4.24 4.23 4.22 4.20 4.20 4.19 4.18 4.18 4.17 4.17 4.16 4.16 4.15 4.14 4.14 4.12 4.12 4.11 4.11 3.89 3.88 3.87 3.71 3.67 3.67 3.65 3.36 3.36 2.38 2.34 2.33 1.79 1.77 1.75 1.75 1.73 1.71 1.62 H₂O 1.60 H₂O 1.42 H₂O 1.40 1.36 1.35 1.33 1.32 1.31 1.31 1.30 1.30 1.29 1.28 1.28 1.28 1.27 1.26 1.25 1.25 1.24 1.23 1.22 1.22 1.20 1.20 1.19 1.18 1.16 1.16 1.14 1.14 1.12 1.12 0.90 0.88 0.87 0.87 0.86 0.86 0.85 0.85 0.84



4.1.5. Continuous Flow Packed Bed Catalytic Reactor enantioselective Cyanoalkylation

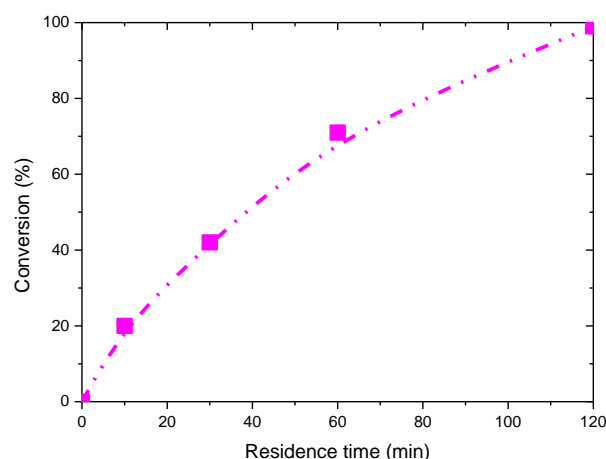


Construction of packed-bed Reactor: 150 cm of 1/16" outer diameter – 0.04" inner diameter PFA-HPLC-tubing were cut and equipped with fluidic connectors (1/4-28-bore fingertight ferules) on both sides. In one side was introduced a string of cotton to act as a "filter/retainer" for the resin-beads. This side was then equipped with a fluidic-adaptor (1/4-28-bore female-to-female). This setup was then weighed, and the weight was noted for later use. Roughly 500 mg of **TG-1** was weighed into a beaker and the weight of the beaker plus resin was noted. **TG-1** was swollen in acetonitrile and the mixture was suspended and taken up in a 2.5 mL SGE gastight syringe and connected to the previously prepared HPLC-Tubing. The mixture was infused so long as the tubing was optically filled with the resin. Another good indicator for complete filling was a sudden jump in counterpressure experienced in the operator's hand. All the remaining material inside the syringe was carefully reintroduced into the beaker, flushing the syringe several times with dichloromethane all while also introducing the flushing liquid into the beaker. The reactor was placed into a freezer overnight, while the solvent mixture was inside the beaker was left to evaporate overnight and was put into a vacuum drying oven the next day for 2 h at 40 °C. The weight difference inside the beaker represents the amount of **TG-1** (270 mg, 94.5 μmol) infused into the reactor. The packed-bed reactor was weighed the next day and based on the density

of acetonitrile/water 7:1 and previously determined weight of **TG-1** inside the reactor, the reactor volume was determined to be $V_R=900 \mu\text{L}$.

Continuous Flow Photoreaction: Roughly 20 mL of a stock solution (0.21 M of effective concentration) was prepared according to the protocol detailed in the general procedure. For this 16 mL of acetonitrile/water 7:1 were used, 1.6 mL of phenylpropanal, 384 μL of radical source, 450 μL of lutidine, 256 mg of nucleophilic catalyst. As the amino-catalyst is inside the packed-bed reactor it was not included in the reaction mixture.

The stock solution was taken up in a 25 mL SGE Gastight syringe and was infused with a variable flow rate to give variable residence times detailed below. Two full reactor volumes were discarded, and the outflow was connected to a Y-connector piece in which at the same time was infused a 2.5 M sodium borohydride in 5% aqueous potassium carbonate solution for the *in situ* reduction.

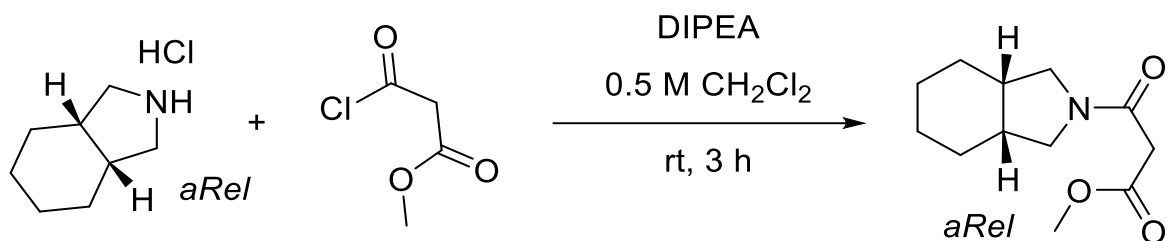


Q_R [$\mu\text{L}/\text{min}$]	Q_R (NaBH ₄) [$\mu\text{L}/\text{min}$]	t_R [min]	Conv.
0	0	0	0%
90	9	10	21%
30	3	30	42%
15	1.5	60	69%
7.5	0.8	120	99%+

The reactor output was collected at the 120 min residence time condition for 157 min to get a theoretical 250 μmol of product. The reaction mixture was diluted with 1 mL methanol and after waiting for the bubbling to subside the, the reaction mixture was directly injected into the prepHPLC system.

After evaporation a 31 mg (71%) of an orange oil were obtained. Chiral HPLC revealed an enantiomeric excess of $ee=93\%$.

4.1.6. Synthesis of Mitiglinide Radical Precursor



in a 250 mL 2-neck-fask was dissolved 8.00 g (49.5 mmol, 1.00 eq) *rac*-hexahydroisindole hydrochloride in 100 mL of dichloromethane by adding 21.6 mL (124 mmol, 2.50 eq) diisopropylethylamine. Into an addition funnel was added 10.0 g (74.2 mmol, 1.50 eq) methyl malonyl chloride and dissolved in 25 mL dichloromethane. The mixture was cooled down to 0 °C and addition over 10 minutes was. Reaction mixture was left to stir at 0 °C for 2 h after which to the reaction mixture was added NaHCO₃ aq sat and left to stir vigorously over night to hydrolyse the malonylchloride. Phases were separated and the organic phase was extracted twice with 1 M HCl. The organic phase was dried over magnesium sulfate, filtered and the volatiles evaporated in vacuo. 12.5 g of a orange oil were obtained. After purification 10.1 g (91%) of a orange oil were obtained.

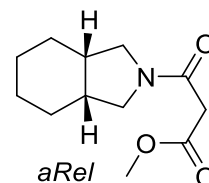
Purification Crude reaction mixture was dissolved in DCM/MeOH, evaporated on 20g ISOLUTE® HM-N (diatomaceous earth) and purified with Grace Reveleris.

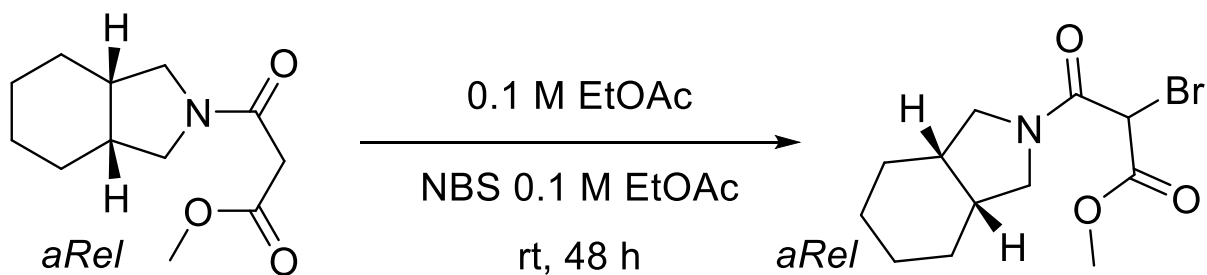
Column: CHROMABOND Flash with 200g MN Silica.
Mobile phase: DCM/MeOH.

¹H NMR (300 MHz, Chloroform-*d*) δ 3.68 (s, 3H), 3.35 (d, *J* = 11.5 Hz, 3H), 2.35 – 2.06 (m, 2H), 1.66 – 1.21 (m, 4H).

¹³C-NMR (75 MHz, Chloroform-*d*) δ 167.96, 164.85, 52.30, 51.11, 49.68, 42.02, 37.53, 35.94, 25.56, 25.54, 22.62, 22.42.

HR-MS *m/z* =calculated 248.1257 [M+Na⁺] found 248.1262 (ESI+APCI) [M+Na⁺]





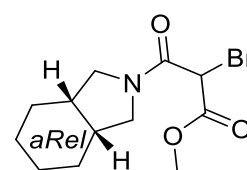
Equipment: 1L RBF with magnetic stirring.

5.10 g (22.6 mmol, 1.00 eq) of maleamide were dissolved in 225 mL of ethylacetate 4.029 g (22.6 mmol, 1.00 eq) of N-bromosuccinimide were dissolved in 225 mL of ethylacetate. The NBS solution was added quickly to the vigorously stirring solution of maleamide. The reaction was left to stir for 60 h. uHPLC-check revealed clean conversion to product. No traces of Side Products or Starting material.

To the reaction mixture was added water and left to stir for 5 min. Phases were separated and the organic phase washed with 150 mL water three times to extract the succinimide byproduct. The organic phase was dried over magnesium sulfate and the volatiles removed in vacuo. 6.80 g (99%) of a orange oil were obtained.

¹H-NMR reveals satisfyingly pure (3w% succinimide, 2w% CH₂Cl₂, 2 w% EtOAC) product. Due to the unstable nature of the alpha-bromo-compound it was decided to not purify it further.

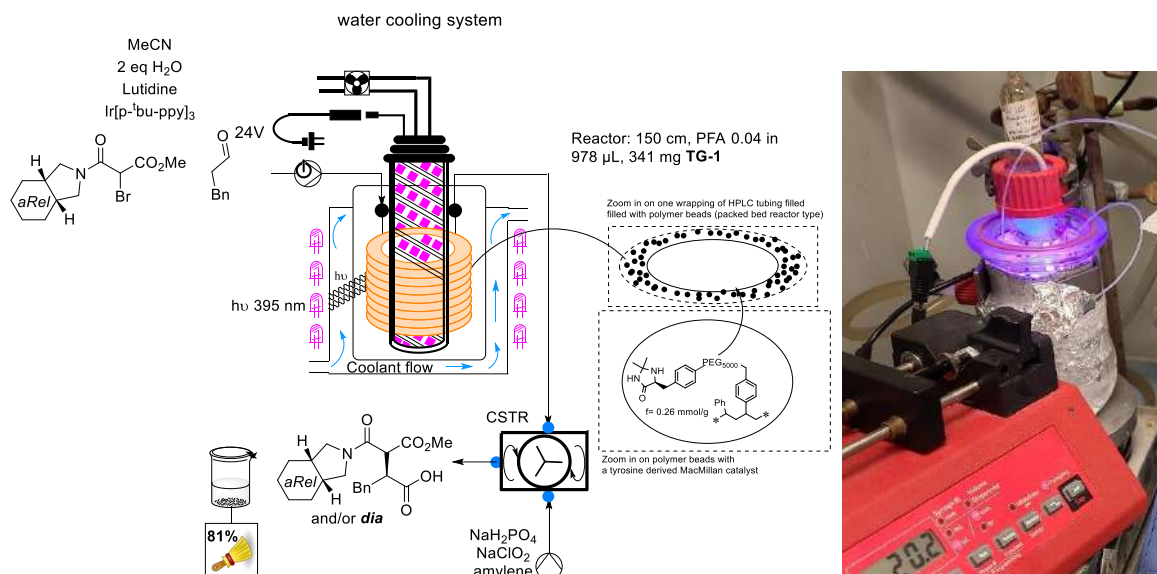
¹H NMR (300 MHz, Chloroform-*d*) δ 4.93 (d, $J = 10.7$ Hz, 1H), 3.83 (s, 3H), 3.64 – 3.23 (m, 2H), 2.75 (s, 0H), 2.28 (dd, $J = 26.9, 6.0$ Hz, 2H), 1.73 – 1.29 (m, 4H).



¹³C-NMR (75 MHz, Chloroform-*d*) δ 177.44, 165.06, 165.00, 163.24, 163.08, 53.76, 51.06, 50.48, 50.35, 43.04, 42.89, 37.64, 37.60, 35.73, 35.65, 29.48, 25.42, 25.40, 25.33, 22.53, 22.28, 22.24.

HR-MS m/z =calculated 326.0362 [M+Na⁺] found (ESI+APCI) 326.0365 [M+H⁺]

4.1.7. Telescoped *in continuo* Synthesis of a Mitiglinide Precursor



Construction of packed-bed Reactor: 180 cm of 1/16" outer diameter – 0.04" inner diameter PFA-HPLC-tubing were cut and equipped with fluidic connectors (1/4-28-bore fingertight ferules) on both sides. In one side was introduced a string of cotton to act as a "filter/retainer" for the resin-beads. This side was then equipped with a fluidic-adapter (1/4-28-bore female-to-female). This setup was then weighed, and the weight was noted for later use. Roughly 500 mg of **TG-1** was weighed into a beaker and the weight of the beaker plus resin was noted. **TG-1** was swollen in acetonitrile and the mixture was suspended and taken up in a 2.5 mL SGE gastight syringe and connected to the previously prepared HPLC-Tubing. The mixture was infused so long as the tubing was optically filled with the resin. Another good indicator for complete filling was a sudden jump in counterpressure experienced in the operator's hand. All the remaining material inside the syringe was carefully reintroduced into the beaker, flushing the syringe several times with dichloromethane all while also introducing the flushing liquid into the beaker. The reactor was placed into a freezer overnight, while the solvent mixture was inside the beaker was left to evaporate overnight and was put into a vacuum drying oven the next day for 2 h at 40 °C. The weight difference inside the beaker represents the amount of **TG-1** (341 mg, 119 μmol) infused into the reactor. The packed-bed reactor was weighed the next day and based on the density of acetonitrile and previously determined weight of **TG-1** inside the reactor, the reactor volume was determined to be $V_R=981 \mu\text{L}$.

Construction of continuous stirred tank reactor: a 4 mL screw-cap vial with two stacked rubber septa was equipped with a stirring bar (conical, 5 mm*12 mm). The septum was punctured in three spots with a thick needle. With the help of tweezers through each of the punctured spots was introduced 1/16" PFA HPLC Tubing which was cut in a roughly 45° angle to get a pointier tip. One of the tubing was used as the outflow while one of the other two was used as the in-flow from the previous photoreaction and the last one was used as the inflow for the sodium phosphate-buffer, sodium chlorite aqueous solution and the amylene – all being independently infused but combined in a X-Mixer.

Continuous Flow Photoreaction: Roughly 20 mL of a stock solution (0.21 M of effective concentration) was prepared according to the protocol detailed in the general procedure. For this 16 mL of acetonitrile were used, 1.6 mL of phenylpropanal, 1.22 g of radical source, 450 µL of lutidine, 6.4 mg of *fac*-Ir[ppy]₃ (Nucleophilic catalyst was excluded due to the observation of significant protodehalogenation). Another difference to the general procedure was the introduction of 2 eq of water to make sure there is water to hydrolyze the iminium-ion formed in the catalytic cycle. As the amino-catalyst is inside the packed-bed reactor it was not included in the reaction mixture. The stock solution was taken up in a 25 mL SGE Gastight syringe and was infused with a static flowrate of 8.15 µL/min into the reactor to give a residence time of $t_R=120$ min. Two full reactor volumes were discarded and the outflow was checked via uHPLC-MS and indeed full conversion was seen. The outflow was then connected to the CSTR as previously detailed.

Continuous Pinnick Oxidation: The previously described X-connector piece was connected to the CSTR. In total three syringes were prepared which were all connected to the X-connector piece.

1st: In a 2.5 mL SGE gastight syringe was taken up a previously prepared 2.1 M solution of sodium chlorite in water. Syringe was connected to a X-connector piece and contents were infused with 3.3 $\mu\text{L}/\text{min}$ (4.00 eq)

2nd: In a 25 mL SGE was taken up a previously prepared 0.21 M solution of NaH_2PO_4 (pH=4). Syringe was connected to a X-connector piece and contents were infused with 8.15 $\mu\text{L}/\text{min}$. (1.00 eq – after full conversion reaction mixture is already at a slightly acidic pH).

3rd: In a 25 mL SGE was taken up a previously prepared 0.21 M solution of amylene in acetonitrile. The Syringe was connected to a X-connector piece and contents were infused with 41 $\mu\text{L}/\text{min}$. (5.00 eq).

The combined flow into the CSTR was roughly 60 $\mu\text{L}/\text{min}$ which manifests itself in a residence time t_R of around 70 min. After waiting one residence time, the reactor efflux was collected showing quantitative consumption of the aldehyde intermediate and formation of the carboxylic acid product. The reactor mixture was collected for 59 min to give a theoretical 100 μmol of product (assuming quantitative conversion). To the reaction mixture was added 100 μL of sat. aq. Sodiumthiosulfate solution and the phases were separated by diluting with 1 mL of water. The aqueous phase was extracted three times with 5 mL of dichloromethane and the volatiles removed *in vacuo*. The remains were subjected to RP-C18 flash chromatography as detailed below to give 28 mg (76%) of a colorless oil.

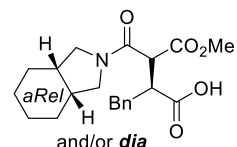
Purification Remains were dissolved in DCM, evaporated on 1.6g ISOLUTE® HM-N (diatomaceous earth) and purified with Grace Reveleris. Column: CHROMABOND Flash with 40g MN RP-18.

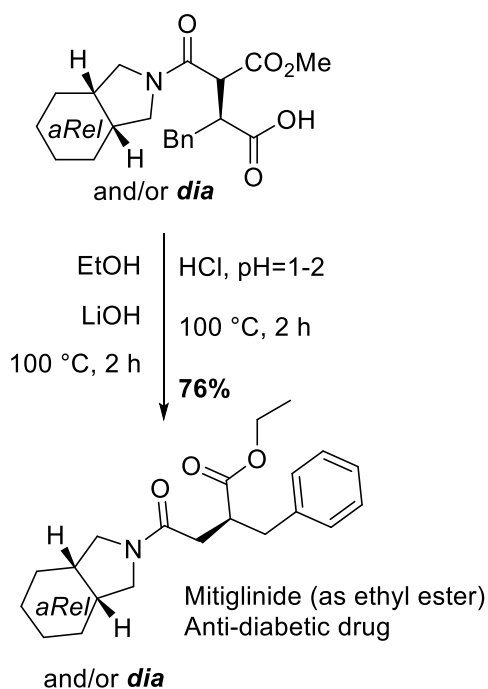
Mobile phase: H₂O (+0.1 HCOOH)/Acetonitrile.

¹H NMR (300 MHz, Chloroform-*d*) δ 7.21 (tq, *J* = 7.4, 3.3 Hz, 1H), 7.09 (t, *J* = 7.5 Hz, 1H), 3.75 – 3.61 (m, 1H), 3.52 (d, *J* = 5.7 Hz, 0H), 3.39 (dt, *J* = 11.1, 5.9 Hz, 1H), 3.30 – 3.10 (m, 0H), 3.03 (dd, *J* = 9.8, 5.7 Hz, 0H), 2.93 – 2.70 (m, 0H), 2.61 (dd, *J* = 10.0, 7.2 Hz, 0H), 2.42 (dd, *J* = 9.8, 7.0 Hz, 0H), 2.12 (tq, *J* = 12.4, 6.6, 6.1 Hz, 1H), 1.64 – 0.99 (m, 3H).

¹³C-NMR (75 MHz, Chloroform-*d*) δ 174.30, 168.02, 167.89, 167.85, 167.71, 137.39, 137.27, 129.25, 129.17, 128.87, 128.77, 128.69, 128.66, 128.60, 127.07, 127.03, 53.07, 53.04, 51.25, 51.05, 50.29, 49.39, 49.20, 37.21, 37.11, 35.91, 35.81, 35.64, 35.55, 25.83, 25.35, 25.16, 25.07, 22.94, 22.37, 22.25, 21.80.

HR-MS *m/z* =calculated 396.1781 [M+Na⁺] found 396.1786 (ESI+APCI) [M+Na⁺]





Equipment: Xelsius-Vial.

87 mg (233 μ mol, 1.00 eq) of acid product were dissolved in 5 mL of Ethanol. To this solution were added 12.00 mg (513 μ mol, 2.20 eq) LiOH and the resulting solution was stirred for two hours at 100 °C. uHPLC-Ch1 revealed full saponification. Reaction was cooled to room temperature and Hydrochloric acid (10%) was added until the pH=1-2 (pH-Paper). The mixture was then heated at 100 °C for one hour. uHPLC-Ch2 revealed product ester formation, acid byproduct and remaining starting material. As the uHPLC showed some unidentifiable peaks it was decided

to not further heat and to quench the reaction with sat. Aq. Sodium hydrogencarbonate. Mixture was diluted with water and dichloromethane. Phases were separated and the aqueous phase was extracted two additional times with dichloromethane. The combined organic phase were dried over magnesium sulfate and the volatiles removed in vacuo. 88 mg of a yellow oil were obtained.

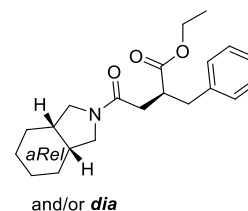
60 mg of a colorless oil were isolated which amounts to an isolated yield of 76%

Purification Remains were dissolved in DCM, evaporated on 1g ISOLUTE® HM-N (diatomaceous earth) and purified with Grace Reveleris.

Column: Grace Reveleris with 12g Grace RP-18.

Mobile phase: H₂O (+0,1 HCOOH)/Acetonitrile.

¹H NMR (300 MHz, Chloroform-*d*) δ 7.53 – 6.94 (m, 5H), 4.19 – 3.90 (m, 2H), 3.59 – 3.12 (m, 4H), 2.94 (ddd, *J* = 13.5, 6.7, 1.8 Hz, 1H), 2.75 (ddd, *J* = 13.2, 8.1, 4.5 Hz, 1H), 2.56 (ddd, *J* = 15.5, 8.9, 5.9 Hz, 1H), 2.15 (ddt, *J* = 32.8, 18.6, 5.5 Hz, 2H), 1.68 – 1.22 (m, 12H), 1.10 (td, *J* = 7.1, 1.7 Hz, 3H).



¹³ C-NMR	(75 MHz, Chloroform- <i>d</i>) δ 175.15, 175.11, 169.91, 138.67, 138.63, 128.98, 128.30, 126.38, 60.42, 50.37, 50.24, 49.53, 49.36, 42.87, 42.81, 37.93, 37.89, 37.49, 37.44, 35.85, 35.83, 35.23, 35.19, 25.72, 25.67, 25.64, 22.66, 22.56, 14.03.
HR-MS	m/z =calculated 366.2040 [M+Na ⁺] found
(ESI+APCI)	366.2040 [M+Na ⁺]
Chiral	Column: Chiralpak AS-3
HPLC	Eluent: Hexane/IPA 90/10 @ 1mL/min
	t _R (minor) 15.5 min, t _R (major) 25.4 min

4.2. Solid Supported Eosin Y and Its Use in (Stereoselective) C-C-Bond Formations

General Description of Reagents and Methods

As oxidation with air is one of the key scopes of this work, no special care was undertaken to work under an inert-gas atmosphere. If not otherwise stated reagents, solvents, and such were used without further purifications. 1,2,3,4-tetrahydroisoquinoline was bought from sigma and distilled and stored over potassium hydroxide before use. Eosin Y was bought from TCI chemicals and was either used without purification or was converted to the sodium salt by addition aqueous sodium hydroxide solution. *N,N*-dimethylformamide was degassed prior to use. *N,N*-diisopropylethylamine was used without prior purification. Merrifield Resin High Loading 1.2 mmol/g was purchased from Merck. Acetonitrile was used in HPLC-grade quality. *N*-phenyl-1,2,3,4-tetrahydroisoquinoline was synthesized as previously published.^[108] The para-bromo derivative thereof was synthesized as previously described.^[109] The para-chloro derivative was synthesized according to a recently published study.^[110] Nitromethane was purchased from Carl Roth. Triethylphosphit was purchased from TCI chemicals. *N*₁,*N*₁-diethyl ethylenediamine **Cat-1** was purchased from Acros Organic and used without further purification. **Cat-2** was purchased from Sigma Aldrich. **Cat-3** was synthesized according to a published study.^[111] **Cat-4** was synthesized according to a known protocol.^[112]

Reactions were monitored by thin layer chromatography (TLC) on Macherey-Nagel pre-coated silica gel plates (0.25 mm) and visualized by UV light. Flash chromatography was performed on Merck silica gel (60, particle size: 0.040–0.063 mm). ^1H NMR ^{13}C NMR and ^{19}F NMR spectra were recorded on Bruker Avance III HD 600, Bruker Avance-400, Bruker Avance-300 or Bruker Avance-250 spectrometer in CDCl_3 as solvents at room temperature. Chemical shifts for protons are reported using residual solvent protons (^1H NMR: $\delta = 7.26$ ppm for CDCl_3) as internal standard. Carbon spectra were referenced to the shift of the ^{13}C signal of CDCl_3 ($\delta = 77.0$ ppm). The following abbreviations are used to indicate the multiplicity in NMR spectra: s - singlet; d - doublet; t - triplet; q - quartet; dd - double doublet; ddd – doublet of doublet of doublets; dt - doublet of triplets; m - multiplet; quint – quintuplet; sext -sextuplet sept - septet; br - broad signal; dq – doublet of quartets.

High resolution mass spectra (HRMS) were acquired using a Bruker solariX XR Fourier transform ion cyclotron resonance mass spectrometer (Bruker Daltonik GmbH, Bremen, Germany) equipped with a 7 T refrigerated actively shielded superconducting magnet. The samples were ionized in positive ion mode using a MALDI or ESI ionization sources.

Automatic weighing and transferring of liquids were made with a Zinssler Analytics custom robot “Calli”.

Samples were evaporated in a parallel fashion by employing a Genevac HT-4X vacuum centrifuge Series II System.

Preparative HPLC-MS was conducted on an Agilent 1260 Infinity Series (Autosampler, Fraction Collector, DAD, Pumps, Check valves, all while coupled to a Agilent 6120 LC-MS Quadrupole mass-spectrometer. MS-traces were generated in positive/negative switching mode and ESI/APCI as ionization method was used in tandem.

uHPLC-MS (ultrahigh performance) was conducted on an Agilent 1260 Infinity Series (Autosampler, Pump was 1290 Infinity Series) all while coupled to an Agilent 6120 LC-MS Quadrupole mass-spectrometer. MS-traces were generated in positive/negative switching mode and ESI/APCI as ionization method was used in tandem.

Chiral HPLC was measured on a Agilent 1100 Series (DAD, Autosampler, Pumps). The respective chiral stationary phase is indicated in the characterization part.

Experimental Procedures

4.2.1. Description of Equipment

LED-Specifications:

Low power: Govee LED Strip 5m, with IR remote control. (12 W/5 m, 2.6 W/m)

High power: METEL: F52-GRE-120812 5m green light 525 nm 2835 120led/m 24V 24W/m

Pumps

Vapour-Tec easyScholar e-series Continuous flow reactor. Especially the peristaltic pumps were used (100 μ L/min-10 mL/min) effective flow rates.

KF-Technologies, NE-300 series Just Infusion.

Packed-Bed-reactor

100 mm x 10 mm (I*ID) Omnifit-Column filled with:

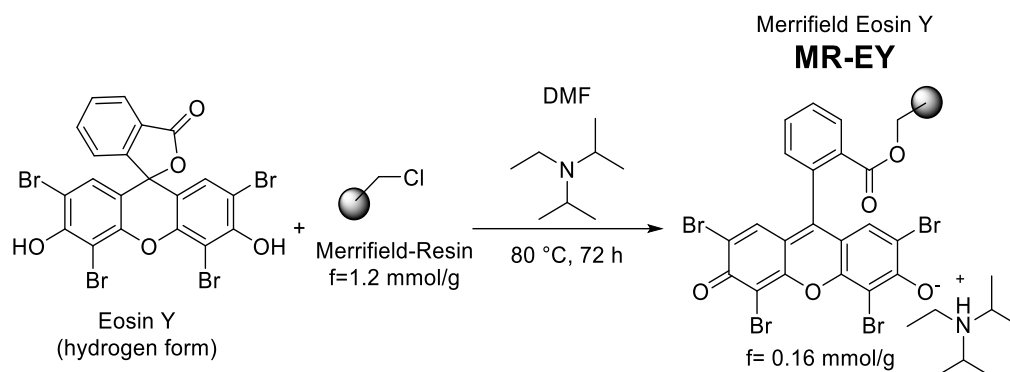
Configuration 5 mm: A total of 42 5 mm glass-balls were filled inside the Omnifit-column (such that the glass-balls were forming a tight-packed configuration, 2 per layer) which was tightly held in place in a vertical position. Inside the column was filled a suspension of 1.24 g of Merrifield Eosin Y in acetonitrile. Regular agitation of the setup ensured complete settling of the solid material inside the reactor. After filling was completed the closing lid with fluidic connection was reattached. The reactor volume $V_R = 1.95$ mL was determined by infusing a 0.1 M solution of anthraquinone and periodically (every 50 μ L) collecting a drop of the outflow on a piece of TLC-plate and checking by a 254 UV-lamp.

Configuration 4 mm: A total of 80 4 mm glass-balls were filled inside the Omnifit-column (such that the glass-balls were forming a tight-packed configuration, 3 per layer) which was tightly held in place in a vertical position. Inside the column was filled a suspension of 1.30 g of Merrifield Eosin Y in acetonitrile. Regular agitation of the setup ensured complete settling of the solid material inside the reactor. After filling was completed the closing lid with fluidic connection was reattached. The reactor volume $V_R = 2.15$ mL was determined by infusing a 0.1 M solution of anthraquinone and

periodically (every 50 μL) collecting a drop of the outflow on a piece of TLC-plate and checking by a 254 UV-lamp.



4.2.2. Synthesis and Characterisation of Solid-Supported Eosin Y MR-EY



In a 250 mL three-necked-flask were weighed exactly 10.0 g (8.33 mmol, 1.00 eq, $f=1.20$ mmol/g) Merrifield-Resin High-Load 100-200 mesh.¹ To this were added 6.48 g (10.0 mmol, 1.20 eq) Eosin Y (hydrogen form). To the flask was then applied a mechanical stirring device. The solid were dispersed in 133 mL *N,N*-dimethylformamide, Mechanical stirring was turned on and it was added 3.48 mL (20.0 mmol, 2.40 eq) diisopropylethylamine. After setting the temperature to 80 °C the dispersion was stirred for exactly 72 h.

After the reaction was completed the reaction mixture was poured into an oven-dried glass sintered funnel (pore size 4, pre-weighed) and special care was taken to remove almost all the material out of the flask with generous amounts of methanol. The residue was infused with a mixture of water/THF/methanol and stirred with a glass rod. After infusing for 5 minutes vacuum was attached and the washing liquid was filtered off. Vacuum was detached and the whole process was repeated 15 times. After this generous washing, the process was repeated for three times using dichloromethane. The washing flasks was changed and the remains in the funnel were dried by running a constant air stream through them for 5 hours by attaching a vacuum. After this time the filter was weighed again and by the difference in weight a preliminary catalyst loading calculated, which amounts to $f = 0.168$ mmol/g.

Elemental analysis of MR-EY: C 80,73, H 6,54, N 0,28

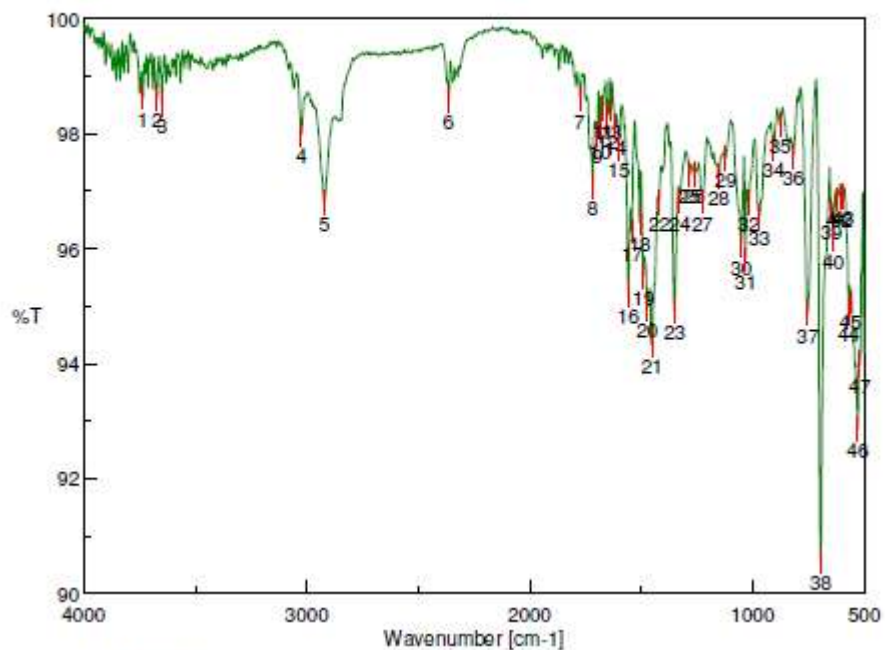
That corresponds to $f = 0.2$ mmol/g

The gravimetric loading ($f = 0.168$ mmol/g) was used in the reactions

¹ Exact weighing was done to ensure later gravimetric preliminary determination of loading.

IR-Spectrum of MR-EY

Peak Find - merrifield eosina.jws

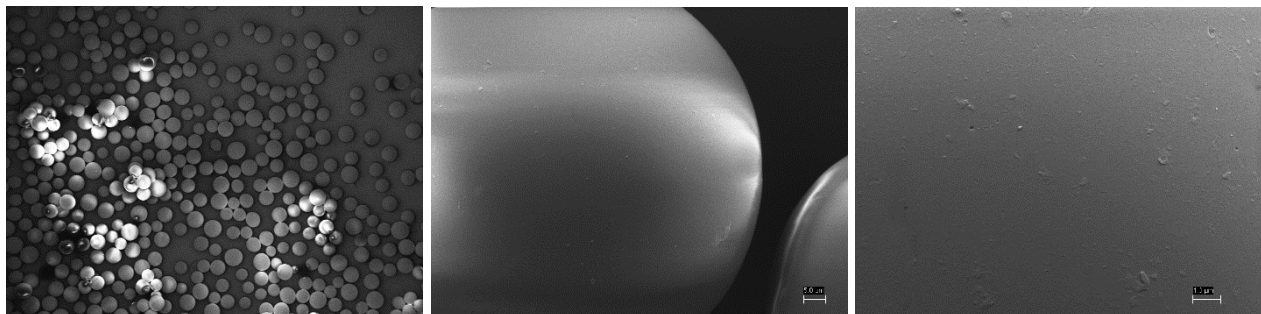


[Result of Peak Picking]

No.	Position	Intensity	No.	Position	Intensity
1	3734.48	98.6362	2	3672.77	98.6184
3	3648.66	98.5185	4	3024.8	97.9819
5	2920.66	96.8038	6	2363.34	98.5871
7	1772.26	98.5996	8	1717.3	97.0894
9	1698.02	97.9906	10	1684.52	98.0685
11	1671.02	98.4196	12	1653.66	98.2399
13	1636.3	98.4288	14	1616.06	98.1205
15	1600.63	97.7409	16	1558.2	95.203
17	1541.81	96.2995	18	1507.1	96.4549
19	1489.74	95.5223	20	1472.38	94.9448
21	1452.14	94.3367	22	1419.35	96.7989
23	1350.89	94.9218	24	1327.75	96.825
25	1282.43	97.2973	26	1263.15	97.2921
27	1224.58	96.8213	28	1152.26	97.2579
29	1121.4	97.5755	30	1051.98	96.0584
31	1032.69	95.808	32	1018.23	96.8081
33	970.019	96.5686	34	905.415	97.7429
35	878.417	98.1582	36	817.67	97.5995
37	754.031	94.8653	38	695.212	90.5565
39	647.965	96.6615	40	638.323	96.1629
41	620.966	96.8618	42	602.646	96.894
43	593.004	96.9096	44	569.862	94.9041
45	562.148	95.0873	46	528.4	92.868
47	518.758	93.9874			

SEM images

Samples were placed on an aluminum stub with carbon tape, golden coated and observed under a FESEM Sigma (Zeiss) equipped with an EDS spectrometer (Bruker). Images were acquired at 5KV at 5mm of working distance.



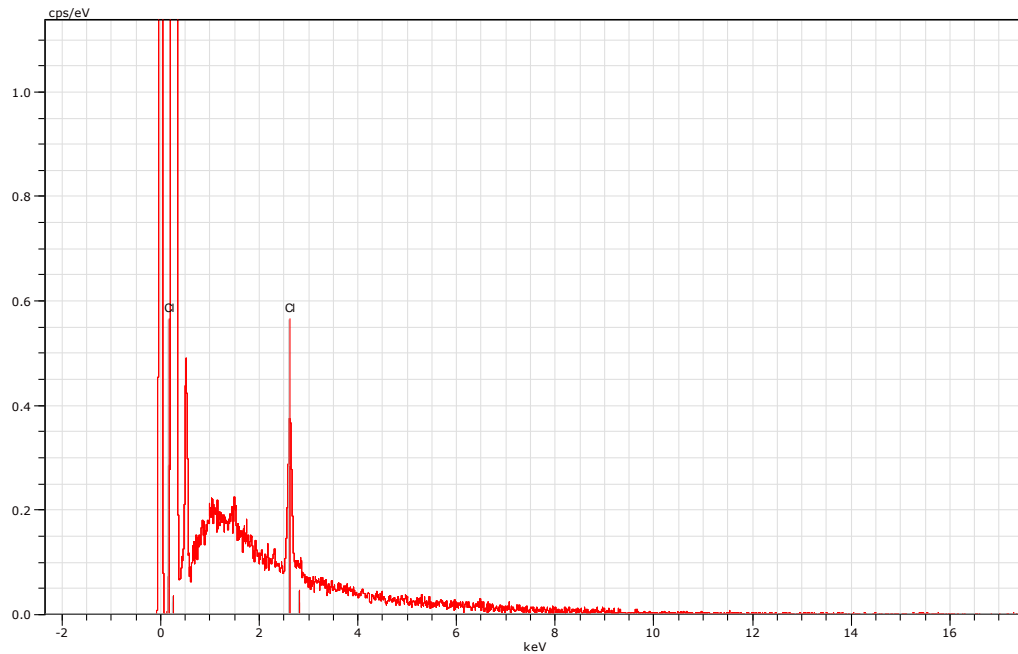
SEM images of commercial Merrifield resin at 150x, 4000x, 25000x magnification



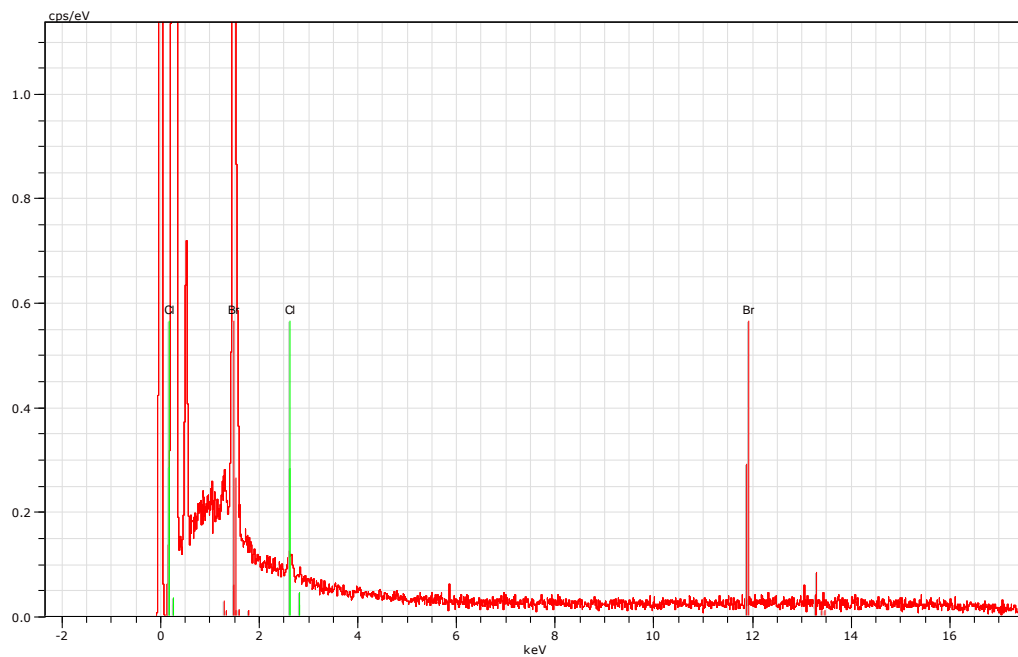
SEM images of MR-EY at 150x, 4000x, 25000x magnification

EDS analysis

Samples were placed on an aluminum stub with carbon tape, golden coated and observed under a FESEM Sigma (Zeiss) equipped with an EDS spectrometer (Bruker). EDS analysis were performed at 20KV



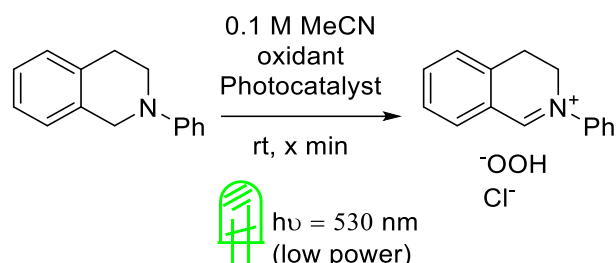
EDS of commercial Merrifield resin



EDS of MR-EY

4.2.3. General Procedures for Batch, Continuous Flow and Packed Bed Catalytic Reactions

General Procedure for Batch Reaction (Screening)



Into a 7 mL screw-neck vial with rubber-teflon septum were placed 105 mg (500 μmol , 1.00 eq) of *N*-Phenyl 1,2,3,4-tetrahydroisoquinoline, followed by 5.00 μmol (1 mol%) of the respective photocatalyst (MR-EY or Na₂Eosin Y). To the vial was added 5 mL acetonitrile. In case of aerobic oxidation, the septum was punctured with a needle, which remained stuck inside the septum. In case of oxidation with tetrochlorocarbon 57.0 μL (600 μmol , 1.20 eq) of which were added to the solution. The vial was subsequently placed roughly in the center of a crystallizing dish (20 cm diameter) which was wrapped with the low power LEDs from the outside. After the later indicated time intervals, an aliquot (20 μL , 2 drops) was taken, dissolved in 1.5 mL acetonitrile and injected into HPLC-MS for quantification.

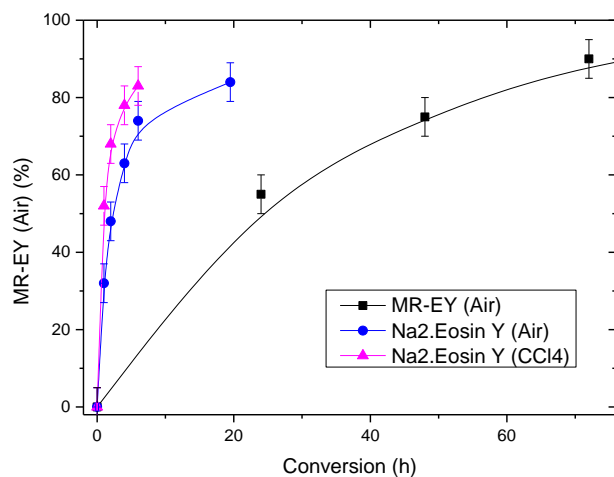
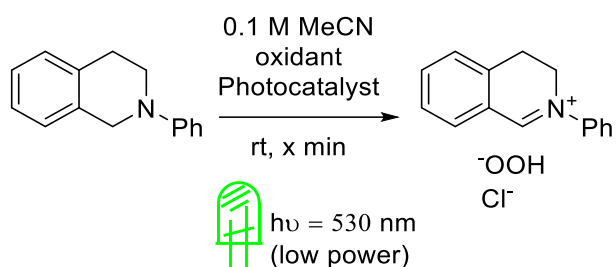
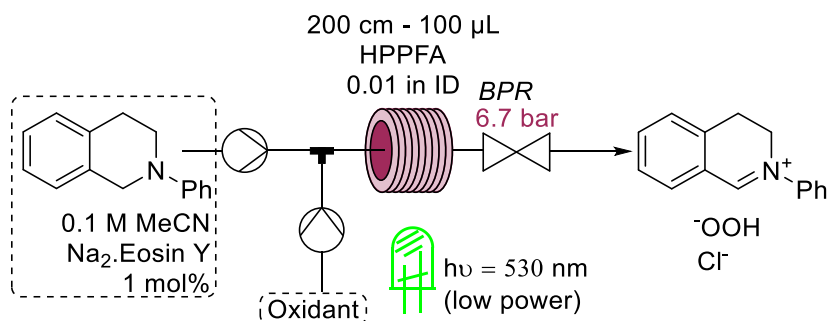


Table 1. Tabular summary of the datapoints inside the conversion graph.

Entry	Reaction Time [h]	Conversion Na ₂ Eosin Y Air [%]	Conversion Na ₂ Eosin Y CCl ₄ [%]	Entry	Reaction Time [h]	Conversion MR-EY [%]
1	0	0	0	7	0	0
2	1	32	52	8	24	55
3	2	48	68	9	48	75
4	4	63	78	10	72	90
5	6	74	83	11	120	100
6	19.5	84	-	-	-	-

General Procedure for Plug-Flow (Microfluidic) Experiments (Screening)

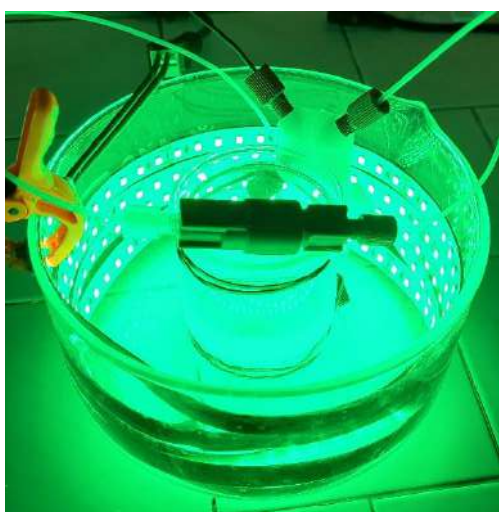
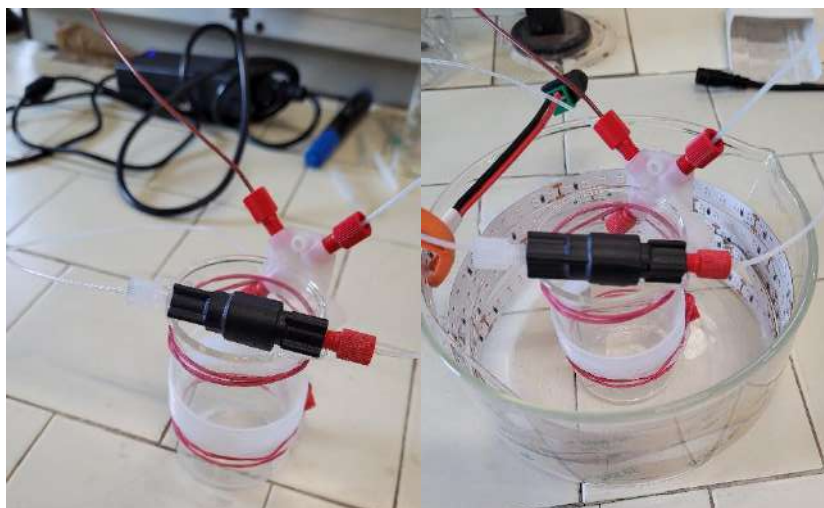


Inside a screw-neck vial was prepared a 0.1 M solution of *N*-Phenyl 1,2,3,4-tetrahydroisoquinoline, 1 mM of Na₂Eosin Y. In case of oxidation with tetrachlorocarbon the same was solution was made with 0.15 M of tetrachlorocarbon.

The solution was taken up in a 2.5 mL SGE gastight syringe and connected to the continuous-flow reactor.

Continuous flow reactor: 200 cm of HPPFA HPLC-tubing was wrapped around a 2 cm diameter glass-tube. The resulting coil-reactor was connected via a Y-connector to the syringe (and the VapourTec peristaltic pump in case of aerobic oxidation), at the intake side. At the output side was connected a back-pressure-regulator (spring-loaded) ensuring 6.7 bar of pressure. The coil-reactor was placed inside the previously described batch-photoreactor inside the crystallization dish as illustrated in the pictures below.

The solution was infused inside the coil-reactor according to the following table and graph. Between or before each collection at a previously varied flow rate, two residence times were discarded until steady state operation of the reactor was reached. Collection of an aliquot: 20 μ L, 2 drops were dissolved in 1.5 mL acetonitrile and injected into HPLC-MS for quantification.



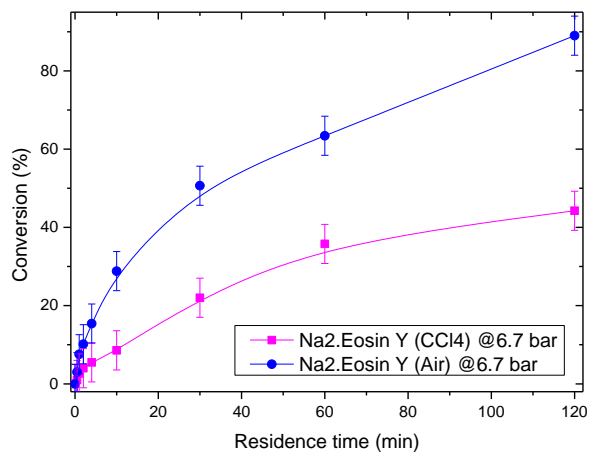
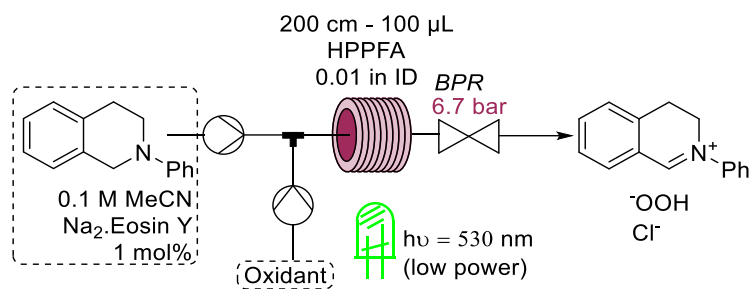
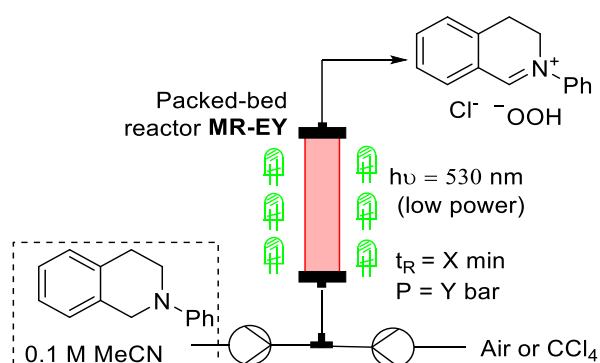


Table 2. Tabular summary of the datapoints inside the conversion graph.

Entry	Residence time [min]	Conversion	
		Na ₂ .Eosin Y Air [%]	Na ₂ .Eosin Y CCl ₄ [%]
1	0	0	0
2	0.5	3	1
3	1	7.6	2.7
4	2	10	4
5	4	15	5.5
6	10	29	8.57
7	30	51	22
8	60	63	36
9	120	89	44

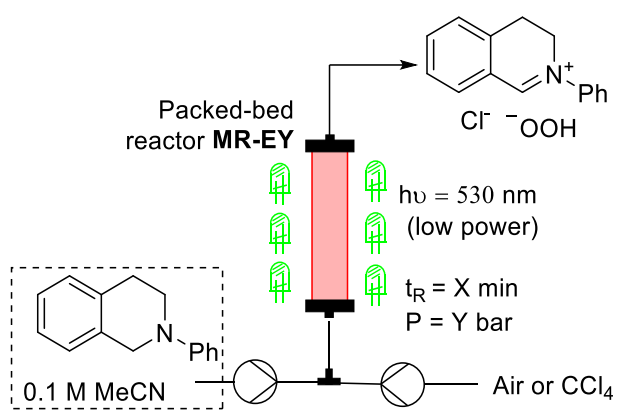
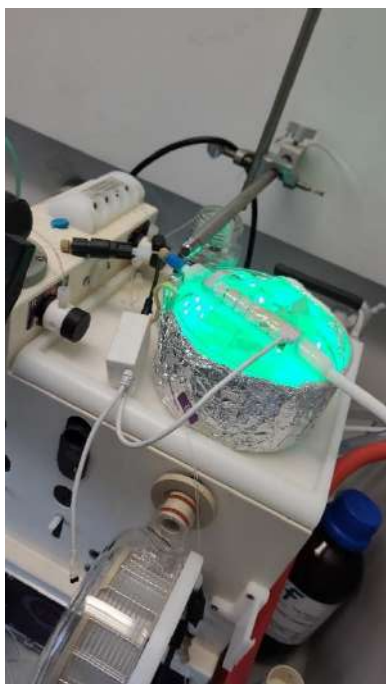
General Procedure for Continuous Flow Packed Reactor Experiments (Screening)



Inside a screw-neck vial was prepared a 0.1 M solution of *N*-Phenyl 1,2,3,4-tetrahydroisoquinoline. The solution was taken up in a 25 mL SGE gastight syringe and connected to the continuous-flow reactor.

Continuous flow reactor: Either configuration (4 mm or 5 mm) was connected via a Y-connector to the syringe and the VapourTec peristaltic pump at the intake side. At the output side was connected a back-pressure-regulator (spring-loaded) ensuring 6.7 bar of pressure, in case of pressurized operation. The catalytic packed-bed reactor was wrapped with the low-power LEDs as previously specified. In case high power LEDs were employed the reactor was placed inside a doubled-walled reactor glass-piece which was connected to in-house water circulation/cooling system. Around this reactor was wrapped the high power LED strip.

The solution was infused into the catalytic packed-bed reactor according to the following tables and graphs. Between or before each collection at a previously varied flow rate, two residence times were discarded until steady state operation of the reactor was reached. Collection of an aliquot: 20 μL , 2 drops were dissolved in 1.5 mL acetonitrile and injected into HPLC-MS for quantification.



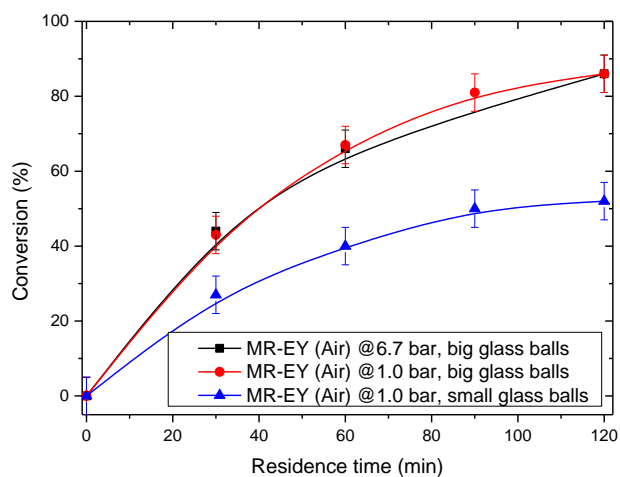


Table 3. Tabular summary of the datapoints inside the conversion graph.

Entry	Residence time [min]	Conversion	Conversion	Conversion
		MR-EY@6.7 bar Big glass balls Air [%]	MR-EY@1.0 bar Big glass balls Air [%]	MR-EY@1.0 bar small glass balls Air [%]
1	0	0	0	0
2	30	44	43	27
3	60	66	67	40
4	90	---	81	50
5	120	86	86	52

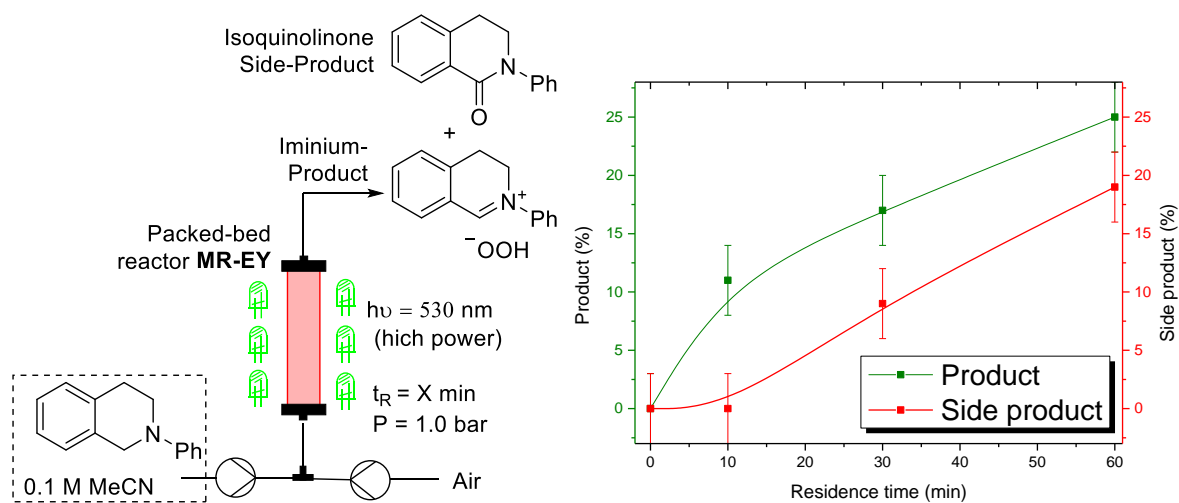
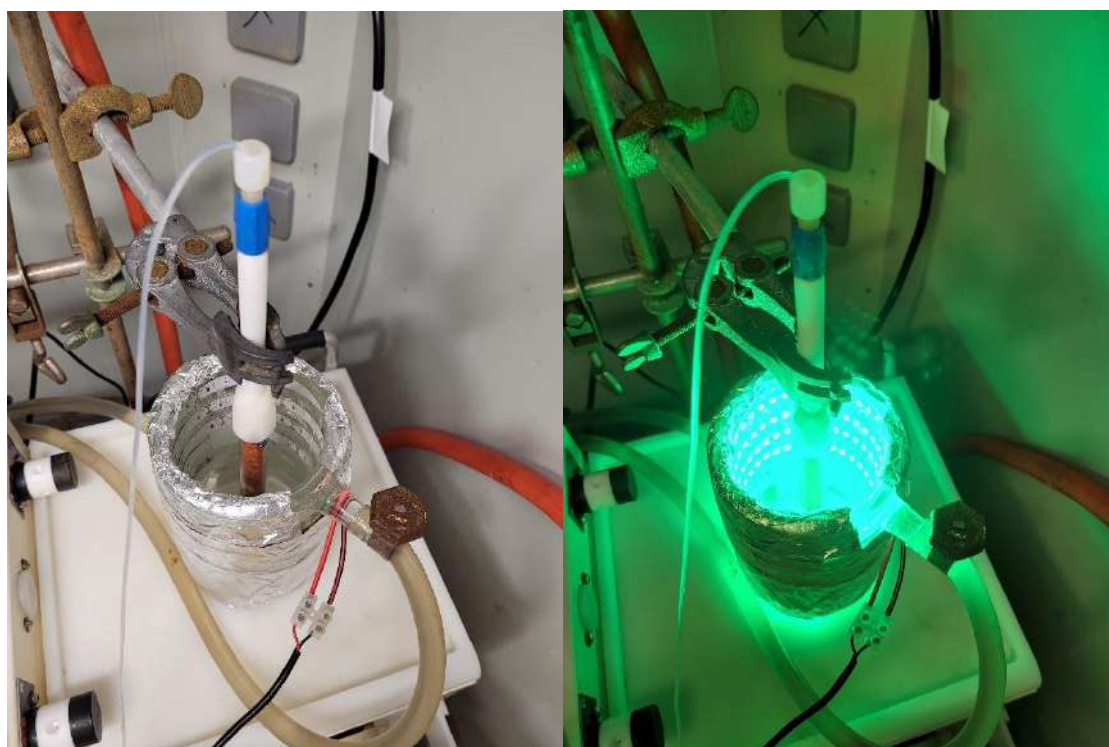
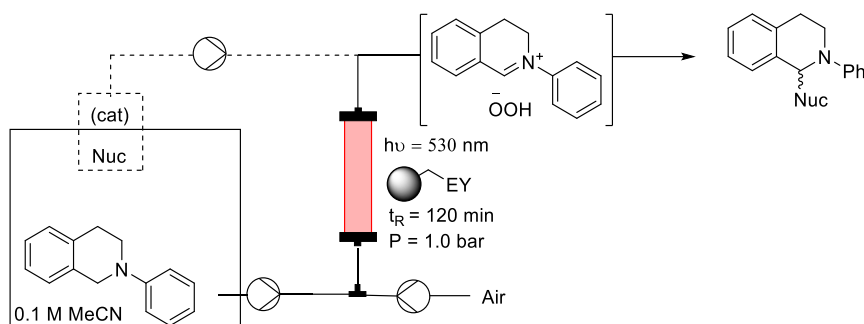


Table 4. Tabular summary of the datapoints inside the conversion graph.

Entry	Residence time [min]	Conversion to product [%]	Conversion to side-product [%]
1	0	0	0
2	10	11	0
3	30	17	9
4	60	25	19



Fluidic Synthesis: General Procedure



Inside a screw-neck vial was prepared a 0.1 M solution of *N*-Phenyl 1,2,3,4-tetrahydroisoquinoline (or its para-chloro/para-bromo derivatives). The solution was taken up in a 25 mL SGE gastight syringe and connected to the continuous-flow reactor.

In case of Aza-Henry reaction, nitromethane was added to generate a 1.0 M thereof. In case of Aza-Michaelis-Arbusov-reaction, triethylphosphite was added to generate a 0.1 M solution thereof.

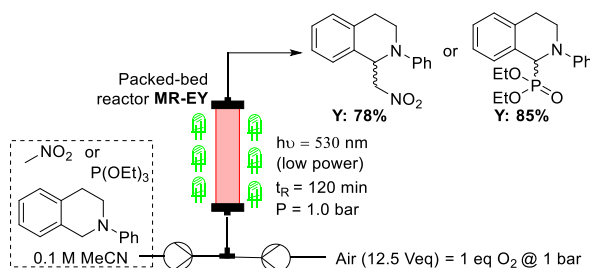
Continuous flow reactor: Configuration (4 mm or 5 mm) was connected via a Y-connector to the syringe and the VapourTec peristaltic pump at the intake side. At the output side was connected a back-pressure-regulator (spring-loaded) ensuring 6.7 bar of pressure, in case of pressurized operation. The catalytic packed-bed reactor was wrapped with the low-power LEDs as previously specified.

The solution was infused into the catalytic packed-bed reactor according to the following tables and graphs. Between or before each collection at a previously varied flow rate, two residence times were discarded until steady state operation of the reactor was reached. Collection of an aliquot: 20 μL , 2 drops were dissolved in 1.5 mL acetonitrile and injected into HPLC-MS for quantification.

After reaching satisfying levels of conversion the output of the packed-bed reactor was collected, or in the case of the diastereoselective Mannich-reaction protocol, connected to a Y-adapter into which was infused a solution of 15.0 M cyclohexanone and 1.0 M of the respective diamino-catalyst. The Y-adapter was inserted through a rubber-septum inside a temperature controlled (either room temperature or pre-cooled

to -10 °C) vial. The overall output was collected inside this vial and stirred for three days.

4.2.4. Fluidic Synthesis and Characterisation of Products



Packed-bed reactor configuration 5 mm was used. The stock solution was infused into the reactor with a flowrate of 16.25 μl/min. Air was infused with a flowrate of 203 μl/min. A total of 120 min of reactor output was collected, which corresponds to 200 μmol of starting material. After collection the sample was diluted with 1 mL of MeOH and subjected as is to C18 prepHPLC-purification. After vacuum centrifugation 42.0 mg (78%) of a orange oil were isolated.

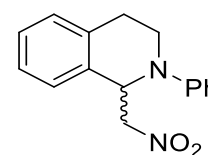
Purification Column: XBridge BEH Prep C18 5 μm, 19 mm X 150 mm.

Mobile phase: Acetonitrile / Water+5mM NH₄HCO₃

Flow rate: 32 ml/min

Gradient:

0-0.5 min	23:77
0.51-10,5 min	98:2
10,5-12,5 min	98:2

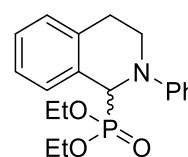


¹H NMR (300 MHz, Chloroform-*d*) δ 7.25 – 6.99 (m, 6H), 6.90 (dd, *J* = 8.0, 1.5 Hz, 2H), 6.81 – 6.73 (m, 1H), 5.47 (t, *J* = 7.2 Hz, 1H), 4.79 (dd, *J* = 11.8, 7.8 Hz, 1H), 4.48 (dd, *J* = 11.8, 6.6 Hz, 1H), 3.68 – 3.43 (m, 2H), 2.98 (dd, *J* = 8.5, 5.9 Hz, 1H), 2.71 (dt, *J* = 16.3, 5.0 Hz, 1H).

MS $m/z = 269.2 [M+H^+]$
(ESI+APCI)

Packed-bed reactor configuration 5 mm was used. The stock solution was infused into the reactor with a flowrate of 16.25 $\mu\text{l}/\text{min}$. Air was infused with a flowrate of 203 $\mu\text{l}/\text{min}$. A total of 120 min of reactor output was collected, which corresponds to 200 μmol of starting material. After collection the sample was diluted with 1 mL of MeOH and subjected as is to C18 prepHPLC-purification. After vacuum centrifugation 59.0 mg (78%) of a orange oil were isolated.

Purification Column: XBridge BEH Prep C18 5 μm , 19 mm X 150 mm
Mobile phase: Acetonitrile / Water+5mM NH_4HCO_3
Flow rate: 32 ml/min



Gradient:

0-0.5 min 23:77

0.51-9,5 min 98:2

9,5-11,5 min 98:2

$^1\text{H NMR}$ (300 MHz, Chloroform-*d*) δ 7.30 (dd, $J = 5.5, 3.4$ Hz, 1H), 7.20 – 7.14 (m, 1H), 7.13 – 7.06 (m, 2H), 6.91 (d, $J = 8.2$ Hz, 2H), 6.72 (t, $J = 7.2$ Hz, 1H), 5.11 (d, $J = 20.0$ Hz, 1H), 4.10 – 3.73 (m, 4H), 3.56 (dt, $J = 12.0, 5.5$ Hz, 1H), 3.07 – 2.86 (m, 2H), 1.17 (t, $J = 7.0$ Hz, 3H), 1.07 (t, $J = 7.0$ Hz, 3H).

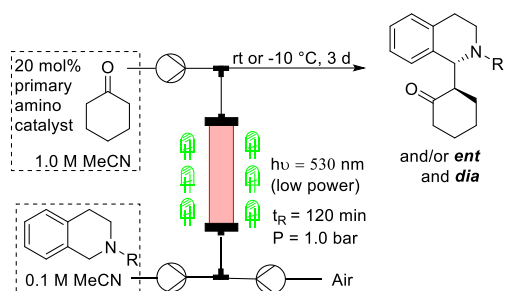
MS $m/z = 346 [M+H^+]$
(ESI+APCI)

Table

5.

Diastereoselective

Mannich-reaction.



Entry	R:	Catalyst	T [°C]	<i>d.r.</i>	<i>ee</i>	Yield
1	Ph		rt	1.5:1	---	64%
2	Ph		rt	1.49:1	<i>Rac</i> (min) 2% (maj)	71%
3	Ph		rt	1.19:1	67% (min) 70% (maj)	64%
4	Ph		rt	1:5.4	33% (min) 45% (maj)	67%
5	Ph		-10	4.9:1	88% (maj) 28% (min)	69%
6	<i>p</i> -Cl-Ph		-10	4:1	90% (maj) 20% (min)	68%
7	<i>p</i> -Br-Ph		-10	3.8:1	87% (maj) 5% (min)	61%

Packed-bed reactor configuration 5 mm was used. The stock solution was infused into the reactor with a flowrate of 16.25 $\mu\text{l}/\text{min}$. Air was infused with a flowrate of 203 $\mu\text{l}/\text{min}$. A total of 120 min of reactor output was collected, which corresponds to 200 μmol of starting material. The Solution containing cyclohexanone and Cat-3 was infused with a flowrate of 3.25 $\mu\text{L}/\text{min}$. After collection the sample was diluted with 1 mL of MeOH and subjected as is to C18 prepHPLC-purification. After Vacuum-centrifugation the following yield were obtained:

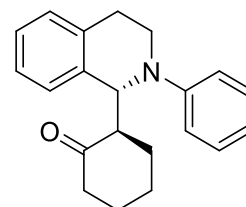
Minor dia: 7.00 mg

major dia: 35.6 mg

combined yield of diastereoisomers Y= 42,6 mg (69%)

from HPLC d.r. was estimated to be 1:4.9

Purification	Column:	XBridge BEH Prep C18 5 μm , 19 mm X 150 mm
	Mobile phase:	Acetonitrile / Water+5mM NH ₄ HCO ₃
	Flow rate:	32 ml/min



Gradient:

0-0.5 min 23:77

0.51-10,5 min 98:2

10,5-12,5 min 98:2

¹H NMR

Major Diastereoisomer

(300 MHz, Chloroform-*d*) δ 7.23 – 6.99 (m, 6H),
6.84 (d, J = 8.2 Hz, 2H), 6.69 (t, J = 7.2 Hz, 1H),
5.53 (d, J = 4.7 Hz, 1H), 3.65 (ddd, J = 13.5, 8.5,
5.3 Hz, 1H), 3.58 – 3.43 (m, 1H), 3.00 – 2.69 (m,
3H), 2.47 – 2.34 (m, 1H), 2.22 (ddd, J = 14.1, 9.1,
5.4 Hz, 1H), 1.91 – 1.69 (m, 3H), 1.71 – 1.44 (m,
3H), 1.34 (q, J = 10.3, 8.5 Hz, 1H).

Minor Diastereoisomer

^1H NMR (300 MHz, Chloroform-*d*) δ 7.36 – 7.22 (m, 1H), 7.21 – 7.09 (m, 2H), 7.09 – 7.00 (m, 3H), 6.74 (d, $J = 8.3$ Hz, 2H), 6.60 (t, $J = 7.2$ Hz, 1H), 5.59 (d, $J = 8.6$ Hz, 1H), 3.47 (dd, $J = 7.3, 5.4$ Hz, 2H), 3.07 – 2.90 (m, 1H), 2.90 – 2.75 (m, 1H), 2.65 (d, $J = 4.9$ Hz, 1H), 2.47 – 2.33 (m, 1H), 2.28 – 2.08 (m, 2H), 2.07 – 1.91 (m, 0H), 1.79 (t, $J = 4.8$ Hz, 1H), 1.69 – 1.40 (m, 3H).

Chiral Lux Amylose 1 nHex/*i*PrOH 95/5 eluent
HPLC Major Diastereoisomer 87% ee
Retention time 8.35 min (minor peak), Retention time 14.47 min (major peak),
Minor Diastereoisomer 30% ee
Retention time 7.93 min (minor peak), Retention time 14.27 min (major peak)
MS $m/z = 306.2$ [M+H⁺]
(ESI+APCI)

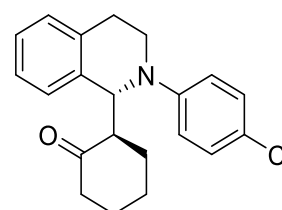
Packed-bed reactor configuration 5 mm was used. The stock solution was infused into the reactor with a flowrate of 16.25 $\mu\text{L}/\text{min}$. Air was infused with a flowrate of 203 $\mu\text{L}/\text{min}$. A total of 120 min of reactor output was collected, which corresponds to 200 μmol of starting material. The Solution containing cyclohexanone and Cat-3 was infused with a flowrate of 3.25 $\mu\text{L}/\text{min}$. After collection the sample was diluted with 1 mL of MeOH and subjected as is to C18 prepHPLC-purification. After Vacuum-centrifugation the following yield were obtained:

(minor): 8.75 mg were isolated after vacuum centrifugation

(major): 33.5 mg were isolated after vacuum centrifugation.

1:3.8 *dr* as estimated from HPLC.

Purification	Column:	XBridge BEH Prep C18 5
	μm , 19	mm X 150 mm
	Mobile phase:	Acetonitrile / Water+5mM
		NH ₄ HCO ₃
	Flow rate:	32 ml/min



Gradient:

0-0.5 min 23:77

0.51-11,5 min 98:2

11,5-13,5 min 98:2

¹H NMR

Major Diastereoisomer

(300 MHz, Chloroform-*d*) δ 7.32 – 7.22 (m, 1H), 7.13 – 7.02 (m, 5H), 6.76 – 6.55 (m, 2H), 5.53 (d, *J* = 8.5 Hz, 1H), 3.56 – 3.32 (m, 2H), 3.03 – 2.75 (m, 2H), 2.72 – 2.57 (m, 1H), 2.47 – 2.33 (m, 1H), 2.28 – 2.06 (m, 2H), 2.00 (dt, *J* = 6.0, 3.2 Hz, 1H), 1.80 (d, *J* = 8.7 Hz, 1H), 1.70 – 1.36 (m, 4H).

Minor Diastereoisomer

(300 MHz, Chloroform-*d*) δ 7.16 – 6.98 (m, 6H), 6.86 – 6.69 (m, 2H), 5.47 (d, *J* = 4.7 Hz, 1H),

3.61 (td, $J = 8.2, 4.2$ Hz, 1H), 3.53 – 3.40 (m, 1H), 2.99 – 2.67 (m, 3H), 2.49 – 2.32 (m, 1H), 2.23 (ddd, $J = 14.1, 9.8, 5.4$ Hz, 1H), 1.95 – 1.69 (m, 2H), 1.70 – 1.43 (m, 2H), 1.41 – 1.09 (m, 1H).

Chiral
HPLC Lux Amylose 1 nHex/*i*PrOH 90/10 eluent
Major Diastereoisomer 89% ee
Retention time 7.94 min (minor peak),
Retention time 10.14 min (major peak),
Minor Diastereoisomer 21% ee
Retention time 11.27 min (minor peak),
Retention time 7.54 min (major peak)

MS
(ESI+APCI) $m/z = 340.4$ [M+H⁺]

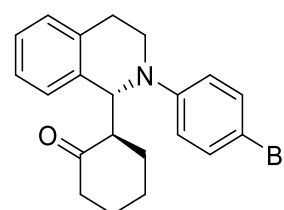
Packed-bed reactor configuration 5 mm was used. The stock solution was infused into the reactor with a flowrate of 16.25 $\mu\text{l}/\text{min}$. Air was infused with a flowrate of 203 $\mu\text{l}/\text{min}$. A total of 120 min of reactor output was collected, which corresponds to 200 μmol of starting material. The Solution containing cyclohexanone and Cat-3 was infused with a flowrate of 3.25 $\mu\text{L}/\text{min}$. After collection the sample was diluted with 1 mL of MeOH and subjected as is to C18 prepHPLC-purification. After Vacuum-centrifugation the following yield were obtained:

(minor): 10 mg were isolated after vacuum centrifugation

(major): 42 mg were isolated after vacuum centrifugation.

1:4 dr from HPLC

Purification Column: XBridge BEH Prep C18 5 μm , 19 mm X 150 mm
 Mobile phase: Acetonitrile / Water+5mM NH_4HCO_3
 Flow rate: 32 ml/min



Gradient:

0-0.5 min 23:77

0.51-11,5 min 98:2

11,5-13,5 min 98:2

^1H NMR

Major Diastereoisomer

(300 MHz, Chloroform- d) δ 7.29 – 7.22 (m, 1H), 7.19 (d, $J = 1.5$ Hz, 1H), 7.07 (q, $J = 4.0, 3.0$ Hz, 3H), 6.70 – 6.50 (m, 2H), 5.54 (d, $J = 8.5$ Hz, 1H), 3.40 (tdd, $J = 11.6, 10.1, 5.6$ Hz, 2H), 3.08 – 2.75 (m, 2H), 2.63 (ddd, $J = 13.2, 8.5, 5.2$ Hz, 1H), 2.47 – 2.36 (m, 1H), 2.28 – 2.06 (m, 2H), 2.01 (dq, $J = 9.0, 2.9$ Hz, 1H), 1.79 (q, $J = 3.9$ Hz, 1H), 1.71 – 1.35 (m, 3H).

Minor Diastereoisomer

(300 MHz, Chloroform-*d*) δ 7.27 – 7.20 (m, 2H),
7.09 (d, $J = 2.7$ Hz, 3H), 6.72 (d, $J = 8.5$ Hz, 2H),
5.48 (d, $J = 4.7$ Hz, 1H), 3.61 (td, $J = 7.8, 4.1$
Hz, 1H), 3.46 (dt, $J = 12.4, 5.7$ Hz, 1H), 2.99 –
2.71 (m, 3H), 2.50 – 2.33 (m, 1H), 2.32 – 2.15
(m, 1H), 1.94 – 1.71 (m, 2H), 1.69 – 1.43 (m,
2H), 1.30 (d, $J = 9.8$ Hz, 1H).

Chiral Lux Amylose 1 nHex/*i*PrOH 95/5 eluent
HPLC Major Diastereoisomer 90% ee
Retention time 10.98 min (minor peak),
Retention time 14.14 min (major peak),
Minor Diastereoisomer 5% ee
Retention time 10.46 min (minor peak),
Retention time 16.85 min (major peak)
MS $m/z = 386.2, 384.2 [M+H^+]$
(ESI+APCI)

4.3. Telescoped, *In Continuo* Synthesis of an API in a Photocatalyzed Stereoselective Way

General Description of Reagents and Methods

All reactions were carried out under a positive pressure of nitrogen (5 cm of mercury, or with a spring loaded silicon oil bubbler set to 100 mbar). Oxygen being an effective quencher of the photoredox-catalyst it was taken special measures to avoid oxygen such as bubbling nitrogen through the stock solution for at least 30 min. As most reactions involved water as (co)-solvent no special care was taken to avoid water residues. If not otherwise stated reagents, solvents and such were used without further purifications. *N,N*-dimethylacetamide was degassed and stored under nitrogen. HPLC-grade water was degassed and stored under nitrogen. Octanal and propanal were flushed through a plug of basic aluminium oxide and then distilled under nitrogen and stored under nitrogen. Propanal when used in the reaction was not added before degassing the stock-solutions but was rather degassed separately each time and then was added to the stock-solutions due to its volatility. 3-phenyl-1-propanal (hydrocinnamaldehyde) was distilled under reduced pressure and then stored under nitrogen. 2,6-lutidine was first refluxed and then distilled over calcium hydride and stored under nitrogen. The benzylic alcohol radical sources were synthesized according to literature described procedures.^[113] The chiral imidazolidinone catalysts (*R*- and *S*-enantiomer) were purchased from Sigma-Aldrich and used as received. Ir[*p*-^tBu-ppy]₃ photoredox-catalyst was purchased from Sigma-Aldrich and used as received.

Reactions were monitored by thin layer chromatography (TLC) on Macherey-Nagel pre-coated silica gel plates (0.25 mm) and visualized by UV light. Flash chromatography was performed on Merck silica gel (60, particle size: 0.040–0.063 mm). ¹H NMR ¹³C NMR and ¹⁹F NMR spectra were recorded on Bruker Avance III HD 600, Bruker Avance-400, Bruker Avance-300 or Bruker Avance-250 spectrometer in CDCl₃ as solvents at room temperature. Chemical shifts for protons are reported using residual solvent protons (¹H NMR: δ = 7.26 ppm for CDCl₃) as internal standard. Carbon spectra were referenced to the shift of the ¹³C signal of CDCl₃ (δ = 77.0 ppm). The following abbreviations are used to indicate the multiplicity in NMR spectra: s - singlet; d - doublet; t - triplet; q - quartet; dd - double doublet; ddd – doublet of doublet

of doublets; dt - doublet of triplets; m - multiplet; quint – quintuplet; sext -sextuplet sept - septet; br - broad signal; dq – doublet of quartets.

High resolution mass spectra (HRMS) were acquired using a Bruker solariX XR Fourier transform ion cyclotron resonance mass spectrometer (Bruker Daltonik GmbH, Bremen, Germany) equipped with a 7 T refrigerated actively-shielded superconducting magnet. The samples were ionized in positive ion mode using a MALDI or ESI ionization sources.

Automatic weighing and transferring of liquids was made with a Zinssler Analytics custom robot “Calli”.

Samples were evaporated in a parallel fashion by employing a Genevac HT-4X vacuum centrifuge Series II System.

Preparative HPLC-MS was conducted on a Agilent 1260 Infinity Series (Autosampler, Fraction Collector, DAD, Pumps, Check valves, all while coupled to a Agilent 6120 LC-MS Quadrupole mass-spectrometer. MS-traces were generated in positive/negative switching mode and ESI/APCI as ionization method was used in tandem.

uHPLC-MS (ultrahigh performance) was conducted on a Agilent 1260 Infinity Series (Autosampler, Pump was 1290 Infinity Series) all while coupled to an Agilent 6120 LC-MS Quadrupole mass-spectrometer. MS-traces were generated in positive/negative switching mode and ESI/APCI as ionization method was used in tandem.

Chiral HPLC was measured on a Agilent 1100 Series (DAD, Autosampler, Pumps). The respective chiral stationary phase is indicated in the characterization part.

Experimental Procedures

4.3.1. Description of Equipment



Figure 59: Photograph of the ignited watercooled high intensity LED photoreactor for cryogenic continuous flow operations. Photograph of the coil-reactor (12.33 m, 0.04 in ID Perfluoroalkoxyalkane (PFA) HPLC-Tubing that is wrapped around the aforementioned photoreactor.

A versatile LED-based photoreactor for continuous flow reactions under *cryogenic conditions* is unprecedented in Literature. The goal is to build a photoreactor for such conditions using only readily available and low-cost equipment that can be found in any organic chemistry laboratory. The herein presented Photoreactor can be immersed in any cryobath for temperature regulation as the LEDs are *hermetically sealed* inside a Pyrex glass tube to avoid glacier formation, which can obstruct efficient irradiation due to the high albedo of water ice that would form from atmospheric moisture. The heat generation which tends to burn high power LEDs under sealed conditions is counteracted by wrapping the LED-Strips around a central sublimator glass-piece which is water cooled. With this innovative reactor design, it is possible to run a continuous flow photoreaction at any temperature by simply immersing the photoreactor and coil reactor couple in a temperature-controlled liquid (Ice-mixtures, dry-ice mixtures, cryostat-baths, oil-baths). The here presented Reactor performed for over 300 h and is still fully operational.



Figure 60: Photographs of the assembled and disassembled water-cooled photoreactor for cryogenic continuous flow operations

Construction of the Photoreactor: The central sublimator glass-piece is first wrapped to the desired length with heavy duty aluminium foil to generate a socket for the LED-strip that possesses high heat conductive properties. Around this first layer is then coiled and glued (doublesided adhesive tape) the LED-strip which is further secured in place at the top and bottom with electric isolating tape. The cable is guided through the silicon rubber seal by puncturing it. The final reactor is then assembled as presented in Figure 2. Video of the assembly can be found separately uploaded under supporting files.

Led-Specifications: Aftertech® 24v 24w UV 1m Strip 120 LEDs SMD5050 ultraviolet (395 nm), with a self-adhesive tape that holds the strip light safely and securely to the photoreactor support. The LEDs wavelength emission profile together with their specific light intensity (expressed as mW cm^{-2}) have been determined before their use. In particular, the spectrum has been obtained by using a compact CCD spectrometer (model CCS200/M) connected to a multimode optical fiber, purchased from Thorlabs. Ultraviolet LEDs are characterized by an almost monochromatic emission profile (with a full width at half-maximum intensity of ca. 10-20 nm) showing a maximum of intensity located at ca. 395 nm (Graphic 1). The light power intensity was thus checked using a Thorlabs PM200 power meter equipped with a S130VC power head with a Si detector. The measured light intensities, though slightly decreasing by moving the maximum of LEDs emission towards longer wavelengths, was $I = 70.94 \text{ mW cm}^{-2}$ (std 0.0034).

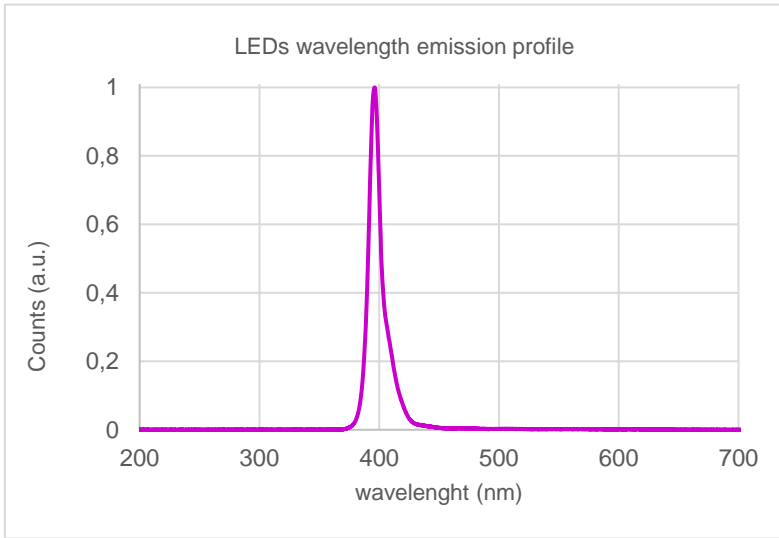


Figure 61. UV- LEDs wavelength emission profile

Continuous Flow Coil Reactor Specifications

Table 19. Specifications for the reactors used in the work. All three coil reactors are made from standard HPLC-Tubing – Material PFA

Entry	Reactor	Reactor Volume	Internal Diameter (Outer Diameter) [in]	Reactor Length [m]	Illuminated Surface Area [cm ²]
1	Microwave-Vial	1 mL	--	---	1
2	Micro-	100 μ L	0.01	2.00	8
3	Small Meso-	1 mL	0.02	5.00	40
4	Meso-	10 mL	0.04	12.33	200

All fluidic connections were made by ¼-28-bore fingertight ferrules and adapters (connectors, Y- and T-type) and were purchased together with the HPLC-tubing. at Cole-Parmer.

Photochemical and Photophysical Considerations for Scalability

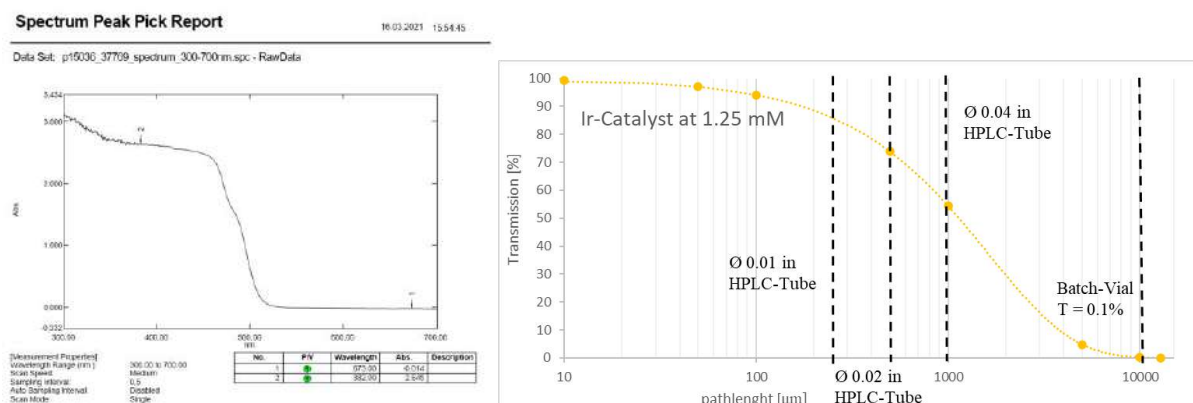


Figure 62: Absorption spectrum of the reaction solution, deaerated measured in a standard single-use cuvette. Calculated transmission curve (log-scale) based on the absorption spectrum. The intersection between the curve and the dashed lines represents the transmission that is to be expected at the respective reactor internal diameter.

Measuring the absorption spectrum of the reactive solution indicates the most suitable reactor type and size for scaling photoredox chemical processes. In the present example the photoredox solution absorbs light with an absorption of $A = 2.63$ au at 395 nm of UV-radiation. Based on this, it is generally sensible to quickly plot the transmission curve of aforementioned solution based on the following formula:

$$T\% = 10^{-A \cdot ID(reactor)}, \quad \text{Equation 31}$$

A : measured absorption, $ID(reactor)$: internal diameter of reactor

Dealing with a negative exponential attenuation it is sensible to scale the x-axis logarithmically to visualize the different internal diameters of the reactors inside the curve. Generally, a good indicator is the transmission cut-off:

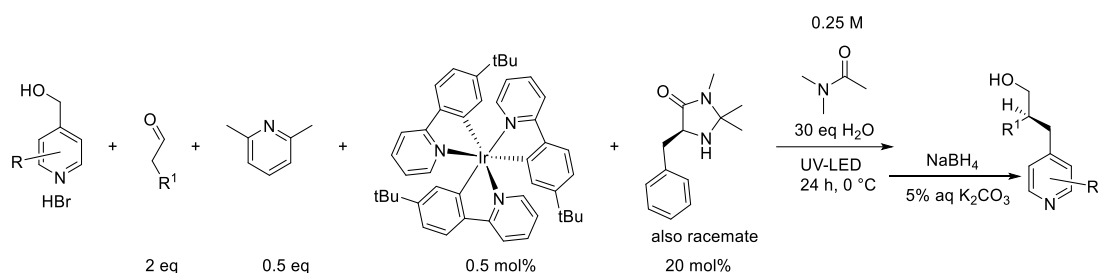
at 0.1% for reactions with a high quantum yield

at 1% for reactions with a low quantum yield

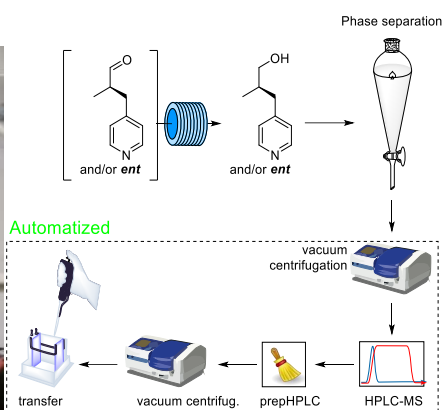
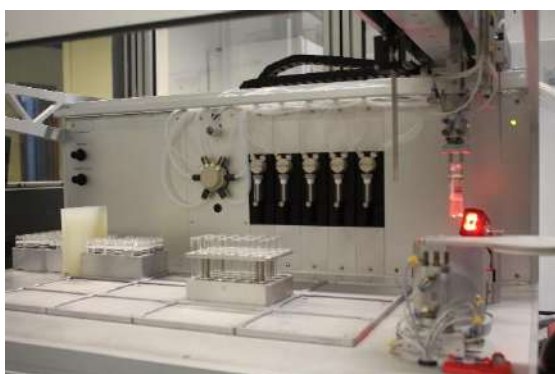
Optimally choosing the internal diameter of the reactor at exactly those transmission cut-offs allows for the most productive process. In practice self-made coil reactors have to be chosen on an availability basis.

In the present example all the employed continuous flow reactors are sized that there are still copious amounts of irradiation left and that several upscaling steps could still be undertaken.

4.3.2. General Procedure for Batch Reactions – Benchmarking the Photoreactor



Benzylic alcohol radical source (250 μ mol, 1.00 eq), (5*S*)-(-)-2,2,3-Trimethyl-5-benzyl-4-imidazolidinon -monohydrochloride 13.0 mg (50 μ mol, 0.20 eq), Ir[4-*t*Bu-ppy]₃ 1.00 mg (12.5 μ mol, 0.005 eq) were placed inside MW-vial, sealed with a aluminium cap with rubber septum and a N₂-atmosphere was applied. *N,N*-Dimethylacetamide (degassed, stored under N₂) 1 mL Distilled water (degassed, stored under N₂) 134 μ L, 2,6-Lutidine (degassed, stored under N₂) 15.0 μ L, (125 μ mol, 0.50 eq), aldehyde (degassed, stored under N₂) (500 μ mol, 2.00 eq) were cannulated under strict N₂-atmosphere. The mixture was degassed by bubbling N₂ for 30 minutes. The vial was placed directly adjacent to the 395 nm high intensity LED photoreactor and was irradiated for 24 h maintaining 0 °C. The reaction was quenched with 10 eq NaBH₄ in 5% aqueous K₂CO₃-Solution at 0 °C and left stirring overnight. 5 mL of dichloromethane were added to the mixture and the aqueous phase was extracted two additional times with 5 mL of dichloromethane. The combined organic phases were dried over magnesium sulfate and the volatiles evaporated in vacuo (HV-rotavap). The resulting remains were purified using preparative RP18-Silica and a gradient of water/acetonitrile with 0.5mM NH₄HCO₃ using an in-house generated protocol for the semi-automated purification, evaporation. For this the workflow is illustrated in figure 4. After the automatic chromatographic purification of the compounds the solvent was evaporated in a parallelized fashion inside a vacuum centrifuge. The tube positions with product containing fractions were submitted automatically to the transfer robot. The robot then backfills the tubes with acetonitrile to redissolve and transfers this to barcode-vials which were weighed by robot before filling. The bar-code vials containing the solutions of the product were then evaporated again in a parallel fashion and the robot after weighing the vials again communicates the final yield.



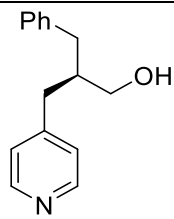
Scheme 43. Semi automatized evaporation, purification, evaporation, transferring, weighing, after manual phase separation. (photos left-to-right: Pipetting and weighing robot, Vacuum centrifuge, analytical/prep. HPLC-MS)

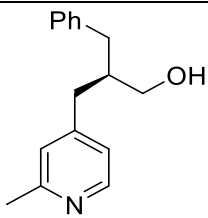
After vacuum centrifugation the compounds were isolated as stated in Table 20. The overall procedure was repeated to generate the racemic samples by carefully weighing the *R*- and *S*-enantiomer of the chiral imidazolidinone catalyst in equal ratio.

Table 20. Results from the batch experiments

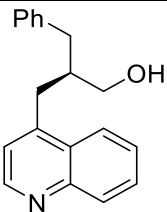
Entry ^[a]	Molecule	ee [%]	Yield [mg], {%}
1	3aa	96	24.3 , 43%
2	3ba	97	19,1 , 32%
3	3ca	96	14.6 , 32%
4	3ab	94	17.0 , 31%
5	3ac	96	16.8 , 44%

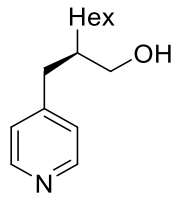
4.3.3. Purification and Characterization of Compounds 3aa, 3ba, 3ca, 3ab, 3ac

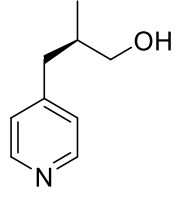
Purification	Crude after workup dissolved in 1 ml of MeOH/MeCN 1:1 and purified by prep-HPLC. Column: XBridge BEH Prep C18 5 μ m, 19 mm X 150 mm Mobile phase: Acetonitrile / Water+5mM NH ₄ HCO ₃ Flow rate: 32 ml/min Gradient: 0-0.5 min 10:90 0.51-12,5 min 80:20 12,5-14,5 min 98:2	 <p>3aa</p>
¹ H NMR	(300 MHz, Chloroform- <i>d</i>) δ 8.47 – 8.35 (m, 2H), 7.31 – 7.01 (m, 7H), 2.68 (ddd, <i>J</i> = 13.7, 7.9, 2.5 Hz, 2H), 2.56 (dd, <i>J</i> = 13.6, 6.6 Hz, 2H), 2.09 (ddt, <i>J</i> = 7.9, 6.4, 1.4 Hz, 1H), 1.82 (s, 2H).	
Chiral HPLC	Chiralpak IA, isocratic 9:1 nHex/EtOH eluent Retention time 17.2 min (minor), Retention time 12.6 min (major),	
MS (ESI+APCI)	<i>m/z</i> = 228.2 [M+H ⁺]	

Purification	Crude after workup dissolved in 1 ml of MeOH/MeCN 1:1 and purified by prep-HPLC. Column: XBridge BEH Prep C18 5 μ m, 19 mm X 150 mm Mobile phase: Acetonitrile / Water+5mM NH ₄ HCO ₃ Flow rate: 32 ml/min Gradient: 0-0.5 min 14:86 0.51-12,5 min 65:35 12,5-14,5 min 98:2	 <p>3ba</p>
--------------	--	---

¹ H NMR	(300 MHz, Chloroform- <i>d</i>) δ 8.30 (d, <i>J</i> = 5.1 Hz, 1H), 7.29 – 7.19 (m, 2H), 7.19 – 7.07 (m, 3H), 6.91 (s, 1H), 3.42 (d, <i>J</i> = 4.9 Hz, 2H), 2.72 – 2.61 (m, 2H), 2.61 – 2.52 (m, 2H), 2.45 (s, 3H), 2.15 – 2.00 (m, 1H), 1.69 (s, 2H).	
Chiral HPLC	Lux Amylose 1, isocratic 95:5 nHex/EtOH eluent Retention time 19.2 min (minor), Retention time 24.0 min (major),	
MS (ESI+APCI)	m/z = 242.2 [M+H ⁺]	

Purification	Crude after workup were dissolved in 1,2 ml of MeOH/MeCN 1:1 and purified by prep HPLC. Column: XBridge BEH Prep C18 5 μm, 19 mm X 150 mm Mobile phase: Acetonitrile / Water+5mM NH ₄ HCO ₃ Flow rate: 32 ml/min Gradient: 0-0.5 min 11:89 0.51-10,5 min 82:18 10,5-12,5 min 98:2	 <p>3ca</p>
¹ H NMR	(300 MHz, Chloroform- <i>d</i>) δ 8.68 (d, <i>J</i> = 4.4 Hz, 1H), 8.02 (dd, <i>J</i> = 8.5, 1.3 Hz, 1H), 7.73 (dd, <i>J</i> = 8.6, 1.4 Hz, 1H), 7.60 (ddd, <i>J</i> = 8.4, 6.9, 1.4 Hz, 1H), 7.39 (ddd, <i>J</i> = 8.3, 6.8, 1.3 Hz, 1H), 7.29 – 7.06 (m, 7H), 3.46 (d, <i>J</i> = 4.7 Hz, 2H), 3.11 (dd, <i>J</i> = 13.7, 8.4 Hz, 1H), 2.99 (dd, <i>J</i> = 13.6, 5.9 Hz, 1H), 2.80 (dd, <i>J</i> = 13.6, 7.5 Hz, 1H), 2.63 (dd, <i>J</i> = 13.5, 7.1 Hz, 1H), 2.26 – 2.12 (m, 1H), 1.73 (s, 2H).	
Chiral HPLC	Lux Amylose 1, isocratic 95:5 nHex/EtOH eluent	

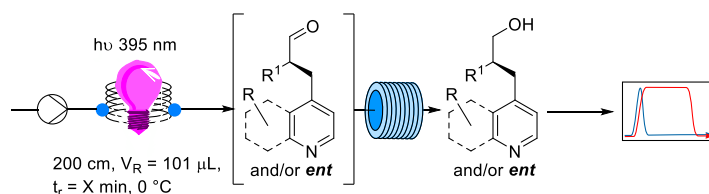
	Retention time 36.9 min (minor), Retention time 39.4 min (major),	
MS (ESI+APCI)	m/z = 278.2 [M+H ⁺]	
Purification	Crude after workup dissolved in 1 ml of MeOH/MeCN 1:1 and purified by prep-HPLC. Column: XBridge BEH Prep C18 5 μm, 19 mm X 150 mm Mobile phase: Acetonitrile / Water+5mM NH ₄ HCO ₃ Flow rate: 32 ml/min Gradient: 0-0.5 min 20:80 0.51-12,5 min 76:24 12,5-14,5 min 98:2	 <p>3ab</p>
¹ H NMR	(300 MHz, Chloroform- <i>d</i>) δ 8.57 – 8.37 (m, 2H), 7.17 – 7.03 (m, 2H), 3.52 (dd, <i>J</i> = 5.3, 2.9 Hz, 2H), 2.72 (dd, <i>J</i> = 13.6, 7.4 Hz, 1H), 2.60 (d, <i>J</i> = 6.9 Hz, 1H), 1.81 (ddd, <i>J</i> = 7.1, 5.2, 1.8 Hz, 1H), 1.69 (s, 1H), 1.48 – 1.15 (m, 11H), 0.94 – 0.77 (m, 3H).	
Chiral HPLC	Chiralpak AS-3, isocratic 98:2 nHex/IPA eluent Retention time 35.5 min (minor), Retention time 39 min (major),	
MS (ESI+APCI)	m/z = 222.2 [M+H ⁺]	

Purification	Crude after workup dissolved in 1 ml of MeOH/MeCN 1:1 and purified by prep-HPLC. Column: XBridge BEH Prep C18 5 μm, 19 mm X 150 mm Mobile phase: Acetonitrile / Water+5mM NH ₄ HCO ₃ Flow rate: 32 ml/min	 <p>3ac</p>
--------------	---	---

	<p>Gradient:</p> <p>0-0.5 min 10:90</p> <p>0.51-12,5 min 56:44</p> <p>12,5-14,5 min 98:2</p>	
¹ H NMR	(300 MHz, Chloroform- <i>d</i>) δ 8.49 – 8.40 (m, 2H), 7.14 – 7.07 (m, 2H), 3.49 (dd, <i>J</i> = 6.0, 0.9 Hz, 2H), 2.82 (dd, <i>J</i> = 13.4, 5.9 Hz, 1H), 2.38 (dd, <i>J</i> = 13.4, 8.4 Hz, 1H), 2.05 – 1.89 (m, 1H), 0.89 (d, <i>J</i> = 6.7 Hz, 3H).	
Chiral HPLC	Chiralpak AS-3, isocratic 9:1 nHex/IPA eluent Retention time 35.5 min (minor), Retention time 39 min (major),	
MS (ESI+APCI)	<i>m/z</i> = 152.2 [M+H ⁺]	

4.3.4. General Procedure for Fluidic Reaction (Screening and Synthesis)

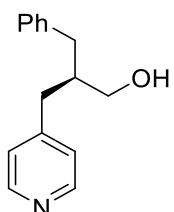
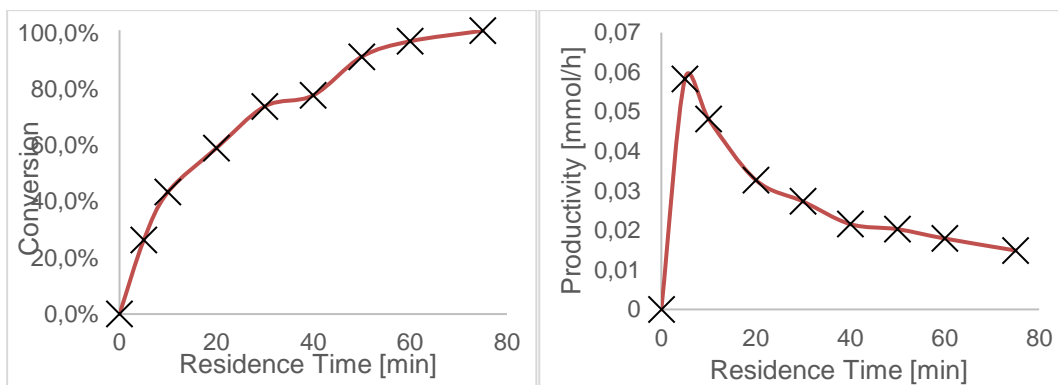
General Procedure for Microfluidic Reaction (screening)



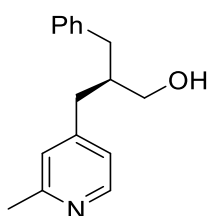
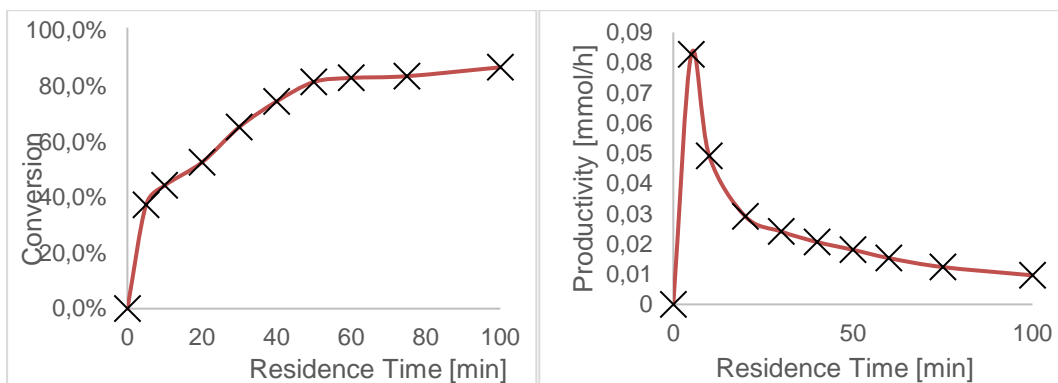
Photoredox stock solution: Benzylic alcohol radical source (250 μmol , 1.00 eq), (5*S*)-(-)-2,2,3-Trimethyl-5-benzyl-4-imidazolidinone -monohydrochloride 13.0 mg (50 μmol , 0.20 eq), Ir[4-*t*Bu-ppy]₃ 1.00 mg (12.5 μmol , 0.005 eq) were placed inside MW-vial, sealed with a aluminium cap with rubber septum and a N₂-atmosphere was applied. *N,N*-Dimethylacetamide (degassed, stored under N₂) 1 mL Distilled water (degassed, stored under N₂) 134 μL , 2,6-Lutidine (degassed, stored under N₂) 15.0 μL (125 μmol , 0.50 eq), aldehyde (degassed, stored under N₂) (500 μmol , 2.00 eq) were cannulated under strict N₂-atmosphere. The mixture was degassed by bubbling N₂ for 30 minutes. Continuous flow reaction: A 2.5 mL SGE gastight syringe was flushed with N₂ three times. The previously prepared solution was taken into the syringe and quickly attached to the apparatus while applying a constant stream of N₂ through the apparatus. The solution was infused through the coil reactor to give the final residence times indicated in the graphs. Between the experiments one full residence time of reactor output was discarded to reach the steady state of the reactor.

NaBH₄- 160 mg (3 mmol, 10 eq) were dissolved in 1 mL of 5% KOH, 200 μL sat. Aq. NaHCO₃ and 1.8 mL of HPLC-Water. 3 mL of this solution were taken into a 3 mL Norminject syringe and connected to the tubing leading into the Y-Connector piece and infused with the same flow rate as the photoredox solution.

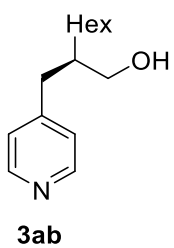
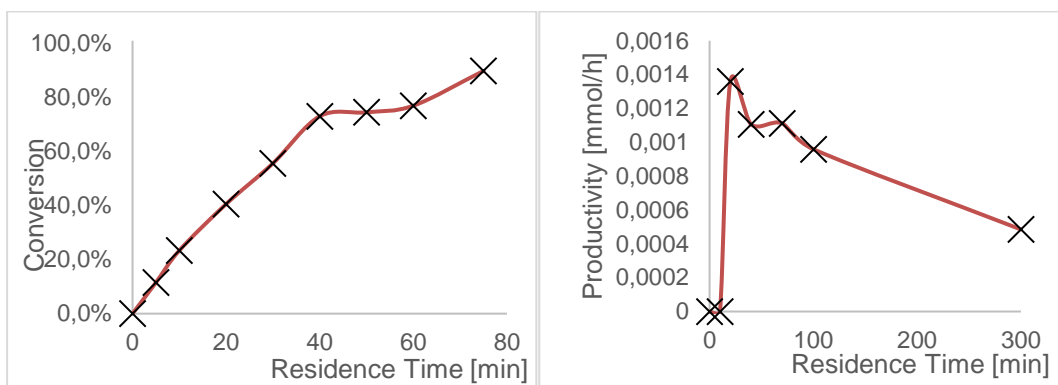
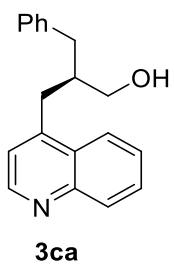
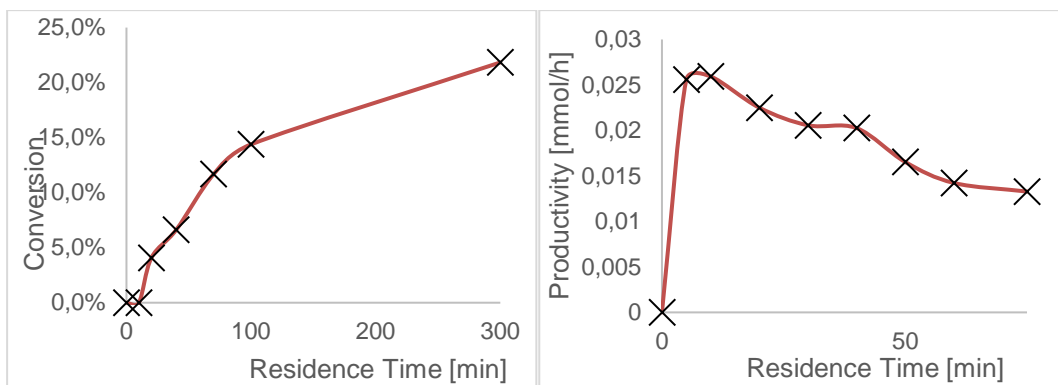
Sampling: After reaching steady state, an aliquot was taken by collecting an idealized 10 μL of the photoredox-solution which were subsequently dissolved in 1 mL of HPLC-MeOH and the resulting mixture was analysed by HPLC-MS to check for the consumption of the starting benzylic alcohol radical source relative to the 2,6-lutidine signal which served as internal standard.

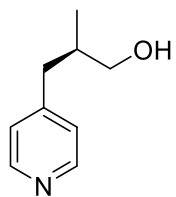
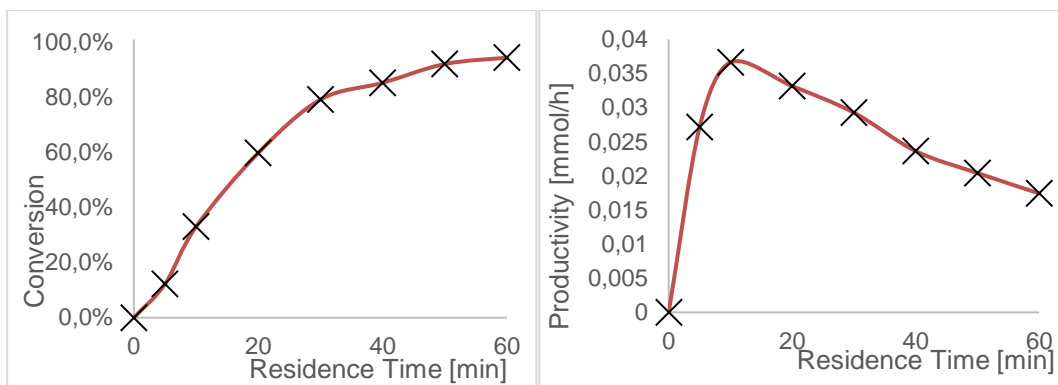


3aa



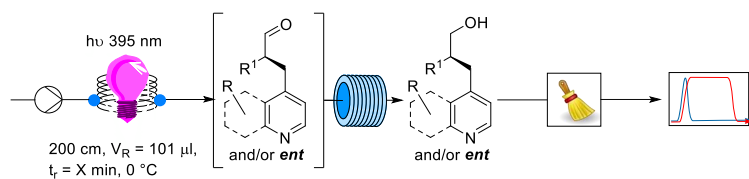
3ba





3ac

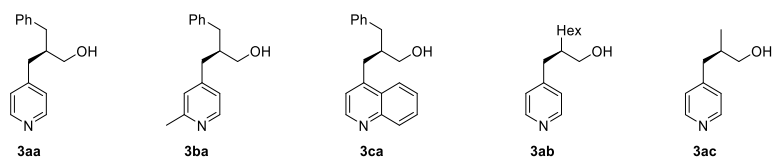
General Procedure for Microfluidic Reactions (Synthesis)



Photoredox stock solution: Benzylic alcohol radical source (250 μmol , 1.00 eq), (5S)-(-)-2,2,3-Trimethyl-5-benzyl-4-imidazolidinone -monohydrochloride 13.0 mg (50 μmol , 0.20 eq), $\text{Ir}[4\text{-tBu-ppy}]_3$ 1.00 mg (12.5 μmol , 0.005 eq) were placed inside MW-vial, sealed with a aluminium cap with rubber septum and a N_2 -atmosphere was applied. N,N-Dimethylacetamide (degassed, stored under N_2) 1 mL, Distilled water (degassed, stored under N_2) 134 μL , 2,6-Lutidine (degassed, stored under N_2) 15.0 μL (125 μmol , 0.50 eq), aldehyde (degassed, stored under N_2) (500 μmol , 2.00 eq) were cannulated under strict N_2 -atmosphere. The mixture was degassed by bubbling N_2 for 30 minutes.

Continuous flow reaction: A 2.5 mL SGE gastight syringe was flushed with N_2 three times. The previously prepared solution (approx.. 0.2 M in concentration) was taken into the syringe and quickly attached to the apparatus while applying a constant stream of N_2 through the apparatus. The solution was infused through the coil reactor to give the final residence times indicated in the graphs. Between the experiments one full residence time of reactor output was discarded to reach the steady state of the reactor.

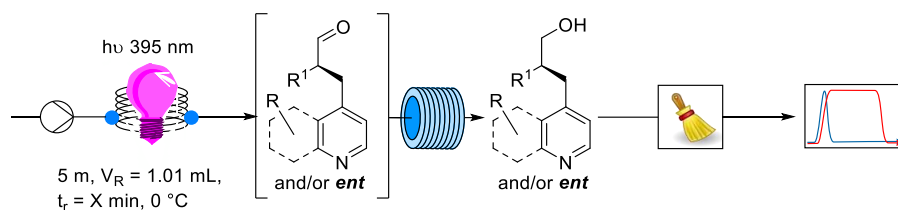
NaBH_4 - 160 mg (3 mmol, 10 eq) were dissolved in 1 mL of 5% KOH, 200 μL sat. Aq. NaHCO_3 and 1.8 mL of HPLC-Water. 3 mL of this solution were taken into a 3 mL Norminject syringe and connected to the tubing leading into the Y-Connector piece and infused with the same flow rate as the photoredox solution. The resulting output of the reactor was collected for the indicated amount of time in Table S3 and the remains were left overnight to be worked up. 5 mL of dichloromethane were added to the mixture and the aqueous phase was extracted two additional times with 5 mL of dichloromethane. The combined organic phases were dried over magnesium sulfate and the volatiles evaporated in vacuo (HV-rotavap). The resulting remains were purified using the automated protocols disclosed in the general procedure After vacuum centrifugation the compounds were isolated as stated in Table S3

Table 21. Results of the Microfluidic Experiments

Entry ^[a]	Molecule	Residence Time [min]	Time of collection [min]	ee [%]	Yield [mg], {%}
1	3aa	30	360	98	16.4 , 30%
2	3ba	35	420	99	23.1 , 38%
3 ^a	3ca	1440	--	91	23.6 , 40%
4	3ab	40	480	94	20.8 , 37%
5	3ac ^b	25	300	96	22.3 , 58%

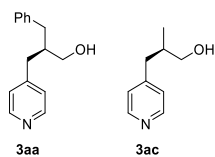
^aStop flow experiment, reaction time 24 h in a 1 mL Reactor, ^bdue to the high water solubility of this compound, additional extraction steps have to be undertaken.

General Procedure for Mesofluidic (1 mL-Coil- Reactor)



Photoredox stock solution: Benzylic alcohol radical source (2.50 mmol, 1.00 eq), (5S)-(-)-2,2,3-Trimethyl-5-benzyl-4-imidazolidinone -monohydrochloride 130 mg (500 μ mol, 0.20 eq), $\text{Ir}[4\text{-tBu-ppy}]_3$ 10.00 mg (125 μ mol, 0.005 eq) were Placed inside MW-vial, sealed with a aluminium cap with rubber septum and a N_2 -atmosphere was applied. *N,N*-Dimethylacetamide (degassed, stored under N_2) 10 mL, Distilled water (degassed, stored under N_2) 1.35 mL, 2,6-Lutidine (degassed, stored under N_2) 150 μ L (1.25 mmol, 0.50 eq), aldehyde (degassed, stored under N_2) (5.00 mmol, 2.00 eq) were cannulated under strict N_2 -atmosphere. The mixture was degassed by bubbling N_2 for 30 minutes.

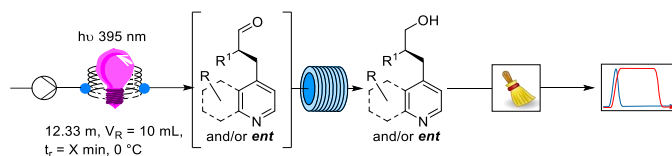
Continuous flow reaction: A 10 mL SGE gastight syringe was flushed with N_2 three times. The previously prepared solution (approx.. 0.2 M in concentration) was taken into the syringe and quickly attached to the apparatus while applying a constant stream of N_2 through the apparatus. The solution was infused through the coil reactor to give the final residence times indicated in the graphs. Between the experiments one full residence time of reactor output was discarded to reach the steady state of the reactor. NaBH_4 - 1.60 g (30 mmol, 10 eq) were dissolved in 10 mL of 5% KOH, 2 mL sat. Aq. NaHCO_3 and 18 mL of HPLC-Water. 24 mL of this solution were taken into a 24 mL Norminject syringe and connected to the tubing leading into the Y-Connector piece and infused with the same flow rate as the photoredox solution. The resulting output of the reactor was collected for the indicated amount of time in Table S4 and the remains were left overnight to be worked up. 5 mL of dichloromethane were added to the mixture and the aqueous phase was extracted two additional times with 5 mL of dichloromethane. The combined organic phases were dried over magnesium sulfate and the volatiles evaporated in vacuo (HV-rotavap). The resulting remains were purified using the automated protocols disclosed in the general procedure. After vacuum centrifugation the compounds were isolated as stated in Table 22

Table 22. Results of the mesofluidic Experiments

Entry ^[a]	Molecule	Residence Time [min]	Time of collection [min]	ee [%]	Yield [mg], {%}
1	3aa	30	36	98	16.2 , 28%
2	3aa	60	72	98	26.8 , 47%
3 ^a	3aa	60	72	96	35.5 , 62%
4	3ac	25	30	96	11.9 , 31%
5	3ac ^b	50	60	95	24.5 , 64%
6	3ac	75	90	95	29.5 , 77%
7 ^a	3ac	50	60	93	11.9 , 31%

^aExperiment conducted at room temperature, ^bdue to the high water solubility of this compound, additional extraction steps have to be undertaken.

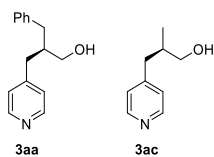
General Procedure for Segmented Mesofluidic Reactions (10 mL-Coil-Reactor)



Photoredox stock solution: Benzylic alcohol radical source (2.50 mmol, 1.00 eq), (5*S*)-(-)-2,2,3-Trimethyl-5-benzyl-4-imidazolidinone -monohydrochloride 130 mg (500 μmol, 0.20 eq), Ir[4-*t*Bu-ppy]₃ 10.00 mg (125 μmol, 0.005 eq) were Placed inside MW-vial, sealed with a aluminium cap with rubber septum and a N₂-atmosphere was applied. *N,N*-Dimethylacetamide (degassed, stored under N₂) 10 mL, Distilled water (degassed, stored under N₂) 1.35 mL, 2,6-Lutidine (degassed, stored under N₂) 150 μL (1.25 mmol, 0.50 eq), aldehyde (degassed, stored under N₂) (5.00 mmol, 2.00 eq) were cannulated under strict N₂-atmosphere. The mixture was degassed by bubbling N₂ for 30 minutes.

Continuous flow reaction: A 25 mL SGE gastight syringe was flushed with N₂ three times. The previously prepared solution (approx.. 0.2 M in concentration) was taken into the syringe and quickly attached to the apparatus while applying a constant stream of N₂ through the apparatus. The solution was infused through the coil reactor to give the final residence times indicated in the graphs. The Photoredox stock-solution was infused through the coil reactor in the time indicated in Table S5 and the syringe pump turned off. Afterwards heptane was infused with the same flow rate to give the final residence time indicated in Table S5.

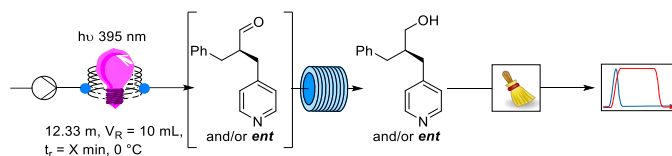
NaBH₄- 1.60 g (30 mmol, 10 eq) were dissolved in 10 mL of 5% KOH, 2 mL sat. Aq. NaHCO₃ and 18 mL of HPLC-Water. 24 mL of this solution were taken into a 24 mL Norminject syringe and connected to the tubing leading into the Y-Connector piece and infused with the same flow rate as the photoredox solution. The resulting output of the reactor was collected for the indicated amount of time in Table S4 and the remains were left overnight to be worked up. 5 mL of dichloromethane were added to the mixture and the aqueous phase was extracted two additional times with 5 mL of dichloromethane. The combined organic phases were dried over magnesium sulfate and the volatiles evaporated in vacuo (HV-rotavap). The resulting remains were purified using the automated protocols disclosed in the general procedure. After vacuum centrifugation the compounds were isolated as stated in Table 23

Table 23. Results of the segmented mesofluidic Experiments

Entry ^[a]	Molecule	Residence Time [min]	Time of collection [min]	ee [%]	Yield [mg], {%}
1	3aa	30	3:40	96	23.2 , 40%
2	3aa	60	7:20	97	20.1 , 35%
3	3aa	120	14:40	97	27.3 , 48%
4 ^a	3ac	25	3	96	3.2 , 8%
5 ^a	3ac ^a	50	6	97	9.5 , 25%
6 ^a	3ac	75	90	95	14.5 , 38%

^adue to the high water solubility of this compound, additional extraction steps have to be undertaken.

Procedure for Mesofluidic Reaction (10 mL-Coil-Reactor)



Photoredox stock solution: pyridine-4-methanol hydrobromide (7.5 mmol, 1.00 eq), (5S)-(-)-2,2,3-Trimethyl-5-benzyl-4-imidazolidinone -monohydrochloride 390 mg (1.25 mmol, 0.20 eq), Ir[4-tBu-ppy]₃ 30.00 mg (375 μmol , 0.005 eq) were placed inside MW-vial, sealed with a aluminium cap with rubber septum and a N₂-atmosphere was applied. *N,N*-Dimethylacetamide (degassed, stored under N₂) 30 mL, Distilled water (degassed, stored under N₂) 4.05 mL, 2,6-Lutidine (degassed, stored under N₂) 450 μL (1.25 mmol, 0.50 eq), 3-phenyl-propanal (degassed, stored under N₂) (15.0 mmol, 2.00 eq) were cannulated under strict N₂-atmosphere. The mixture was degassed by bubbling N₂ for 30 minutes.

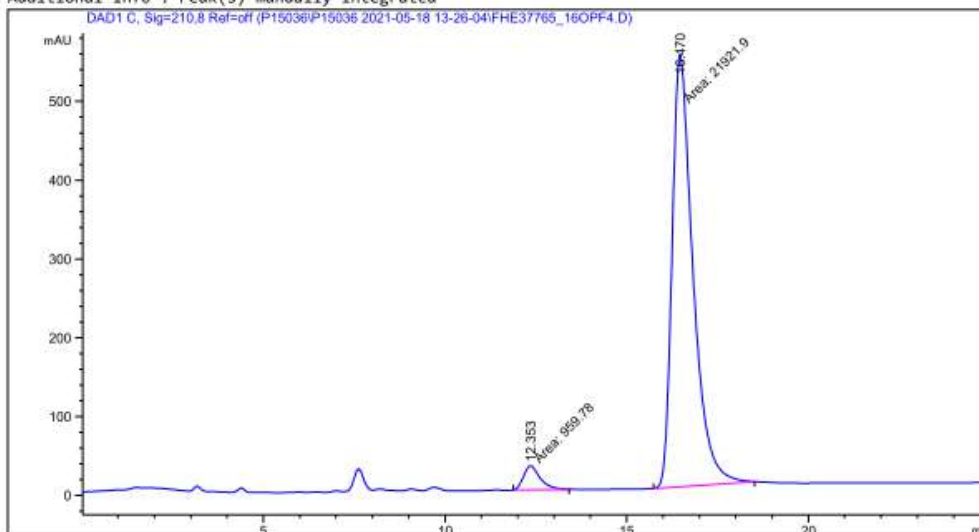
Continuous flow reaction: A 25 mL SGE gastight syringe was flushed with N₂ three times. The previously prepared solution (approx.. 0.2 M in concentration) was taken into the syringe and quickly attached to the apparatus while applying a constant stream of N₂ through the apparatus. The solution was infused through the coil reactor to give the final residence times of 60 min. Two full residence times of reactor output were discarded.

NaBH₄- 1.60 g (30 mmol, 10 eq) were dissolved in 10 mL of 5% KOH, 2 mL sat. Aq. NaHCO₃ and 18 mL of HPLC-Water. 24 mL of this solution were taken into a 24 mL Norminject syringe and connected to the tubing leading into the Y-Connector piece and infused with the same flow rate as the photoredox solution. An aliquot from the reactor output revealed 60% consumption of the starting material. The resulting output of the reactor was collected for 72 min (1.2 reactor volumes, 2.5 mmol of hypothetical yield) and the remains were left overnight. 50 mL of dichloromethane were added to the mixture and the aqueous phase was extracted two additional times with 50 mL of dichloromethane. The combined organic phases were dried over magnesium sulfate and the volatiles evaporated in vacuo (HV-rotavap). The resulting remains were purified using preparative RP18-Silica and a Gradient of water/acetonitrile with 0.5 mM

NH₄HCO₃. After vacuum centrifugation 220 mg of Product was isolated in 38% Yield and with an ee of 92%.

```

=====
Acq. Operator   : SYSTEM                      Seq. Line :    1
Acq. Instrument : HPLC                      Location  : Vial 72
Injection Date  : 5/18/2021 1:28:38 PM      Inj       :    1
                                           Inj Volume: 10.000 µl
Different Inj Volume from Sample Entry! Actual Inj Volume : 4.000 µl
Method          : C:\CHEM32\1\DATA\P15036\P15036 2021-05-18 13-26-04\P15036_CHIRALPACK_IA_90-
                : 10.M (Sequence Method)
Last changed    : 5/18/2021 1:26:04 PM by SYSTEM
Additional Info  : Peak(s) manually integrated
    
```



Area Percent Report

```

Sorted By      : Signal
Multiplier     : 1.0000
Dilution       : 1.0000
Use Multiplier & Dilution Factor with ISTDs
    
```

Signal 1: DAD1 C, Sig=210,8 Ref=off

Peak #	RetTime [min]	Type	Width [min]	Area [mAU*s]	Height [mAU]	Area %
1	12.353	MM	0.5244	959.78027	30.50532	4.1945
2	16.470	MM	0.6662	2.19219e4	548.44763	95.8055

Totals : 2.28817e4 578.95295

*** End of Report ***

4.3.5. Calculation of Productivity and Space-Time-Yield

Table 24. Calculation of STY and productivity

Entry	Method	Yield	t _{collection} until 250 μmol [h]	P [mmol/h]	Rel. Factor	Residence time t _R [h]	STY [mmol/ml *h]	Rel-Factor
1	Batch (1.2 mL)	43 %	24	4.5E-3	1	24	0,003673	1
2	Microfluidic	43 %	6	1.3E-2	2.8	0.5	0,123	33,48837
3	1 mL Meso	47 %	1.2	9.8E-2	22	1	0,09635	26,23256
4	10 mL Meso	38 %	0.12	7.9E-1	176	1	0,0779	21,2093

$$P = \frac{n_{\text{prod}} * \%Y}{t_{\text{collection}} * 100\%}$$

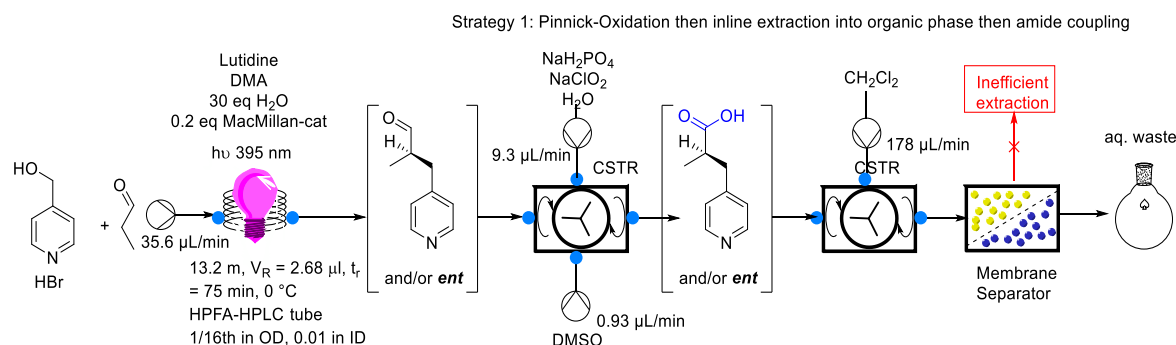
$$STY = \frac{n_R * \%Y}{V_R * t_R * 100\%}$$

As to rule out effects of reaction scale that will change isolated yield (e.g. purification methods, work-up methods). All of the reactions were performed on the same scale by collecting reactor outputs for the given time it would take to have the same amount of moles as under batch conditions (250 μmol). Then the above formula was used to calculate P, in which n_{prod} stands for the (idealized) quantitative yield of product. %Y stands for isolated yield in % and t_{collection} stands for collection time until the idealized n_{prod} would be collected.

When calculating the space-time-yield (STY) the above formula was used, where n_R and V_R are the moles and volume inside the reactor, t_R is residence time, %Y stands for isolated yield in %.

4.3.6. Procedures for the Telescoped Process

Telescoping: Inline oxidation to the carboxylic acid then extraction



Photoredox stock solution: Benzylic alcohol radical source 935 mg (4.92 mmol, 1.00 eq), (5S)-(-)-2,2,3-Trimethyl-5-benzyl-4-imidazolidinone 215 mg (998 μmol, 0.20 eq), Ir[4-*t*Bu-ppy]₃ 20.25 mg (24.6 μmol, 0.005 eq) were placed inside 25 mL conical flask, sealed with rubber septum and a N₂-atmosphere was applied. *N,N*-Dimethylacetamide (degassed, stored under N₂) 20 mL, Distilled water (degassed, stored under N₂) 2.66 μL, 2,6-Lutidine (degassed, stored under N₂) 285 μL (2.46 mmol, 0.50 eq) were added using syringe in the flask under strict N₂-atmosphere. The mixture was degassed by bubbling N₂ for 30 minutes. Propionaldehyde (degassed, stored under N₂) 1.74 mL (24.6 mmol, 2.00 eq) has been also degassed for 30 minutes and added to the conical flask: the resulting mixture has been degassed 10 minutes.

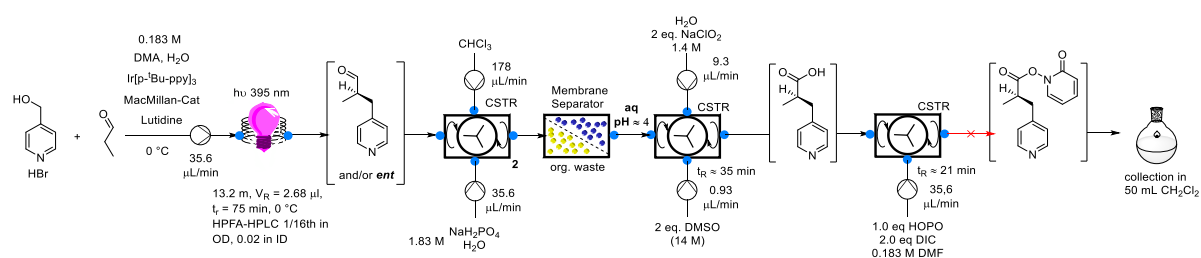
Continuous flow photoredox reaction: A 10 mL SGE gastight syringe was flushed with N₂ three times. The previously prepared solution (0.183 M) was taken into the syringe and quickly attached to the apparatus while applying a constant stream of N₂ through the apparatus. The first 75 min of elution has been wasted.

Continuous flow Pinnick-oxidation: In a 10 mL SGE syringe was taken up a 10 mL of solution of 1.83 M sodium dihydrophosphate mixed with 1.83 M sodium chlorite in distilled water. The mixture was infused into the first CSTR after infusing DMSO into the same CSTR that was previously taken up in a 250 μL SGE syringe. The first residence time of infusion (40 min) is discarded. The output of the CSTR is connected to the next CSTR in the cascade.

Continuous Extraction: dichloromethane (5 volume equivalents) was infused in second CSTR. Residence time (extraction time) is approximately 9 min.

Continuous Phase separation: The output of the second CSTR was infused into a Zaiput continuous Phase separator (Laboratory scale) with a 0.5 μm hydrophobic membrane inside. After experiencing successful phase separation two full residence times were infused and the mixture was collected. After checking the organic phase for the carboxylic acid (tlc 9:1 dichloromethane/methanol) also the aqueous phase was checked, and the product was found inside it. These findings discouraged the further development of an organic phase driven amide coupling due to the excellent water solubility of the carboxylic acid.

Telescoping: First extraction then oxidation then aqueous amide coupling



Photoredox stock solution: Benzylic alcohol radical source 935 mg (4.92 mmol, 1.00 eq), (5S)-(-)-2,2,3-Trimethyl-5-benzyl-4-imidazolidinone 215 mg (998 μmol , 0.20 eq), $\text{Ir}[4\text{-}t\text{Bu-ppy}]_3$ 20.25 mg (24.6 μmol , 0.005 eq) were placed inside 25 mL conical flask, sealed with rubber septum and a N_2 -atmosphere was applied. *N,N*-Dimethylacetamide (degassed, stored under N_2) 20 mL, Distilled water (degassed, stored under N_2) 2.66 μL , 2,6-Lutidine (degassed, stored under N_2) 285 μL (2.46 mmol, 0.50 eq) were added using syringe in the flask under strict N_2 -atmosphere. The mixture was degassed by bubbling N_2 for 30 minutes. Propionaldehyde (degassed, stored under N_2) 1.74 mL (24.6 mmol, 2.00 eq) has been also degassed for 30 minutes and added to the conical flask: the resulting mixture has been degassed 10 minutes.

Continuous flow photoredox reaction: A 10 mL SGE gastight syringe was flushed with N_2 three times. The previously prepared solution (0.183 M) was taken into the syringe and quickly attached to the apparatus while applying a constant stream of N_2 through the apparatus. The first 75 min of elution has been wasted.

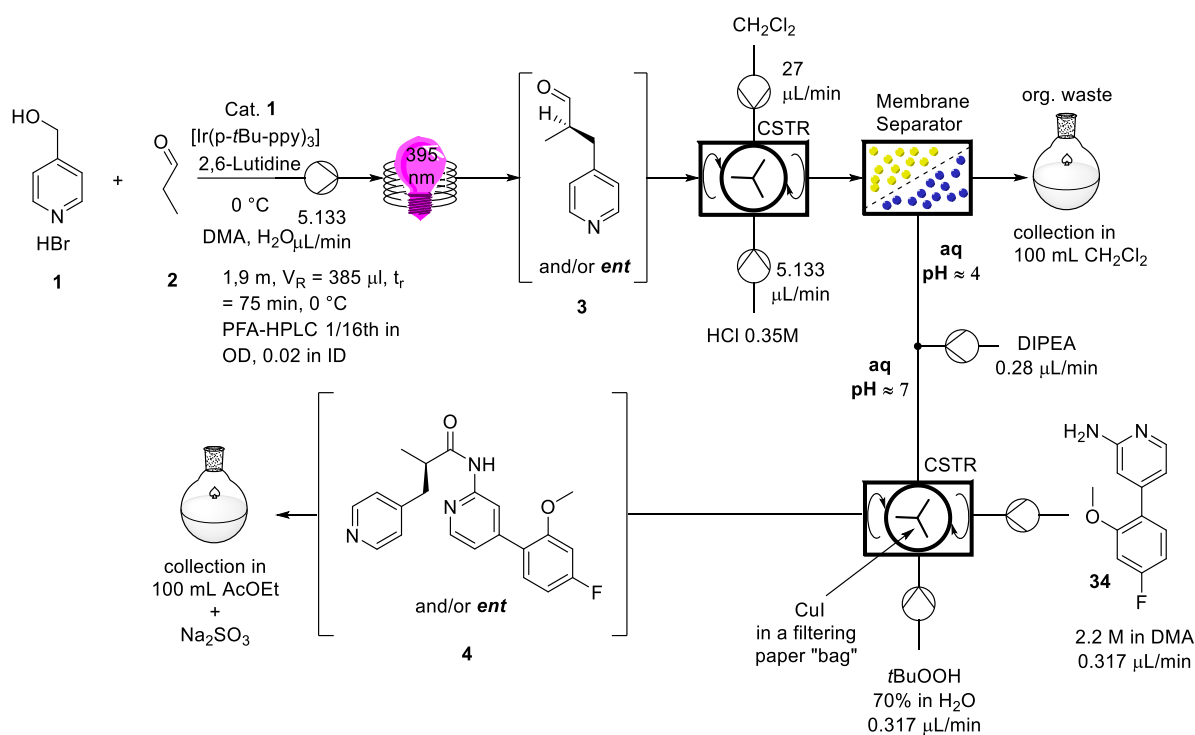
Continuous Extraction: In a 10 mL SGE syringe was taken up 10 mL of a solution of 1.83 M sodium dihydrophosphate. dichloromethane (5 volume equivalents) was infused into the first two CSTRs. Residence time (extraction time) is approximately 18 min.

Continuous Phase separation: The output of the second CSTR was infused into a Zaiput continuous Phase separator (Laboratory scale) with a 0.5 μm hydrophobic membrane inside. This time the aqueous output was of interest and thus was further infused into a third CSTR.

Continuous flow Pinnick-oxidation: In a 10 mL SGE syringe was taken up a 10 mL of solution of 1.83 M sodium chlorite in distilled water. The mixture was infused into the third CSTR after infusing DMSO into the same CSTR that was previously taken up in a 250 μL SGE syringe. The first residence time of infusion (35 min) is discarded. The output of the third CSTR is infused into the fourth CSTR for the aqueous amide coupling.

Continuous flow aqueous amide coupling: into a 10 mL SGE syringe was taken up a solution of 546 mg (4.92 mmol, 1.00 eq) 2-hydroxy pyridine oxide (HOPO) together with 1.54 mL (9.84 mmol, 2.00 eq) diisopropylcarbodiimide in 27 mL dimethylformamide ($c=0.183\text{ M}$). This solution was then infused into the fourth CSTR and the first residence time was discarded. The output was collected in dichloromethane under stirring for 2 full residence times. After unsuccessful HOPO-active ester formation (indicated by tlc, acid remained in aqueous phase) the aqueous phase was evaporated and the remains were purified by normal phase flash column chromatography (5% methanol in dichloromethane) to give the carboxylic acid product in 74% yield.

Fully Telescoped fully continuous Synthesis of the API



Photoredox stock solution: Benzylic alcohol radical source 290 mg (1.53 mmol, 1.00 eq), (5*S*)-(-)-2,2,3-Trimethyl-5-benzyl-4-imidazolidinone 66.6 mg (305 μmol , 0.20 eq), Ir[4-*t*Bu-ppy]₃ 6.3 mg (7.6 μmol , 0.005 eq) were placed inside 25 mL conical flask, sealed with rubber septum and a N₂-atmosphere was applied. *N,N*-Dimethylacetamide (degassed, stored under N₂) 6.1 mL, Distilled water (degassed, stored under N₂) 825 μL , 2,6-Lutidine (degassed, stored under N₂) 89.0 μL (763 μmol , 0.50 eq) were added using syringe in the flask under strict N₂-atmosphere. The mixture was degassed by bubbling N₂ for 30 minutes. Propionaldehyde (degassed, stored under N₂) 547 μL (7.63 mmol, 2.00 eq) has been also degassed for 30 minutes and added to the conical flask: the resulting mixture has been degassed 10 minutes.

Continuous flow photoredox reaction: A 10 mL SGE gastight syringe was flushed with N₂ three times. The previously prepared solution (0.183 M) was taken into the syringe and quickly attached to the apparatus while applying a constant stream of N₂ through the apparatus. The first 75 min elution has been wasted.

Continuous flow extraction: a 25 mL SGE gastight syringe has been flushed with N₂ three times and then filled with dichloromethane, another 10 mL SGE gastight syringe has been flushed with nitrogen three times and then equipped with 0.35M HCl (aq.).

Under strong flux of nitrogen in a CSTR equipped with a stirring bar, were rapidly connected the syringe with DCM, the syringe with 0.35M HCl and the output of the photoredox flow reaction; the pH at the output of the CSTR has been tested between 3 and 4 with pH-indicator paper. The membrane separator has been connected, fluxed for some minutes with nitrogen from the output and then connected to the CSTR: the organic output of the CSTR was collected in a 50 mL flask and discarded. A complete reactor volume has been wasted (80 minutes).

Continuous flow neutralization: the pH at the aqueous output of the extraction has been tested 4 with pH indicator paper. The output has been connected to a T connector. A 250 μ L syringe has been fluxed with nitrogen three times, charged with *N,N*-Diisopropylethylamine and connected to the T connector. pH at the output of the T-shaped connector has been tested to be 7. The output of this T-connector was connected to the last CSTR, containing a filtering paper bag loaded with CuI (1.00 g, 5.25 mmol).

Continuous flow amidation: In a vial cold 4-(4-fluoro-2-methoxyphenyl)pyridin-2-amine 100 mg (458 μ mol, 1.00 eq) was diluted with 210 μ L of DMA to obtain an homogeneous 2.2 M solution; this solution has been charged in a 250 μ L SGE syringe and connected to the CSTR.

In another 250 μ L SGE syringe was added the same volume of *Tert*-butyl hydrogen peroxide 70% and connected to the CSTR.

The CSTR output was dropped inside a flask containing 20 mL of AcOEt and 500 mg of Na₂SO₃. After 180 min the flask has been changed with another one containing 20 mL of AcOEt and 500 mg of Na₂SO₃.

The product has been purified by preparative-TLC using 8% EtOH in DCM (violet spot under UV light).

Yield 22%

R_f = 0.52 8% EtOH in DCM

Purified by Preparative TLC

¹H NMR (300 MHz, CDCl₃) δ 8.51 (s, 2H), 8.32 (s, 1H), 8.22 (d, J = 5.2 Hz, 1H), 7.82 (d, J = 14.6 Hz, 2H), 7.34 (t, J = 7.4 Hz, 2H), 7.24 – 7.17 (m, 1H), 6.87 – 6.63 (m, 2H), 3.85 (d, J = 7.5 Hz, 5H), 3.20 – 3.03 (m, 1H), 2.91 – 2.54 (m, 2H), 1.29 (d, J = 4.7 Hz, 3H).

^{13}C NMR (75 MHz, CDCl_3) δ 173.63, 164.16 (d, $J = 248.2$ Hz), 151.29, 150.08, 148.42 (d, $J = 8.2$ Hz), 147.34, 131.74 (d, $J = 10.1$ Hz), 124.46, 121.11, 114.45, 107.69 (d, $J = 21.4$ Hz), 99.82 (d, $J = 25.8$ Hz), 56.03, 43.85, 39.34, 29.85, 18.06.

^{19}F NMR (282 MHz, CDCl_3) δ -109.66.

Exact Mass = 366.1611 m/z (TOF ESI+; calculated: 366.1610 m/z)

Chiral HPLC: PHENOMENEX LUX 3u Amylose-1, 70 Hex 30 EtOH 0,1 DEA, 1 mL/min, P=97 bar. Retention time: 9.287 min, 13.313 min ee 95%

4.4. Photochemistry *in Continuo* Deep Dive – A Critical Examination of Important Parameters

General Description of Reagents and Methods

All reactions were carried out under a positive pressure of nitrogen (5 cm of mercury, or with a spring loaded silicon oil bubbler set to 50 mbar). As most reactions involved water as (co)-solvent no special care was taken to avoid water residues. If not otherwise stated reagents, solvents, and such were used without further purifications. HPLC-grade water was degassed and stored under nitrogen. 1,1,3,3-Tetramethylguanidine, $(\text{Ir}[\text{dF}(\text{CF}_3)\text{ppy}]_2(\text{dtbpy}))\text{PF}_6$, [4,4'-Bis(1,1-dimethyl-ethyl)-2,2'-bipyridine] nickel (II) dichloride, 4'-Brom-acetophenone and Z-Pro-OH were purchased from Sigma and used without further purification. 2,4,5,6-Tetra(9H-carbazol-9-yl)-1,3-Dicyanobenzene (4CzIPN) was bought from AmBeed and used without further purification. Biphenyl was bought from Sigma in the analytical standard quality.

Reactions were monitored by thin layer chromatography (TLC) on Macherey-Nagel pre-coated silica gel plates (0.25 mm) and visualized by UV light. Flash chromatography was performed on Merck silica gel (60, particle size: 0.040–0.063 mm). ^1H NMR ^{13}C NMR and ^{19}F NMR spectra were recorded on Bruker Avance III HD 600, Bruker Avance-400, Bruker Avance-300 or Bruker Avance-250 spectrometer in CDCl_3 as solvents at room temperature. Chemical shifts for protons are reported using residual solvent protons (^1H NMR: $\delta = 7.26$ ppm for CDCl_3) as internal standard. Carbon spectra were referenced to the shift of the ^{13}C signal of CDCl_3 ($\delta = 77.0$ ppm). The following abbreviations are used to indicate the multiplicity in NMR spectra: s - singlet; d - doublet; t - triplet; q - quartet; dd - double doublet; ddd – doublet of doublet of doublets; dt - doublet of triplets; m - multiplet; quint – quintuplet; sext -sextuplet sept - septet; br - broad signal; dq – doublet of quartets.

High resolution mass spectra (HRMS) were acquired using a Bruker solariX XR Fourier transform ion cyclotron resonance mass spectrometer (Bruker Daltonik GmbH, Bremen, Germany) equipped with a 7 T refrigerated actively-shielded superconducting magnet. The samples were ionized in positive ion mode using a MALDI or ESI ionization sources.

Automatic weighing and transferring of liquids was made with a Zinssler Analytics custom robot "Calli".

Samples were evaporated in a parallel fashion by employing a Genevac HT-4X vacuum centrifuge Series II System.

Preparative HPLC-MS was conducted on a Agilent 1260 Infinity Series (Autosampler, Fraction Collector, DAD, Pumps, Check valves, all while coupled to a Agilent 6120 LC-MS Quadrupole mass-spectrometer. MS-traces were generated in positive/negative switching mode and ESI/APCI as ionization method was used in tandem.

uHPLC-MS (ultrahigh performance) was conducted on a Agilent 1260 Infinity Series (Autosampler, Pump was 1290 Infinity Series) all while coupled to an Agilent 6120 LC-MS Quadrupole mass-spectrometer. MS-traces were generated in positive/negative switching mode and ESI/APCI as ionization method was used in tandem.

Chiral HPLC was measured on a Agilent 1100 Series (DAD, Autosampler, Pumps). The respective chiral stationary phase is indicated in the characterization part.

4.4.1. Description of Equipment

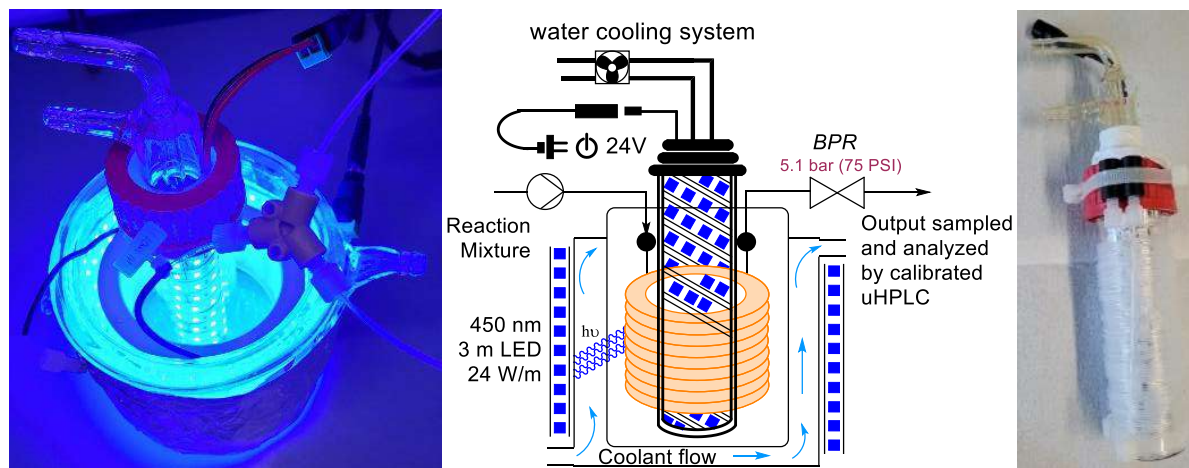


Figure 63. Depiction and photographs of the continuous flow reactor (plug-flow) and the photoreactor setup.

A versatile LED-based photoreactor for continuous flow reactions under *cryogenic conditions* is unprecedented in Literature. The goal is to build a photoreactor for such conditions using only readily available and low-cost equipment that can be found in any organic chemistry laboratory. The herein presented Photoreactor can be immersed

in any cryobath for temperature regulation as the LEDs are *hermetically sealed* inside a Pyrex glass tube to avoid glacier formation, which can obstruct efficient irradiation due to the high albedo of water ice that would form from atmospheric moisture. The heat generation which tends to burn high power LEDs under sealed conditions is counteracted by wrapping the LED-Strips around a central sublimator glass-piece which is water cooled. With this innovative reactor design, it is possible to run a continuous flow photoreaction at any temperature by simply immersing the photoreactor and coil reactor couple in a temperature-controlled liquid (Ice-mixtures, dry-ice mixtures, cryostat-baths, oil-baths). The here presented Reactor performed for over 300 h and is still fully operational.



Figure 64. Photographs of the assembled and disassembled water-cooled photoreactor for cryogenic continuous flow operations

Construction of the inside-out Photoreactor: The central sublimator glass-piece is first wrapped to the desired length with heavy duty aluminium foil to generate a socket for the LED-strip that possesses high heat conductive properties. Around this first layer is then coiled and glued (double-sided adhesive tape) the LED-strip which is further secured in place at the top and bottom with electric isolating tape. The cable is guided through the silicon rubber seal by puncturing it. The final reactor is then assembled as presented in Figure 53. Video of the assembly can be found separately uploaded under supporting files.

Construction of the outside in photoreactor. A photoreactor was build based on a jacketed-water cooled reactor purchasable from <https://www.neubert-glas.de> (catalogue number: 5020-06-0250) Around the glass body were wrapped the later described UV-LED-strips and fixed in position with adhesive tape. Contacts were sealed with electrical isolating tape and everything was once again wrapped with several layers of aluminium foil. The aluminium foil cover was then wrapped with parafilm to protect it from eventual chemical exposure. The whole reactor ensemble is displayed in Figure 65. It is conceivable to connect a temperature regulated circulating liquid and thus perform reactions under elevated temperatures.



Figure 65. Assembly of the double walled glass photoreactor-couple with the central photoreactor on top of the VapourTec EasyScholar system.

Led-Specifications: Striscia LED Blue (460 nm) ORBLUF52120812 (ledpoint) 24 W/m with a self-adhesive tape that holds the strip light safely and securely to the photoreactor support. The LEDs wavelength emission profile together with their specific light intensity (expressed as mW cm^{-2}) have been determined before their use. In particular, the spectrum has been obtained by using a compact CCD spectrometer (model CCS200/M) connected to a multimode optical fiber, purchased from Thorlabs. Ultraviolet LEDs are characterized by an almost monochromatic emission profile (with a full width at half-maximum intensity of ca. 10-20 nm) showing a maximum of intensity located at ca. 458 nm. The light power intensity was thus checked using a Thorlabs

PM200 power meter equipped with a S130VC power head with a Si detector. The measured light intensities, though slightly decreasing by moving the maximum of LEDs emission towards longer wavelengths, was $I = 540 \text{ mW cm}^{-2}$ (std 2.7).

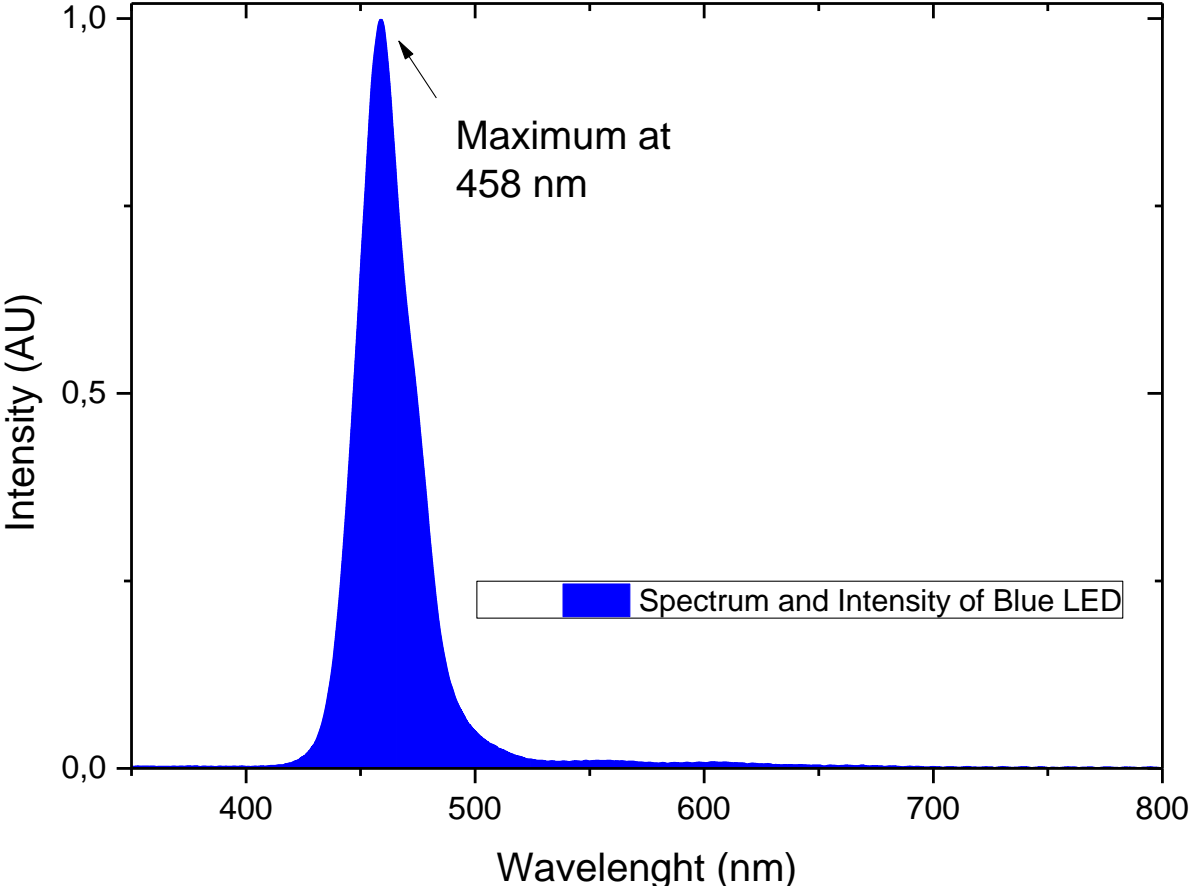


Figure 66. Graph of UV- LEDs wavelength emission profile

Continuous Flow Coil Reactor Specifications

Table 25. Specifications for the reactors used in the work. All three coil reactors are made from standard HPLC-Tubing – Material PFA

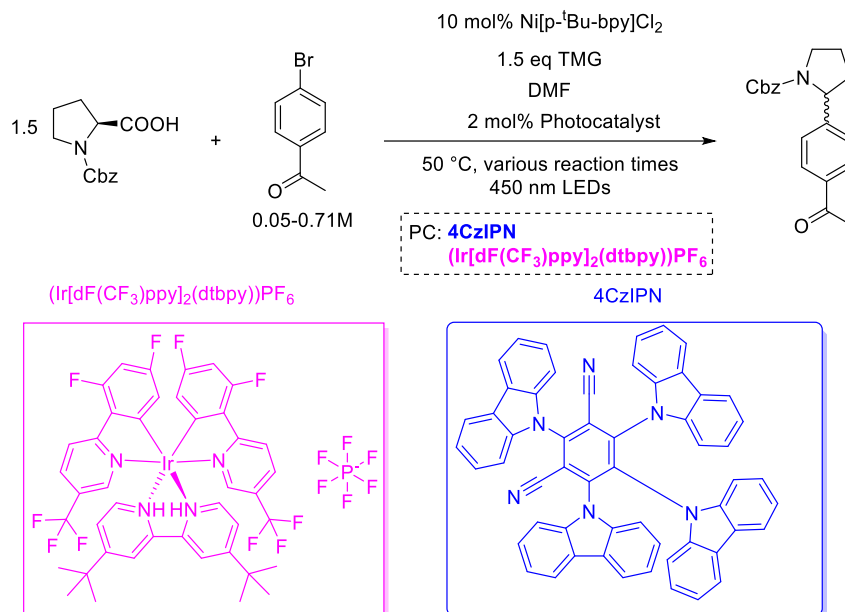
Entry	Reactor	Reactor Volume	Internal Diameter (Outer Diameter) [in]	Reactor Length [m]	Illuminated Surface Area [cm ²]
1	50 mL RBF	50 mL	--	---	28 ^[a]
2	Micro-	100 µL	0.01	2.00	16
3	Small Meso-	0.5 mL	1/16	0.025	12.5
4	Meso-	5 mL	0.04	6.2	160

[a] estimated based on a half sphere of 20 mL that gets irradiated laterally.

All fluidic connections were made by ¼-28-bore fingertight ferules and adapters (connectors, Y- and T-type) and were purchased together with the HPLC-tubing. at Cole-Parmer.

4.4.2. General Procedure for the Preparation of Stock-Solutions for Batch and Flow Reactions

MacMillan's decarboxylative sp^3 - sp^2 -cross-coupling by merging Ni- and photoredox-catalysis



Into a Vial of the appropriate size (4 mL screw-cap in case of Microfluidic reaction, 50 mL round-bottom-flask with NS 29 mm opening and rubber septum in the case of batch and mesofluidic conditions) were placed (order is unimportant) 1.00 eq of 4-bromoacetophenone, 1.50 eq of Z-Pro-OH, 0.10 eq of [4,4'-Bis(1,1-dimethyl-ethyl)-2,2'-bipyridine] nickel (II) dichloride, 0.02 eq of either the Iridium-PC or 4CzIPN, 0.20 eq of biphenyl as internal standard and nitrogen was applied. The mixture was dissolved in the appropriate amount of solvent (note that in the case of the concentrated solution effective concentration had to be considered and dissolution was achieved by sonification). To this mixture as then added 1.50 eq of 1,1,3,3-Tetramethylguanidine. The respective Vial or flask was further protected from incident irradiation by wrapping it with aluminium foil. No degassing was carried out only the headspace atmosphere was exchanged to nitrogen. In case of Microfluidic process, the contents were taken up in an inertised 2.5 mL SGE gastight syringe and infused into the coil-reactor via ¼-28-bore fluidic connections. In case of Mesofluidic process the round-bottom flask was punctured by a PEEK-tubing and connected to the peristaltic pumps of the VapourTec EasyScholar via ¼-28 bore fluidic connectors. The coil reactor was equipped with a 5.1 bar (75 PSI) back-pressure regulator and the output was collected in standard Erlenmeyer-Flasks. When sampling for the uHPLC-MS assay was undertaken, a few drops were collected in a GC-vial and diluted with methanol and the

mixture was then analysed by the autosampler of the uHPLC-MS. Collection of the product for characterisation purposes was done using 4CzIPN as photocatalyst, the 5 mL mesofluidic reactor and at a residence time of 20 min. The output of the reactor was collected for 4 minutes to give 1 mL of crude reaction mixture. The DMF was evaporated in a steady stream of compressed air over night. The remains were dissolved in dichloromethane and ammonium chloride solution (half saturated) and the phases separated. The aqueous layers were extracted two additional times with dichloromethane. The volatiles were removed *in vacuo* and then in high vacuum. The final product was obtained by normal phase silica flash chromatography using a gradient of EtOAc/cyclohexane to yield xx mg (xx%) of the final product as a yellow solid.

Purification Crude reaction mixture was dissolved in DCM/, evaporated on 5g ISOLUTE® HM-N (diatomaceous earth) and purified with Grace Reveleris.

Column: CHROMABOND Flash with 20 g MN Silica.

Mobile phase: EtOAc/cyclohexane.

¹H NMR (300 MHz, Chloroform-*d*) δ 8.05 – 7.59 (m, 2H), 7.44 – 6.93 (m, 6H), 6.77 (dd, *J* = 16.2, 7.9 Hz, 1H), 5.23 – 4.71 (m, 3H), 3.61 (t, *J* = 6.4 Hz, 2H), 2.55 – 2.34 (m, 3H), 2.39 – 2.11 (m, 1H), 1.78 (tq, *J* = 10.2, 6.2, 5.4 Hz, 3H)..

MS m/z =342.2 [M+H⁺]
(ESI+APCI)

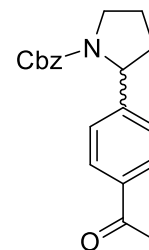
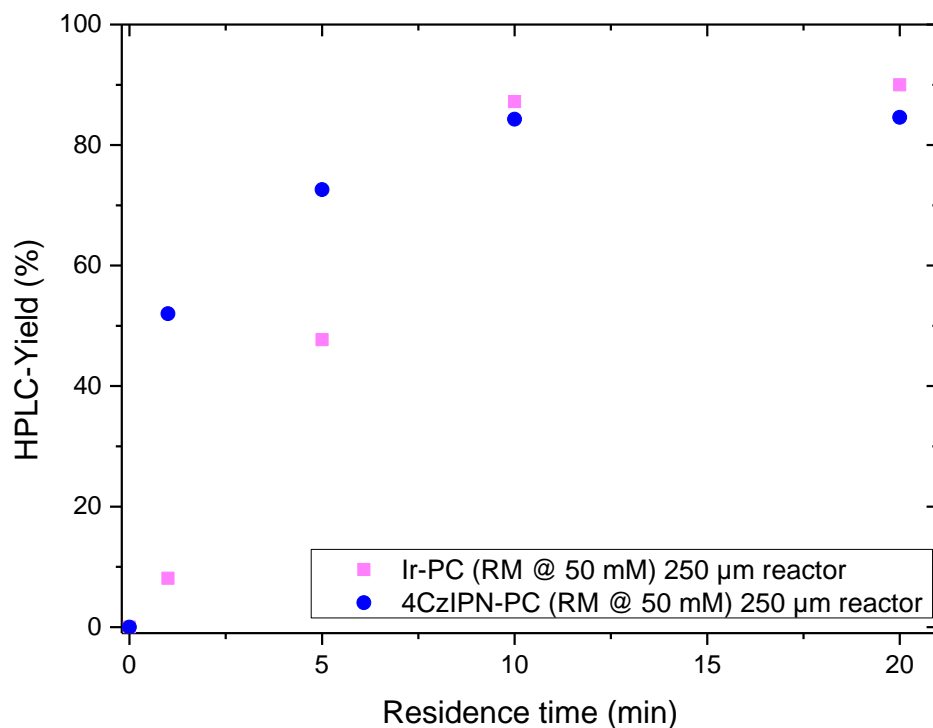
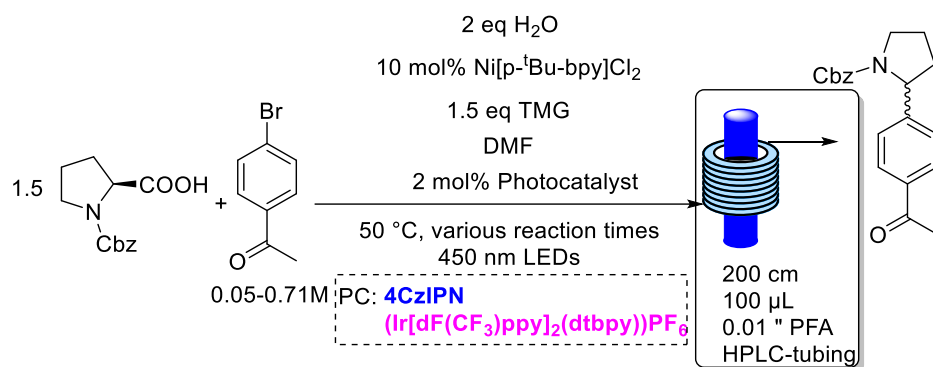


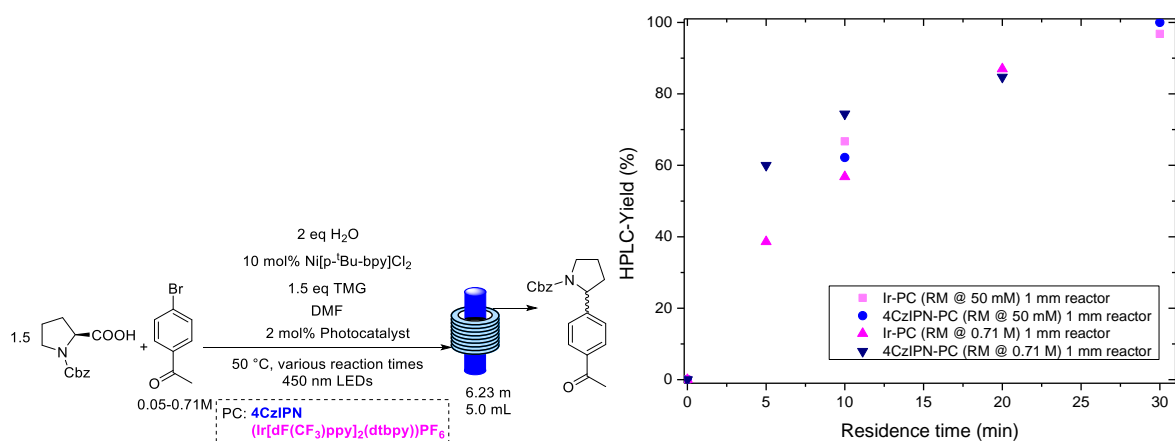
Table 26. Batch experiments for benchmarking purposes.

Entry	Catalyst	Reaction time [h]	HPLC-Yield
1	Ir-PC	23	77
2	4CzIPN	23	75



Scheme 44. Depiction of the reaction conditions with reactor specifications under microfluidic conditions. Depiction of reaction progress as a function of residence time.

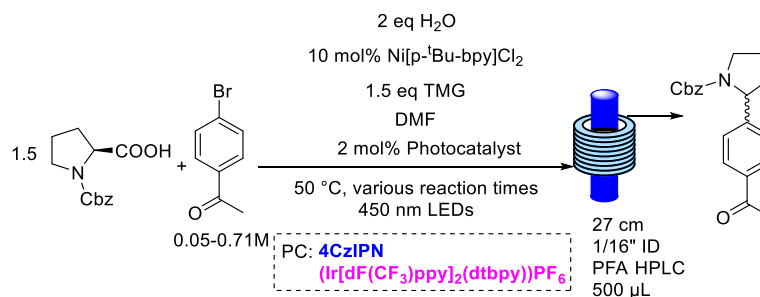
Entry	Residence time [min]	Flow rate [μl/min]	HPLC-Yield	
			Iridium	4CzIPN
1	0	0	0	0
2	5	50	47,7	72,6
3	10	25	87,2	84,3
4	20	12.5	90	84,6



Scheme 45. Conversion curve of unintensified microfluidic conditions against their intensified conditions.

Entry	Residence time [min]	Flow rate [$\mu\text{L}/\text{min}$]	HPLC-Yield Ir@0.05M	Ir@0.71M	HPLC-yield 4CzIPN@0.05M	HPLC-yield 4CzIPN@0.71M
1	0	0	0	0	0	0
2	5	1000	----	38,6	----	60
3	10	500	66,7	56,8	62,2	74,4
4	20	250	----	87	-----	84,7
5	30	167	96,8	----	100	-----

Table 27. Results of small meso fluidic experiment.



Entry	Catalyst	Residence time [min]	Flow rate [$\mu\text{L}/\text{min}$]	HPLC-Yield
1	Ir-PC	10	50	75
2	4CzIPN	30	16.7	59

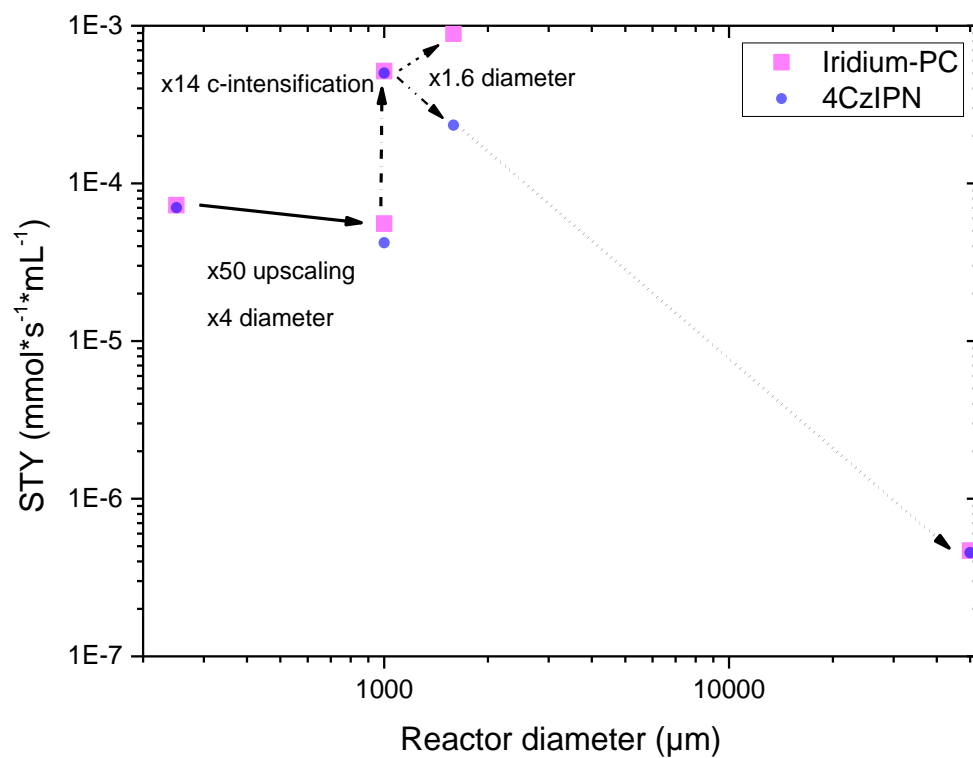


Figure 67. Space-time-yield as a function of the reactor diameter.

Entry	Reactor diameter [μm]	STY [mmol*s ⁻¹ *mL] Iridium-PC	Residence time [min]	Flow rate [μL/min]
1	250	7,27E-5	10	10
2	1000	5,16E-4	20	250
3	1588	8,91E-4	10	50
4	50000	4,687E-7	1380	---
5	1000	5,56E-5	10	500
Entry	Reactor diameter [μm]	STY [mmol*s ⁻¹ *mL] 4CzIPN	Residence time [min]	Flow rate [μL/min]
1	250	7,02E-5	10	10
2	1000	5,01E-4	20	250
3	1588	2,34E-4	30	16.7
4	50000	4,54E-7	1380	
5	1000	4,2E-5	20	250

4.4.3. Measurement of Molar Extinction Coefficient to Determine Transmission Through Reaction Medium

Generally when engaging in upscaling of a photochemical process the knowledge about the transmission behaviour is of utmost importance. For this the molar extinction coefficient needs to be measured. This is a quite simple measurement the only things needed are:

- A UV-Vis spectrometer
- A cuvette (best the 1 mm micro cuvettes)
- Your reaction mixture and a dilution protocol of it.

For the dilution protocol of the reaction mixture a several factor 2 or factor 5 dilution is required. Usually 3 measurement points plus the $c=0$ (just solvent) are enough to get a good linear correlation. By taking an aliquot and diluting it with the corresponding amount of solvent the respective dilution protocol is made. Each of the solutions will be measured and the absorption value will be noted. Then a linear correlation between the absorption values and the concentration of each solution is made. The slope of the linear correlation marks the molar extinction coefficient of your solution. It is advisable to mark two things:

1. The concentration may be set to the limiting reagent, the photocatalyst or whatever else is inside the reaction mixture – not important with the later calculations. It is very important that the chemical entity of what is set as the concentration is not changed later. This sounds clunkier than it is, an example may be helpful. Example: You set the chemical entity of what marks your molar extinction coefficient to be the photocatalyst. So, under no circumstances the concentration of your limiting reagent or other ingredients can be used as the calculation base later! Stick to one.
2. Use a Microcuvette with a low pathlength and volume. This will save reaction mixture and means you do not have to dilute as many times. If such a microcuvette is used, the slope of the linear correlation will not represent the molar extinction coefficient. Only the multiplication of the slope with fraction of the pathlength/1 cm will represent the molar extinction coefficient. Example: you use a 1 mm cuvette your slope has to be multiplied by $1 \text{ cm}/1 \text{ mm}=10$ to get the accurate molar extinction coefficient.

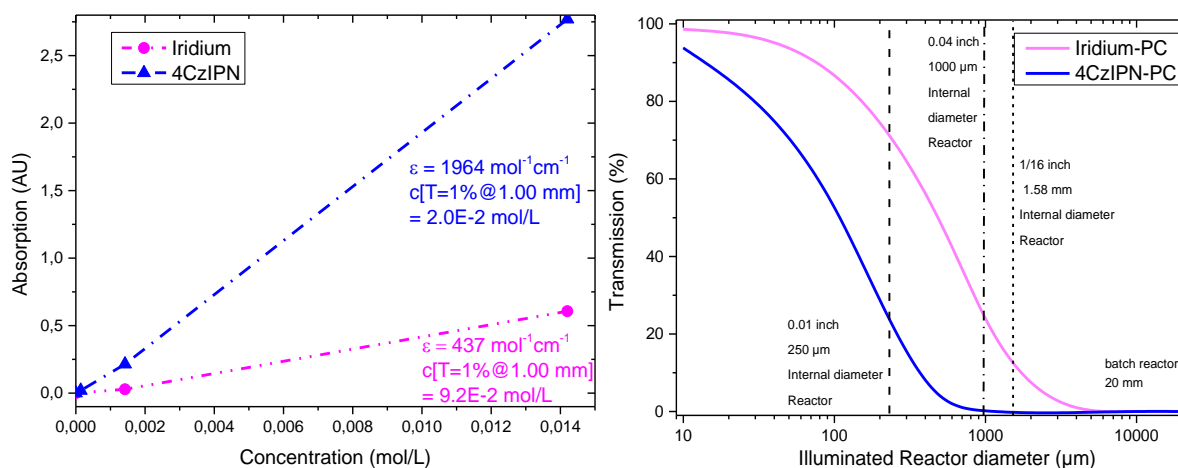


Figure 68. Graphical display of the determination of the molar extinction coefficient and the optimum concentration of the reaction mixture. Calculated transmission curve with inlayed lines with the corresponding reactor diameters.

In Figure 68 is displayed the graph for the determination of the molar extinction coefficient. In the present study a 1 mm micro-cuvette was used and the original reaction mixture was concentrated as high as possible (0.71 M bromoacetophenone, 0.014 M in terms of photocatalyst) and diluted three times by a factor of 10. The resulting solution were analyzed by UV-Vis spectrometry where their respective absorption values were measured.

$$A = \epsilon cl \leftrightarrow c = A/\epsilon l \quad \text{Equation 32}$$

By rearranging the Lambert-Beer law Equation 32 and setting the values for $A=2$ (99% of photons get absorbed), $l=1 \text{ mm}$ (desired reactor diameter, any value can be set here) and the value of the molar extinction coefficient ϵ , that was just determined, the optimum concentration may be calculated. Based on the optimum concentration by using again a variation of the Lambert-Beer law the transmission as a function of reactor diameter may be calculated:

$$T = 10^{-\epsilon cl} \quad \text{Equation 33}$$

Table 28. Measurement values for the determination of the molar extinction of either reaction mixtures.

Entry	c [mol/L]	Absorption [AU]	
		Iridium PC	4CzIPN
1	0	0	0
2	1.4E-3	0	0.02
3	1.4E-2	0.029	0.22
4	1.4E-1	0.61	2.77

4.4.4. Irradiation from One Side versus Both Sides. And How to Read the Diffusion Graph

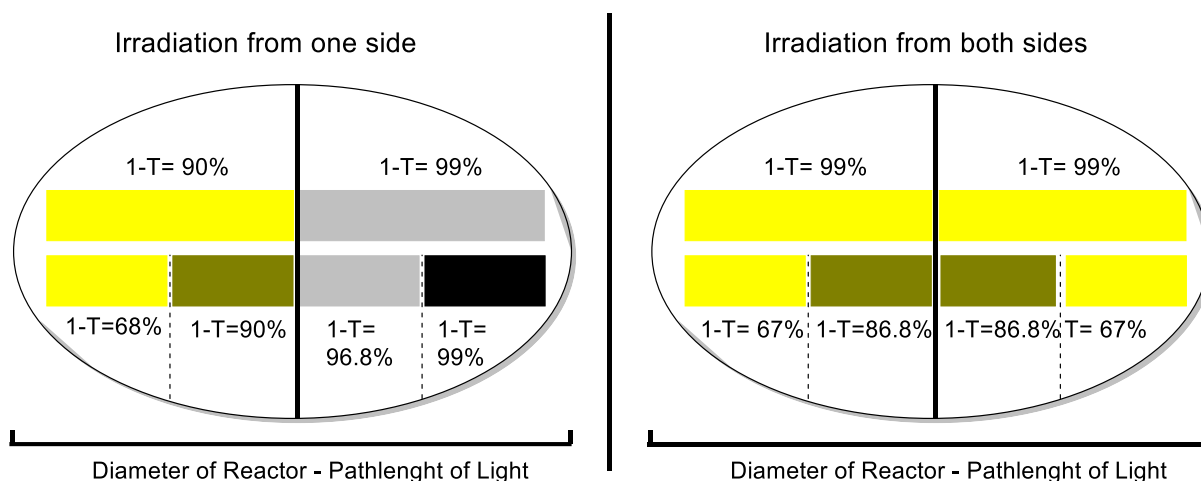


Figure 69. Transmission (T) profile of a reactor cross-section. Left is displayed the case where irradiation is taking place only from one side of the reactor. Right is displayed the case where irradiation is taking place from both sides of the reactor. Dark zones, as characterized by low transmission zones, are much less prevalent on the right side.

In the case of irradiation from only one side the dimensions of the flow reactor become limiting very fast. As we can see in Figure 69 at best half of the reactor will receive efficient irradiation performing the reaction at a concentration that will absorb 99% of photons ($1-T=99\%$). If irradiation occurs from both sides most of the reactor will receive efficient irradiation. There is an argument to be made that the middle quarters do not receive efficient irradiation. All things considered there must be some diffusion going on from the dark zones to the bright zones. If the reaction mixture that absorbs 99% of

all photons is present, diffusion time will limit to half (a quarter) of the reactor and thus the diffusion time may be read out from Figure 70. Alternatively the Einstein-Smoluchovski equation may be used to calculate the diffusion time.

$$t_{mixing} = \frac{L^2}{D} \tag{Equation 34}$$

If diffusion time is significantly slower than the reaction kinetics will allow the reaction to proceed, it means there has to be dealt with an inefficient reactor.

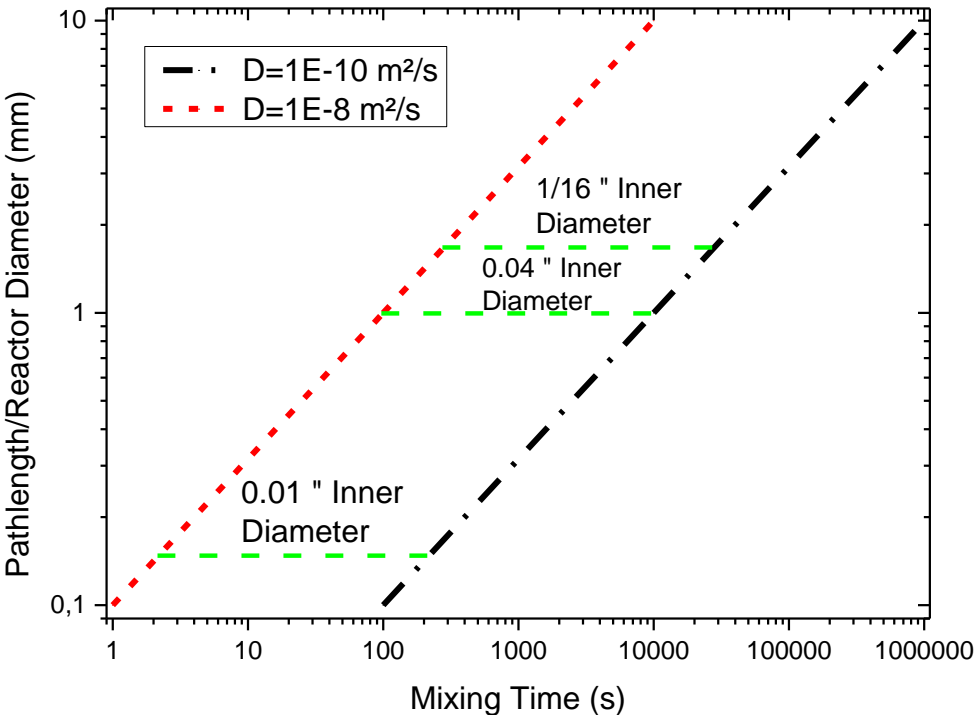


Figure 70. Reactor size (Diameter) versus mixing time. In small reactors laminar flow regimes are predominant, leading to mixing being limited by diffusion.

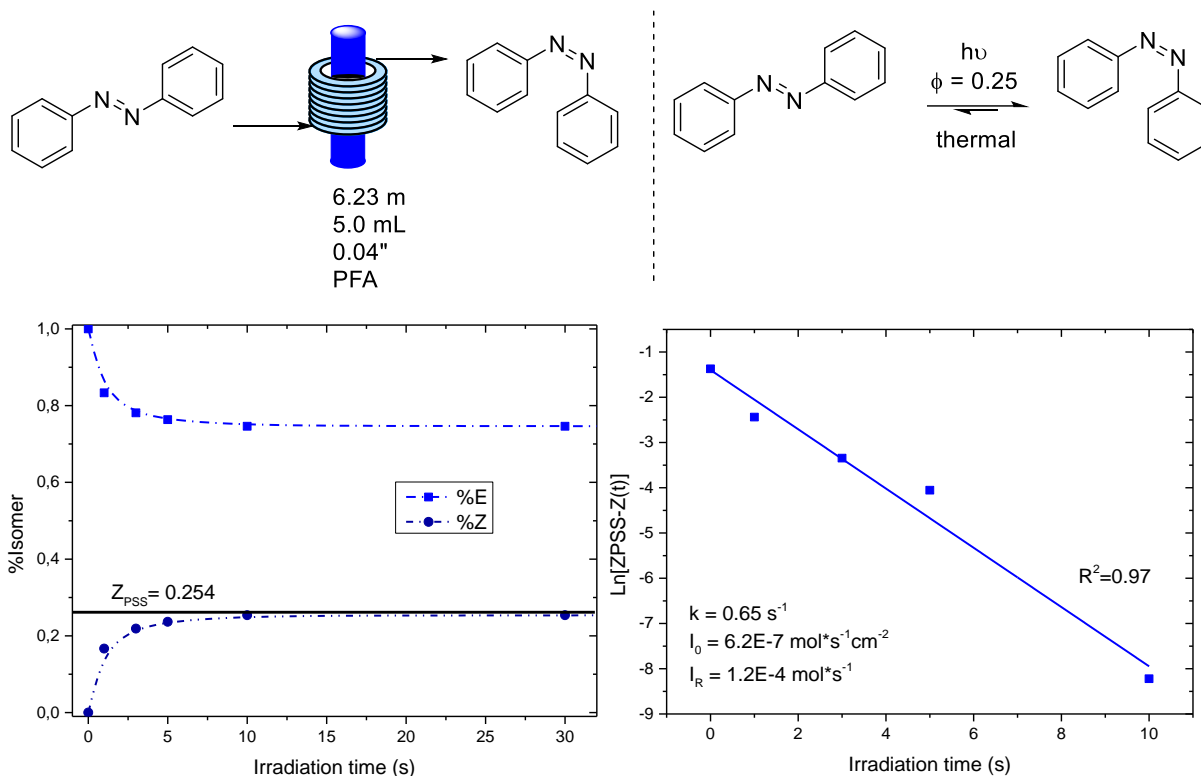
4.4.5. Actinometry and Photonflux Consideration.

It is sensical that running an efficiently irradiated reactor at some point the number of incident photons will be rate-limiting. To know the full capabilities of a photoreactor + continuous flow reactor it is important to determine the photonflux I_R inside your reactor. Only then can you estimate the highest achievable productivity or STY. The most convenient way to measure the photonflux is to use the azobenzene actinometer recently introduced by Roseau and coworkers.^[106] In Scheme 46 is displayed the underlying principle of the this actinometer: A well described *E/Z*-Isomerisation reaction for which the quantum yield was determined to be $\Phi=0.25$. So every four photons absorbed one isomerization will take place. The ratio of *E/Z*-isomer can be conveniently measured by ¹H-NMR.

Procedure of Actinometry Using Azobenzene

In a container of the operator's choice was prepared a solution of 0.01 M azobenzene in acetonitrile (note: enough solution is required to flush the reactor several dozens of times). The container is then darkened by wrapping it copious amounts of aluminium foil. The container is then connected to the fluidic delivery device, such as a peristaltic pump, syringe pumps (in tandem with switch valve) or other. The lamps of the photoreactor are turned on and the solution is infused to give residence times of seconds to dozens of seconds. The outflow is collected in a darkened container (note: It is best to use non-transparent tubing for the in-flow and out-flow tubings, the reactor obviously must be made of transparent tubing). The collected outflow of the reactor is transferred to a NMR-tube and quickly measured (note: A "dark" room is best suited for this purpose). The distinctively different signals in the aromatic region are integrated and the values recorded (I_Z and I_E respectively). Set the value for the *E*-isomer to a number of the operator's choice, it is only important to not change during the course of an experiment as to not mess up the ratio. Calculate the abundance of *Z*-isomer according to Equation 35:

$$\%Z = \frac{I_Z}{I_E + I_Z} \quad \text{Equation 35}$$



Scheme 46. Illustration of the actinometry experiments: Graph of *E*- vs *Z*-Isomer against irradiation time (residence time). Graph of first order rate kinetics, based on the first graph, to determine the kinetic constant from which the incident photonflux I_R inside the reactor (also photonflux per unit area I_0) can be calculated.

In theory a curve of % of either isomer as a function of irradiation time as displayed in Scheme 46 should be obtained with a %*Z*-isomer approaching the equilibrium state or Photostationary state (Z_{PSS}). Next with the obtained values a first order rate kinetics was undertaken. For this the measurement points were subtracted from the Z_{PSS} and a logarithm was applied and according to Equation 36 a linear correlation was obtained as displayed in Scheme 46:

$$\ln[Z_{PSS} - Z(t)] = kt \quad \text{Equation 36}$$

$Z(t)$ marks the %*Z*-isomer at a set irradiation time t . The constant k that can directly be obtained from the slope of the graph now just was substituted in Equation 37.

$$I_R = A_{irrad} I_0 = A_{irrad} \frac{Z_{PSS} k}{\phi_{azobenzene} \varepsilon_{azobenzene} \ln 10} \quad \text{Equation 37}$$

The values for ϕ , ε can be looked up at Roseau, M.; De Waele, V.; Trivelli, X.; Cantrelle, F. X.; Penhoat, M.; Chausset-Boissarie, L. *Helv. Chim. Acta* **2021**, 104 (7).

The only value that is missing is the irradiated surface area of the reactor. This is not a measured value but rather a calculated value. Based on some basic geometric principles e.g. the lateral surface area of a tubular coil reactor boils down to calculating the lateral surface area of a cylinder:

$$A_{coil-reactor} = 2\pi r h \quad \text{Equation 38}$$

If the irradiation is taking place from only one side than the value has to be halved.

If a chip reactor with cuboid channels is used it is even simpler to calculate the surface area:

$$A_{chip-reactor} = 2 * width * length \quad \text{Equation 39}$$

Again if the irradiation is taking place from only side the value has to be halved.

4.4.6. Predicting Reactor Performance Using Photons equivalents

Once the photonflux inside the reactor is obtained and it is made sure the reactor is irradiated efficiently. The performance of the reactor may be estimated. But first the quantum yield of the reaction is required. If you are fortunate enough the value is published somewhere – if not it is not a big deal to determine it yourself as you know already the photonflux inside your reactor. The calculation that must be made boils down to setting into correlation the moles of product in your reactor (numerator) and divided by the number of photons in the reactor denominator. C_{prod} has to be measured by a good assay such as with a calibrated GC/HPLC- or an NMR-assay. To get an accurate quantum yield it is important that the reaction has not gone to high levels of conversion! If a plateau in conversion is reached the values you get for C_{prod} will significantly skew your quantum yield.

$$\Phi = \frac{c_{prod} V_R}{I_R (1 - T) t_R} \quad \text{Equation 40}$$

Again without the term (1-T) that was hopefully determined before even trying to use photon equivalents nothing works in photochemistry.

In principle all the values that are needed for the prediction of reactor performance are now at hand. What is of interest to the chemist/engineer is most likely the volumetric flowrate multiplied by the initial concentration to get a good feeling about how high is

the reactor performance. Assuming an efficient photoreactor is at hand and it needs to be calculated how many moles of product per time unit may be obtained after irradiation with one photon equivalent according to the following equations.

$$\frac{\Phi I_R(1 - T)}{q c_0} = E q_{\text{photon}} \quad \text{Equation 41}$$

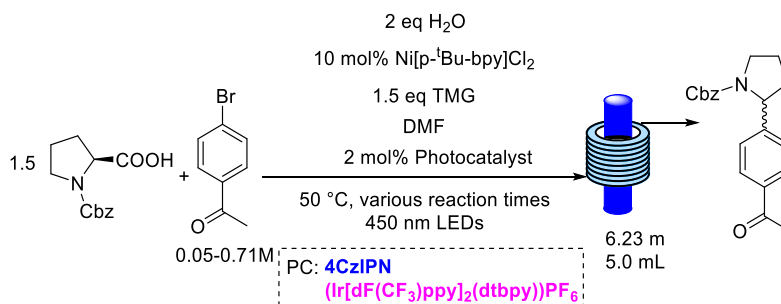
$$E q_{\text{photon}} = 1 \leftrightarrow P = q c_0 = \Phi I_R(1 - T) \quad \text{Equation 42}$$

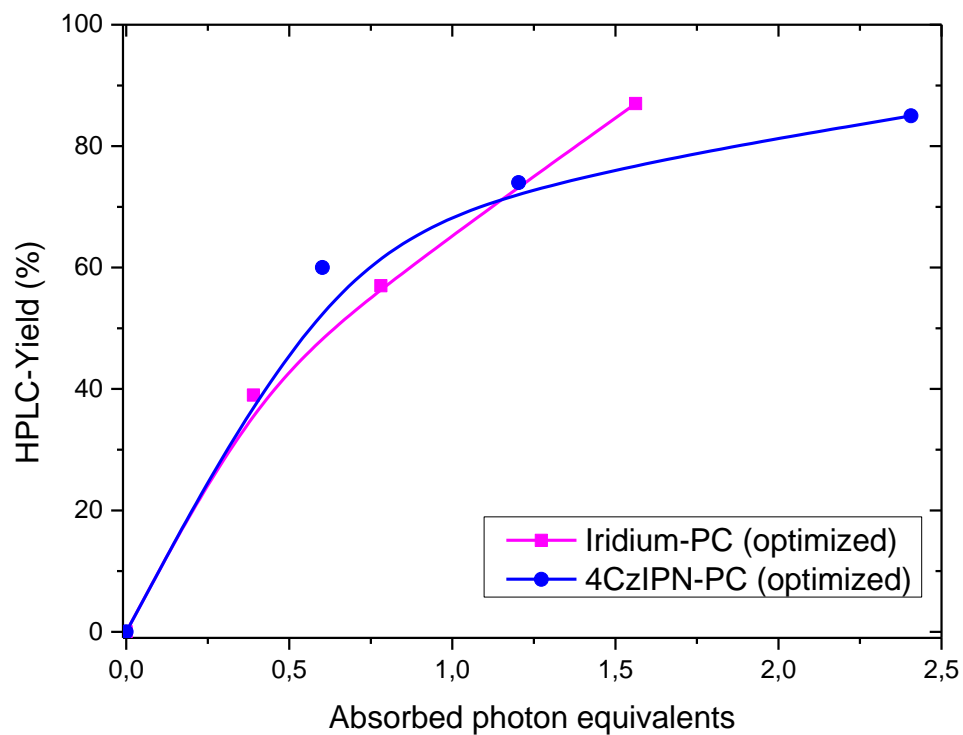
Ideally not a single value for the photon equivalents is determined but a conversion curve of the reaction is measured by varying the flowrate inside the reactor

For this the typical conversion curve as function of the residence time may be modified by modifying Equation 42.

$$\frac{\Phi I_R(1 - T)t_R}{V_R c_0} = E q_{\text{photon}} \quad \text{Equation 43}$$

Instead of plotting t_R now the photon equivalents may be plotted as the function of the Assay %yield.





Scheme 47. Graph of the HPLC-yield as a function of the absorbed photon equivalents.

Entry	Photon eq. Iridium-PC	HPLC-yield [%]	Photon eq. 4CzIPN	HPLC-yield [%]
1	0	0	0	0
2	0,39046	39	0,60162	60
3	0,78092	57	1,20324	74
4	1,56183	87	2,40649	85

5. Bibliography

- [1] G. Ciamician, *Science (80-)*. **1912**, 36, 385–394.
- [2] D. Cambié, C. Bottecchia, N. J. W. Straathof, V. Hessel, T. Noël, *Chem. Rev.* **2016**, 116, 10276–10341.
- [3] J. A. Balzani V., Ceroni P., *Photochemistry And Photophysics - Concepts, Research, Application*, **2014**.
- [4] D. M. Arias-Rotondo, J. K. McCusker, *Chem. Soc. Rev.* **2016**, 45, 5803–5820.
- [5] N. A. Romero, D. A. Nicewicz, *Chem. Rev.* **2016**, 116, 10075–10166.
- [6] F. Herbrink, P. Camarero González, M. Krstic, A. Puglisi, M. Benaglia, M. A. Sanz, S. Rossi, *Appl. Sci.* **2020**, 10, 5596.
- [7] M. B. Plutschack, B. Pieber, K. Gilmore, P. H. Seeberger, *Chem. Rev.* **2017**, 117, 11796–11893.
- [8] B. J. Reizman, K. F. Jensen, *Acc. Chem. Res.* **2016**, 49, DOI 10.1021/acs.accounts.6b00261.
- [9] C. J. Mallia, I. R. Baxendale, *Org. Process Res. Dev.* **2016**, 20, DOI 10.1021/acs.oprd.5b00222.
- [10] M. B. Plutschack, B. Pieber, K. Gilmore, P. H. Seeberger, *Chem. Rev.* **2017**, 117, 11796–11893.
- [11] D. R. Snead, T. F. Jamison, *Angew. Chemie - Int. Ed.* **2015**, 54, 983–987.
- [12] C. Sambigiato, T. Noël, *Trends Chem.* **2020**, 2, 92–106.
- [13] N. Yazdanpanah, Z. K. Nagy, *The Handbook of Continuous Crystallization*, **2020**.
- [14] U. Shah, “No Title,” can be found under <https://www.slideshare.net/SyedMuhammadUsmanSha/difference-between-batchmixed-flow-amp-plugflow-reactor>, **2019**.
- [15] C. G. Hill, T. W. Root, **2014** □□□□□ □□□□□.
- [16] P. T. Anastas, J. C. Warner, *Green Chem. Theory Pract. Oxford Univ. Press. New York* **1998**.
- [17] V. Hessel, D. Kralisch, N. Kockmann, T. Noël, Q. Wang, *ChemSusChem* **2013**, 6, DOI 10.1002/cssc.201200766.
- [18] J. Wegner, S. Ceylan, A. Kirschning, *Adv. Synth. Catal.* **2012**, 354, DOI 10.1002/adsc.201100584.
- [19] M. Benaglia, A. Puglisi, *Catalyst Immobilization Methods and Applications*, Wiley-VCH Verlag, **2020**.
- [20] C. Rodríguez-Escrich, M. A. Pericàs, *Chem. Rec.* **2019**, 19, DOI 10.1002/tcr.201800097.
- [21] R. Porta, M. Benaglia, V. Chiroli, F. Coccia, A. Puglisi, *Isr. J. Chem.* **2014**, 54, 381–394.
- [22] R. Porta, F. Coccia, R. Annunziata, A. Puglisi, *ChemCatChem* **2015**, 7, 1490–1499.
- [23] S. Guizzetti, M. Benaglia, J. S. Siegel, *Chem. Commun.* **2012**, 48, 3188–3190.
- [24] R. Porta, M. Benaglia, R. Annunziata, A. Puglisi, G. Celentano, *Adv. Synth. Catal.* **2017**, 359, 2375–2382.
- [25] S. Mondini, A. Puglisi, M. Benaglia, D. Ramella, C. Drago, A. M. Ferretti, A. Ponti, *J. Nanoparticle Res.* **2013**, 15, 2025.
- [26] R. Porta, M. Benaglia, A. Puglisi, A. Mandoli, A. Gualandi, P. G. Cozzi, *ChemSusChem* **2014**, 7, 3534–3540.
- [27] V. Chiroli, M. Benaglia, F. Cozzi, A. Puglisi, R. Annunziata, G. Celentano, *Org.*

- Lett.* **2013**, *15*, 3590–3593.
- [28] Deepa, S. Singh, *Adv. Synth. Catal.* **2021**, *363*, 629–656.
- [29] D. A. Nicewicz, D. W. C. MacMillan, *Science (80-.)*. **2008**, *322*, 77–80.
- [30] E. R. Welin, A. A. Warkentin, J. C. Conrad, D. W. C. MacMillan, *Angew. Chemie Int. Ed.* **2015**, *54*, 9668–9672.
- [31] H.-W. Shih, M. N. Vander Wal, R. L. Grange, D. W. C. MacMillan, *J. Am. Chem. Soc.* **2010**, *132*, 13600–13603.
- [32] E. D. Nacsa, D. W. C. C. MacMillan, *J. Am. Chem. Soc.* **2018**, *140*, 3322–3330.
- [33] D. A. Nagib, M. E. Scott, D. W. C. Macmillan, **n.d.**, DOI 10.1021/ja9053338.
- [34] G. Cecere, C. M. König, J. L. Alleva, D. W. C. MacMillan, *J. Am. Chem. Soc.* **2013**, *135*, 11521–11524.
- [35] A. Bahamonde, P. Melchiorre, *J. Am. Chem. Soc.* **2016**, *138*, 8019–8030.
- [36] G. E. M. Crisenza, D. Mazzarella, P. Melchiorre, *J. Am. Chem. Soc.* **2020**, *142*, 5461–5476.
- [37] E. de Pedro Beato, D. Mazzarella, M. Balletti, P. Melchiorre, *Chem. Sci.* **2020**, *11*, 6312–6324.
- [38] A. Puglisi, M. Benaglia, M. Cinquini, F. Cozzi, G. Celentano, *European J. Org. Chem.* **2004**, *2004*, 567–573.
- [39] V. Chirolì, M. Benaglia, A. Puglisi, R. Porta, R. P. Jumde, A. Mandoli, *Green Chem.* **2014**, *16*, 2798–2806.
- [40] M. Benaglia, G. Celentano, M. Cinquini, A. Puglisi, F. Cozzi, *Adv. Synth. Catal.* **2002**, *344*, 149–152.
- [41] D. Brenna, R. Porta, E. Massolo, L. Raimondi, M. Benaglia, *ChemCatChem* **2017**, *9*, 941–945.
- [42] N. R. Guha, R. M. Neyyappadath, M. D. Greenhalgh, R. Chisholm, S. M. Smith, M. L. McEvoy, C. M. Young, C. Rodríguez-Esrich, M. A. Pericàs, G. Hähner, et al., *Green Chem.* **2018**, *20*, 4537–4546.
- [43] T. Ritter, *FLUOROALKYLATION REAGENTS AND USES THEREOF*, **2015**.
- [44] B. Altava, M. I. Burguete, E. García-Verdugo, S. V. Luis, *Chem. Soc. Rev.* **2018**, *47*, 2722–2771.
- [45] A. Puglisi, M. Benaglia, R. Annunziata, V. Chirolì, R. Porta, A. Gervasini, *J. Org. Chem.* **2013**, *78*, 11326–11334.
- [46] M.-Y. Rong, L. Yang, J. Nie, F.-G. Zhang, J.-A. Ma, *Org. Lett.* **2019**, *21*, 4280–4283.
- [47] J. Chatt, G. J. Leigh, A. P. Storace, D. D. A. Squire, B. J. Starkey, *J. Chem. Soc. A Inorganic, Phys. Theor. Chem.* **1971**, 899–904.
- [48] S. Cañellas, C. Ayats, A. H. Henseler, M. A. Pericàs, *ACS Catal.* **2017**, *7*, 1383–1391.
- [49] S. Wang, J. Izquierdo, C. Rodríguez-Esrich, M. A. Pericàs, *ACS Catal.* **2017**, *7*, 2780–2785.
- [50] R. M. Neyyappadath, R. Chisholm, M. D. Greenhalgh, C. Rodríguez-Esrich, M. A. Pericàs, G. Hähner, A. D. Smith, *ACS Catal.* **2018**, *8*, 1067–1075.
- [51] J. Lai, S. Sayalero, A. Ferrali, L. Osorio-Planes, F. Bravo, C. Rodríguez-Esrich, M. A. Pericàs, *Adv. Synth. Catal.* **2018**, *360*, 2914–2924.
- [52] V. Chirolì, M. Benaglia, F. Cozzi, A. Puglisi, R. Annunziata, G. Celentano, V. Golgi, I.-Milano, *S. Farmaceutiche*, **2013**, 2011–2014.
- [53] T. H. Graham, B. D. Horning, D. W. C. MacMillan, *Org. Synth.* **2011**, *88*, 42–53.
- [54] B. Schweitzer-Chaput, M. A. Horwitz, E. de Pedro Beato, P. Melchiorre, *Nat. Chem.* **2019**, *11*, 129–135.

- [55] R. Quarrell, T. D. W. Claridge, G. W. Weaver, G. Lowe, *Mol. Divers.* **1996**, *1*, 223–232.
- [56] S. Kim, M. Jahandar, J. H. Jeong, D. C. Lim, *Curr. Altern. Energy* **2019**, *3*, DOI 10.2174/1570180816666190112141857.
- [57] E. Arceo, I. D. Jurberg, A. Álvarez-Fernández, P. Melchiorre, *Nat. Chem.* **2013**, *5*, 750–756.
- [58] M. Neumann, K. Zeitler, *Org. Lett.* **2012**, *14*, 2658–2661.
- [59] H. Laverty, K. M. Orrling, F. Giordanetto, M. Poinot, E. Ottow, T. W. Rijnders, D. Tzalis, S. Jaroch, *J. Med. Dev. Sci.* **2016**, *1*, 20.
- [60] A. R. Bogdan, B. P. Mason, K. T. Sylvester, D. T. McQuade, *Angew. Chemie Int. Ed.* **2007**, *46*, 1698–1701.
- [61] W. Huang, J. Da Cen, *Synth. Commun.* **2007**, *37*, DOI 10.1080/00397910701392590.
- [62] D. A. Nicewicz, D. W. C. MacMillan, *Science (80-)*. **2008**, *322*, 77–80.
- [63] E. Speckmeier, T. G. Fischer, K. Zeitler, *J. Am. Chem. Soc.* **2018**, *140*, 15353–15365.
- [64] D. Cambié, J. Dobbelaar, P. Riente, J. Vanderspikken, C. Shen, P. H. Seeberger, K. Gilmore, M. G. Debije, T. Noël, *Angew. Chemie - Int. Ed.* **2019**, *58*, 14374–14378.
- [65] A. Sridhar, R. Rangasamy, M. Selvaraj, *New J. Chem.* **2019**, *43*, 17974–17979.
- [66] P. Li, G.-W. Wang, X. Zhu, L. Wang, *Tetrahedron* **2019**, *75*, 3448–3455.
- [67] Q.-Y. Meng, J.-J. Zhong, Q. Liu, X.-W. Gao, H.-H. Zhang, T. Lei, Z.-J. Li, K. Feng, B. Chen, C.-H. Tung, et al., *J. Am. Chem. Soc.* **2013**, *135*, 19052–19055.
- [68] Z. Li, W. Zhang, Q. Zhao, H. Gu, Y. Li, G. Zhang, F. Zhang, X. Fan, *ACS Sustain. Chem. Eng.* **2015**, *3*, 468–474.
- [69] A. Dhakshinamoorthy, M. Opanasenko, J. Čejka, H. Garcia, *Catal. Sci. Technol.* **2013**, *3*, 2509.
- [70] G. Kumar, P. Solanki, M. Nazish, S. Neogi, R. I. Kureshy, N. H. Khan, *J. Catal.* **2019**, *371*, 298–304.
- [71] C.-A. Wang, Y.-W. Li, X.-L. Cheng, J.-P. Zhang, Y.-F. Han, *RSC Adv.* **2017**, *7*, 408–414.
- [72] X. Yu, Z. Yang, B. Qiu, S. Guo, P. Yang, B. Yu, H. Zhang, Y. Zhao, X. Yang, B. Han, et al., *Angew. Chemie Int. Ed.* **2019**, *58*, 632–636.
- [73] X. Yu, Z. Yang, B. Qiu, S. Guo, P. Yang, B. Yu, H. Zhang, Y. Zhao, X. Yang, B. Han, et al., *Angew. Chemie - Int. Ed.* **2019**, *58*, 632–636.
- [74] D. A. Nicewicz, D. W. C. MacMillan, *Science (80-)*. **2008**, *322*, 77–80.
- [75] E. Sugiono, M. Rueping, *Beilstein J. Org. Chem.* **2013**, *9*, 2457–2462.
- [76] X. F. Tang, J. N. Zhao, Y. F. Wu, Z. H. Zheng, S. H. Feng, Z. Y. Yu, G. Z. Liu, Q. W. Meng, *Org. Biomol. Chem.* **2019**, *17*, 7938–7942.
- [77] E. B. Corcoran, J. P. McMullen, F. Lévesque, M. K. Wismer, J. R. Naber, *Angew. Chemie* **2020**, *132*, 12062–12066.
- [78] K. Donnelly, M. Baumann, *J. Flow Chem.* **2021**, 1–19.
- [79] U. Heiser, A. Niestroj, *N-Pyridinyl Carboxamides as Cyclin-Dependent Kinase Inhibitors Useful in the Treatment of Diseases*, **2011**, WO2011110612.
- [80] M. Cassandri, R. Fioravanti, S. Pomella, S. Valente, D. Rotili, G. Del Baldo, B. De Angelis, R. Rota, A. Mai, *Front. Pharmacol.* **2020**, *11*, DOI 10.3389/fphar.2020.01230.
- [81] N. Fattahi, M. Ayubi, A. Ramazani, *Tetrahedron* **2018**, *74*, 4351–4356.
- [82] M. Badland, R. Crook, B. Delayre, S. J. Fussell, I. Gladwell, M. Hawksworth, R.

- M. Howard, R. Walton, G. A. Weisenburger, *Tetrahedron Lett.* **2017**, *58*, 4391–4394.
- [83] D. Q. Dong, S. H. Hao, H. Zhang, Z. L. Wang, *Chinese Chem. Lett.* **2017**, *28*, 1597–1599.
- [84] L. Marzo, S. K. Pagire, O. Reiser, B. König, *Angew. Chemie - Int. Ed.* **2018**, *57*, DOI 10.1002/anie.201709766.
- [85] T. H. Rehm, *Chem. - A Eur. J.* **2020**, *26*, 16952–16974.
- [86] T. H. Rehm, *ChemPhotoChem* **2019**, DOI 10.1002/cptc.201900247.
- [87] D. Cambié, T. Noël, *Top. Curr. Chem.* **2018**, *376*, DOI 10.1007/s41061-018-0223-2.
- [88] E. B. Corcoran, M. T. Pirnot, S. Lin, S. D. Dreher, D. A. DiRocco, I. W. Davies, S. L. Buchwald, D. W. C. Macmillan, *Science (80-.)*. **2016**, *353*, DOI 10.1126/science.aag0209.
- [89] Z. Zuo, D. T. Ahneman, L. Chu, J. A. Terrett, A. G. Doyle, D. W. C. MacMillan, *Science (80-.)*. **2014**, *345*, DOI 10.1126/science.1255525.
- [90] Z. Zuo, H. Cong, W. Li, J. Choi, G. C. Fu, D. W. C. MacMillan, *J. Am. Chem. Soc.* **2016**, *138*, DOI 10.1021/jacs.5b13211.
- [91] F. Lévesque, M. J. Di Maso, K. Narsimhan, M. K. Wismer, J. R. Naber, *Org. Process Res. Dev.* **2020**, *24*, DOI 10.1021/acs.oprd.0c00373.
- [92] M. González-Esguevillas, D. F. Fernández, J. A. Rincón, M. Barberis, O. De Frutos, C. Mateos, S. García-Cerrada, J. Agejas, D. W. C. Macmillan, *ACS Cent. Sci.* **2021**, *7*, DOI 10.1021/acscentsci.1c00303.
- [93] L. D. Elliott, M. Berry, B. Harji, D. Klauber, J. Leonard, K. I. Booker-Milburn, *Org. Process Res. Dev.* **2016**, *20*, DOI 10.1021/acs.oprd.6b00277.
- [94] K. C. Harper, E. G. Moschetta, S. V. Bordawekar, S. J. Wittenberger, *ACS Cent. Sci.* **2019**, *5*, DOI 10.1021/acscentsci.8b00728.
- [95] A. Steiner, P. M. C. Roth, F. J. Strauss, G. Gauron, G. Tekautz, M. Winter, J. D. Williams, C. O. Kappe, *Org. Process Res. Dev.* **2020**, *24*, DOI 10.1021/acs.oprd.0c00239.
- [96] TED, **2013**.
- [97] TED, **2017**.
- [98] Z. Amara, J. F. B. Bellamy, R. Horvath, S. J. Miller, A. Beeby, A. Burgard, K. Rossen, M. Poliakoff, M. W. George, *Nat. Chem.* **2015**, *7*, 489–495.
- [99] Periodic Videos, **2015**.
- [100] R. A. Howie, L. D. Elliott, S. Kayal, X. Z. Sun, M. W. D. Hanson-Heine, J. Hunter, C. A. Clark, A. Love, C. Wiseall, D. S. Lee, et al., *Org. Process Res. Dev.* **2021**, *25*, DOI 10.1021/acs.oprd.1c00089.
- [101] H. W. Hsieh, C. W. Coley, L. M. Baumgartner, K. F. Jensen, R. I. Robinson, *Org. Process Res. Dev.* **2018**, *22*, DOI 10.1021/acs.oprd.8b00018.
- [102] M. S. Oderinde, A. Varela-Alvarez, B. Aquila, D. W. Robbins, J. W. Johannes, *J. Org. Chem.* **2015**, *80*, DOI 10.1021/acs.joc.5b01193.
- [103] F. Herbrük, M. Sanz, A. Puglisi, S. Rossi, M. Benaglia, *Chem. - A Eur. J.* **2022**, *28*, DOI 10.1002/chem.202200164.
- [104] Y. Su, N. J. W. Straathof, V. Hessel, T. Noël, *Chem. - A Eur. J.* **2014**, *20*, DOI 10.1002/chem.201400283.
- [105] J. Rabani, H. Mamane, D. Pousty, J. R. Bolton, *Photochem. Photobiol.* **2021**, *97*, DOI 10.1111/php.13429.
- [106] M. Roseau, V. De Waele, X. Trivelli, F. X. Cantrelle, M. Penhoat, L. Chausset-Boissarie, *Helv. Chim. Acta* **2021**, *104*, DOI 10.1002/hlca.202100071.

- [107] T. H. Graham, B. D. Horning, D. W. C. MacMillan, *Org. Synth.* **2011**, *88*, 42.
- [108] C. R. Johnson, M. I. Ansari, A. Coop, *ACS Omega* **2018**, *3*, 10886–10890.
- [109] H. Ueda, K. Yoshida, H. Tokuyama, *Org. Lett.* **2014**, *16*, 4194–4197.
- [110] M. He, X. Yu, Y. Wang, M. Bao, *J. Org. Chem.* **2021**, *86*, 14720–14731.
- [111] A. Rostami, E. Sadeh, S. Ahmadi, *J. Polym. Sci. Part A Polym. Chem.* **2017**, *55*, 2483–2493.
- [112] C. Cassani, R. Martín-Rapún, E. Arceo, F. Bravo, P. Melchiorre, *Nat. Protoc.* **2013**, *8*, 325–344.
- [113] E. D. Nacsa, D. W. C. MacMillan, *J. Am. Chem. Soc.* **2018**, *140*, 3322–3330.